ABSTRACT

Water bodies contamination is a global and serious environmental concerns. An increase in the world's population, growing industrialization, and exploitation of natural resources are the reasons of water contamination. Several heavy metals are continuously released into water bodies and caused for deleterious of aquatic environment. The expanding industrial, agricultural, and urban activities including the metal plating, paints and dyes, textiles, fertilizers, tanneries, medicines, battery production, and mineral processing industries. Heavy metals are toxic, bio-accumulative, and non-biodegradable; they are hazardous to aquatic life and human being, leading to a variety of ailments and chronic health issues. Arsenic, chromium, mercury, and lead are highly hazardous or even lethal to the living being even at low levels. These heavy metals enter into the biological system primarily through the food, water, and/or the air. Arsenic, a pervasive element in Earth's crust, and its presence at levels beyond the acceptable limit (10 μg/L) in both surface and ground water is endangering human health which can cause cancer and skin lesions in human being. Similarly, lead is highly toxic element and causes serious health issues at extremely low concentrations, that includes the reproductive, neurological, and cardiovascular abnormalities. Chromium is widely employed for various industrial applications including oxidative dying, the production of pigments, and the manufacturing of textiles has led to severe environmental and health issues. Epigastric pain, carcinogenic effects, bleeding, and severe diarrhea are some of the toxic effects of chromium to humans. Fluoride, an inorganic pollutant causes dental and skin fluorosis, muscle fibre degeneration, skin rashes, low hemoglobin levels, urinary tract malfunctioning, abnormalities in red blood cells, abdominal pain, excessive thirst, headaches, nervousness, tingling in the fingers and toes, and reduced immunity. Simialrly, the persistent organic contaminants are hazardous compounds that have a negative impact on human health. They are accumulated and spread across the food chain from one species to other due to their persistency to remain for extended periods of time in the environment. Among the persistent organic pollutants, diclofenac sodium is nonsteroidal anti-inflammatory drug. The diclofenac sodium is often detected in aqueous effluents due to its wide spread use. Because of its low biodegradability and

high persistency, diclofenac sodium is bioaccumulated and showed severe health problems. On the other hand, the water-soluble cationic dye of the xanthene class, Rhodamine B is seemingly enters into the waterbodies from different industries. It is extensively used as a food additive. It is known neurotoxic and carcinogenic to both humans and animals.

The development of efficient methods of removing hazardous inorganic and organic pollutants from water has received considerable attention in recent time. The advanced treatment methods *viz.*, advanced oxidation process, ion exchange, reverse osmosis, membrane separation, and electrocoagulation are demonstrated to remove inorganic and organic contaminants, however, these methods are required with high capital and operating costs. On the other hand, adsorption is regarded as the efficient wastewater treatment method due to its widespread use, low initial costs, simple design, and ease of operation. The method provides selective and efficient removal of various inorganic and organic pollutants from various polluted waterbodies using adsorbents.

The selection of adsorbents inherently possess the high specific surface area, numerous sorption sites, low cost, eco-friendly, and ease of modification and handling. In a line, nanomaterials are useful alternatives, is explored extensively in recent time. Natural, affordable, non-toxic minerals are used as adsorbents in the treatment of contaminated water due to its high ion exchange capacity, hydrophilicity, physical and chemical stability. Ionic species present in an aqueous solution is readily adsorbed onto the clay surface. Graphene oxide (GO) is contained with various functional groups *viz*., hydroxy, carboxyl, and epoxy groups which impart hydrophilic nature and is a suitable adsorbent for the adsorption of different inorganic and organic contaminants. But due to its hydrophilic nature with fine suspended or colloidal particles makes it difficult in phase separation. The functionalization of graphene oxide with organic or inorganic materials makes is easy for phase separation also the introduction of additional functional groups make the solid selective for several pollutants. In addition, the need to obtain materials with low costs employing greener method spurred the development of numerous environment friendly routes for preparation processes. The synthesis of graphene oxide using natural carbohydrates is being utilized in present investigation.

Therefore, the present investigation aims to synthesise the novel nanocomposites materials precursors to the naturally available sugarcane juice and *in situ* magnetite the nanocomposite material. A greener and sustainable approach was adopted in the facile synthesis of materials. Further, materials were employed in the treatment of aquatic environment contaminated with various inorganic and organic pollutants.

The synthesized solid materials *viz.*, graphene oxide (GO), magnetite graphene oxide (MGO), and magnetite graphene oxide clay nanocomposites (MGOBN) along with the pristine bentonite are characterized by the scanning electron microscopy (SEM), transmission electron microscope (TEM) reveals the heterogenous surface with the presence of Fe_3O_4 nanoparticles onto the graphene oxide or bentonite surfaces. The X-ray diffraction (XRD) results reveal the formation of graphene oxide and magnetite graphene oxide and a Fourier transform infrared (FT-IR) spectra shows the presence of various functional groups. Similarly, a vibrating sample magnetometer (VSM) measure the magnetization of magnetite graphene oxide (MGO) and magnetite graphene oxide clay nanocomposites (MGOBN), and a BET (Brunauer-Emmett-Teller) surface area analyzer showed high specific surface area and mesoporous of these solids. The zeta potential analyzer reveals the negative charges carried by the solid materials.

Graphene oxide (GO) and magnetite graphene oxide (MGO) were utilized for the removal of arsenic (III), and arsenic (V) whereas bentonite (BN), graphene oxide (GO), magnetite graphene oxide (MGO), and magnetite graphene oxide clay nanocomposite with 1:2 ratio (MGOBN@1:2) was employed for fluoride removal. MGO solid showed very high removal efficiency for arsenic (III), and arsenic (V) whereas MGOBN@1:2 showed high removal efficiency in removing fluoride. pH *Ca* 3-4 favored greatly the elimination of these pollutants and an increase in pollutant's concentrations (1.0 to 30.0 mg/L) did not impact significantly the elimination efficiency of solids. The sorption capacities estimated by Sips isotherm were 26.59 and 35.97 mg/g for the arsenic (III) and arsenic (V), respectively using the MGO. Whereas the fluoride removal capacity was 17.81 mg/g using the MGOBN@1:2 nanocomposite. The simultaneous removal of arsenic (V) and fluoride were modeled with the expanded Sips equation and the optimized capacities were 31.88 and 6.57 mg/g, respectively for

arsenic (V) and fluoride using the MGO solid. The pollutants are forming an 'inner sphere complexes' at the solid surface and the kinetic data showed that the uptake of arsenic and fluoride followed the pseudo-second-order rate kinetics. The nanocomposite beads showed high loading capacities i.e., 1.54 mg/g for fluoride using MGOBN@1:2-beads and $1.55x10^2$ mg/g and 1.15 $x10^2$ mg/g for arsenic (III) and arsenic (V), respectively using the MGO-beads under the column experiments. The materials were tested for several natural water implications and showed promising in eliminating these pollutants. Moreover, the solids were regenerated using the phosphate solution (0.05 M) for arsenic and acetate solution (0.01 M) for fluoride and the sorption desorption results showed that the removal efficiency of solid was not affected even for five repeated cycles. The MGO showed efficiency in the removal of arsenic, chromium and copper simultaneously using an archeological bamboo chip sample. The nanocomposite materials are promising in large scale implications for the remediation of water contaminated with arsenic and fluoride.

Further, in the removal of lead (II) and chromium (VI) by MGOBN, the removal efficiency was favored with an increase in pH, however; the lower pH favored the elimination of chromium (VI). The extent of lead (II) and chromium (VI) removal by MGOBN was increased significantly with an increase in pollutant concentrations (1.0 to 30.0 mg/L). The Sips isotherm estimated adsorption capacities for lead (II), and chromium (VI) to 32.48 mg/g and 5.17 mg/g, respectively. The theoretical modelling using the Sips expanded equation revealed the removal efficiency of nanocomposite solid MGOBN for lead (II) and chromium (VI) to 27.5 mg/g and 25.15 mg/g, respectively, in the 1:1 molar ratios of lead (II) and chromium (VI). Similarly, the MGO could remove the arsenic (V) and lead (II) with capacities of 52.7 mg/g and 88.0 mg/g for, respectively, and for arsenic (V) and chromium (VI) is 60.5 mg/g and 19.2 mg/g, respectively for their 1:1 molar ratio. The lead (II), and chromium (VI) are rapidly sorbed at the MGOBN solid and kinetic data agrees well to the pseudo-second-order and fractal-like-pseudo-second-order rate kinetics. The lead sorption proceeds with 'ion-exchange' surface process and forming an 'inner-sphere surface complexation' at the solid surface, whereas chromium is partly sorbed with weaker forces and forming an 'outer-sphere complexes' at the surface. The nanocomposite solid showed high selectivity in the removal of lead (II) and chromium (VI) in the

spiked natural water sample. Fairly a high percentage recovery (>95%) of pre-sorbed lead (II) and chromium (VI) from solid surface for four successive batch operations using the 0.1 mol/L of HCl and H_2SO_4 was achieved and repeated use of nanocomposite solid pointed the potential of nanocomposite solid in the sustainable unit operations.

Furthermore, the nanocomposite solid MGOBN is employed in the removal of organic pollutants *viz.*, diclofenac sodium and Rhodamine B. High removal percentage of diclofenac sodium was obtained a lower pH conditions, however; the Rhodamine B showed higher removal efficiency at pH~6.0. The isotherm modelling of diclofenac sodium fits well to the Langmuir and Sips isotherms, whereas Rhodamine B follows the Langmuir isotherm. The adsorption capacities estimated by the Sips isotherm was 55.01 mg/g and 12.68 mg/g, respectively for diclofenac sodium and Rhodamine B. According to the kinetic data, diclofenac sodium and Rhodamine B uptake followed pseudo-second-order and fractal-like pseudo-second-order rate kinetics. At the solid surface, diclofenac sodium and Rhodamine B were aggregated with relatively stronger forces and forming "inner-sphere-complexes". The MGOBN showed potential in removing diclofenac sodium and Rhodamine B in the spiked natural water. The pre-adsorbed diclofenac sodium and Rhodamine B from MGOBN were fully desorbed by using 0.1 M HCl for five consecutive cycles and indeed the removal efficiency of solid was not altered even for five repeated cycles.

The results demonstrated that the facile, novel, greener, and economically viable magnetite graphene oxide clay nanocomposites showed potential in removing a variety of inorganic and organic contaminants from aqueous solutions. The materials could be employed in a large-scale treatment of wastewaters contaminated with these pollutants. A sustainable and facile treatment process could possibly be promising in unit operations.

MAGNETITE GRAPHENE OXIDE - CLAY NANOCOMPOSITES IN THE REMEDIATION OF AQUATIC ENVIRONMENT CONTAMINATED WITH ARSENIC AND FLUORIDE

A THESIS SUBMITTED IN PARTIAL FULFILMENT OF THE REQUIREMENTS FOR THE DEGREE OF DOCTOR OF PHILOSOPHY

NGAINUNSIAMI

MZU REGISTRATION NUMBER: 3173 of 2009-10

Ph.D. REGISTRATION NUMBER: MZU/Ph.D/1104 of 24.04.2018

DEPARTMENT OF CHEMISTRY

SCHOOL OF PHYSICAL SCIENCES

JUNE, 2023

MAGNETITE GRAPHENE OXIDE - CLAY NANOCOMPOSITES IN THE REMEDIATION OF AQUATIC ENVIRONMENT CONTAMINATED WITH ARSENIC AND FLUORIDE

BY
NGAINUNSIAMI
Department of Chemistry

Under the supervision of

Prof. DIWAKAR TIWARI

Submitted
In partial fulfilment of the requirement of the Degree of Doctor of Philosophy in Chemistry of Mizoram University, Aizawl.

MIZORAM UNIVERSITY
Department of Chemistry
(A DST-FIST Supported Department)
Tanhril, Aizawl, Mizoram. PIN: 796004

Prof. Diwakar Tiwari, Dean (SPS)

Thesis Certificate

This is to certify that the thesis entitled *'Magnetite Graphene- oxide clay nanocomposites in the remediation of aquatic environment contaminated with arsenic and fluoride'* submitted by ***Miss Ngainunsiami*** for the degree of ***Doctor of Philosophy*** in the Mizoram University, Aizawl, Mizoram, embodies the record of original investigations carried out by her under my supervision. She has been duly registered and the thesis presented is worthy of being considered for the award of the Ph.D. degree. This work has not been submitted for anydegree in anyother university.

Dated:28th June, 2023. (DIWAKAR TIWARI)

Supervisor

Tanhril Campus, Aizawl 796004 Phone : 9862323015
Fax : (0389) 233 0834 E-mail : diw_tiwari@yahoo.com

DECLARATION OF THE CANDIDATE

Mizoram University

June 2023

I, Ngainunsiami, hereby declare that the subject matter of this thesis is the record of work done by me, that the contents of this thesis did not form the basis of the award of any previous degree to me or to do the best of my knowledge to anybody else, and that the thesis has not been submitted by me for any research degree in any other University/Institute.

This is being submitted to Mizoram University for the degree of Doctor of Philosophy in Chemistry.

Dated: 28th June, 2023

(NGAINUNSIAMI)

Candidate

Prof. N. MOHONDAS SINGH)

Head

(Prof. DIWAKAR TIWARI)

Supervisor

ACKNOWLEDGEMENT

I thank Almighty God for blessing me with health, strength, and knowledge to accomplish this work. Without his grace and mercy, this work would not have been possible.

I have a great pleasure to express my gratitude to my mentor and supervisor, *Prof. Diwakar Tiwari*, Department of Chemistry, Mizoram University. His dedication and most of all his overwhelming attitude had been solely responsible for the completion of my work. He is always ready to provide a fresh perspective and scholarly advice during my entire tenure. His timely advice, scrutiny, and scientific approach have greatly aided me in completing this work.

I sincerely extends my thank and grateful to *Prof. N. Mohondas Singh , Head, Department of Chemistry, MZU*, and other faculty members *viz*., *Prof Muthukumaran, R., Dr. Zodinpuia Pachuau, Dr. N. Mohondas Singh, Dr. A. Bimolini Devi, Dr. Manjeet Singh, Dr. Joydeep Das,* and *Dr. R. Lalrempuia*, for their constant encouragement and useful advice they have offered me throughout my academic career in the University. My heartfelt special thanks is extended to *Dr. Lalhmunsiama and Dr. Ved Prakash Singh* for his incentive and helpful suggestions in completing my research works.

I am grateful to acknowledge the close cooperation and support I received from all of my colleagues in the Department of Chemistry. I'd like to thank *Dr. J. Lalmalsawmi, Dr. R. Malsawmdawgnzela*, *Dr. Levia Lalthazuala, Dr. CVL Hmingmawia, Mr. Himangshu Dihingsia, Mr. Ricky Lalawmpuia, Mr.Sarikokba, Ms. Lalmalsawmdawngliani, Melody Lalhruaitluangi, Ms. Swagata Goswami*, *Mr. Lalruatkima Ralte, Ms. Barsha Rabha, Ms. Hmingsangzuali and Mr. Vanhmingliana* for assisting me with my laboratory work. It is my pleasure to mention the assistance of *Mr. Brojendro Singh Shagolsem*, Sr. Laboratory Technician, and *Mr. John Vanlalhruaia*, Technical Assistant, Chemistry Department.

Mydeepest gratitude to my parents and all of my family members for their love and support during my tenure for the degree, as well as their comforts and prayers; I can't repaythementirely, but I thank and appreciate them fromthe bottom of my heart.

NGAINUNSIAMI

CONTENTS

CHAPTER 3

CHAPTER 4

List of figures:

Figure 3.9: Effect of pH in the removal of **(a)** arsenic (III) and arsenic (V); and **(b)** fluoride using the nanocomposite materials ([arsenic (III)/ or arsenic (V)/ or Fluoride ions]: 10.0 mg/L; Solid dose: 2.0 g/L; Temperature: 25±1°C, Agitation speed: 180 rpm).

Figure 3.10: Effect of initial sorptive concentration in the removal of arsenic (III), arsenic (V) by MGO, and fluoride by MGOBN@1:2 [pH: 3.0 for arsenic (III) & arsenic (V), 4.1 for fluoride); solid dose: 2.0 g/L: temperature: 25±1°C, agitation speed: 180 rpm].

Figure 3.11: Langmuir, Freundlich, and Sips isotherms for the sorption of arsenic (III), arsenic (V) using MGO and fluoride using MGOBN@1:2 [pH: 3.0 for arsenic (III) & arsenic (V), 4.1 for fluoride); solid dose: 2.0 g/L: temperature: 25±1°C, agitation speed:180 rpm].

Figure 3.12: (a) Sips isotherm modeling in the sorption of fluoride and arsenic (V) in the single component system; and Sips modelling for the binary systems; **(b)** arsenic (V); and **(c)** fluoride in the simultaneous removal of fluoride and arsenic (V) at varied molar ratios using MGO solid (pH: 3.0; solid dose: 2.0 g/L; temperature: 25±1°C, agitation speed: 180 rpm).

Figure 3.13: (a) Effect of contact time in the removal of arsenic (III), arsenic (V) by MGO, and fluoride by MGOBN@1:2 solids [Pollutant concentrations: 10.0 mg/L; (pH: 3.0 for arsenic (III) & arsenic (V), 4.1 for fluoride); Solid dose: 2.0 g/L; Temperature: 25°C, Agitation speed: 180 rpm]; and **(b)** pseudo-first order and pseudo-second order fitting of kinetic data in the uptake of arsenic (III), arsenic (V) by MGO, and fluoride by MGOBN@1:2 solids.

Figure 3.14: Effect of background electrolyte concentrations in the removal of arsenic (III), arsenic (V) by the MGO solid and fluoride by MGOBN@1:2

([Arsenic (III)/ or arsenic (V), Fluoride]: 10.0 mg/L; pH: 3.0 for arsenic (III) & arsenic (V), and 4.1 for fluoride; solid dose: 2.0 g/L; temperature: 25°C, agitation speed: 180 rpm).

Figure 3.15: Effect of co-existing ions in the removal of arsenic (III) and arsenic (V) by MGO and fluoride by MGOBN@1:2 ([Pollutant concentrations: 10.0 mg/L; cations/anions concentrations: 50.0 mg/L; pH: 3.0 for arsenic (III) & arsenic (V), and 4.1 for fluoride; solid dose: 2.0 g/L; temperature: 25°C, agitation speed: 180 rpm).

Figure 3.16: Breakthrough curves for the removal of fluoride by MGOBN@1:2-Beads, and arsenic (III) and arsenic (V) by MGO-Beads (Pollutant concentrations: 10.0 mg/L; flow rate: 1.0 mL/min; pH: 4.14 for fluoride, and pH: 3.04 for arsenic (III)/or arsenic (V); the amount of solid loaded: 2 g for fluoride, 0.5 g for arsenic (III), and 1.0 g for arsenic (V); Temperature: 25°C).

Figure 3.17: Removal of arsenic (III), arsenic (V), and fluoride in distilled water (DW) and natural water (NW) samples using MGO and MGOBN@1:2 materials at varied sorptive concentrations (Pollutants concentration: 10.0 mg/L; pH: 3.0 @ arsenic (III) & arsenic (V), and 4.1 for fluoride, solid dose: 2.0 g/L; temperature: 25±1°C, agitation speed:180 rpm).

Figure 3.18: (a) Repeated use of MGO, and MGOBN@1:2 materials in the removal of arsenic (III), arsenic (V), and fluoride. (Pollutant concentration: 10.0 mg/L; pH: 3.0 for arsenic (III) & arsenic (V), 4.1 for fluoride, solid dose: 2.0 g/L; temperature: 25°C, agitation speed: 180 rpm; desorptive solution: acetate (0.01M) for fluoride and 0.05M phosphate (0.05M) for arsenic (III) and arsenic (V)); and **(b)** Percentage desorption of pollutants in a repeated cycle of desorptions using acetate (0.01 M) and phosphate solutions (0.05 M).

Figure 3.19: Removal of arsenic, copper, and chromium from CCA solution using various doses of MGO nanocomposite [pH of CCA solution: 3.0; contact time: 4 h; temperature: 25±1°C, agitation speed:180 rpm].

Figure 3.20: Effect of pH in the removal of **(a)** lead (II); and **(b)** chromium (VI) by BN, GO, MGO, and MGOBN solids ([Pollutants]: 10.0 mg/L; Solids dose: 2.0 g/L).

Figure 3.21: Effect of sorptive concentrations in the removal of lead (II) and chromium (VI) using MGOBN [pH: 4.0 for lead (II), 3.6 for chromium (VI); Solid dose: 2.0 g/L].

Figure 3.22: Langmuir, Freundlich and Sips isotherms for the sorption of lead (II), and chromium (VI) using MGOBN [pH: 4.0 for lead (II), 3.6 for chromium (VI); Solid dose: 2.0 g/L].

Figure 3.23: **(a)** Sips isotherm modeling for the sorption of lead (II) (pH: 3.7 and 4.0), Cr (VI) (pH: 3.7 and 3.0), and As (V) (pH: 3.0 and 4.0) in the single component system; expanded Sips modelling for the binary systems for the simultaneous removal at varied molar ratios of **(b)** lead (II) and chromium (VI) (pH: 3.7) where q1: adsorption capacity of Pb (II) in Pb:Cr, q2: adsorption capacity of Cr (VI) in Pb:Cr using MGOBN; **(c)** arsenic (V) and lead (II) (pH: 4.0) where q1: adsorption capacity of As (V) in As:Pb, q2: adsorption capacity of Pb (II) in As:Pb using MGO; and **(d)** arsenic (V) and chromium (VI)) (pH: 3.0) using MGO solid where q1: adsorption capacity of As (V) in As:Cr, q2: adsorption capacity of Cr (VI) in As:Cr.

Figure 3.24: **(a)** Effect of contact time in the removal of lead (II), and chromium (VI) by MGOBN; **(b)** Pseudo-first-order, pseudo-second-order, and fractal-like pseudo-second-order kinetic fitting for the sorption of lead (II), and

concentration: 10.0 mg/L; pH: 3.6 for diclofenac sodium and 4.0 for Rhodamine B, solid dose: 2.0 g/L; temperature: 25°C, agitation speed: 180 rpm; desorptive solution: 0.1 M HCl

List of Tables:

CHAPTER 1
INTRODUCTION

1. INTRODUCTION

1.1. BACKGROUND

Water is important for maintaining the quality of life in addition to being a necessary part of life itself. It is a special resource that cannot be replaced. 71% of the earth's surface is covered by water; hence, water is not a scarce resource but the concern is fresh water resources since most of the water is salty or not easily accessible to humans. The majority of water on Earth (97%) is contained excessively with salt. Freshwater makes up only 2.5% of the total amount of water on Earth, and the majority of this is frozen in glaciers and ice caps. Only a small portion of the freshwater is present on the ground or in the air; the majority is located as groundwater (United States Geological Survey, 2009), thus, groundwater is sometimes described as the 'hidden sea'.

Although fresh water is a renewable resource, the world's groundwater supply is progressively declining. According to the WHO/UNICEF JMP 2020 Annual Report update, 2.0 billion people, or 26% of the world's population, do not have access to "safely managed drinking water" which refers to water that is safe and readily available at home. This comprises 1.2 billion people who have basic water service, but it is provided outside the home, is sporadic, or is hazardous. The other 0.8 billion people either used unprotected water sources (367 million), required more than 30 minutes of walking to fetch water from outside the house (282 million) or were forced to use untreated water from rivers or lakes (122 million) that are seemingly contaminated. Lack of water is having negative repercussions on every population on every continent and is severely affecting developing countries because of their rapid growth both in industries and urbanization (Rana et al., 2017). The depletion of water is severely observed in Asia, South America, and North America (Gleeson et al., 2012). The developing world, notably Africa, still relies on questionable water supplies for everyday needs and is plagued by persistent water issues and including waterborne diseases (UNESCO, 2014). In India, less than 50% of the population has access to fresh and safe drinking water, and is properly managed. The waterborne pathogens still account for *Ca.* 80% of diseases in India. The establishment of wastewater treatment

facilities is a significant component of this endeavor, still only 20% of communities in India had access to wastewater treatment facilities which is primarily due to inadequate infrastructural facilities in addition to the lack of energy requirement for such facilities to operate (Fosshage, 2014). It was estimated that 1.96 million homes are bound to use chemically contaminated water, primarily from fluoride and arsenic. And two-thirds of India's 718 districts are struggling with severe water shortages. Due to the widespread usage of drilling over the past few decades, India is known as the country with the highest rate of groundwater depletion in the world (JMP, 2017). Infected/or contaminated water is killing more people than cancer, AIDS, conflicts, or accidents, according to a report from the Third World Academy of Sciences (TWAS, 2002). Additionally, it was predicted that 1.8 billion individuals drink water tainted with *Escherichia coli* (an indicator of faecal contamination) (Bain et al., 2014). Diseases associated with water, such as cholera, diarrhea, malaria, dengue fever, and others, claim the lives of millions of people. Over 25,000 people each day die from water-related diseases worldwide, and 5000 children die from water-related diseases each day (Bcee, 2020). About 1.8 million children die every year from diarrhea and other infections, with developing countries accounting for the majority of these deaths (Johnston et al., 2011).

Water supplies are at risk due to the factors such as climate change, water pollution, water conflict, and water scarcity, with water pollution being the greatest threat to global water supplies. Recent population growth, fast urbanization, and industrialization all played a significant role in severe water contamination and the Groundwater serves as the main supplement for microbial pathogens. The most prevalent inorganic pollutants are metals and salts, with heavy metals being the most significant (Hu et al., 2010) and some of the organic contaminants include pesticides, insecticides, fertilizers, hydrocarbons, phenolic compounds, plasticizers, biphenyls, lubricants, surfactants, and medicines (Ali et al., 2012). The release of effluents from the industries such as chemical, tannery, metal extraction, battery production, paint, pigment, paper, glass, and polishing causes significant surface water contamination (Selvam et al., 2017). These substances are dangerous to aquatic life as well as to human health. The effluents of these industries deteriorate the quality of waterbodies even at trace levels (Gupta et al., 2020). Since heavy metal ions showed a strong

affinity for hemoglobin, the body quickly accumulates these substances that results in several negative side effects, including cancer, nephritic syndrome, cholera, typhoid fever, ringworms, dysentery, skin irritation, and liver-related problems (Pan et al., 2019).

Maintaining water quality is becoming exceedingly challenging around the world since the availability of ground/surface water is limited due to pollution and significant costs associated with removing contamination, salt removal, and undesirable particle separation. As a result, wastewater remediation has received greater attention and is in practice in developed or developing nations. Different technologies are developed for eliminating various harmful contaminants from wastewater, which include photodegradation, precipitation, coagulation and flocculation, membrane separation, and ion exchange (Khan et al., 2019). However, because of their shortcoming in terms of operation costs, performance efficiency, application for a variety of pollutants, and reusability, these technologies are typically not appealing (Blackburn, 2004; Tiwari et al., 2015). Adsorption, in contrast, is a well-known, adaptable, practical, and extremely effective pollution treatment technology due to its inherent benefits, such as simplicity of use, low cost, reusability, and absence of secondary pollutant formation (Yagub et al., 2014). The type and concentration of the pollutants present in the wastewater determine the appropriate adsorbent for the treatment of a particular wastewater with a particular chemical pollution profile. Adsorbents with high surface areas, wide pore volumes, and appropriate functionalities are useful for adsorption processes (Wang et al., 2013). Nano-size adsorbents achieve the goal of efficient treatment of water contaminated with a variety of contaminants due to their small size, high surface area, high reactivity, and a large number of active sites (Lata and Samadder, 2016). Activated carbon, silica gel/beads, activated alumina, pillared clays, polymeric resins, zeolites, mesoporous oxides, and metal-organic frameworks are a few of the numerous porous materials that have shown variable degrees of efficacy in eliminating harmful pollutants from aqueous medium. Among them, carbonaceous-based adsorbents such as fullerene, carbon nanotubes, and activated carbon typically exhibit high adsorption capacity (Ren et al., 2011). Lately, graphene-based carbon composite materials are the most intriguing two-dimensional (2D) functional materials. These materials display remarkable qualities like a large

surface area, a high density of oxygenated functional groups on sheets, extravagant π electron mobility on the surface of the carbon lattice area, etc., (Liu et al., 2011). Therefore, these materials received greater attention in their wider role in wastewater treatment technologies.

1.2. SOURCE, FATE, AND TOXICITY OF POLLUTANTS

Rapid industrialization, population growth, and urbanization have all contributed significantly to serious pollution of the air, water, and soil. The presence of several naturally occurring, anthropogenic, and industrial-bound pollutants such as fluoride, heavy metals, variety of pharmaceutical products and dyes, significantly degrade the water quality, resulting in serious health problems and the marine ecosystem. The group of metals and metalloids with high atomic densities exceeding 4 g/cm^3 that are poisonous at low metal concentrations are often referred to as "heavy metals" (Aprile and De Bellis, 2020). Due to their prolonged existence in biological systems, the slow accumulation of heavy metals in water bodies or development in the environment via the food chain, and potential health risks pose serious and adverse impacts on living organisms or the environment as a whole. The known heavy metals that include arsenic, copper, cadmium, lead, zinc, mercury, chromium, nickel, molybdenum, cobalt, and manganese showed harmful effects on human health at low to higher concentrations (Engwa et al., 2019) .

The term "emerging pollutants" (EPs) refers to a broad spectrum of synthetic chemicals used in modern society, including pesticides, cosmetics, personal care items, and pharmaceutical compounds. Since these micro-pollutants are persistent, partly biodegradable, and harmful even at low levels, the presence of organic micro-pollutants poses severe environmental issues. The monitoring agencies have detected a significant concentration of several pharmaceutical and personal care products (PPCPs) in waterbodies, sediments, groundwater, and even in drinking water.

1.2.1. Arsenic

Arsenic is an allotropic pnictogen ubiquitous metalloid with atomic number 33 and an atomic weight of 74.92. It occurs naturally in the earth's crust as a trace element. Arsenic is the 53rd most prevalent element, accounting for approximately 1.5 ppm (0.00015%) of the Earth's crust (Rieuwerts, 2017), ranking to be 20th in abundance on earth's crust. Arsenic is found as a pure elemental crystal or in a variety of minerals, usually in conjunction with sulfur metals. Among the 200 different mineral forms of As, the three primary arsenic forms are distinguished: arsenates (60%), sulfides, and sulfosalts (20%). Native arsenic and silicates make up the remaining components (Nriagu, 1994). Arsenic is found in the environment in a variety of forms, depending on the predominant physicochemical conditions: Arsenate (+5), arsenite (+3), elemental arsenic (0), and arsine (-3) are the four oxidation states of arsenic. Arsenic (III) and arsenic (V) are the most often seen oxidation states of arsenic in the environment, particularly in soil and water, while arsenic (III) predominates in a reducing environment.

The amount of arsenic in water varies depending on the type of waterbody. The local geology, hydrology, and geochemical properties of the aquifer materials influence the presence of arsenic in natural waters (Bhattacharya et al., 1997). Uncontrolled human activities also resulted in arsenic contamination of the environment. Human activities such as the smelting of metal ores, the use of arsenical insecticides and pesticides, and the application of wood preservatives are the major sources of arsenic in the environment. The presence and source of arsenic in groundwater rely on several variables, including adsorption-desorption, precipitation-dissolution, oxidation-reduction, ion exchange, particle size, organic content, biological activity, and aquifer features (Robertson, 1989). In the ocean, arsenic concentrations were reported to range from 1 µg/L to 2 µg/L (Chappell et al., 2003).

Arsenic is categorized as "toxic" and "hazardous for the environment" in its elemental form as well as in its compounds of sulfate and trioxide. Arsenic trioxide, arsenic pentoxide, and arsenate salts are classified as category 1 carcinogens by the European Union (EU) and the International Agency for Research on Cancer (IARC) (Domínguez-González et al., 2014; Lee et al., 2015). In the 1930s, a method of treating

wood with chromate copper arsenate (also known as CCA or Tanalith) was developed, and for many years, this treatment was the most prevalent commercial application. The toxicity of arsenic prevents bamboo from insects, bacteria, and fungi (Rahman et al., 2004). CCA was banned from consumer items in 2004, at the initiative of the European Union and the United States (Mandal and Suzuki, 2002). Arsenic was often used as agricultural toxins and insecticides. Additionally, a number of agricultural toxins and pesticides are contained with arsenic. For instance, lead hydrogen arsenate is a typical insecticide used for fruit trees, however, exposure to this substance caused brain damage. To promote weight gain, boost feed efficiency, and guard against disease, arsenic is added to the feed of pigs and poultry (Nachman et al., 2005). Chickens are fed feed contained with minutes quantities of arsenic (Nachman et al., 2005). Inorganic arsenic is more dangerous than organic arsenic compounds, which also aid in the growth of chickens. The arsenic in chicken feed can change into a hazardous inorganic form in specific circumstances. Natural sources of exposure for humans include mineralized groundwater, ore weathering, and volcanic ash. In addition, arsenic is found in food, water, soil, and air (CSEM,2010). Although all plants absorb arsenic, it is more prevalent in seafood, green vegetables, rice, apple, and grape juice. Inhaling dust and pollutants from the atmosphere is another way to become exposed. In the Victorian era, arsenic was frequently employed in interior design, particularly in wallpaper (Hawksley and Lucinda, 2016). Multiple pathways exist for arsenic to enter into the human body. Ingestion, inhalation, and cutaneous adsorption are the typical ways of exposure. The skin and lungs of human absorbs the arsenic.

The toxicity of arsenic is categorized into two parts: acute and sub-acute or chronic toxicity. Typically, consuming contaminated food or water results in acute arsenic toxicity that necessitates immediate medical intervention. The most common early symptoms of acute arsenic toxicity include hematuria, dysphasia, colicky atypical discomfort, projectile vomiting, copious diarrhea, and burning and dry mouth and throat. Dehydration quickly leads to shock, facial edema, heart irregularities, and muscle spasms (Done and Peart, 1971). The cardiovascular, neurological, gastrointestinal, respiratory, and hematopoietic systems are the principal targets of subacute arsenic toxicity. Loss of appetite, nausea, vomiting, dry mouth, shooting pains, diarrhea, nervous weakness, tingling in the hands and feet, jaundice, and

erythema are possible side effects. Longer contact caused dry, falling hair, brittle nails, dermatitis, darkened skin that was exfoliating, and a hormy condition on the palms and soles (Pinto and Mcgill, 1953). As compared to its oxidized pentavalent state, trivalent arsenic is around 60 times more hazardous and inorganic arsenic compounds are approximately 100 times more toxic than organic arsenic.

The recommended level of total arsenic in drinking water by the World Health Organization is 10 µg/L. Natural arsenic pollution of groundwater and surface water is believed to affect more than 140 million people in at least 70 different countries, according to a report published by a UNICEF consultant (Ravenscroft, 2007). The majority of naturally occurring arsenic pollution in groundwater is reported in South Asia and South America (Shaji et al., 2021). The most badly impacted nations are Bangladesh, India, China, Nepal, Vietnam, Cambodia, Laos, Myanmar, Indonesia, the USA, and Indonesia (McArthur, 2019). Numerous studies show that Bangladesh's shallow aquifers are seriously harmed by the elevated amounts of arsenic contamination (Edmunds et al., 2015). Arsenic levels in groundwater ranged from 0.5 to more than 4600 µg/L. Out of 64 districts in Bangladesh, 59 of them have levels that are higher than the WHO limit of 10 µg/L for drinking water, which has an impact on more than 85 million people (Huq et al., 2020). A population of more than 50 million people in India is reportedly at risk due to groundwater arsenic poisoning. Shallow aquifers from 5 Indian states *viz.*, Assam, Bihar, Chhattisgarh, Uttar Pradesh, and West Bengal are having high levels of arsenic (>10 ppb) in their groundwater (CGWB, 2018).

1.2.2. Fluoride

An inorganic anion called fluoride (F) is found in minerals naturally. Fluoride enters the environment through the interaction of fluorite salts with minerals in soil or rocks. Fluoride is the 13th most abundant element in the earth's crust (Tomar et al., 2013). Through a process known as the fluorine cycle, fluorides are released into the biosphere through the natural weathering of specific types of basement rocks such as amphiboles (hornblende), micas (biotite and muscovite), fluorite and apatite, and human activities. Especially in metropolitan settings, fluoride is naturally present in

precipitation, groundwater, freshwater, and saltwater sources. The average seawater fluoride concentration is 1.1 mg/L and with a typical range of 0.86 to 1.4 mg/L (Government of British Columbia, 2015). Fluoride concentrations in freshwater fluctuate with several parameters. In general, the concentration of surface water in rivers and lakes ranges from 0.01-0.3 mg/L (Liteplo et al.2002). Both natural and anthropogenic sources of fluoride pollute the aquatic environment. The natural causes of groundwater pollution are connected to geogenic processes, such as the weathering and erosion of fluoride-rich minerals including fluorite, topaz, and biotite, and also the discharge of fluoride as a result of volcanic activity, fumarolic gases, hydro-geothermal vents, and marine aerosols (Bhatnagar et al., 2011). Industrial sources of fluoride contamination include the discharge of waste from aluminum smelters, toxic waste from coal-fired power plants, and factories that manufacture various materials (such as glass, ceramic, plastics, pesticides, disinfectants, etc.), while agricultural sources include unrestricted long-term use of phosphatic fertilizer or the irrigation of crops with fluoride-enriched water (Kimambo et al., 2019). Fluoride enters the food chain via contaminated soil, water, and air. Consuming contaminated food products is regarded as an additional significant source of fluoride exposure to humans (Brahman et al., 2014). Furthermore, toxicities that occur in food crops as a result of contaminated plant-growing environments reduce their yield and nutritional values (Bustingorri , 2014).

The most common symptom of prolonged fluoride exposure is skeletal fluorosis, which permanently alters the bones and joints as well as dental fluorosis. Fluorosis of the teeth or the skeleton is reported in humans at fluoride concentrations greater than 1.5 mg/L. Since young children's body tissues are still developing and growing, children under the age of 12 are most vulnerable to fluorosis. Further, fluorosis is not medically curable (Miretzky and Cirelli, 2011). Dental fluorosis causes teeth to become stained and pitted, and in extreme conditions, the entire enamel is badly harmed. Skeletal fluorosis is characterized by fluoride buildup in the bones, which results in structural alterations to the bones as well as stiffness and pain in the joints. Damage to organs other than the skeletal system, such as the liver, kidneys, brain, reproductive, and digestive systems, is known toxicity of fluoride (Barbier et al., 2010).

Fluoride pollution in drinking water is a global problem since more than 200 million people encounter drinking water with elevated fluoride concentrations (Chai et al., 2013). Fluorosis affects a large number of individuals worldwide, particularly in China, Spain, Iran, Brazil, Jordan, Canada, India, Ethiopia Pakistan, Mexico, Japan, and Thailand. It was further reported that approximately 35 and 26 million people respectively from China and India are at risk from fluoride (Jadhav et al., 2015a).

1.2.3. Lead

Lead is the most widely distributed heavy metal in the world and is a soft, malleable, toxic substance with a high molecular weight (Li et al., 2002). Lead, a component of the earth's crust is a naturally occurring element present in trace amounts in soils, plants, and water. With a crustal abundance of 14 ppm, lead ranks as the 38th most plentiful element in the Earth's crust. Galena (PbS), cerussite ($PbCO_3$), anglesite ($PbSO_4$), and pyromorphite ($Pb_5(PO_4)_3Cl$) are the primary lead ore mineral. Lead is typically extracted as a byproduct from ores that also contain impurities including antimony, copper, arsenic, zinc, tin, bismuth, and silver (Gulson, 2008). The primary sources of lead in the environment include waste products from the production of storage batteries, paint and ammunition, petroleum refineries, and lead mining runoff (Wang et al., 2010). The manufacturing of storage batteries consumes the most lead, followed by the production of gasoline additives by the petroleum sector (Gürel et al., 2005). Despite its usefulness, lead pollution has emerged as one of the most widespread and elusive threats to the environment and public health (Şölener et al., 2008a).

Humans are frequently exposed to lead through lead-containing activities such as lead smelter and ignition, pottery, boat construction, lead-based paintwork, lead-containing pipelines, battery reprocessing, grids, the production of armament, pigment, and book printing (Wani et al., 2015). Even at low concentrations, lead is extremely harmful to all living beings, including humans. Lead poisoning is a serious consequence throughout the history of mankind. One of the main sources of lead poisoning is water pipes that enter residences (Moore, 1977). Comparatively low lead exposure was used to study the oxidative stress of DNA, membranes, and proteins indicating potential negative effects on oxidative stress (Roy et al., 2015). Employees

exposed to lead showed impaired respiratory function and had higher blood lead and zinc protoporphyrin levels (Jurdziak et al., 2015). The immunological system, the cardiovascular system, the kidneys, and the central nervous system are thought to be among the organ systems that are severely impacted by lead's absorption into the bloodstream (Bergeson, 2008). Ionic lead (Pb^{2+}) showed a high affinity for enzymes, ligands, and biomolecules that contain thiols (-SH) and phosphate ions (PO_4^{3-}). Further, the kidney, liver, and brain cells are experienced reduced functions or complete breakdown as a result of the inhibition of the biosynthesis of heme units, which affects the membrane permeability of the organs. Anemia and an elevation of blood pressure are also linked to prolonged lead exposure. High lead exposure during pregnancy results with miscarriage and male fertility is found to be decreased by chronic lead exposure (Sokol and Berman, 1991). The signs of lead poisoning include forgetfulness, neurological problems, numbness of the muscles, and irritability (Wani et al., 2015). Many body tissues, including the lungs, brain, liver, spleen, and kidneys store lead in addition to the bones, blood and, teeth. It was discovered that low levels of lead were excreted in faeces as well as in perspiration, hair, and nails. The intriguing is that the lead has no physiological function in the body, despite having numerous negative effects (Kosnett et al., 2007).

1.2.4. Chromium

Chromium is a transition heavy metal, which is derived from the Greek term Chroma, which means "color,". It is found to be hazardous to a variety of human organs. Chromium is one of the elements that are most readily available on Earth, ranking 22 (Barnhart, 1997). Chromium deposits are found in the Earth's crust. Chromium compounds are released into the environment through the erosive processes of rocks containing chromium. Two crucial native chromium minerals are mined either open-pit or underground: chromite (iron chromium oxide) and magnesiochromite. Chromium is mostly obtained from industries that use chromium such as the steel manufacturing sector, electroplating, tannery, chemical production, and textile manufacturing (Sankararamakrishnan et al., 2006). Two-fifths of the world's chromite ores are located in South Africa followed by Kazakhstan about a third. Other notable countries are India, Turkey, and Russia. India accounts for 14% of global output, and

Sukinda Mines Valley in Odisha solely produces 98% of the country's chromium. Black Smith Institute Report ranks the Sukinda mines Valley as the fourth-most chromium-contaminated area on earth (Das and Singh, 2011). The groundwater and soil contained variable oxidation states of chromium (ranging from- 4 to + 6). Chromium exists with the more oxidized +6, or hexavalent state, or the trivalent state that is likely to be oxidized but to a smaller extent than its hexavalent state (Saha et al., 2011). The steel industry uses metallic chromium to produce stainless steel and polish steel. Chromium is also used in alloys, tanneries, fabric dyes, and mordants. Chromium compounds are employed in the production of magnetic tape, oxidizing paints & pigments, ceramic coatings, glues & adhesives, fillers for plastics, wood preservatives, and the prevention of water corrosion (Mohan and Karthikeyan, 1997). Chromium is extensively used in industries, hence, higher contents of chromium (VI), chromic acid, and other oxidizing products are released into the atmosphere, soil, and water bodies, posing serious environmental issues (Guertin et al., 2004).

Metal speciation, which determines chromium's adsorption, and transport, affects the toxicity of chromium. Moreover, because of being more soluble and bioavailable than chromium (III), chromium (VI) is 1000 times more toxic compared to chromium (III) (Saha et al., 2011). Chromium (VI) is having low density, high toxicity, and non-biodegradable nature and poses a larger risk to human health. Chromium (VI) is having low density, high toxicity, and non-biodegradable poses a high risk to human health. It has been associated with several health problems when it enters the gastrointestinal tract in human, including liver and kidney damage, extensive dermatitis, GI tract damage, human lung cancer, cardiovascular illness, etc. (Tchounwou et al., 2012). The toxic effects of chromium (VI) also include upper respiratory tract irritants, rhinitis, and nasal septal damage. Around 3 million disability-adjusted life years (DALYs) are thought to be affected by diseases associated with chromium exposure, which puts millions of people at risk worldwide (Fuller et al., 2015). The IARC classifies chromium as a potentially carcinogenic substance because it alters the DNA transcriptional activation and results in significant chromosomic abnormalities (IARC,1982) .

1.2.5. Diclofenac Sodium

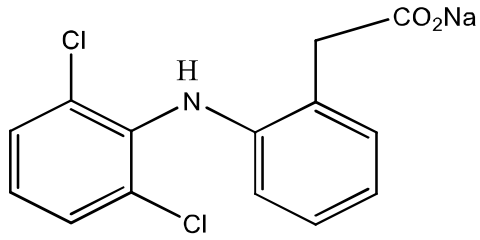

Figure: 1.1. Structure of Diclofenac Sodium

Diclofenac (2-(2,6-dichloranilino) phenylacetic acid) is a non-steroidal anti-inflammatory drug (NSAID) broadly prescribed as an antipyretic, analgesic, and anti-inflammatory drug. It is frequently referred to as the "world's most popular painkiller." Diclofenac sodium is often used to treat diseases including arthritis and acute injuries to reduce inflammation and relieve pain. Furthermore, it functions as an analgesic and antiuricosuric. Both topical and oral administration of diclofenac sodium is common in the treatment. Eyedrops containing diclofenac sodium are also used to treat painful traumatic corneal abrasions (Wakai et al., 2017). With a prescribed daily dose of 100 mg, diclofenac sodium is thought to be consumed globally at a rate of about 940 tonnes annually (Altman et al., 2015). The water bodies are greatly contaminated with diclofenac sodium with a level as high as µg /L ((Lonappan et al., 2016). It was reported that a maximum concentration of diclofenac sodium was 4900 µg/L detected in Pakistani rivers (Scheurell et al., 2009). The wastewater treatment plants as well as natural processes including soil retention, biodegradation, and photo-transformation could help to lower the diclofenac sodium concentration. Diclofenac sodium is detected in samples from various water sources, including rivers, and surface waters due to the improper or inefficient treatment of conventional treatment plants ((Lonappan et al., 2016). It was demonstrated that the existing WWTP effluents contained very high levels of diclofenac sodium even up to 16 µg/L (Lonappan et al., 2016). Similarly, the high concentration of diclofenac sodium (1030 µg/L) was found in river water in Germany (Heberer, 2002). In Norway, Finland, and Switzerland, it was detected in the wastewater influent between 0.19 to 1.9 µg/L (Krzmarzick & Novak, 2014).

The presence of diclofenac sodium in the aquatic environment showed a detrimental impact on aquatic life (Ebele et al., 2017). Studies indicated that diclofenac sodium is accumulated in the body of a variety of fishes and invertebrate species that impact severely the development, reproduction, and metabolism (Acuña et al., 2015). Although Diclofenac sodium is present in the aquatic environment in very low quantities, its persistence results in compounded harmful consequences (Lonappan et al., 2016). Hence, extended exposure to diclofenac sodium even at a concentration of 5 µg/L, rainbow trout showed alterations in gills, livers, and kidneys (Pérez-Estrada et al., 2005). Diclofenac sodium causes harmful effects on renal and gastrointestinal tissues in various vertebrate taxa (Oaks et al., 2004). Even at environmentally acceptable dosages, diclofenac sodium disrupts the metabolic processes of fish and causes tissue damage (Saravanan et al., 2011).

1.2.6. Rhodamine B

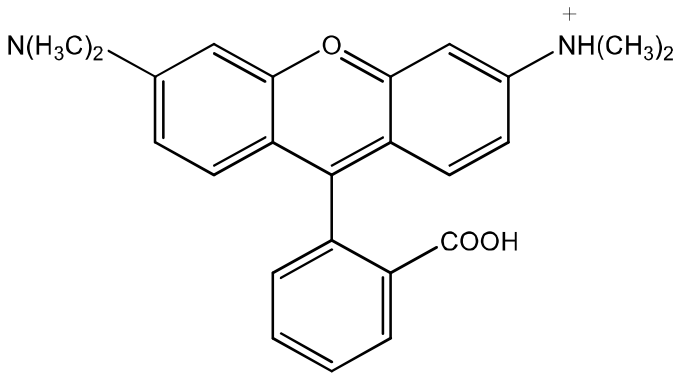

Figure:1.2. Structure of Rhodamine B

Rhodamine-B (RhB) is a water-soluble cationic fluorescent dye that belongs to the xanthene derivatives. It is used as primarily color paper and inks and also frequently employed as a tracer dye, for example, to establish the rate and direction of water flow and transport. In the paper printing, fabric dyeing, paint, and tanning sectors, rhodamine B are having widespread uses. Plastics, fibers, rubber, ceramics, and food sectors are just a few of the items that employ dyes extensively.

Rhodamine B when combined with food, frequently enters into the biological systems and stresses cells and tissues through oxidative stress (Sulistina and Martini, 2020). Acute poisoning of Rhodamine B is occurred with short-duration exposure, while long-term exposure through the food causes cancer or liver damage (Mahdi et al., 2019). Rhodamine B overdose is linked to abdominal pain, dehydration, malabsorption, protein-losing gastroenteropathy, weight loss, dysentery, and electrolyte imbalance (Sulistina and Martini, 2020). The Rhodamine B dye is contained with complex aromatic structure, which makes it difficult to degrade, and also, restrict light penetration in the aquatic system thereby impact severely the photosynthetic activity of aquatic life (da Rosa et al., 2018)

1.3. VARIOUS REMOVAL METHODS FOR INORGANIC POLLUTANTS (ARSENIC, FLUORIDE, LEAD, AND CHROMIUM) AND PERSISTENT ORGANIC POLLUTANTS (DICLOFENAC SODIUM AND RHODAMINE B)

1.3.1. Inorganic pollutant

One of the most significant environmental issues is the contamination of the aquatic environment with a variety of inorganic pollutants. Natural anthropogenic sources also increase their production and the release of inorganic pollutants into the aquatic environment and pose a serious global problem (Guleria et al., 2022). To increase inorganic pollutant adsorption from the aquatic environment, extensive studies are demonstrated and also reviewed elsewhere (Soni et al., 2020; Carolin et al., 2017). Researchers are investigating the mechanism of sorption and trying to obtain insights into solid/solution interfacial studies (Abbas et al., 2018). Generally, inorganic water pollutants are divided into three categories *viz*: Metals/ metalloids, acid, and organic form (Borah et al., 2020). Metals especially the heavy metals in water bodies are a serious concern on a global level. With the increased use of several agricultural, industrial, medicinal, home appliances, and technological applications, human exposure is increased significantly (He et al., 2005). Cadmium, arsenic, mercury, chromium, and lead are among the various metal inorganic pollutants which

cause serious consequences to human health because of their high levels of toxicity (Borah et al., 2020). In the case of the acid form of inorganic pollutants, nitrogen oxides (NO, NO_2) and sulphur dioxide emissions from automobiles and power plants are rising dramatically as a result of human interest and greater industrialization. The nitric acid and sulfuric acid which are derived in the atmosphere by these gases, acid rain, or contaminated snow enter into the environment, which alters the pH of natural water (Borah et al., 2020). Similarly, the organic form of inorganic compounds easily contaminates drinking water sources and causes human health in the long run. Several harmful organic compounds constitute the primary source of water contamination in the country. Numerous other organic chemicals, such as organic solvents, dioxins, furans, polychlorinated biphenyls, pesticides, and other derivatives of nitrogen are included in this group of contaminants (Borah et al., 2020).

1.3.2. Persistent Organic pollutants (POPs)

POPs are persistent by definition, and this characteristic is typically connected with their chemical stability (Miniero and Iamiceli, 2008). Organic pollutants' physicochemical characteristics, such as Henry's constant (H), the n-octanol/water partition coefficient (K_{ow}), the sorption coefficient (K_D), and the partition coefficient between soil organic carbon and water (K_{OC}), all play a significant role in their fate and speciation in the environment (Grassi et al., 2013). Based on the unit operations and procedures frequently employed in wastewater treatment plants (WWTP), different persistent organic pollutants have different removal efficiencies (Barceló, 2003). The mechanical and biological stages of treatment were utilized in traditional municipal WWTPs. The filtration, sedimentation, and flotation techniques are part of the mechanical stage's goal in removing suspended particles. Under aerobic and anoxic conditions, the traditional activated sludge (CAS) method is typically used for biological treatment. Volatilization, or changing an organic pollutant from its dissolved state in water to a gaseous state, is another method for removing it from municipal wastewater.

The conventional wastewater treatment techniques fall short in their ability to eliminate efficiently the POPs. Therefore, there is a necessity of employing advanced treatment steps in removing these persistent chemicals from conventional treatment plants. Advanced oxidation processes (AOPs), as they are known, use a different

strategy, are relying on the oxidation of organic contaminants by potent oxidants, principally the hydroxyl radicals produced by ozone, hydrogen peroxide, and other substances (Bartolomeu et al., 2018). The application and evaluation of biological processes, membrane filtration, and advanced oxidation processes are often used for the removal of organic micropollutants. However, each removal method has benefits and drawbacks (Silva et al., 2012).

Several methods are demonstrated for the removal of inorganic pollutants and persistent organic pollutants that include ion exchange, oxidation, phytoremediation, adsorption, membrane technologies, chemical precipitation, electrokinetic, electrocoagulation, etc. These methods are briefly summarized below:

1.3.2.1. Ion exchange

Ion exchange is a common physicochemical method to eliminate contaminants from an aqueous medium. Ion exchange is a phenomenon that occurs when ions are exchanged between solid and liquid media through a chemical reaction. The ions held electrostatically on the surface of the solid phase are swapped with ions with a similar charge from the solution (Katsoyiannis and Zouboulis, 2006). The ion exchange process effectively removes inorganic contaminants and makes them accessible for recycling. The exchange materials are both synthetic and natural resins. Ion-exchange resins are used for removing various kinds of inorganic pollutants depending on the kind of functional groups present on the solid surface. This method uses reinforced, frequently-regenerated resins that pass through contaminated water and recycle the exchanged ions.

1.3.2.2. Advanced Oxidation process

One of these techniques is the *in situ* production of extremely reactive and nonselective hydroxyl radicals (·OH). The advanced oxidation process relies on highly reactive hydroxyl radicals, which carry out the oxidation of the pollutant. The radicals are anticipated to effectively interact with wastewater contaminants and readily degrade them, hence; are found efficient in wastewater treatment options (Huang et

al., 1993). The oxidation process includes the mineralization of organic pollutants to their end product (CO_2) or oxidation-reduction processes that use strong oxidizers to convert pollutant compounds to their metabolite products (Liu et al., 2009).

1.3.2.3. Membrane technologies

To remove inorganic pollutants from wastewater, membrane technology is received greater attention. Reverse osmosis (RO) and nanofiltration (NF) membranes are two membrane filtration methods that are found efficient in removing the inorganic and organic micro-contaminants (Silva et al., 2012). Adsorption, size exclusion, and charge repulsion are three parameters that are principally responsible for the elimination by membrane filtration. The membrane technology is a pressure-driven process. Membranes, which are made of synthetic materials with a vast number of pores, serve as selective barriers that prevent contaminants to pass through. Pressure-driven membrane filtrations are often classified into two types: (i) low-pressure membrane processes like microfiltration (MF) and ultrafiltration (UF); and (ii) high-pressure membrane processes like reverse osmosis (RO) and nanofiltration (NF). The RO membrane is superior to the NF membrane because reverse osmosis has smaller pores than nanofiltration, and it can hold more organic pollutants than nanofiltration. RO will therefore provide nearly full elimination, however, the increased energy use makes it more unappealing (Bolong et al., 2009).

1.3.2.4.Chemical precipitation

Chemical precipitation is the most widely used technique for separating (ionic) dissolved metals from solutions which is achieved by making the ionic metals insoluble or making the solution extremely saturated through pH changes, electro-oxidizing potential, or co-precipitation with precipitating agents.

Hydroxide precipitation also known as precipitation by pH and Sulfide precipitation are two of the most frequently utilized chemical precipitation techniques (Yadav et al., 2019). Since hydroxide precipitation offers more benefits than sulphide precipitation, including lower costs, greater simplicity, and easier pH control, hydroxide precipitation is the more widely used of the two. The different metal hydroxide solubilities are covered between the pH value of 8.0-11.0 which is further

by sedimentation and flocculation making it simple to extract the metal hydroxides (Fu and Wang, 2011). Even though several hydroxides have been employed for the precipitation of metals, lime remains the base of choice for hydroxide precipitation due to its affordability and ease of handling (Baltpurvins, 1997).

1.3.2.5. Phytoremediation

Phytoremediation is a group of environment friendly green technologies that primarily relies on plants (aquatic, semi-aquatic, and terrestrial) and associated enzymes, microorganisms etc. These materials remove, degrade, or immobilize the water contaminants of various origins i.e., from soil, sediment, and aquatic medium (Dhir, 2013). The metal uptake and transport are the basis of the phytoremediation process. To increase the effectiveness of phytoremediation, it is aided or induced by chelators, microbial inoculations, soil amendments, and nanoparticle administration. Natural or continuous phytoremediation and chemically altered phytoremediation are the two methods for phytoremediation (Alkorta et al., 2004).

Natural or continuous phytoremediation is basically dependent on exploiting naturally occurring hyperaccumulator plants that exhibit extreme metal accumulation in shoots as well as unusual resistance to metal toxicity in the roots surrounding the media (Assunção et al., 2003). Low biomass, poor growth and low metal translocation in hyperaccumulator plants, poor solubility of metallic elements in medium, and poor absorption of the element by roots are some of the disadvantages of natural phytoremediation (Prasad, 2004). These restrictions are overcome by a chemically altered phytoremediation by the use of chelating ligands that are present in aquatic media at concentrations of μg/L such as ethylene diamine tetra-acetic acid (EDTA), diethyl triamine penta-acetic acid (DTPA), 1, 3-propylene-diamine-tetra-acetic acid (PTDA), and nitrilo-tri-acetic acid (NTA) (Knepper, 2003).

1.3.2.6.Biological treatment

The approach adopted in the biological treatment plants to purify contaminated water is based on activated sludge, since only a part of impurities is removed during primary settling, chemical precipitation, and aerating volatilization, steps. Biological treatment relies on microbial activity to remove nutrients and oxidize

materials having high carbon content (Eckenfelder and O'Connor, 2013). Activated sludge and biological trickling filters are core components of sewage treatment plants that quickly transform aqueous organic molecules into biomass, which is then segregated from the aqueous solution by sedimentation (Johnson and Sumpter, 2001). Additionally, biological treatment partially eliminates a variety of emerging micro-pollutants, especially polar ones and these compounds are released through the treatment plant effluents (Petrovic, 2003).

1.4. ADSORPTION

Adsorption is a phenomenon of gases or solutes adhering to a solid or liquid surface, resulting in a mass transfer process (Hu and Xu, 2020). Due to the unbalanced forces, the residual surface energy is created in the molecules or atoms on the surface of the solids which allows the other substance to get attracted to the surface of the solid by the unbalanced forces. When the adsorbate species are in contact with the highly porous solid surface resulting in the intermolecular force of attraction between the adsorbate and the solid surface (Rashed, 2013). In adsorption mechanisms, the solute is trapped (on the solid surface) and is referred to as adsorbate, and the solid on which it is trapped is referred to as an adsorbent. Adsorption is the term used to describe this surface phenomenon of adsorbent.

1.4.1. CLASSIFICATION OF ADSORPTION

According to the type of interactive force between the atoms, molecules, or ions of the adsorbent and adsorbate, adsorption is classified into two categories: chemisorption and physisorption. Similarly, based on the bulk adsorbate concentrations, the adsorption is classified into two types: positive adsorption and negative adsorption.

1.4.1.1. Physisorption or physical adsorption

Adsorption that is controlled by physical interaction as opposed to chemical bonding is known as physisorption. Physical forces, such as van der Waals forces, hold

the adsorbate to the surface of the adsorbent. The physical adsorption is driven by intermolecular forces, hence, there is a minimal binding force, low adsorption heat, and a rapid rate of adsorption and desorption at the surface. Further, the physisorbed substances are desorbed easily from the surface, the physical adsorption is apparently reversible in nature (Deng et al., 2019).

1.4.1.2. Chemisorption or chemical adsorption

Adsorbates are attached to the adsorbent (atoms or molecules) by a strong chemical interaction (covalent bonds) referred to as chemisorption. Adsorbates transfer, exchange, or share electrons with adsorbents in this process. The adsorption is often intense, irreversible, and often monolayer aggregation. It is temperature-dependent and increases as the temperature rises, indicating the presence of an activation energy barrier (Butt et al., 2013). Contrary to physisorption, chemisorption takes a longer duration to take place.

1.4.1.3. Positive and negative adsorption

Positive adsorption is defined as when the bulk equilibrium concentration of adsorbate is lower than the adsorbed concentration of adsorbate at the surface whereas a process is referred to as negative adsorption if the bulk concentration of adsorbate is higher than its concentration at the adsorbent surface.

1.4.2. FACTORS AFFECTING THE ADSORPTION PROCESS

Adsorption is affected by several factors, some of which are briefly described here. These variables also affect the mechanism driving the adsorption process (King et al. 1974)

1.4.2.1. Nature of adsorbent

Increasing the surface area of the adsorbent generally improves adsorption since there are more sites available for adsorption. When an adsorbent surface possesses a high surface charge, oppositely charged species are drawn to the surface while similarly charged species are only partially adsorbed (King et al., 1974).

1.4.2.2. Nature of adsorbate

The adsorption process is significantly influenced by the adsorbate's structure, volume, and chemical characteristics. The charge on the sorbate species, the presence of active binding sites on the surface, and the polarity of the adsorbent impact the uptake of the adsorbate.

1.4.2.3. Nature of the solvent

The solute and surface interaction is weakened as a result of interactions between the solvent and/or the surface, which affects the adsorption. The solvent's chemical composition and polarity are crucial characteristics in the adsorption process.

1.4.2.4. Solution pH

pH is a crucial factor in adsorption processes. The solution pH considerably influences the adsorbate's solubility and speciation, which has a significant impact on the adsorption process (Wang et al., 2008). The surface charge of the adsorbent is significantly influenced by pH and affects the adsorption process.

1.4.2.5. Sorptive concentration

The sorptive concentration controls the adsorbent's ability to bind to specific initial adsorbate concentrations, making it a crucial component of the adsorption process (Banerjee and Chattopadhyaya, 2017). Raising the initial concentration of adsorbate led to an increase in the amount of removal (Mnasri-Ghnimi & Frini-Srasra, 2019). The adsorbate components are transported through mass transfer under a chemical potential gradient. The adsorbate species are moved in the direction of a decreasing concentration in which transportation takes place from a high-concentration region to a low-concentration region. The gradient is zero when equilibrium is reached.

1.4.2.6. Temperature

Temperature is an important factor affecting the rate of adsorption. Temperature plays a major role in the adsorption process at the liquid-solid interfaces. The increase in solution temperature impacts the kinetics of adsorption and the physisorption is usually suppressed in increasing the solution temperature whereas the chemisorption is enhanced with an increase in temperature (Li et al., 2009). Increase in solution temperature, the rate of adsorbate molecule diffusion is usually increased (Mekatel et al., 2015). However, was reported that specific adsorption declines as the temperature rises (Rahmani et al., 2010).

1.5. COMMONLY EMPLOYED ADSORBENT

Numerous materials are explored as adsorbents for the efficient elimination of pollutants from aqueous medium. Nevertheless, some of the commonly used adsorbents are discussed below:

1.5.1. Activated Carbon

The phrase "Activated Carbon (AC)" refers to carbonaceous material having high porosity, and a large specific surface area. Activated carbon most common adsorbent for removing contaminants from wastewater. The process that produces activated carbon involves dehydration and carbonizing raw materials first followed by activating them. AC is an extremely porous structure and possesses a large surface area between 600 and 2000 m^2/g (Bhatnagar and Sillanpää, 2010). The structural features, porous structure with high surface area, and chemical composition, which are easily adjusted by chemical treatment are the properties that make activated carbon efficient in wastewater treatment technologies (Ahmaruzzaman, 2008). The commercially available activated carbons are micro-porous in terms of pore size, making them efficient adsorbents for small compounds. The adsorption of large molecules is beneficial when using mesoporous-activated carbons. Activated carbon (AC) was made from *Glebionis Coronaria* L (Tounsadi et al., 2016) and the carbonization

temperature, activation temperature and time, and the ratio of impregnation are crucial components involved in the synthesis of AC. There are two forms of activated carbons: powder-activated carbon (PAC) and granular-activated carbon (GAC). PAC is more effective than GAC in removing micro-pollutants (Odabasi and Büyükgüngör, 2016). Although it is typically used to remove organic contaminants, activated carbon is effective at removing a number of heavy metals as well. Arsenic elimination from aqueous solutions was accomplished using manganese-coated activated carbon materials made from areca nut waste and rice hulls (Lalhmunsiama et al., 2012a).

1.5.2. Zeolites

In general, zeolites are hydrated alumino-silicates with a microporous form that attenuates a variety of cations without causing any structural changes. Zeolites are having three-dimensional, negatively charged lattice structures (Ghasemi et al., 2018). Zeolites are widely employed in wastewater treatment to remove a variety of pollutants. Zeolites are having strong ion-exchange capacity, comparatively high specific surface area, and most importantly, low cost. Among the several zeolites, clinoptilolite is the most prevalent. Other zeolites include mordenite, erionite, chabazite, ferrierite, analcime, and phillipsite (Wang and Peng, 2010). Zeolites are being used as alternatives to traditional materials in industries for the adsorptive removal of a variety of water contaminants. For the selective removal of cations from aqueous solutions, zeolites' ion exchange and adsorption characteristics are both utilized (Ahmaruzzaman, 2008). Aluminum-loaded shirasu-zeolite was used in the elimination of As(V) from drinking water (Xu et al., 2002).

1.5.3. Activated Alumina

Activated alumina is a porous, granular substance with excellent sorption characteristics having a diameter of 0.3-0.6 mm and a surface area of 200 to 300 m^2/g (Bhatnagar and Sillanpää, 2010). Al_2O_3 that has been partially hydroxylated is found in a variety of non-equilibrium forms in activated alumina (AA). The hydroxyl groups in a hydrous alumina precursor are normally destructed when heated, producing an

activated alumina solid structure with high porosity. AA is being studied as an adsorbent after being used as an adsorptive medium for the decontamination of arsenic from water resources. The adsorption capacity of AA was found to range from 0.003 to 0.112 g of arsenic per gram of AA. It comes in a variety of mesh sizes, and particle size influences pollutant removal efficiency.

1.5.4. Bio-sorbent and Biomass

Bio-sorbents are receiving interest due to their widespread availability and eco-friendliness which contain natural polymers, particularly polysaccharides like chitin and its derivative chitosan. Bio-sorbents are inherently low-cost and have a high extent of amino and hydroxyl functional groups. Chitin, a long-chain polysaccharide, and its derivatives are among the most efficient adsorbents for the removal of many aquatic contaminants, including heavy metals and other toxic ions. Arsenic removal from water using batch and dynamic processes was accomplished by converting powdered chitosan derived from shrimp shells into beads (Chen and Chung, 2006).

Biomass is a diverse group of materials having varied chemical properties. Biomass is used often used as adsorbent material since is found renewable, biodegradable, and non-toxic substance (Chi et al., 2020). Industrial, natural, and agricultural waste products such as soy protein, nut shells, potato peels, tea leaves, algae, and microbial-based materials are examples of typical biomass adsorbent materials (Han et al., 2022). Biomass is being utilized more frequently for the treatment of wastewater since its natural abundance. Some biomass-derived sorbents for different metals include algae, fungi, and bacteria. Brierley, 1990 examines the sorption of toxic metal ions by bacteria, fungi, and algae.

1.5.5. Industrial and municipal waste

Industrial waste byproducts and residues are used as inexpensive adsorbents to remove organic chemicals, heavy metals, and colors from aqueous waste fluids. Industrial solid wastes/by-products like fly ash and red mud are employed as adsorbents for the removal of a variety of pollutants. Fly ash is a waste product

available in large quantities during the burning of coal in thermal power plants. The main components of fly ash include silica, carbon, alumina, ferric oxide, etc., making it a useful material as an adsorbent (Montalvo et al., 2017). Fly ash has a 15.6 m^2/g surface area and its characteristics vary greatly by its precursor source (Wang et al., 2005). A new adsorbent for the removal of As(V) from wastewater was obtained using iron-rich fly ash (Li et al., 2009). Additionally, it was noted that red clay which is heated and acidified found effective in the removal of arsenic from aqueous solutions (Altundoğan et al., 2002).

1.5.6. Carbon nanotubes (CNTs)

Carbon nanotubes are hollow graphitic tubes with two-dimensional structures at the nanoscale (Bharati et al., 2017). There are primarily two types of carbon nanotubes used: multi-walled and single-walled carbon nanotubes. Based on the two-dimensional shape of the sheets, CNTs are further divided into three types *viz.*, zigzag, armchair, and chiral nanotubes (Fiyadh et al., 2019). They are employed as absorbents because of their high surface area. CNTs are having unique properties viz., high mechanical strength, high electrical conductivity, and high surface area (Ajayan, 1999). Adsorption is primarily caused by a chemical contact (bond) between the metal ions and the CNT's surface active sites such as electrostatic attractions, sorption-precipitation, and ion exchange (Al-Khaldi et al., 2013).

1.6. REVIEW OF LITERATURE

The single atomic layer of graphite is known as "graphene". It was first introduced in 1986 (Peng et al., 2017). Graphene is a hexagonal, closely packed honeycomb-like crystal lattice of sp^2 hybridized carbon atoms arranged in a two-dimensional (2D), one-atom-thick layer connected through π and σ bonds. This substance serves as the foundation for all graphitic forms; when separated, graphite (3D) sheets generate graphene; when rolled up, graphene layers become carbon nanotubes (1D); and when folded, graphene produces fullerene (0D). Graphene possesses thermal conductivity of 5300 W/Mk, mobility of charge carriers, electrical conductivity (~ 2000 S/cm), and mechanical properties (Young modulus~1100 GPa,

specific magnetism and large theoretical surface area (~ 2630 m^2/g) (Shen et al., 2012) which is significantly greater than carbon nanotubes (1315 m^2 /g) and graphite (10 m^2 /g). Optically, graphene is transparent to light by 97.3% (Baig et al., 2019). Graphene is 200 times more powerful than steel. It also exhibits a significant amount of stiffness. In terms of basic research and potential applications in a variety of research areas, graphene is particularly appealing due to its intriguing mechanical and physico-chemical properties: high strength, electrical and thermal conductivity, exceptional chemical stability and charge mobility, flexibility, and minimal thickness (Novoselov et al., 2012). Both top-down which include epitaxial growth on SiC, chemical vapour deposition (CVD), and solution-based reduction of graphene oxide, and bottom-up organic material synthesis techniques including microwave heating and micromechanical exfoliation of graphite are used to produce graphene (Mbayachi et al., 2021). Graphene has the potential to be used as a promising sorbent for environmental remediation applications, such as the wastewater treatment from harmful inorganic and organic species, due to its enormous surface area, shape, and chemical characteristics, but graphene is typically quite hydrophobic and has high surface energy, which results in weak dispersion and incompatibility with the majority of organic solvents as a result surface modification is required (Kumar et al., 2017).

Graphene oxide (GO), a monolayer graphite oxide, is produced when graphene is oxidized and exfoliated. The most common technique of making it involves chemically oxidizing graphite which produces extended graphene oxide layers decorated with epoxy and hydroxyl and carboxylic acid functional groups (Mkhoyan et al., 2009) and due to the presence of these functional groups, the usual thickness of GO single layers is about 0.7-1.2 nm, which is substantially bigger than the thickness of pristine graphene (0.335 nm) (Peng et al., 2017). GO's hydrophilic nature and high negative charge density are attributed primarily to the oxygen-containing functional groups (Ramesha et al., 2011). Due to its role as an origin for the low-cost and widespread production of graphene-based products, GO has drawn significant scientific interest. GO is also known to have significant hydrophilicity, which indicates that it is readily dissolvable in water. It is suitable for application in a variety of disciplines, including wastewater treatment, due to the functional groups it contains. Although the hydrophilicity of GO guarantees that heavy metals and the

aqueous phase interact as much as possible, it also makes it challenging to separate GO-based adsorbents from treated water after adsorption. Additionally, the restricted number of surface functional groups and tendency of GO to clump together after adsorption limit its ability to adsorb, which lowers its performance. The modification of GO using several other materials was therefore addressed to alleviate its shortcomings. The functionalization of GO has a wide range of options because of the various oxygenated functional groups on GO.

The oxygen functions provide the GO surface a negative charge, which helps the cationic organic dyes to bind to it electrostatically. Through the "π-π" interaction, the aromaticity in the GO can likewise combine with the aromatic organic contaminant. Because of the existence of the reactive species, the functionalization of the GO is simpler. The carboxylic acid, which is found on the edges of the GO sheets, is more reactive than the other functionalities found in the GO (Tang et al., 2011). The epoxy group can likewise be further functionalized similarly. The nucleophilic assault might quickly break open the epoxy ring on the GO (Gao, 2015). The GO's hydroxyl group is another reactive moiety that can be used to create functionalized GO. As a nucleophile, the hydroxyl group readily targets ketones to connect the desired branch or functionality that contains a ketone to the GO (McGrail et al., 2014). GO can also be functionalized with inorganic particles like metal, non-metal, and their oxide nanoparticles in addition to organic functionalization.

GO-based nanoparticles have been used to remove heavy metals, according to other reports. Due to its beneficial characteristics, such as having significant specific surface areas and a large number of oxygenated functional groups with a high affinity for heavy metal ions, such as carboxyl, hydroxyl, and carbonyl groups, GO has attracted a lot of attention from the adsorption of heavy metals. Anionic heavy metal removal is made possible by the ability to protonate oxygen-containing functional groups, which act as the active sites for the adsorption of negatively charged ions in solutions with lower pH levels. This means that at lower pHs, the electrostatic attraction between the positively charged adsorbent and the negatively charged heavy metal ions is what primarily drives the adsorption of oxyanion heavy metals such as chromium and arsenic ions. For instance, to remove both arsenic (III) and arsenic (V) from an aqueous solution, Chen et al., (2015) decorated carboxylated graphene

oxide (GO- COOH) with akaganeite (β-FeOOH) to create the nanocomposite β-FeOOH@GO-COOH. arsenic (III) and arsenic (V) ions were drawn to the oxygen from the Fe-O bonding, which served as the site of complexation. As a result, in the pH range of 4 to 11, both arsenic ion adsorption efficiency increased by up to 100%. With adsorption capacities of 77.5 mg/g and 45.7mg/g for arsenic (III) and arsenic (V) respectively by the nanocomposite. Additionally, 80% removal efficiency demonstrating a high recycle rate was maintained for both arsenic (III) and arsenic (V). By modifying GO with hydrated zirconium oxide ($ZrO(OH)_2$) nanoparticles through a hydro-thermal co-precipitation reaction, Luo et al., (2013) created a substance known as GO-$ZrO(OH)_2$ for an arsenic adsorbent. In comparison to $ZrO(OH)_2$ nanoparticles, GO-$ZrO(OH)_2$ nanocomposites had a higher specific surface area. It demonstrated significant arsenic (III) and arsenic (V) adsorption capabilities over a wide pH range. According to the Langmuir adsorption model, the maximum adsorption capacities for arsenic (III) and arsenic (V) were calculated to be 95.15 mg/g and 84.89 mg/g, respectively. These values were 3.54 and 4.64 times more than those for $ZrO(OH)_2$ nanoparticles. The better dispersion of $ZrO(OH)_2$ nanoparticles in the GO substrate was credited with the higher adsorption capacity. Additionally, GO-$ZrO(OH)_2$ showed outstanding regeneration and anti-interference properties toward the coexisting anions. To create new arsenic adsorbents, several graphene oxide-based materials were chemically coupled with iron compounds. Due to its small particle size, hydrophilicity, and density, Chandra et al.,(2010) used a chemical technique to produce composites of magnetized-reduced GO (M-rGO). The hybrids displayed greater binding capacities for both arsenic (III) (7.81 mg/g) and arsenic (V) (4.23 mg/g) when compared to bare magnetized particles. The composites can be segregated by an external magnetic field and were extremely paramagnetic at ambient temperature, which is significant. Akaganeite graphene oxide (β-FeOOH@GO) nanocomposites were made by in situ-induced hydrolysis of ferric chloride in the presence of graphene oxide (Liu et al., 2016a).

Since functional groups act as the active site for the functionalization of GO to produce composites containing metals, organic molecules, or other heteroatoms, the use of oxygen-containing functional groups for the functionalization of GO to remove cationic heavy ions has increased significantly. X-ray photoelectron spectroscopy

(XPS) and Fourier transform infrared spectroscopy (FT-IR) measurements of the functional groups before and after adsorption have consistently shown direct graphene materials are difficult to separate from water, however, magnetic nanoparticles have the advantages of quick gathering and separation. Magnetic graphene-based nanocomposites have been produced to bypass the unpleasant and laborious procedure of centrifugation or filtration.

Relation between the presence of these functional groups and the formation of new bonds with the adsorbed heavy metals (Bian et al., 2015). A few stacked GO nanosheets were created and employed by Zhao et al., (2011) to adsorb lead (II) ions in water. From 1.0 to 8.0 pH, the sorption was enhanced. The results followed the Langmuir isotherm model, with endothermic and spontaneous processes, and sorption capacities of 842, 1150, and 1850 mg/g at 293, 313, and 333 K, respectively. Strong exterior complex formation between lead (II) and oxygen-containing groups was the cause of the excellent sorption. Commercial GO was functionalized by co-precipitation with Fe-Mg double hydroxide (Huang et al., 2018). Both GO and Fe-Mg hydroxide's oxygen-containing bonds had combined to remove heavy metals, mostly by complexation and ion exchange via OH ions.

Numerous investigations revealed that Fe_3O_4 added to graphene showed remarkable performance with long-term energy and financial viability in the elimination of chromium (VI)(Fan et al., 2012a) and lead (II) (Zhang et al., 2013). Arsenic (III) (Vadahanambi et al., 2013) and lead (II) (Yang et al., 2012) were removed more effectively from graphene when it was coated with iron oxide nanoparticles. Further, the synthesis of magnetic graphene nanocomposites with Fe-Fe_2O_3 nanoparticles in their core-shell resulted in materials with a potent magnetism and high binding potential for chromium (VI) (Zhu et al., 2012) and arsenic (III). Additionally, graphene was decorated with nanoscale iron particles, which demonstrated improved magnetic properties, catalytic adsorption, and reduction of chromium (VI) (Jabeen et al., 2011) and lead (II) (Jabeen et al., 2013) in comparison to raw iron nanoparticles

GO-based nanomaterials with various functionalizations have a greater potential to adsorb fluorine in aqueous systems. An analysis comparing the modification of GO nanolayers with alumina GO/Al_2O_3 and alumina -Al_2O_3 as an adsorbent was carried out by Xu et al., (2020). The GO/Al_2O_3 adsorption capacity was

increased to 4.68 mg/g concerning γ -Al_2O_3, which is determined to be 3.04 mg/g. This increase is mostly attributable to the GO structure, which permits a surface area of 326.22 m^2 /g, somewhat more than the γ -Al_2O_3's reported 316.17 m^2 /g. As a result of the pore volume reduction for the GO/Al_2O_3, the porous structure is also altered, encouraging the occurrence of active sites following the alteration. Chen et al.,(2013) demonstrated a defluoridation process with strong second-order kinetics to achieve equilibrium within 60 min with a maximum adsorption capacity of 17.67 mg /g at ambient temperature. By depositing basic aluminum sulfate in graphene hydrogel using a homogeneous precipitation process, a novel effective adsorbent for fluoride was prepared (BAS@GHG). At pH 7.2 and 298 K, the BAS@GHG composites' maximum adsorption capacity for fluoride was discovered to be 33.4 mg/g. Due to a ligand exchange process between the hydroxide ions and fluoride ions, BAS is thought to result in the high fluoride adsorption capacity in composites, whereas GHG acts as a porous matrix that can give a significant surface area and aid in the diffusion of the adsorbate. For the removal of fluoride ions (F^-), graphene oxide with eggshells (GO/ES) has been investigated as an adsorbent with the maximum F^- adsorption capacity (56 mg/g)

The water pollutants caused by the dyes and pigments are particularly harmful to aquatic life. Sun et al., (2011a) created a combination of magnetized and RGO to form MRGO and used it to capture rhodamine B dyes in an aqueous solution. Rhodamine B dyes have 91% percentage removal capabilities with sorption capacities of 13.15 and mg /g. Ramesha et al., (2011) employed exfoliated and reduced graphene oxide (EGO) both for the adsorption of rhodamine B in an aqueous solution. Owing to strong electrostatic interactions between GO and dye molecules, excellent sorption occurred. Tiwari et al., (2013) employed RGO hydrogel for rhodamine B adsorption in an aqueous solution, removal capacity was about 97% in 2 hours. The cation-anion and $\pi - \pi$ interactions are the cause of sorption. The results were supported by pseudo-second-order kinetics and Freundlich models. Even after three consecutive cycles, 100% rhodamine B removal capabilities were discovered, claiming the suitability for industrial and environmental remediation. A reduced graphene oxide/ZnO composite was created by Wang et al., (2012) and used to investigate rhodamine B adsorption. After four rounds, 99% of the sorbent had recovered. Sui et al. (2012) also created

graphene-carbon nanotubes composite to eliminate rhodamine B from an aqueous solution by heating graphene oxide and carbon nanotubes in the presence of vitamin C Rhodamine B's sorption capabilities were 150.2 mg /g which is a result of $\pi - \pi$ and electrostatics interactions between the dye and the adsorbent.

To assess the potential use of GO as an adsorbent for pharmaceutical waste removal, the adsorption of diclofenac sodium by GO was investigated by Hiew et al., (2019). For diclofenac, GO synthesized using the modified hummers method showed a maximum adsorption capacity of 653.91 mg/g which is attributed due to the $\pi - \pi$ interaction, hydrogen bonding, and hydrophobic attraction. The adsorption of diclofenac sodium by GO was compatible with the pseudo-second-order kinetic and Langmuir adsorption models. According to FTIR studies, the active binding sites for diclofenac sodium in GO may be hydroxyl, carboxyl, and alkoxy. The outcomes offered convincing proof that goes is a potential adsorbent for diclofenac sodium elimination in an aqueous solution. Adsorption tests were carried out by Jauris et al., (2016) to assess the rGO's ability to remove the diclofenac sodium from aqueous solutions prepared by the use of the modified hummers method. At 25 °C, rGO interaction with DCF was due to the electrostatic interaction, hydrogen bonding, and the $\pi - \pi$ interaction which shows a maximum adsorption capacity of 59.67 mg/g. Graphene oxide nanosheets (GON) synthesized via the modified hummers method were used to study sodium diclofenac's (DCF) adsorption by Guerra et al., (2021). The pseudo-second-order model performed better when fitted to the kinetic data at 25 °C, which points to a chemisorptive mechanism with a maximum adsorption capacity of 128.74 mg /g at 25 °C, and the elimination efficiency was 74% after 300 minutes in which the removal was attributed due to the hydrogen bonding , $\pi - \pi$ interaction, hydrophobic and electrostatic interactions.

The name "clay" denotes a naturally occurring substance made mostly of fine-grained aluminosilicate components, which typically reach plasticity at the proper water concentrations and turn hard when dried or burnt. Clay comprises phyllosilicates and other substances that increase the plasticity of materials (Guggenheim, 1995). With a few notable exceptions, the crystalline structure of clay minerals consists of sheets that are rigidly organized in structural layers. Each layer is made up of two, three, or four sheets. Tetrahedra $[SiO_4]^{4-}$, often referred to as tetrahedral "T," or octahedra

$[AlO_3(OH)_3]^{6-}$, also known as octahedral "O," are the building blocks that make up these sheets. Smaller metal cations make up the interiors of tetrahedrons and octahedrons; oxygen occupies their apices, where some are coupled to protons as (OH). With each sheet, all these essential structural components are arranged to create a hexagonal network. The charge of the layers is determined by the quantity and ratio of sheets in the basic structural elements (Lee and Tiwari, 2012) .

The crystalline clay minerals can be broadly divided into seven groups: (i) the two-sheet phyllosilicates typically seen in kaolinite and serpentine, where the T:O ratio is 1:1 and the charge of the two-sheet layer (unit cell) is 0 e/uc (electron charges per unit cell). (ii) Three-sheet phyllosilicates, a class of micas with a T:O ratio of 2:1 and a charge of 2 e/uc on the three-sheet layer. (iii) The expanding three-sheet phyllosilicates of the vermiculite group, (iv) The smectites group, which consists of aggressively expanding three-sheet phyllosilicates with a T:O ratio of 2:1 and a charge of 0.5 to 1.2 e/uc where T:O ratio is 2:1 and the charge of the three-sheet layer (unit cell) ranges from 1.2 to 1.8 e/uc. (v) The talc group and pyrophyllite, which are non-swelling three-sheet phyllosilicates with a T:O ratio of 2:1 and a charge of 0 e/uc. (vi) The chlorites family of four-sheet silicates, with a T:O:O ratio of 2:1:1 with a charge ranging from 1.1 to 3.3 e/uc. (vii) The group of sepiolite and palygorskite minerals with a layer-fibrous structure (Lee and Tiwari, 2012) .

Bentonite is a type of natural clay that mostly consists of the smectite and kaolinite families. Smectite is a three-sheet phyllosilicate that is fairly expanding, with a T:O ratio of 2:1 with a charge ranging from 0.5 to 1.2 e/uc (negative charge). The term "smectite groups" refers to non-metallic clay made of hydrated sodium aluminum silica. Al^{3+} is substituted for Si^{4+} in the tetrahedral sheets and Mg^{2+} or Zn^{2+} is substituted for Al^{3+} in the octahedral layer as a result of the isomorphous substitution, which also results in a net negative charge on the clay surface (Zhu et al., 2000). As a result, bentonite has a high cation exchange capacity (CEC). Due to its large specific surface area, it can be used to adsorb or absorb a variety of polar or ionic substances whereas the kaolinite and serpentine groups contain two-sheet phyllosilicates with a T:O ratio of 1:1 and a charge of 0 e/uc per unit cell.

The environment's chemistry and the kinetics of reactions that take place as clay minerals form and develop regulate the ionic substitutions in the structure.

Exchangeable cations are found in the interlamellar area owing to isomorphous substitution occurring inside silicate layers (Konta, 1995). Cations adsorbed in the interlayer region automatically balance out the negative charge of structural layers. K^+, Na^+, Ca^{2+}, Mg^{2+}, and H^+ are the exchangeable cations that are most frequently found in the interlayer gaps. Because of its substantial surface area and high exchange rates, clay can absorb substances. Clay may draw and hold cations, including heavy metals, due to the negative charge on the structure of its minerals (Bailey et al., 1999). Therefore, the clay minerals' electrical charge combined with their microporosity, surface functional groups, and exchangeable cations in the crystal structure makes them a potential natural adsorbent for attenuating a variety of pollutants from aqueous solutions (Lee and Tiwari, 2012).

Clays are therefore used in numerous research to demonstrate how well they can remove various metal ions. Srivastava et al., (1989) examined the effectiveness of montmorillonite and kaolinite in removing lead(II). It was discovered that montmorillonite has a substantially higher lead(II) adsorption capacity than kaolinite, and that sorption capacity rises with increasing pH. The adsorption on montmorillonite also adheres to the Langmuir adsorption model. Chantawong et al., (2001) investigated the adsorption of lead(II) on Thai kaolin and clay mostly composed of kaolinite and illite. The maximal lead(II) adsorption capacities of the two materials were determined to be 1.41 and 4.29 mg/g, respectively. Both the Freundlich and Langmuir isotherm models of adsorption were used. Additionally, it was noted that lead(II) uptake from aqueous solution was significantly decreased by the presence of co-ions like cadmium (II), chromium (VI), copper (II), nickel (II), and zinc (II).

It is generally known that clay and clay minerals may be used to remove fluoride from water. Clays with significant gibbsite or aluminum oxide content have a huge capacity for fluoride adsorption (Bhatnagar et al., 2011). High-affinity adsorption of negatively charged ions at close to neutral pH is explained by the positively charged surface of the clay minerals. Clay and clay minerals' ability to remove fluoride is affected by a variety of variables, including the medium's pH, ionic strength, and thermodynamic conditions (Gitari et al., 2015; Meenakshi et al., 2008) reported that mechanochemical activation of kaolinites using an oscillatory disc mill increased surface area from 15.11 m^2/g (raw kaolinite) to 32.43 m^2/g, which ultimately resulted

in the creation of new active surfaces and elevated fluoride adsorption capacity (from 0.096 mg/g to 0.106 mg/g). Gogoi and Baruah, (2008) observed significant defluoridation using concentrated sulphuric acid-activated kaolinite concerning raw kaolinite which is due to the intra-particle diffusion and the adsorption at the surface, with the maximum sorption capacity of the acid-activated clay varying between 0.0450 mg/g and 0.0557 mg/g at various temperatures. According to Hamdi and Srasra, (2007) research, a Tunisian clay with kaolinite and a negligible quantity of smectite have a fluoride adsorption capability of up to 93.45 mg/g. When treated sequentially with hydrochloric acid and sodium hydroxide base, laterite adsorption capabilities were reported to be improved (Maiti et al., 2011)The surface area of treated laterite increased as a result of the acid-base treatment, going from about 17.5 m^2 / g to 178 m^2/g, and the highest capacity for fluoride adsorption on treated laterite was discovered to be 39.1 mg/g which was through the electrostatic interaction and ligands exchange. The use of kaolinite clay to remove the fluoride ion by electrostatic interaction from an aqueous solution was investigated by Nabbou et al., (2019).The best pH range for removing the most fluoride is between 4 and 6, and the equilibrium period is 120 minutes. Pseudo-second-order models are used to characterize adsorption kinetics systems. The Langmuir method yields a value of 0.556 mg/g for the adsorption capacity. According to thermodynamic data, fluoride adsorption enhanced with rising temperature from 30 to 55 °C, going from 0.45 mg/g (90%) to 0.48 mg/g (96%) The endothermic character of fluoride adsorption is indicated by the positive value of ΔH_0. The adsorption mechanism was spontaneous, according to ΔG_0', negative value. The fluoride adsorption into kaolinite clay is unaffected by the nitrate and chloride ions that coexist with it in water. Sulfate and carbonate, on the other hand, reduce the removal of fluoride.

The pristine clay minerals showed negligible adsorption capability and selectivity towards many organic pollutants having non- or low polarity and the anionic contaminants such as arsenic (V), arsenic (III), chromium (VI), etc., even though clay minerals are naturally porous materials and demonstrated suitability for adsorption of several metal ions. Due to the fact that the hydration of the clay mineral surface tends to make the interlayer regions less accessible to aromatic molecules, clay minerals have a negligible attraction for organics (Lee and Tiwari, 2012). Furthermore, clay particles

are even less desirable as adsorbents for treating industrial water treatment due to the challenges associated with recovering them from solutions after the adsorption process. This ultimately makes the regeneration of these colloidal particles very challenging. Once more, the adsorption capabilities of these clay minerals are significantly reduced when they are regenerated for usage (Unuabonah and Taubert, 2014). Most clay materials exhibited reduced ability for settling, which restricted their practical application in various wastewater treatment processes.

The performance of clays as the adsorbent can be improved through a variety of modification techniques. The creation of clay/ graphene nanocomposites was reported by Nethravathi et al., (2008) prepared by the colloidal dispersions of graphene oxide- octylamine- intercalated (GO-OA) and bentonite- cetyltrimethyl ammomium (CTA) bromide. Zhang et al., (2015) examined the utilization of a nanocomposite of reduced graphene oxide and montmorillonite (GCM) prepared via a simple solvent method for the removal of chromium (VI) from aqueous solutions by the electrostatic interaction with the maximum adsorption capacity of 12.86 mg/g following the pseudo-second-order kinetics and Freundlich isotherm. The removal of lead (II) was also investigated which involved the use of montmorillonite pillared GO as an adsorbent showing a very high maximum adsorption capacity of 285 mg/g (Liu et al., 2015). Furthermore, the study of the intercalation of Fe-Mn oxides and hexadecyltriammomium bromide (HDTMA-Br) led to the effective synthesis of a hybrid clay-based adsorbent for arsenic (III) and arsenic (V) which follows Langmuir isotherm with the adsorption capacity of 7.99 mg/g for arsenic (III), and 7.32 mg/g for arsenic (V) in with spontaneous and exothermic adsorption process. Batch tests revealed that arsenic (III) removal was best at pH levels of 4-6 while arsenic (V) removal was best at pH limits of 4-8. When 0.01 M HCl was used as the desorbing agent, up to 7 adsorption-desorption cycles of inorgano-organo-modified kaolin clay were completed. Nanocomposites of magnetic montmorillonite clay (MtMag) and magnetic- organic clay (O100MtMag) prepared by the exchange of $HDTMA^{+}$, 100 % montmorillonite CEC was investigated for their ability to adhere to arsenate (Barraqué et al., 2021). The maximum arsenic (V) sorption capacity was discovered at pH 4.0 (9 mg /g and 7.8 mg/ g by MtMag and O100MtMag, respectively), declining under neutral and alkaline conditions.

1.7. SCOPE OF THE PRESENT INVESTIGATION

Concern over environmental aquatic contamination caused by organic and inorganic micropollutants is serious environmental concerns around the globe. It is crucial to keep the aquatic environment free from variety of contaminants as to protect the human and marine life. One of the keys is to focus on several important issues, including effective and viable treatment technologies for the remediation of aquatic environments. To safeguard the aquatic ecosystem and terrestrial life, it is necessary to remove or eliminate these pollutants from aqueous waste or effluent waters before releasing them into water bodies. There is no doubt that the current water and wastewater treatment facilities are built to provide the best possible treatment and removal of contaminants, particularly those that are included in the standards that are now in effect. However, the current wastewater treatment facilities are ineffective at removing the persistent micro-pollutants such as pharmaceuticals, personal care items, endocrine disrupting substances, etc., or potential heavy metal toxic ions. Advanced treatment is therefore crucial to enhance the efficiency and efficacy of current treatment facilities. Adsorption is recognized as a convenient and economical method because it facilitates the removal of numerous water pollutants using naturally abundant materials. Carbon is historically the most adaptable material for water filtration. Water has traditionally been purified using carbon compounds such as activated carbon, soot, charcoal, and carbon nanotubes. One of the most fascinating new additions to the carbon family is graphene and its derivatives. Graphene is a two-dimensional honeycomb single sheet with a sp^2-linked network of carbon atoms that has a very large specific surface area. The high surface area, low electrical conductivity, extraordinary dispersibility in water, presence of oxygen-containing functional groups, and ease of modification of graphene oxide have increased its adsorptive capacity for cations, anions, and basic chemicals. The greener technique using the bottom-up route to synthesize graphene-oxide nanosheets precursor to carbon source by dehydrogenation process overcomes Hummers method for carbon being more versatile and inexpensive. Carbohydrates with a 1:2:1 carbon, hydrogen, and oxygen ratio is used as a carbon source in the hydrothermal condition to produce graphene oxide.

However, the use of graphene-oxide is limited to some extent due to its difficult separation from aqueous solutions due to its high dispersibility and hydrophilicity. Due to its ability to separate when exposed to an external magnetic field, the introduction of magnetic nanoparticles in conjunction with graphene-oxide avoid the limitations. Numerous naturally occurring materials are being thoroughly researched as adsorbents for decontamination of polluted water. Clay has attracted extensive interest for its usage as adsorbents. The electrical charge of clay minerals, as well as the porosity at the micro level, surface functional groups, and exchangeable cations found within the crystal structure, make it a potential natural adsorbent for various contaminants in the remediation of contaminated waters.

Keeping this in mind, the current study focuses on the development of magnetite graphene oxide clay nanocomposites as a precursor to locally available sugarcane for the preparation of graphene oxide. A more feasible, environmentally friendly, low-cost, and efficient treatment method was offered for the elimination of arsenic (V), arsenic (III), lead (II), chromium (VI), fluoride, diclofenac Sodium, and Rhodamine B from aqueous solutions under different physico-chemical parametric studies. The batch reactor operations along with multiple parametric investigations allowed to propose a plausible mechanism involved at the solid/solution interface. Additionally, the operation of the column reactor offers the solids loading capacity for these contaminants under dynamic conditions, which is helpful for actual implications of materials in the wastewater treatment plan or even for scaling up laboratory data to large-scale treatment.

CHAPTER 2
METHODOLOGY

2 METHODOLOGY

2.1 MATERIALS AND APPARATUSES

2.1.1. Chemicals

All chemicals and reagents obtained are Analytical or equivalent grade and are utilized without further purification. Table 2.1 provides detailed information on the chemicals used in the present work.

Table 2.1: List of chemicals used for the experimental works.

Sl.No.	Chemicals used	Chemical Formula	Assay (%)	CAS Number	Company
1	Sodium (meta) arsenite	$NaAsO_2$	99	7784- 46-5	HiMEDIA, India,
2	Sodium arsenate dibasic heptahydrate	$Na_2(AsHO_4).7H_2O$	99	10048-95-0	HiMEDIA, India,
3	Sodium Fluoride	NaF	99	7681-49-4	SRL, India
4	Lead (II)Nitrate	$Pb(NO_3)_2$	99	10099-74-8	MERCK, India
5	Potassium dichromate	$K_2Cr_2O_7$	99.5	7778-50-9	MERCK, India
6	Rhodamine B	$C_{28}H_{31}ClN_2O_3$	99	81-88-9	HiMEDIA, India,
7	Diclofenac sodium salt	$C_{14}H_{10}Cl_2NNaO_2$	99	15307-79-6	Sigma Aldrich, USA
8	Ammonia solution	NH_4OH	25	1336-21-6	SDFCL, India
9	Sodium Alginate	NaC_6H_7O	≥99	9005-38-3	SDFCL, India
10	Ammonium ferrous sulphate	$NH_4Fe(SO_4)_2.6H_2O$	≥99	7783-85-9	SDFCL, India

11	Ammonium ferric sulphate	$NH_4Fe(SO_4)_2.12H_2O$	≥99	7783-83-7	MERCK, India
12	Calcium chloride	$CaCl_2$	95	10043-52-4	MERCK, India
13	Ethanol	CH_3CH_2OH	≥99	64-17-5	Qualigens Fine Chemicals, India
14	Sulphuric acid	H_2SO_4	98	7664-93-9	HiMEDIA, India
15	Hydrochloric acid	HCl	36.5	7647-01-0	Merck
16	Glycine	$C_2H_5NO_2$	≥99	56-40-6	HiMEDIA, India
17	Sodium hydroxides	NaOH	≥97	1310-73-2	HiMEDIA, India
18	Disodium hydrogen phosphate anhydrous	Na_2HPO_4	98	7558-79-4	Merck, India
19	Ethylenediamine - tetraacetic acid	$C_{10}H_{16}N_2O_8$	98	60-00-4	Qualigens Fine Chemicals, India
20	Oxalic Acid	$C_2H_2O_4$	98	144-62-7	MERCK, India
21	Magnesium sulphate heptahydrate	$MgSO_4.7H_2O$	99	10034-99-8	Loba Chemie, India
22	Calcium chloride dihydrate powder	$CaCl_2 .2H_2O$	99.5	10035-04-8	MERCK, India
23	Manganese (II) chloride anhydrous	$MgCl_2$	≥98	7786-30-3	MERCK, India
24	Nickel(II) chloride anhydrous	$NiCl_2$	98	7718-54-9	MERCK, India
25	Nitric acid	HNO_3	65	7697-37-2	HiMEDIA, India
26	Perchloric acid	$HClO_4$	60.0	7601-90-3	HiMEDIA, India

27	Acetic acid	CH_3COOH	≥99.8	64-19- 7	Merck

2.1.2. Sugarcane juice, bentonite clay, and natural water samples

Native sugarcane juice used as a precursor for graphene oxide was collected from Ngaizel, Aizawl district, Mizoram (India), and the bentonite clay (BN) was mined close to Bhuj, Gujarat (India). The bentonite clay was rinsed multiple times with distilled water (DW), dried at 90°C in a hot-air oven (Relitech Co., India), and ground to a fine powder to get 100 BSS (British Standard Sieve). The natural water samples were collected from river, spring, stream, and waterfall sources spread over five distinct locations in the Aizawl region of Mizoram (India). Each place is fully described in Table 2.2, along with its GPS coordinates. Prior to using these water samples, it was filtered using Whatman filter paper (pore size 20 μm). Several physical-chemical parametric investigations of these water samples were conducted as listed in Table 2.3. The water quality was tested using multiparameter equipment that evaluated a range of parameters, including pH, conductivity, resistivity, salinity, and total dissolved solids. A multiphotometer (Hanna Instruments, USA; Model: H183300) was used to analyze the dissolved sulphate, phosphate, fluoride, and nitrate in the real water samples using the standard photometers reagents of phosphate, fluoride, nitrate, and sulphate as HI93713-0, HI93729-0, HI93728-0, HI9751-0, respectively. The samples were examined for contaminants, such as various elements, using an AAS (Atomic Absorption Spectrometer), (Model: AA-7000 Series, Shimadzu, Japan) instrument. The NPOC (Non-purgeable Organic Carbon) and IC (Inorganic Carbon) were obtained using the TOC analyzer (Shimadzu, Model: TOC-VCPH/CPN, Japan). Furthermore, the water samples were spiked with arsenic (III), arsenic (V), fluoride ions, lead(II), chromium(VI), diclofenac sodium, and Rhodamine B and subjected to the removal of these pollutants using nanocomposite materials.

Table 2.2: Details of GPS coordinates of real water samples collected for experiments.

Location	Source	GPS Coordinates
Tlawng, Sairang (Aizawl)	River	Latitude: 23.830385 Longitude: 92.625935 Elevation: 349.01±11m
Chiahpui (Aizawl)	River	Latitude: 23.822641 Longitude: 92.621647 Elevation: 263.2±12m
Tuikhur (Durtlang N, Aizawl)	Spring	Latitude: 23.794722 Longitude:92.729941 Elevation:1191.54±11m
Pukpui, Aizawl	Waterfall	Latitude: 23.817507 Longitude: 92.623275 Elevation: 138.37±24m
Lengpui, (Aizawl)	Stream	Latitude: 23.830385 Longitude: 92.625835 Elevation: 349.61±11m

2.1.3. Materials and instrumentation

Glass beads (0.5 mm to 1 mm and 3-4 mm) were purchased from HiMedia, India for packing of glass column (Spectra/Chrom Aqueous Column, USA; 1 cm inner diameter and 30 cm of length). The sorptive solution of the pollutant was pumped upward using a peristaltic pump (KrosFlo Research I Peristaltic Pump, Spectrum Laboratories Inc., California, USA), Syringe filters with a porosity of 0.45 µm and a diameter of 25 mm was obtained from Whatman, the USA and utilized for batch tests to filter the test solutions. The atomic absorption spectrometer was

employed for analyzing the total arsenic and lead. The calibration curves were obtained using the standard solutions of respective elements, which had concentrations of 1.0, 3.0, and 7.0 µg/ for As (III)/As (V) and 3.0, 5.0, and 7.0 mg/L for Pb (II). A multiphotometer parameter (Hanna Instruments, USA; Model: H183300) was used to analyze the fluoride using the fluoride reagent (HI93729-0). Cr VI), diclofenac sodium, and Rhodamine B were analyzed using a UV-Vis spectrophotometer (Shimadzu Model: UV 1800, Japan). The calibration curves were obtained using the standard sorptive solutions of 1.0, 5.0, 10.0, 15.0, 20.0, and 25.0 mg/L for Cr (VI), diclofenac sodium, and Rhodamine B and analyzed at the λ_{max} of 350, 277 and 553 nm, respectively. The pH of solutions was determined using a digital pH meter (Labtronics; Model: LT-50 microprocessor pH meter, India). The solid materials were annealed in a furnace using (Nabertherm; 30-3000°C; P330; Germany). To dry the solid samples, a hot-air oven (Relitech Co., India) was employed. Solids were weighed using an electronic balance (HPB220, Wensar, India). Water was purified using the Milli-Q Water Purification System (Direct-Q Et Direct-Q UV), USA and the water is having a conductivity of 0.056 µS/cm.

A scanning electron microscope (SEM; JEOL, JSM 7100F; Oxford Xmax), and transmission electron microscope (TEM; JEOL, JEM 2100; Oxford Xtreme) were used for obtaining the surface morphologies of nanocomposites. Furthermore, the elemental composition was determined using energy-dispersive X-ray (EDX, Oxford instruments X-MaxN) spectroscopy in conjunction with a scanning electron microscope (SEM). The FT-IR data of solids were collected using a Fourier transform infrared spectrometer (FT-IR-Shimadzu, Model: IR Affinity-1S, Japan). An X-ray diffraction (XRD) spectrometer (X'Pert PRO, MPD, PANalytical, Netherlands) was used to obtain the X-ray diffraction pattern of solids. The magnetism of the nanocomposites was obtained using a vibrating sample magnetometer (VSM; brand: Lakeshore; model:7400 series), and specific surface area and pore volumes of solids were obtained using a BET (Brunauer-Emmett-Teller) surface area analyzer (3 Flex version 4.03, Micromeritics, USA). The NanoPlus AT, a Zeta/nanoparticle analyzer, was used to determine the Zeta potential of the nanocomposites.

2.1.4. Reagents

The stock solutions of arsenic (III), arsenic (V), fluoride, chromium (VI), lead (II), diclofenac sodium, and Rhodamine B, each having a concentration of 50 mg/L, were prepared by dissolving an appropriate amount of analyte in purified water and by successive dilutions of stock solutions the required concentrations of analyte were obtained. The pH meter was calibrated using standard buffer solutions of pH 4.01, 7.00, and 10.01 from Hanna Instruments. The pH of the experimental solutions was adjusted to freshly prepared standard solutions of 0.1 mol/L HCl or 0.1 mol/L NaOH. A variety of photometers reagents using HI93713-0, HI93729-0, HI93728-0, and HI9751-0 were used to analyze the quantitative estimations of phosphate, fluoride, nitrate, and sulphate, respectively.

2.2. Methods for the preparation of a nanocomposites

2.2.1. Washing of bentonite clay powder

5 g of bentonite powder which was mined near Bhuj, Gujarat (India) was washed thoroughly with distilled water to remove impurities and sand particles and dried in the hot-air oven at 90°C and crushed to obtain 100 BSS (British Standard Sieve). The solid powder was labeled as Bentonite (BN) as shown in Figure 1(a).

2.2.2. Synthesis of graphene oxide

The graphene oxide is synthesized by a greener approach by utilizing sugarcane juice. The *bottom-up* approach using sugarcane juice as a precursor material yielded graphene oxide. In a beaker, 1 L of sugarcane juice was heated to 100 °C until the water molecules evaporated, resulting in a deep yellowish-red syrup. This was cooled at room temperature. Further, the sugarcane syrup was treated with 100 mL of concentrated sulfuric acid (98%) for complete dehydration. Inside the beaker, a column of black carbon formed which was washed with 400 mL of 5 M HCl to remove the remaining impurities. The slurry was then washed with purified water several times until it reaches to neutral pH. The material was dried in an oven at 70°C and then

annealed for 5 hours in a furnace at 600°C. The obtained solid material was termed graphene oxide (GO). The image of GO is represented in Figure 1(b).

2.2.3. Synthesis of magnetite graphene oxide

The *in situ* chemical co-precipitation of Fe^{2+} and Fe^{3+} with the GO resulted in the formation of magnetite graphene-oxide. The detailed method is as: 2 g of graphene oxide was suspended in 800 mL of a solution containing 6.8 g of $(NH_4)_2Fe(SO_4)_2 \cdot 6H_2O$ (4.33 mmol) and 10.04 g of $NH_4Fe(SO_4)_2.12H_2O$ (8.66 mmol). The solution mixture was continuously stirred at 50 °C in an atmosphere of N_2. The solution mixture was sonicated for 10 mins while 10 mL of an aqueous solution containing 8 mol /L of NH_4OH was added dropwise to precipitate the iron oxides. The solution mixture pH reaches between 11 and 12. The reaction mixture was stirred at 50°C for another 60 min. The decantation process was used to separate the supernatant from the precipitate. The solid was finally washed with 150 mL of absolute alcohol three times. The contaminants such as sulphate and ammonium ions were eliminated using an excess of purified distilled water washings and the solid was then separated using a permanent magnet. The composite was then dried in an oven and termed magnetite graphene oxide (MGO) also shown in figure 2(c)

2.2.4. Synthesis of magnetite graphene oxide - clay nanocomposites

1 g of MGO was taken in a beaker with 1 L of purified water and the solution mixture was sonicated in a sonication bath for two hrs. Similarly, 1g of BN was taken in 1 L of purified water and sonicated simultaneously for 2 hrs. After sonication, the MGO and BN solution mixtures were mixed, and the resulting slurry was agitated at 950 rpm for 96 hours in a magnetic stirrer and, later solid was separated by a permanent magnet followed by drying in an oven at 80°C. The sample was named magnetite graphene-oxide clay nanocomposite (MGOBN). The image of MGOBN is shown in Figure 2 (d) and Figure 2(e) shows the images of MGOBN toward the external magnet. Likewise, another MGOBN@1:2 composite was obtained by

utilizing the MGO, and BN with a 1:2 weight ratio in a similar manner as detailed above.

2.2.5. Synthesis of magnetite graphene oxide clay - nanocomposites beads

1 g of Na-alginate biopolymer powder was mixed and stirred with 75 mL of distilled water till the homogenized polymer solution was formed. Further, 5 g of MGOBN was added to the homogenized sodium alginate slurry and stirred for 2 hours. The slurry was transferred to a separating funnel to which a small pipe with a hole size of 0.2 cm was attached at the bottom of the separating funnel. The separating funnel was clamped to a burette stand under which 2% $CaCl_2$ solution was kept in a beaker. The slurry was dropped into the calcium chloride solution. The beads of the nanocomposite materials were obtained in the $CaCl_2$ solution which was separated after 4 hours and then washed with distilled water and dried in a hot air oven at 70°C. The beads are labeled as MGOBN beads and shown in Figure 2(f). Likewise, MGOBN@1:2 beads were obtained by taking the same amount of MGOBN@1:2 solid in the preparation process.

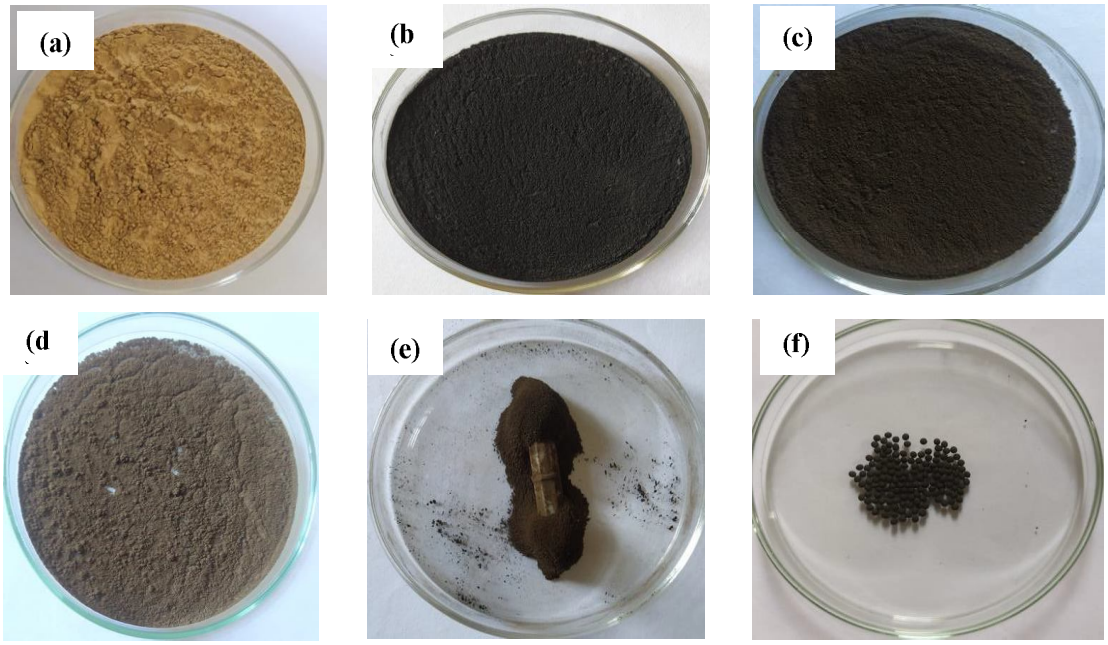

Figure 2.1: Pictures of **(a)** BN; **(b)** GO; **(c)** MGO; **(d)** MGOBN; **(e)** MGOBN attracted towards magnets; and **(f)** MGOBN beads.

2.3. Characterization of materials

The surface morphology of BN, GO, MGO, and MGOBN are obtained using the scanning electron microscope (SEM)(FESEM): JEOL, JSM 7100F; Oxford Xmax) (Operational condition: SEI Resolution: 15 kV, 46 Magnification: 10-1000000, Accelerating Voltage: 0.2-30 kV, Probe Current: 1 pA to 400 nA and Electron Gun used: In-Lens Schottky field emission gun). Furthermore, the elemental composition was determined using energy-dispersive X-ray (EDX, Oxford instruments X-MaxN) spectroscopy in conjunction with a scanning electron microscope. Similarly, to understand the surface morphology, shape and size of nanocomposites were obtained using a transmission electron microscope (TEM) (HRTEM:JEOL, JEM 2100; Oxford Xtreme). The solids powder was dispersed in isopropyl alcohol by sonication and drop cast on the TEM grid (Lacey carbon-coated copper grid-300 Mesh). The grid was dried in a vacuum desiccator and then coated with gold (2.0 nm). The sample was analyzed using the secondary electron detector at 30 kV acceleration voltage.

The materials *viz.*, BN, GO, MGO, and MGOBN were characterized by the Fourier transform infrared spectrometer (FT-IR-Shimadzu, Model: IR Affinity-1S, Japan). The sample holder was cleaned with chloroform and about 10 mg of the powder solid sample was placed in a sample holder. The solids were exposed to infrared light from the FT-IR instrument that ranges in wavelength from 10,000 to 100 cm^{-1}. The molecules in the sample transform the absorbed radiation into rotational and/or vibrational energy. The resultant signal, which appears as a spectrum at the detector in wavenumbers ranging from 4000 cm^{-1} to 400 cm^{-1}, represents the sample's molecular fingerprint. Because each molecule or chemical structure provides a distinct spectral fingerprint, FT-IR analysis is a useful technique for identifying specific molecules. To determine the phase structure, particle size, miller indices and lattice parameters of power materials, an X-ray diffraction (XRD) spectrometer (X'Pert PRO, MPD, PANanalytical, Netherlands) was used. The X-ray diffraction data were collected at a scan rate of 0.033 of 2θ illuminations and with the generator set to 30 mA and 40 kV. The magnetism properties such as saturation magnetization (M_o), remnant induction (M_R), and coercivity (H_c), of MGO and MGOBN solids is obtained

using a Vibrating Sample Magnetometer (VSM), Make: Lakeshore, Model:7400 series). The analysis is conducted based on the Faraday's law of Induction which explains that an electric field is created when a magnetic field change. The sample is vibrated by an electronic vibrator at a defined frequency and stabilized the amplitude. Voltage corresponding to the magnetic moment of the sample is induced in the pickup coils as a result of flux variations. It is possible to determine the magnetic moment of the sample by calibrating this voltage to the magnetic moment using calibration standards and detecting the magnetic field. The software measures the magnetic moment. Also, this software allows the calculation of the parameters of a hysteresis loop. The magnetic field system includes an electromagnet (Magnetic field is higher than 0.5 T at a gap of 25 mm in iron cores), dual polarity power supply, Gauss meter (Range: 20 k Gauss to 1 Gauss), and embedded magnetic flux detector. The control system includes a built-in software interface for collecting and analyzing the data, and a built-in data acquisition system.

A BET surface area analyzer (3 Flex version 4.03, Micromeritics, USA) based on liquid nitrogen desorption and adsorption isotherms was used to perform the BET analyses. The results provide the material's physical structure such as specific surface area, pore size, and pore volumes. The surface area of material is often correlated with various properties such as shelf life, dissolution rates, moisture retention, and catalytic activity. The NanoPlus AT, a Zeta/nanoparticle analyzer (Particulate system), was used to determine the Zeta potential of the nanocomposites which uses a diode laser as laser source, avalanche photodiode as a detector and provides the measurement range between -500 to +500 mV Zeta potential, laser wavelength of 660 nm, and uses a dual laser power of 30 mW and 70 mW with the measurement angle of 15° + 30°. The conductivity ranges vary up to 200 mS/cm.

2.3.1. pH_{PZC} determination of the powder material

The pH level at which there is no net surface charge on the solid surface is known as the point of zero charge pH (pH_{PZC}) (Lalchhingpuii et al., 2017a). The surface has a net positive charge when the pH is less than pH_{PZC} and a net negative charge when the pH is more than pH_{PZC}. Determining these solids' point of zero charge

is useful for understanding the adsorption process. The pH drift method was used to determine the solid's pH_{PZC} (Lalhmunsiama et al., 2013). In a series of 100 mL of 0.1 M NaCl was dissolved in CO_2-free purified water. The CO_2 was degassed by bubbling the nitrogen gas for 5 minutes and covered with parafilm paper to prevent further reabsorption of CO_2 gas. To a prepared series of 100 mL of 0.1 M NaCl solutions taken in different narrow-mouth bottles 0.1 M HCl or 0.1 M NaOH solutions were added to each bottle's solution to adjust the pH from 2 to 11. In each bottle, 0.1 g of the solid was added, and it was sealed tightly and stirred for 24 h at 25°C. The solutions' final pH was recorded and a graph was drawn between $pH_{Initial}$ and pH_{Final}, and the zero charge was obtained at the point where this curve and the linear $pH_{Initial} = pH_{Final}$ plot intersected.

2.4. Batch reactor experiments

The adsorption of pollutants is carried out for various parametric conditions *viz*., the effects of sorptive pH, initial sorptive concentrations, contact time, background electrolytes, and co-existing ion under the batch operations. The parametric studies provide insights of the sorption mechanism and demonstrates the mechanism involved at the solid/solution interface (Tiwari et al., 2007). By dissolving the appropriate amounts of analytes in purified water, the stock solutions of 50.0 mg/L of arsenic (III), arsenic (V), chromium (VI), lead (II), fluoride, diclofenac sodium, and Rhodamine B in 1.0 L of each sorptive were prepared. To improve the solubility of these pollutants in purified water, the solutions were subjected to sonication for 5 minutes. The sequential dilution procedure was used to achieve the necessary concentration for the batch reactor trials. 0.05 g of the solid sample was placed in 25 mL of 10 mg/L sorptive solutions to study the adsorption of arsenic (III), arsenic (V), chromium (VI), lead (II), fluoride, diclofenac sodium, and Rhodamine B. To adjust the pH of the sorptive solution, dropwise additions of the 0.1 mol/L HCl / 0.1 mol/L NaOH solutions were made. Rotary flask shaker (Scientech., India) was used to equilibrate the solution mixture for 24 hours at 25±1°C. A 0.45 µm syringe filter was used to filter the equilibrated solution. The bulk sorptive concentration of arsenic (III), arsenic (V), and

lead (II) were measured using an AAS, and chromium (VI), diclofenac sodium, and Rhodamine B by UV-Vis spectrophotometer at the wavelength of 350 nm, 277 nm, and 553 nm, respectively for these pollutants. For fluoride, a multiphotometer parameter was utilized. Equation 2.2 was used to calculate the removal efficiency.

$$\text{Removal efficiency (\%)} = \frac{C_0 - C_e}{C_0} \times 100 \quad \ldots(2.1)$$

where C_o and C_e are the initial and final sorptive concentrations, respectively

2.4.1. Effect of pH

In the adsorption process, the pH of a solution is a crucial variable as it significantly impacts on various parameters such as rate of ionization as well as the speciation of the various pollutants, the dissociation of functional groups of adsorbent, and the charge on the surface of the adsorbent. The aqueous chemistry of the solution as well as the adsorbents binding surface is affected by the pH of the solution (Ai et al., 2011). The sorptive solution pH for arsenic (III), arsenic (V), chromium (VI), fluoride, diclofenac sodium, and Rhodamine B were maintained in the range of pH 2.0 and 10.0 and between pH 2.0 and 6.0 for lead (II). The sorptive solutions with the sobent were equilibrated at constant temperature of 25±°C for 24 hours to achieve apparent equilibrium between the solid/solution interface. The sorption tests were carried out as already demonstrated previously in Chapter 2, section 2.4. The results were presented as removal efficiency (%) as a function of pH of sorptive solution

2.4.2. Effect of sorptive concentration

To overcome the mass transfer gradient resistance between the solution and solid phase in batch sorption process, the initial sorptive concentration in the solution is a significant factor (Dang et al., 2009a). Additionally, it facilitates the use of equilibrium state adsorption isotherms models to demonstrate the type of interaction involved at the solid/solution interface as well to optimize the removal capacities based on different assumptions (Dawodu and Akpomie, 2014). Therefore, a systematic sorption studies were conducted varying the sorbate initial concentrations.

For arsenic (III), arsenic (V), chromium (VI), lead (II), fluoride, diclofenac sodium, and Rhodamine B the effect of the initial sorptive concentration was investigated varying the sorbate concentrations from 1.0 mg/L to 30.0 mg/L at the sorptive pH of 3.0, 3.0, 3.6,4.0, 4.1, 3.7 and 4.0 respectively for the arsenic (III), arsenic (V), chromium (VI), lead (II), fluoride, diclofenac sodium, and Rhodamine B. The sorbtive solutions were equilibrated with the sorbent 24 hours at constant temperature of 25±1°C in the shaker. The detail sorption procedure is given in Chapter 2, section 2.4. The results were presented as a function of the initial sorptive concentration against the removal efficiency (%). Furthermore, simultaneous removal of arsenic (V) and fluoride was studied using the MGO solid at pH of 3.0 at a steady temperature of 25±1°C. The simultaneous studies were performed with the different molar ratios of arsenic (V) to fluoride (i.e., 1:1, 1:2, 2:1). Likewise, the simultaneous removal of arsenic (V) and lead (II) at pH 4.0, arsenic (V) and chromium (VI) at pH of 3.0 were performed using the MGO solid, and lead (II) and chromium (VI) using the MGOBN solid at pH of 3.7.

2.4.3. Adsorption isotherm modeling

Equilibrium adsorption isotherm models are developed based on many fundamental presumptions. The known isotherm models are Langmuir, Freundlich, Brunauer-Emmett-Teller, Redlich-Peterson, Dubinin-Radushkevich, Temkin, Toth, Koble-Corrigan, Sips, Khan, Hill, Flory-Huggins, and Radke-Prausnitz models. Due to their simplicity and, in certain circumstances, their ubiquity, some of the models are having prominence to demonstrate the sorption process. While the popularity of an isotherm model in connection to the process application is typically a consequence of its mathematical simplicity, and the accuracy of an isotherm model is typically a function of the number of independent parameters provided with the model (Malek and Farooq, 1996).

When the sorptive solution is in contact with the adsorbent for a sufficient amount of time, a state of adsorption equilibrium is reached. The interface concentration and bulk solution concentrations appearing to be in a dynamic equilibrium. The mathematical relationship, which is typically represented graphically

by the solid phase concentration against its residual concentration, plays a crucial role in modelling analysis, operational design, and practical application of the adsorption process. Information about the adsorption mechanism, surface features, and degree of adsorbent affinities are provided by its physicochemical parameters and the underlying thermodynamic hypotheses (Thiele, 1953).

Thus, the common adsorption isotherm models *viz.*, Langmuir, Freundlich and Sips isotherms are used using the equilibrium state sorption data. To estimate the various variables used in the equations, a non-linear least square fitting method was adopted. To do this, the residuals between the data calculated and data measured values are reduced using the Microsoft Excel add-ins "Solver" and the unknown parameters are optimized for minimizing the least square sum.

2.4.3.1. Langmuir adsorption Isotherm

The Langmuir isotherm model presumes monolayer adsorption, which means that the adsorbed layer is of a molecular thickness and adsorption occurs at a predetermined number of fixed localized sites that are identical and equivalent in nature, with no lateral interaction and steric hindrance between the adsorbed molecules, even on adjacent sites. The term "Langmuir isotherm" refers to homogenous adsorption, when each molecule has a constant enthalpy and sorption activation energy and each site has an identical affinity for the adsorbate (Swain et al., 2013).

The non-linear Langmuir adsorption model (Lalhmunsiama et al., 2016a) is used to estimate the sorption capacity (q_o) of solid at different equilibrium state sorbate concentrations (Equation 2.2):

$$q_e = \frac{q_m K_L C_e}{1+K_L C_e} \quad \ldots(2.2)$$

where q_e is the amount of solute adsorbed per unit weight of adsorbent (mg/g) at equilibrium; C_e is the equilibrium bulk sorptive concentration (mg/L); q_m the Langmuir monolayer adsorption capacity i.e., the amount of solute required to occupy all the available sites in a unit mass of solid sample (mg/g) and K_L is the Langmuir constant (L/g).

2.4.3.2. Freundlich adsorption Isotherm

The Freundlich isotherm is the earliest known isotherm describes the non-ideal and reversible adsorption, not restricted to the formation of monolayer. With the non-uniform distribution of adsorption heat and affinities throughout the heterogeneous surface, this empirical model is used for multilayer adsorption. On activated carbon and molecular sieves, Freundlich isotherm is now frequently used in heterogeneous systems, particularly for organic chemicals or highly interacting species (Foo & Hameed, 2010). In Equation 2.3, the Freundlich equation is given in its non-linear form (Lalhmunsiama et al., 2016a).

$$q_e = K_F C_e^{\frac{1}{n}} \quad \text{...(2.3)}$$

where q_e and C_e are the amount adsorbed (mg/g) and bulk sorptive concentrations (mg/L) at equilibrium, respectively, and K_F and $\frac{1}{n}$ are the Freundlich constants referring to adsorption capacity and adsorption intensity or surface heterogeneity, respectively.

2.4.3.3. Sips adsorption Isotherm

The Freundlich and Langmuir models were combined resulted with the Sips isotherm. The Sips model estimates the adsorption in heterogeneous systems and overcome the Freundlich isotherm's restriction on rising adsorbate concentration. Sips isotherm assumes that the surface is homogeneous but that the sorption is a collaborative process because of interactions between the sorbates. The Sips isotherm behaviour is identical to that of the Freundlich equation, with the distinction that, when the concentration is high enough, it has a finite saturation limit. The Sips isotherm equation is represented in Equation (2.4) in its non-linear form (Repo et al., 2010):

$$q_e = \frac{q_m (K_S C_e)^{n_S}}{1+(K_S C_e)^{n_S}} \quad \text{...(2.4)}$$

where , K_S (L /mg) is the Langmuir equilibrium constant, q_m(mg/g) is the maximum adsorption capacity of adsorbents, and n_s is the Freundlich heterogeneity factor, C_e the equilibrium bulk sorptive concentration (mg/L) and q_e the Langmuir monolayer adsorption capacity.

The Sips isotherm is further used for the simulation of competitive sorption of pollutants in its binary form as shown in Equation (2.5) and (2.6) (Repo et al., 2010).

$$q_1 = \frac{q_{m1}(K_{s1}C_{e1})^{n_{s1}}}{1+(K_{s1}C_{e1})^{n_{s1}} + (K_{s2}C_{e2})^{n_{s2}}} \quad \ldots(2.5)$$

$$q_2 = \frac{q_{m2}(K_{s2}C_{e2})^{n_{s2}}}{1+(K_{s1}C_{e1})^{n_{s1}} + (K_{s2}C_{e2})^{n_{s2}}} \quad \ldots(2.6)$$

where K_{s1} and K_{s2} (L /mg) are analogous to the Langmuir affinity constants, q_{m1}(mg/g) and q_{m2} (mg/g) is the maximum adsorption capacity of adsorbents, C_{e1} and C_{e2} the equilibrium bulk sorptive concentrations (mg/L), q_1 and q_1 are the expanded Sips adsorption capacities and n_{s1} and n_{s2} are the heterogeneity constants, 1 and 2 denotes for two different pollutants.

The modeling of the binary-component system was performed by taking a varied molar ratio of sorptive concentrations of two components (i.e., 1:1, 1:2, 2:1) for arsenic (V) and fluoride ions at pH 3.0 for arsenic (V) and pH 4.0 for lead (II), arsenic (V) and chromium (VI) at pH 3.0 and lead (II) and chromium (VI) at pH 3.7.

2.4.4. Effect of contact time

In wastewater treatment, the study of sorption kinetics is crucial because it provides important insights into the reaction pathways and makes it possible to determine the mechanism of sorption processes (Zou et al., 2006). It is observed that the nature of the adsorbent, its accessible active sites, and the accessibility of the pollutants to the active sites are all factors that affect the removal of pollutants to reach their apparent equilibrium state, which varies from one pollutant to another. To build effective wastewater treatment facilities, it is crucial to forecast the rate at which the pollutant is removed from aqueous solutions (Ho and McKay, 1999). The impact of contact time was investigated over a range of time intervals while maintaining initial sorptive concentrations of 10.0 mg/L. The outcome of the studies was shown as percent removal of pollutants against the contact time.

2.4.5. Adsorption kinetic modeling

A reasonable explanation for the mechanisms and kinetics involved in the uptake of pollutants by the employed materials, the kinetic modelings were conducted with the known kinetic models. The reaction orders of adsorption systems based on the capacity of the adsorbents as well as the reaction orders based on solution concentration were previously reported in numerous kinetic models (Ho, 2006).

The most popular kinetic models for describing the adsorption of a solute from an aqueous solution are the pseudo-first-order equation and pseudo-second-order equations. The pseudo-second-order kinetic model describes the chemisorptive type uptake, which are primarily caused by valency forces and ion exchange between the adsorbent and adsorbate (Momčilović et al., 2011).

2.4.5.1. Pseudo-first-order kinetic model

PFO kinetics is known as the Lagergren rate equation. In this model, the difference between the amount of adsorbate adsorbed on adsorbents at equilibrium is determined by the adsorption process (Mahdavinia and Mosallanezhad, 2016). When one of the reactants is present in extreme excess or is kept at a constant concentration in relation to the other component, the reaction is demonstrated with pseudo-first order kinetics. Equation (2.7), is the pseudo-first-order kinetic model (Azizian, 2004) in its non-linear form, which was applied to fit the time dependence sorption data . The pseudo–first–order kinetic model which is theoretically derived by the Lagergren could show the properties of the Langmuir rate at initial times of adsorption or close to equilibrium.

$$q_t = q_e(1 - e^{k_1 t}) \qquad \ldots(2.7)$$

where q_t and q_e are the amount of sorbate removed at time t and removal capacity at equilibrium, k_1 is the rate constant for pseudo-first order kinetics. Excel 'add-ins' Solver was used with user-defined functions to minimize the residuals between the model-calculated and model-measured values.

2.4.5.2.Pseudo-second-order kinetic model

Based on the presumption that chemisorption is the rate-limiting phase, the pseudo-second-order kinetic model predicts the adsorption mechanism. In this condition, the adsorption rate is dependent on adsorption capacity not on concentration of adsorbate (Sahoo and Prelot, 2020). Equation (2.8) represents the pseudo-second-order kinetic equation (Azizian, 2004). Similarly, theoretical studies indicate that the rate coefficient of pseudo-second-order model, i.e., k_2 is virtually a complex function of the initial concentration of the sorbing species

$$q_t = \frac{k_2 q_e^2 t}{1+ k_2 q_e t} \quad ...(2.8)$$

where q_t and q_e are the amount of sorbate removed at time 't' and removal capacity at equilibrium, k_2 is the rate constant for pseudo-second-order kinetics.

2.4.5.3. Fractal-like pseudo-second order kinetic

The fractal-like pseudo-second-order (FL–PSO) model approach basically imply to the fact that there are different paths of adsorption that take place in adsorption and the adsorption rate coefficient is a function of time (Haerifar and Azizian, 2012). The equation for fractal-like pseudo-second-order (FL–PSO) in its non-linear form is given in equation (2.9) (Haerifar and Azizian, 2012).

$$q_t = \frac{k q_e^2 t^{\alpha}}{1+ k q_e t^{\alpha}} \quad ...(2.9)$$

where q_t and q_e are the amount of sorbate removed at time 't'. The constants k and α are referred to as the rate constant and fractal constant, respectively.

2.4.6. Effect of background electrolyte

The background electrolyte demonstrates the sorption process. The nonspecific and specific adsorption are distinguished using the background electrolyte concentrations. Physisorption, also known as non-specific adsorption, that involves

relatively weaker forces and forming outer-sphere complexes, whereas chemically adsorbed inner-sphere complexes, more selective, and less reversible reactions are characteristics of specific adsorption (Bradl, 2004). Ionic strength as the background electrolyte concentrations showed a significant impact on outer sphere complexes, which simply include electrostatic interactions, but inner-sphere complexes, which involve considerably stronger covalent or ionic binding, showed insignificant impact (Scheidegger et al., 1996). Furthermore, the ionic strength also governs electrostatic interaction. Thus, by raising the ionic strength of the sorptive solution, whether electrostatic forces or the physisorption, is decreased significantly since the background ions created a surface charge layer at the solid surface and caused screening effect. A systematic sorption studies were conducted varying the background electrolyte concentrations (NaCl, KCl, and $NaNO_3$) from 0.001 to 0.5 mol/L in the sorptive solutions with the pollutants' concentration of 10.0 mg/L. The $NaNO_3$ was used for the arsenic (III), and arsenic (V) at pH of 3.0, KCl for fluoride at pH 4.0 pH and NaCl for lead (II), chromium (VI), diclofenac sodium and Rhodamine B at pH of 4.0, 3.6, 3.7 and 4.0, respectively. A solid dose of 2.0 g/L was introduced to the sorptive solutions to equilibrate it for 24 hrs. The sorption process was conducted as demonstrated previously Chapter 2, section 2.4. Further, the percentage removal of pollutants was presented as a function of background electrolyte concentrations.

2.4.7. Effect of co-existing ions

It is very important to investigate the effect of co-existing ions on the adsorption of adsorbate because a variety of ions may be present in polluted water and may compete with adsorbate for binding sites on the surface of the adsorbent. The sorption of arsenic (III), and arsenic (V), at pH 3.0, lead (II), and Rhodamine B at 4.0 pH, whereas chromium (VI), fluoride, and diclofenac sodium at pH 3.6, 4.1, 3.7 respectively were performed separately in the presence of various cations and anions, and the sorptive solutions were given a solid dosage of 2 g/L to equilibrate for 24 hours. 50.0 mg/L was used as the coexisting ion concentration. The anions used were ethylenediaminetetraacetic acid (EDTA), oxalic acid, glycine, and phosphate, while the cations were manganese (II), magnesium (II), calcium (II), and nickel (II)

2.4.8. Column reactor studies

Column experiments were carried out using a glass column (1 cm inner diameter) filled with 0.5 g of MGO beads for arsenic (III) and 1g of MGO beads for arsenic (V) and 2 g MGOBN@1:2 beads for fluoride taken in the middle of the column. The remaining column was filled with small sized glass beads , sand (0.5 g), and pebbles (1 g) below and above of the MGOBN@1:2 beads. Arsenic (III), arsenic (V), and fluoride's initial sorptive concentrations were kept at 10.0 mg/L, with arsenic (III), arsenic (V), and fluoride's pH of 3.0, 3.0, and 4.1, respectively. A peristaltic pump was used to pump sorptive solution from the bottom of column at a constant flow rate of 1.0 mL/min. Fraction Collector, collected the effluent solutions of column. The collected effluents were filtered using a 0.45 m syringe filter, and their concentrations were measured using an AAS for arsenic (III) and arsenic (V), and a multiphotometer for fluoride.

The breakthrough curve was obtained by drawing curve between the column data (C_e/C_o) and the throughput volume (L). Further, Using the Thomas equation (Equation 2.10) (Thomas, 1944), the breakthrough data were further used to estimate the loading capacity of column loaded with the MGO beads and MGOBN beads for the pollutants under dynamic conditions:

$$\frac{C_e}{C_o} = \frac{1}{1+e[K_T\,(q_o m - C_o V)]/Q} \qquad \ldots(2.10)$$

where C_e and C_o are the concentrations of effluents and influent solutions of arsenic (III), arsenic (V), or fluoride; K_T refers to the Thomas rate constant (L/min/mg); q_o is the maximum amount of pollutants loaded (mg/g) in the column under the specified column conditions; m is the amount of adsorbent taken in column (g); V is the throughput volume (L); and Q is the flow rate of pumped pollutants' solution (L/min). The column data were then fitted to a non-linear Thomas equation using the least square fitting method to estimate two unknown variables, i.e., K_T and q_o. Microsoft Excel 'add-ins' Solver was used with user-defined functions to minimize the residuals between the model-calculated and model-measured values.

2.4.9. Application in the natural water matrix

The sorption experiment was carried out using the natural water samples collected from different water sources *viz.*, river, stream and spring in various regions of the Aizawl area to assess the practical implacability of the synthesized material in the removal of arsenic (III), arsenic (V), fluoride, lead (II), chromium (VI), diclofenac sodium, and RB spiked in natural water sample. This would make it possible to model the sorption process onto a realistic water matrix. Using a multiphotometer instrument, several water quality parameters, including pH, conductivity, resistivity, salinity, total dissolved solids, phosphate, sulphate, nitrate, and fluoride, were measured for these water samples. Using an atomic absorption spectrometer, the metal concentrations of Fe, Zn, Mn, Ca, Pb, and Cu were determined. The inorganic carbon and NPOC values of the real water samples were obtained using a TOC analyzer. As a stock solution, real water was spiked with arsenic (III), arsenic (V), fluoride, lead (II), chromium (VI), diclofenac sodium, and Rhodamine B to make it 100 mg/L. This stock solution was then further utilized for experiments under dilution. The pH of the pollutant solutions was adjusted by the dropwise addition of 0.1 mol/L HCl or 0.1 mol/L NaOH. The pH was adjusted to 3.04, 3.04, 3.61,4.01, 4.14, 3.71, and 4.01 for arsenic (III), arsenic (V), chromium (VI), lead (II), fluoride, diclofenac sodium, and Rhodamine B, respectively. Further, 2 g/L solid was introduced and the sorption experiments were performed as demonstrated previously Chapter 2, Section 2.4. The equilibrated solutions were filtered with the syringe filter and subjected for the pollutants' concentration measurements. The bulk sorptive concentration of arsenic (III), arsenic (V), and lead (II), was measured using an AAS, and chromium (VI), diclofenac sodium, and Rhodamine B concentration were measured using UV-Vis spectrophotometer. Similarly, the fluoride concentration was measured using a multiphotometer parameter.

2.4.10. Application of MGO over Chromated Copper Arsenate (CCA)

Chromated copper arsenate coating on bamboo chips was a technique employed for the preservation of bamboo which were used for the construction of

bungalows during olden days. The same archeological bamboo chips were obtained from the Lakher Pioneer Mission,1905, LORRAIN Bungalow, Serkawr, Siaha District, Mizoram (India). 1 g bamboo chip was wet digested in 10 mL of concentrated HNO_3 and solution mixture was heated at 80°C for 30 min. It was cooled at room temperature. Further, 3 mL of 70% $HClO_4$ was added, and then it was heated once again for evaporation to reduce the total volume of *Ca* 5 mL. The transparent solution was cooled at room temperature and diluted to a total volume of 50 mL. Further, the applicability of MGO was studied for the simultaneous removal of chromium, copper and arsenic using the solid doses of 1 mg, 2 mg and 5 mg in 10 mL of diluted bamboo chip solution. The removal process was followed as demonstrated previously Chapter 2, section 2.4. The arsenic, copper and chromium were estimated using the AAS and UV-Vis spectrophotometer, respectively.

2.4.11. Regeneration and reusability

MGO, MGOBN and MGOBN@1:2 were regenerated and reused for the sorption/desorption experiments. MGO for arsenic (III) and arsenic (V) and MGOBN for lead (II), chromium (VI), diclofenac sodium and the Rhodamine B, whereas MGOBN@1:2 for fluoride was conducted for the sorption/desorption experiments. The experiments were accomplished by the use of suitable desorbing reagent with optimized molar concentrations. HCl solution was employed as an eluent for lead (II), diclofenac sodium, and Rhodamine B and H_2SO_4 for chromium (VI) whereas acetate solution used for the desorption of fluoride and phosphate solution for arsenic (V) and arsenic (III). The sorption experiment was carried out for 25 mL of arsenic (III) and arsenic (V) at the concentration of *Ca.*10 mg/L at pH *Ca.*3.0 using 50 mg of MGO in three beakers and kept in a shaker for 24 hours. The bulk solutions were analyzed using AAS for the sorbate concentrations. The solid which is loaded with the sorbate ions was dried at 60°C for 2 hrs and introduced for the desorption experiments. The dried solid was taken in 25 mL of phosphate solutions (0.05, 0.01, and 0.1 M) and shaken for 2 hours, the supernatant solution was analyzed for total arsenic using the AAS. The material was washed with water and again dried at 60°C. The same was used for the next cycle of adsorption and desorption process and repeated for four consecutive

cycles. The same procedure was followed for the sorption/desorption experiments for the lead (II), diclofenac sodium, and Rhodamine B using HCl as a desorbing solution (0.1, 0.01, 0.05 M), H_2SO_4 for chromium (VI) whereas acetate solution for fluoride where MGOBN was an adsorbent. The pre-adsorbed and desorption was analyzed using an AAS, UV-Vis spectrophotometer, whereas, for fluoride, a multiphotometer parameter was used. The MGOBN@1:2 was used as an adsorbent and acetate solution was employed as eluent (0.1 M, 0.01 M, 0.05 M). The percentage desorption was calculated using Equation (2.11).

$$\% \text{ Desorption} = \frac{Concentration\ of\ pollutant\ desorbed}{Concentration\ of\ pollutant\ adsorbed} \times 100 \qquad \ldots(2.11)$$

The figures and tables represented the three repeated experimental results to obtain the mean value ±SE. 'Solver' from the Microsoft Excel add-ins was used to simulate the non-linear sorption isotherms and kinetics to reduce the difference between observed and calculated data.

CHAPTER 3

RESULTS AND DISCUSSION

3. RESULTS AND DISCUSSION

3.1. PHYSICO- CHEMICAL PARAMETRIC ANALYSIS OF FIVE NATURAL WATER SAMPLES

The five natural water samples are collected from various water sources *viz.*, river, stream, spring, and waterfall from different parts of Aizawl, Mizoram (India). These water samples are tested for several physico-chemical parametric analyses and results are given in Table 3.1. The pH of the samples is almost neutral and ranged from 7.0 to 8.2. The natural water sample contains a substantial amount of inorganic carbon i.e., 16.554 mg/L, 17.652 mg/L, 14.506 mg/L, 16.396 mg/L, and 16.004 mg/L, respectively for the Tlawng river, Chiahpui river, *Tuikhur* spring, Pukpui waterfall and Lengpui stream with a lesser content of non-purgeable organic carbon (NPOC) i.e., 1.749 mg/L, 1.443 mg/L, 1.679 mg/L, 1.434 mg/L, and 1.043 mg/L, respectively for the Tlawng river, Chiahpui river, *Tuikhur* spring, Pukpui waterfall, and Lengpui stream. Copper, aluminium, lead, and nickel are present in trace amounts in these water samples. However, relatively the water sample contained with high content of calcium and magnesium. The concentrations of calcium and magnesium were found to be in the range of 37.0 to 117.0 mg/L and 3.0 to 11.0 mg/L, respectively for different natural water samples. The presence of high inorganic carbon with Ca and Mg indicated that the water is contained with carbonates and bicarbonates of calcium and magnesium. Phosphate is present at its low values i.e., 0.56, 0.2, 0.17, 0.3, and 0.4 mg/L for Tlawng river, Chiahpui river, *Tuikhur* spring, Pukpui waterfall, and Lengpui stream, respectively and sulphate is also within the permissible level i.e., 9.0, 4.0, 2.0, 4.0, and 4.5 mg/L respectively for the Tlawng river, Chiahpui river, *Tuikhur* spring, Pukpui waterfall, and Lengpui stream water samples.

Table 3.1: Physico-chemical quality parameters of five natural water samples.

Natural water	TOC (mg/L	Cations (mg/L)	Anions	Physical properties
Tlawng, Sairang, (Aizawl)	NPOC:1.749 TC: 17.861 IC: 16.554	Cu: 0.053 Ca: 66.0 Pb: 0.775 Ni: 0.028 Fe: ND Mn:ND Al: 0.04 Mg: 10.0	Sulphate: 9 mg/L Phosphate: 0.56 mg/L Nitrate: 2.0 µg/L	pH: 8.1 Salinity: 0.12 PSU Oxd. & red. Potential: 160.7 MV Resistivity: 0.0043 $M\Omega cm^{-1}$ Conductivity: 219 μScm^{-1} TDS: 105 ppm
Chiahpui, (Aizawl)	NPOC: 1.443 TC: 18.211 IC: 17.652	Cu: 0.06 Ca: 117 Pb: 0.012 Ni: 0.096 Al: 0.03 Mg: 11.0	Sulphate: 4 mg/L Phosphate: 0.2 mg/L Nitrate: 2.30µg/L	pH: 7.9 Salinity: 0.14 PSU Oxd. & red. Potential: 160.7 MV Resistivity: 0.0045 $M\Omega cm^{-1}$ Conductivity: 199 μScm^{-1} TDS: 107 ppm
Tuikhur (Durtlang N, Aizawl)	NPOC: 1.679 TC: 16.862 IC: 14.506	Cu: 0.036 Ca: 30 Pb: 0.0752 Ni: 0.192 Al: 0.01 Mg: 3.0	Sulphate: 2 mg/L Phosphate: 0.17 mg/L Nitrate: 3.0 µg/L	pH: 7.9 Salinity: 0.12 PSU Oxd. & red. Potential: 204.8 MV Resistivity: 0.0044 $M\Omega cm^{-1}$ Conductivity: 257 μScm^{-1} TDS: 113 ppm

Pukpui waterfall, (Aizawl)	NPOC:1.434 TC: 15.328 IC: 16.396	Cu: 0.07 Ca: 37.0 Pb: 0.01 Ni: 0.06 Al: 0.01 Mg: 4.0	Sulphate: 4 mg/L Phosphate: 0.3 mg/L Nitrate: ND	pH: 7.8 Salinity: 0.11 PSU Oxd. & red. Potential: 201.2 MV Resistivity: 0.003 $M\Omega cm^{-1}$ Conductivity: 225 μScm^{-1} TDS: 115 ppm
Lengpui stream, (Aizawl	NPOC:1.043 TC: 16.731 IC: 16.004	Cu: 0.05 Ca: 35.0 Pb: 0.01 Ni: 0.05 Al: 0.01 Mg: 4.5	Sulphate: 4.5 mg/L Phosphate: 0.4 mg/L Nitrate: 4.0 µg/L	pH: 7.0 Salinity: 0.21 PSU Oxd. & red. Potential: 203.1 MV Resistivity: 0.002 $M\Omega cm^{-1}$ Conductivity: 214 μScm^{-1} TDS: 113 ppm

3.2. CHARACTERIZATION OF MATERIALS

3.2.1. SEM- surface morphology of materials

The surface morphology of bentonite (BN), graphene oxide (GO), magnetite graphene oxide (MGO), and magnetite graphene oxide-clay nanocomposite (MGOBN) materials are discussed using the SEM micrographs of these solids (*Cf* Figure 3.1(a-d)). Bentonite (BN) exhibits a layered structure i.e., the phyllosilicates are arranged in layers. The surface is heterogenous and possesses large distribution of meso- to macropores on the surface. GO, on the other hand, show a compressed wrinkled edge with a layered structure. The material is porous and heterogenous. The MGO and MGOBN, display a more compact and heterogeneous surface structure. The SEM micrographs of MGO and MGOBN display the spatial distribution of magnetite

nanoparticles randomly on the surface of the graphene oxide or bentonite clay. Furthermore, the layers of MGOBN, the wrinkled graphene oxide, and magnetite nanoparticles are dispersed smoothly and showed meso- to macro-pores on their surface. Similarly, the SEM image of magnetite graphene oxide (GO-Fe_3O_4) showed the random distribution of Fe_3O_4 nanoparticles on the surface of graphene oxide (GO) (Neolaka et al., 2020).

Furthermore, the SEM/EDX spectrum of BN, GO, MGO, and MGOBN are shown in Figure. 3.1(e-h) along with the quantitative data (weight and atomic percentages) included in Table 3.2. The EDX spectrum of graphene oxide (GO) contains C and O elements. Similarly, the MGO showed an additional EDX peak of iron indicating the presence of magnetite in MGO. Further, peaks of the Si, Al, Na, Ti, and K are clearly seen in the BN due to the presence of phyllosilicates with some of the exchangeable ions. Similarly, the MGOBN is contained with these elements and along with iron, confirmed the presence of magnetite in the nanocomposite material.

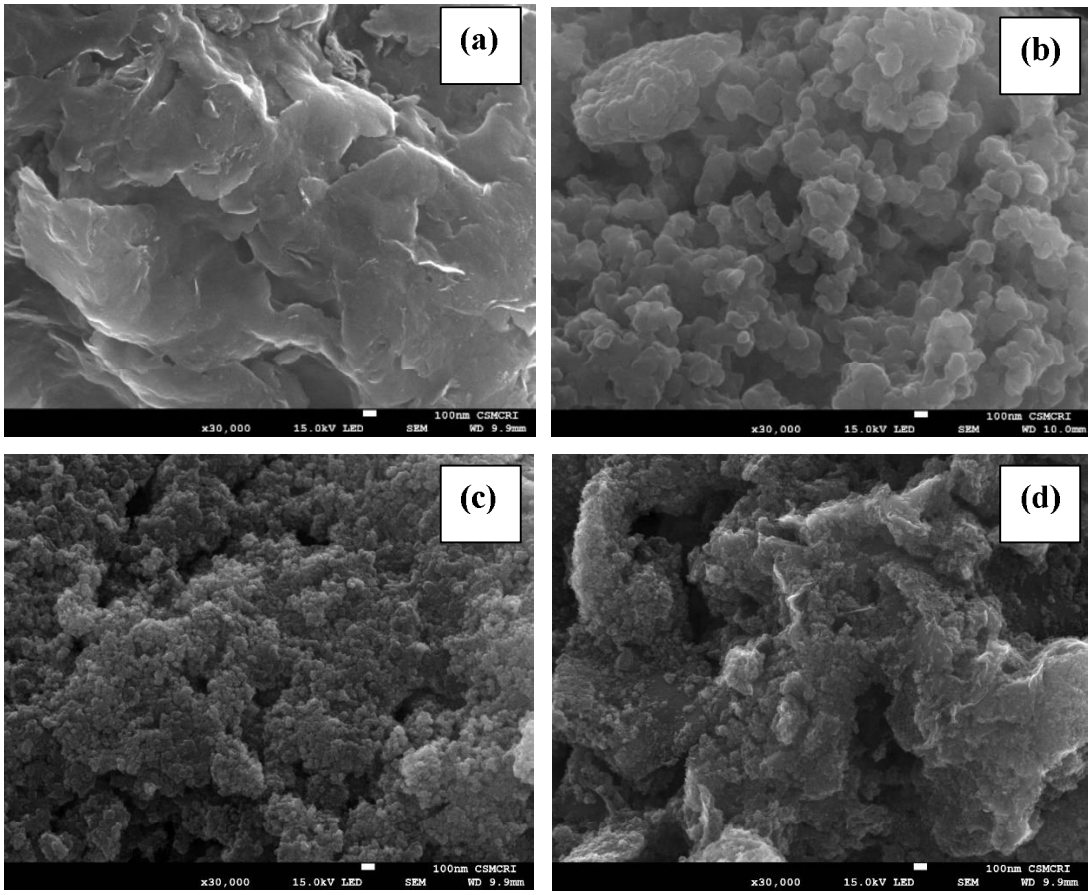

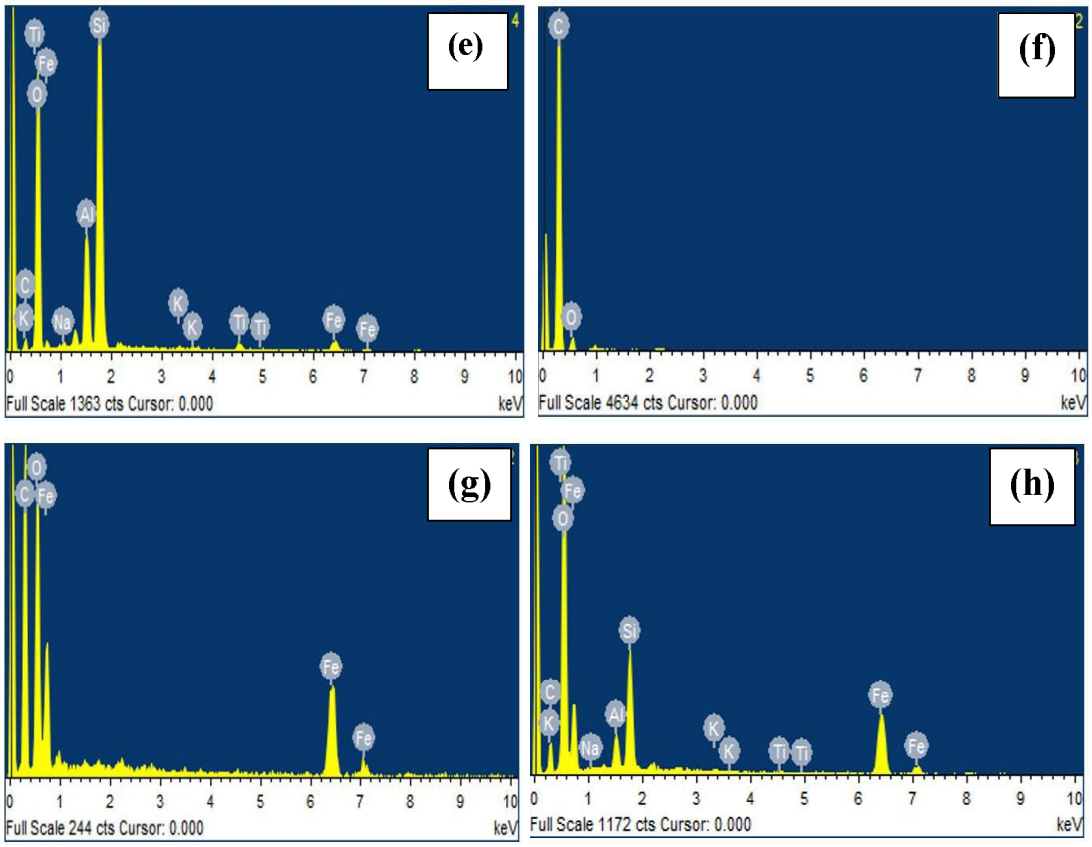

Figure 3.1: SEM micrographs of **(a)** BN; **(b)** GO; **(c)** MGO; and **(d)** MGOBN; and EDX spectra of **(e)** BN; **(f)** GO; **(g)** MGO; and **(h)** MGOBN.

Table 3.2: Weight and atomic percentage of the elements present in the BN, GO, MGO, and MGOBN solid samples using the SEM/EDX analysis.

Elements	Weight %				Atomic %			
	BN	GO	MGO	MGOBN	BN	GO	MGO	MGOBN
C K	6.73	86.91	40.47	13.18	10.85	89.84	56.68	22.48
O K	51.71	13.09	33.85	45.61	62.54	10.16	35.59	58.40
Fe K	5.32	-	25.68	30.19	1.84	-	7.73	11.08
Na K	0.44	-	-	0.09	0.32	-	-	0.08
Al K	7.51	-	-	2.33	5.38	-	-	1.77
Si K	26.50	-	-	8.33	18.26	-	-	6.07
K K	0.34	-	-	0.13	0.17	-	-	0.07
Ti K	1.45	-	-	0.15	0.59	-	-	0.06

3.2.2. TEM- Surface Morphology of the material

TEM micrographs of GO, MGO, and MGOBN are shown in Figure 3.2 (a-c). It reveals that the GO surface possesses to have a uniform surface, which has thick stacks with a thin wrinkled sheet, borders that appear to be torn off, and some voids visible within the sheet. The magnetite nanoparticles are uniformly deposited on the surface of the GO and GO-BN in the TEM images of MGO, and MGOBN. A spatial but uniform distribution of almost spherical nanoparticles of magnetite is observed on the surfaces of GO-BN and MGOBN. Moreover, heterogeneity was seen in the MGOBN solid due to the presence of phyllosilicates in the sample. Further, Figures 3.2 (d) and (e) respectively depict the mean particle size distribution of the magnetite nanoparticles in the MGO and MGOBN solids calculated using ImageJ software. The average particle size was determined using the ImageJ software and was found to be 11.88 nm and 12.44 nm, respectively for MGO and MGOBN solids. Moreover, it was determined that the magnetite nanoparticle is having a d-spacing of 0.296 nm obtained using ImageJ software, principally because of diffraction from the (220) plane of magnetite (*Cf.* Figure 3.3(c)). In an earlier report the reduced graphene oxide – gold nanoparticles showed a similar thick stack structure with multiple wrinkled graphene oxide (El-Maghrabi et al., 2021). The spherical-shaped Fe_3O_4 nanoparticles were uniformly distributed on the surface of reduced graphene oxide as observed in the TEM image of rGO/Fe_3O_4. Furthermore, the mean particle size of Fe_3O_4 was found to be 8.86 nm in rGO/Fe_3O_4 (Kahsay et al., 2020).

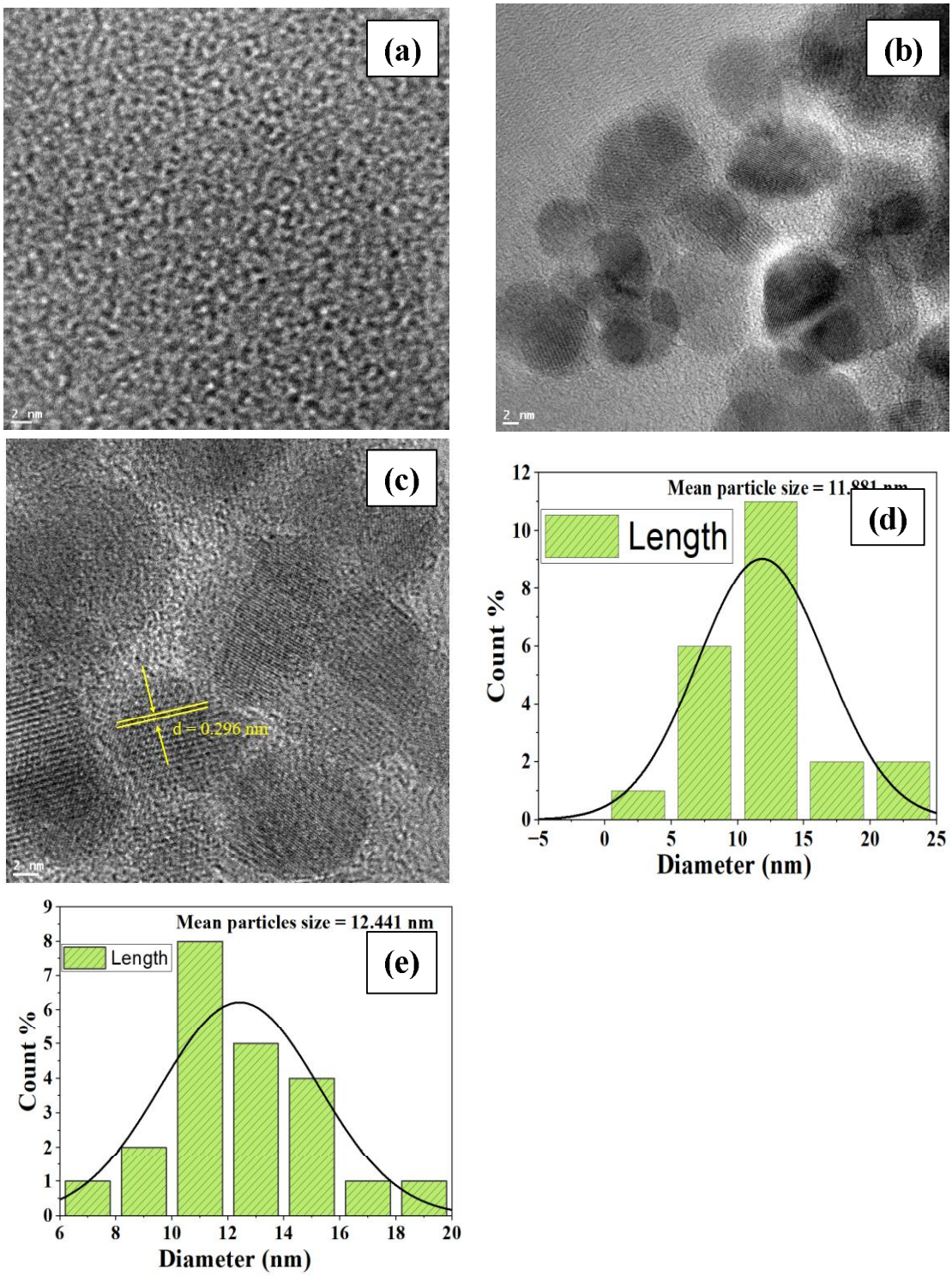

Figure 3.2: TEM micrographs of **(a)** GO; **(b)** MGO; and **(c)** MGOBN; and mean particle sizes of **(d)** MGO; and **(e)** MGOBN.

3.2.3. X-ray Diffraction (XRD) analysis

The XRD diffraction pattern of bentonite (BN), graphene oxide (GO), magnetite graphene oxide (MGO), and magnetite graphene oxide clay nanocomposite (MGOBN) are shown in Figure.3.3. The bentonite is predominantly contained with quartz and montmorillonite mineral phases. The distinctive diffraction peaks at the 2θ values of 20.65°, 26.43°, 36.47°, 49.99°, 59.8°, and 68.08°, which correspond to the quartz phase and 19.85°, 36.62°, and 50.0° for the montmorillonite mineral phases. Graphene oxide on the other hand exhibits broad characteristic diffraction peaks at the 2θ values of 26.04° and 43.09° (Kumar & Jiang, 2016). Additionally, the MGO reveals the diffraction peaks at the 2θ values of 30.18°, 35.56°, 43.18°, 53.55°, 57.19°, and 62.86° due to the face-centered cubic (fcc) magnetite nanoparticles with diffraction planes of (220), (311), (400), (422), (511) and (440), respectively (JCPDS No. 019-029). Moreover, it was also found that the $d_{(hkl)}$ spacings for the magnetite nanoparticles of the (220), (311), (400), (422), (511), and (440) planes were 2.96, 2.53, 2.09, 1.71, 1.61, and 1.48 Å, respectively. Similarly, the Fe_3O_4 nanoparticles in magnetite graphene oxide anchored sulfonic acid (Fe_3O_4@GO-SO_3H) showed the diffraction peaks at the 2θ values of 30.21°, 35.71°, 43.31°, 53.70°, 57.35°, and 62.77° (Dhamodharan et al., 2019).

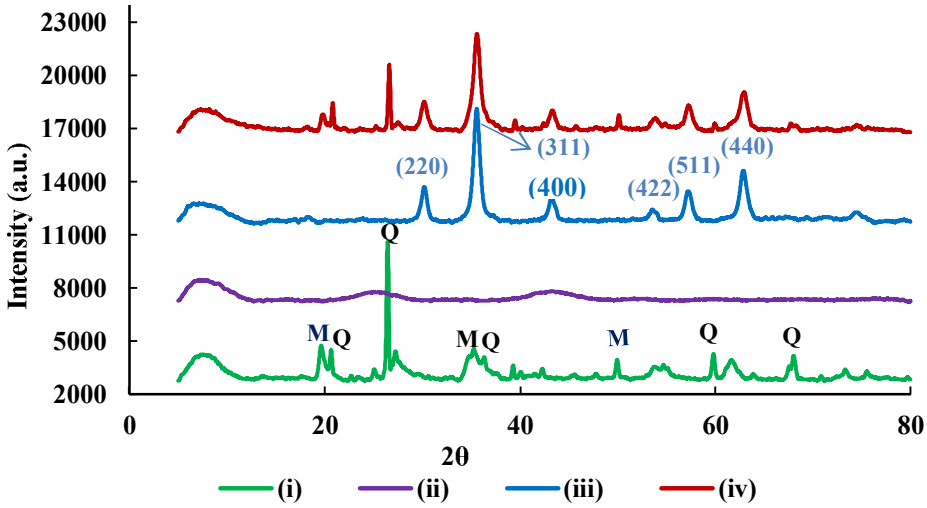

Figure 3.3: X-ray diffraction pattern of **(i)** BN; **(ii)** GO; **(iii)** MGO; and **(iv)** MGOBN solids.

3.2.4. Fourier-transform infrared spectroscopic (FT-IR)

The FT-IR spectra of BN, GO, MGO, and MGOBN are shown in Figure.3.4. The solid material BN displays Si-O and Si-O-Si-O-Al stretching vibrations at wavenumbers of 513 cm^{-1}, 918.11 cm^{-1}, and 987.55 cm^{-1}, respectively (Xu et al., 2020). A vibrational peak at 3618 cm^{-1} is due to the Al-O-H stretching vibrations. Oxygen-containing functional group of GO shows the vibrational band at 1712 cm^{-1}, which is due to the stretching vibration of C=O of graphene oxide, and C-OH stretching vibration has appeared at 3402 cm^{-1}. The C-O-C epoxide, the C-O stretching vibrations, as well as the stretching vibration of the C=C in the aromatic ring, were observed at 883 cm^{-1} (Boruah, 2012), 1172 cm^{-1}, and 1589 cm^{-1}, respectively (Marcano et al., 2010). The presence of magnetite nanoparticles was confirmed by the appearance of two distinct vibrational peaks at 551 and 631 cm^{-1} (Fe-O) (Belachew & Bekele, 2020). The aromatic C=C stretch vibration was observed at 1578 cm^{-1} for both GO and MGO solids (Su et al., 2017). Fe-O bond in MGOBN nanomaterial undergoes a red shift from 551 cm^{-1} to 532 cm^{-1} due to the creation of a Fe-O-Si or Fe-O-Al bond. A

similar redshift from 578 cm^{-1} to 540 cm^{-1} was observed by activated clay-magnetite (AC-Fe_3O_4) (Belachew & Bekele, 2020). A peak at 1651 cm^{-1} occurred due to the formation of -COO^- after the incorporation of magnetite into the GO (Alizadeh et al., 2017). Al-O-H and H-O-H stretching vibrational peaks of solid bentonite were observed at 3626 cm^{-1} and 3425 cm^{-1}, respectively. C-O stretching was also recorded at 1026 cm^{-1} in these solids.

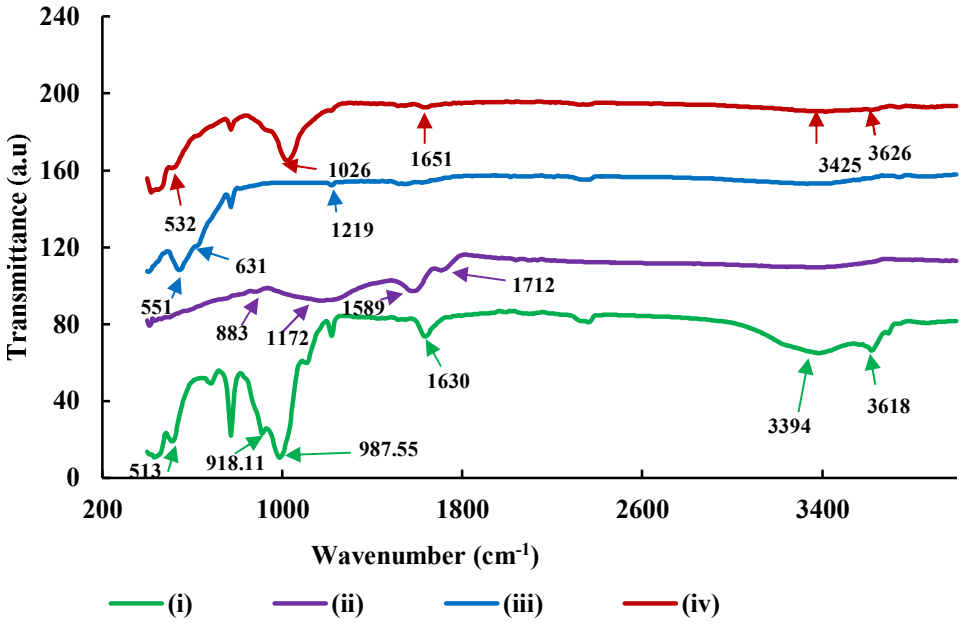

Figure.3.4: FT-IR spectra of **(i)** BN; **(ii)** GO; **(iii)** MGO; and **(iv)** MGOBN.

3.2.5. Vibrating sample magnetometer analysis

MGO and MGOBN were subjected to magnetic analyses using a magnetometer. Figure 3.5(a&b) depicts the magnetic field dependency of the magnetization observed at 298 K. Both MGO and MGOBN exhibit typical paramagnetic behavior. MGO and MGOBN had saturation magnetization intensities of 35 and 17 emu/g, respectively, and were sufficient for magnetic separation using a standard magnet. The MGOBN saturation magnetization is relatively less than the MGO which is explained due to the lesser content of magnetite nanoparticles in the composite material. Furthermore, the magnified hysteresis loops were depicted in the

inset graph in Figure 3.5 (a&b). The MGO and MGOBN nanocomposites had a 1.262 emu/g and 0.405 emu/g remanent magnetization (Mr), respectively whereas the coercivity (Hc) was found to be -23.47 Oe and -14.16 Oe, respectively for MGO and MGOBN at 298 K. Similar results were obtained with the reduced in saturation magnetization for the Fe_3O_4@ graphene oxide nanoparticles (Fe_3O_4@GO) and having the magnetization intensity of 11.5 emu/g, a significantly lower value compared to the Fe_3O_4 having an intensity of 86.59 emu/g. The reduction in the saturation magnetization was attributed due to the lesser content of Fe_3O_4 in Fe_3O_4@GO solid with the remanent magnetization and coercivity of 2.0 emu/g and 160 Oe, respectively for Fe_3O_4@GO solids (Fu & Zhu, 2016).

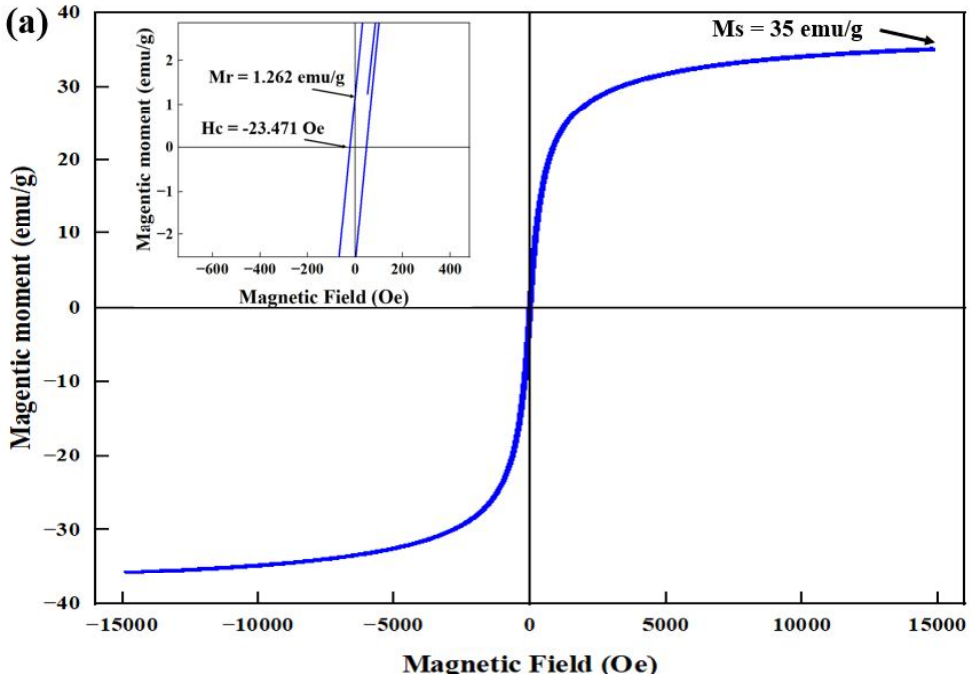

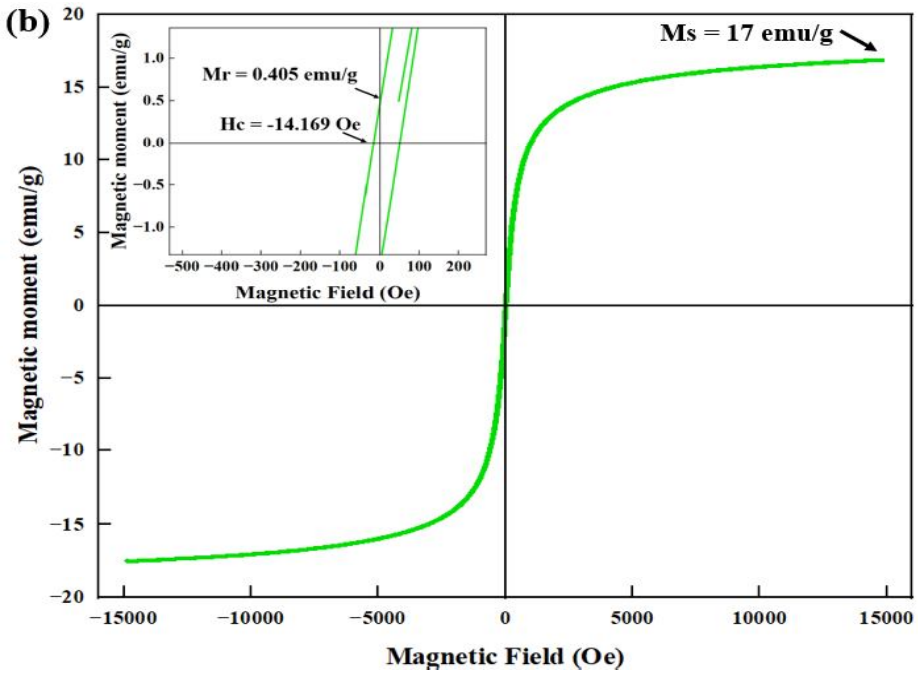

Figure 3.5: Magnetic hysteresis curves for **(a)** MGO; and **(b)** MGOBN; [Inset: Magnified magnetic hysteresis showing the remanent magnetization (Mr) and coercivity (Hc) for **(a)** MGO; and **(b)** MGOBN] using vibrating sample magnetometer.

3.2.6. Brunauer, Emmett, and Teller (BET) surface area analyses

The Brunauer, Emmett, and Teller (BET) method was employed for obtaining the specific surface area, pore size, pore volume, and pore-size distribution of BN, GO, MGO, and MGOBN, and the results are shown in Table 3.3. It is observed that the BET-specific surface areas of BN, GO, MGO, and MGOBN were 164.010, 428.551, 238.645, and 195.842 m^2 /g, respectively. The specific surface area for GO was comparatively high with a small pore diameter and low pore volume. However, the surface area decreases in the case of MGO, and MGOBN, which is due to the distribution of magnetite nanoparticles over the pores of GO. It was previously reported that iron-oxide graphene oxide composite showed a significant decrease in specific surface area and an increase in pore diameter and pore volume as compared to bare graphene oxide (Su et al., 2017b). Moreover, the nitrogen adsorption-desorption isotherms for BN, GO, MGO, and MGOBN are presented in Figure 3.6 (a). The solid materials *viz* BN, GO, MGO, and MGOBN exhibit Type IV type isotherms demonstrating that the materials are having a mesoporous structure with a random pattern of pore size, and adsorption

hysteresis of H3 type loop was observed for the BN, GO, and MGOBN solids, which is indicative of plate-like particles forming slit-shaped pores. Similarly, the MGO which showed the H1 type loop referred to the porous materials having narrow pore size distributions. Furthermore, Figure 3.6(b) shows the BN, GO, MGO, and MGOBN pore width distributions versus the different pore volumes. The desorption peak of BN, GO, MGO, and MGOBN occurred at the pore widths of 40.1 Å, 39.4 Å, 37.3 Å, and 40.3 Å, respectively. All the solid materials fall in the pore width range between 2-50 nm thereby exhibiting mesoporous structure. Similarly, the magnetite graphene oxide and chitosan microspheres (MGOCS) possessed a mesoporous structure and type IV type isotherm (Shan et al., 2022).

Table 3.3: BET surface area, BJH adsorption pore volume, adsorption average pore diameter, and BJH desorption pore width for the BN, GO, MGO, and MGOBN solids.

Parameters	**BN**	**GO**	**MGO**	**MGOBN**
BET-specific surface area (m^2/g)	164.01	428.55	238.645	195.84
Pore volume BJH adsorption (cm^3/g)	0.15	0.17	0.35	0.27
Adsorption average pore diameter (Å)	36.85	29.18	59.05	56.14
BJH desorption pore width (Å)	40.11	39.48	37.32	40.31

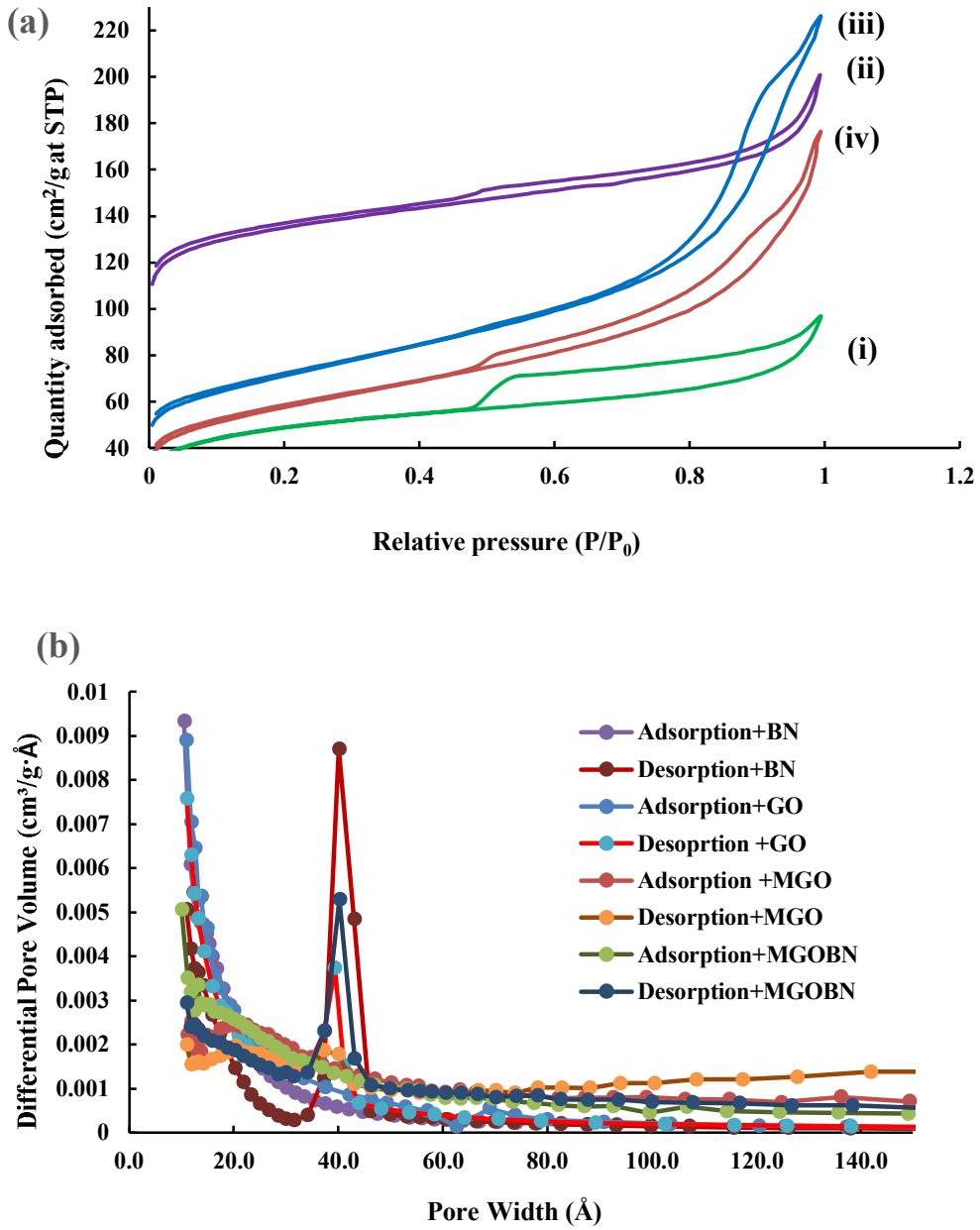

Figure 3.6: (a) N_2 adsorption-desorption isotherms obtained for **(i)** BN, **(ii)** GO, **(iii)** MGO; and **(iv)** MGOBN; and **(b)** pore size distribution of BN, GO, MGO, and MGOBN solids.

3.2.7. Zeta Potential Analysis

Figure 3.7 depicts the zeta potential curves of these solids i.e., BN, GO, MGO, and MGOBN, and these solid materials exhibit a negative zeta potential of -43.54, -28.98, -23.01, and -30.19 mV, respectively. BN possesses a negative zeta potential

value which is due to the presence of aluminate and silicate groups in clay, whereas in the case of GO is due to the ionization surface functional groups viz., hydroxyl and carboxyl groups, leaving the negative charges at the surface. MGO negative zeta potential is ascribed due to the ionization of carboxylic and hydroxyl groups. Zeta potentials greater than -30 mV are regarded to form stable suspensions for particles (Cao et al., 2016). Furthermore, graphene oxide in graphene oxide-wrapped magnetite nanoclusters showed a negative zeta potential due to the presence of hydroxyl and carboxyl group ionization (Ganesan et al., 2018).

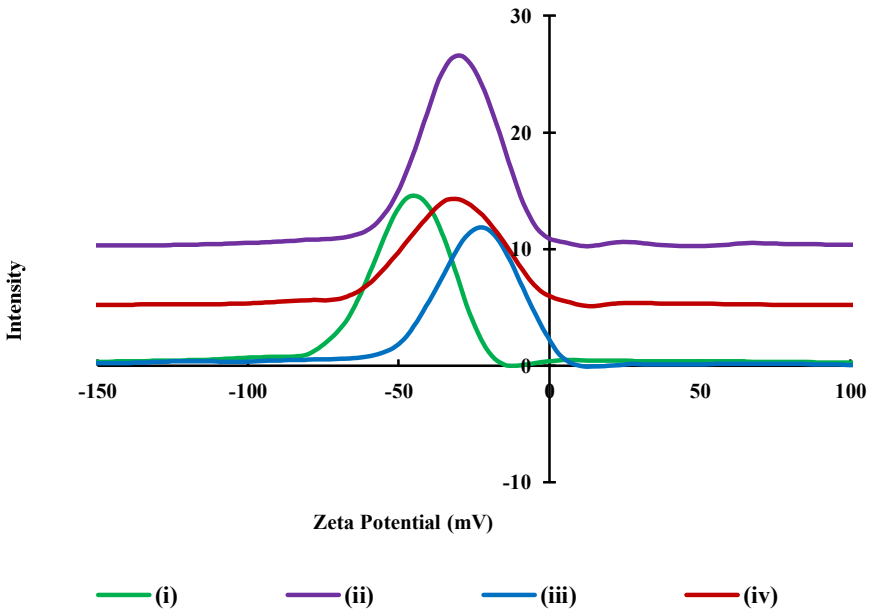

Figure 3.7: Zeta potential for **(i)** BN; **(ii)** GO; **(iii)** MGO; and **(iv)** MGOBN.

3.2.8. Point of zero charge (pH_{PZC}) values

The pH_{PZC} of the BN, GO, MGO, and MGOBN solids were obtained and are shown graphically in Figure 3.8 and the values are given in Table 3.4. the pH_{PZC} of the solid was found to be 6.8, 4.0, 6.5, and 5.3, respectively for the BN, GO, MGO, and MGOBN solids.

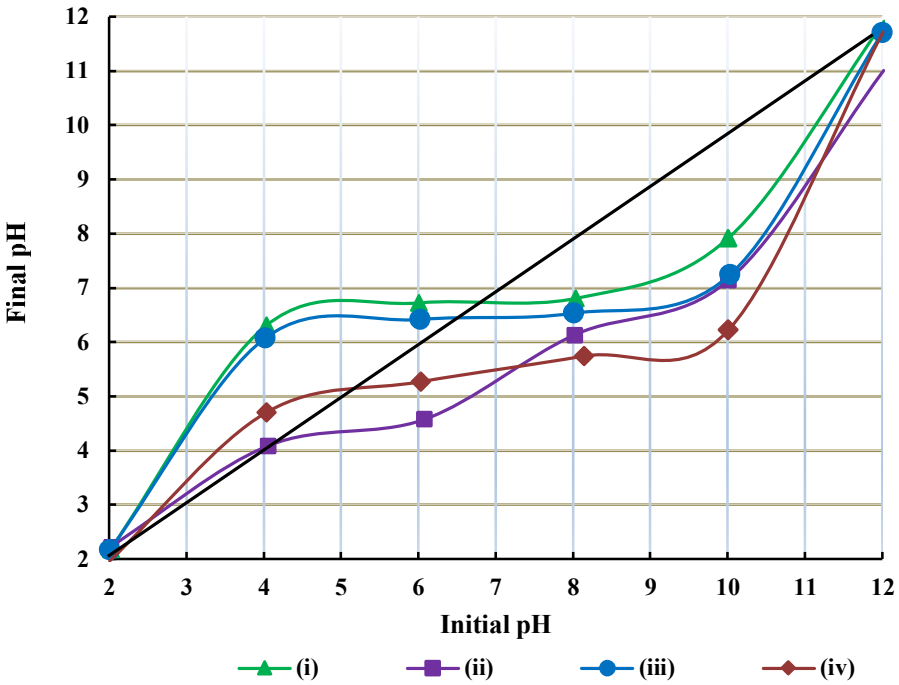

Figure 3.8: Plot of initial pH versus final pH for **(i)** BN;**(ii)** GO; **(iii)** MGO; and **(iv)** MGOBN.

Table 3.4: The pH_{PZC} values of the BN, GO, MGO, and MGOBN solids**.**

Solid materials	**pH_{PZC}**
BN	6.8
GO	4.0
MGO	6.5
MGOBN	5.3

3.3. BATCH REACTOR STUDIES FOR ARSENIC (III), ARSENIC (V), AND FLUORIDE

3.3.1. Effect of pH

As stated in Chapter 2, section 2.4, the adsorption of arsenic (III) and arsenic (V) was conducted for varied pH values i.e., pH 2.0 to 10.0. Figure 3.9 (a) depicts the percentage removal of arsenic (III) and arsenic (V) using GO and MGO solids at different pH values. Results showed that the change in solution pH showed varied impact on the uptake of arsenic species. A high percentage removal of arsenic (III) was almost unaffected within the pH region *Ca* 2.0 and 5.0, however, a modest drop in percentage removal was observed by an increase in pH from *Ca* 5.0 to 8.7. On the other hand, the percentage removal of arsenic (V) was slightly increased with an increase in pH from *Ca* 2.0 to 3.0, however, a further increase in pH from *Ca* 3.0 to 8.7 caused for a significant decrease in the percentage uptake of arsenic (V).

The speciation of arsenic species and the surface properties of solid material in an aqueous medium for varied pH values could explain the pH dependence uptake of arsenic by these solids i.e, GO and MGO. The point of zero charge pH of the solid materials i.e. GO and MGO was found 4.0 and 6.5, respectively. This showed that the solid surface possessed a net negative charge above this pH and a net positive charge below to this pH, as represented in Equation (3.1). This is due to surface dissociation/association of surface functional groups.

$$\equiv M{-}OH_2^+ \equiv M - OH \underset{pH_{PZC}}{\leftrightarrow} \equiv M - O^- \qquad ...(3.1)$$

where –OH represents the collective surface functional group of GO or MGO.

Arsenic (III) predominantly exists to its nonionic species (H_3AsO_3) within a wide pH range *Ca* 2.0 to 8.0. However, pH>8.0, the anionic species ($H_2AsO_3^-$) are formed due to the acidic dissociation of H_3AsO_3 (Yoon et al., 2017; Thanhmingliana et al., 2016). The high percentage uptake of arsenic (III) at a wide pH range by the GO and MGO was due to the high affinity of these solids towards the arsenic (III) and also no electrostatic repulsive forces hindered the uptake of arsenic (III) species by these solids within the studied pH region (*Cf* Figure 3.9 (a). These results inferred that a surface complexation of arsenic (III) at the active sites of a solid is the driving force of

sorption by the GO and MGO solids (Kang et al., 2017). It is further observed that the MGO nanocomposite showed a significantly enhanced percentage uptake of arsenic (III) compared to the bare GO. The presence of magnetite nanoparticles synergizes the uptake of arsenic (III) in addition to facilitating in the phase separation of solid once unit operation completed (Liu et al., 2015).

On the other hand, the uptake of arsenic (V) is predominantly affected with change in solution pH. Arsenic (V) exists in various oxyanionic species and the speciation studies revealed that within the pH region 2.0-7.0, the $H_2AsO_4^-$ species dominates. However, further increase in pH (7.0-9.0), the $HAsO_4^{2-}$ anionic species are dominated (Yoon et al., 2017). Therefore, the arsenic (V) is predominantly present to its anionic species throughout the studied pH range. Electrostatic attraction primarily controls the arsenic (V) adsorption on the GO and MGO nanocomposites (Guo et al., 2015; Kang et al., 2017). An increase in percentage uptake of arsenic (V) by the GO and MGO nanocomposites in the initial pH region (pH ~2.0-4.0) is primarily due to the electrostatic attraction of $H_2AsO_4^-$ species by the positively charged solid surface. However, further increase in pH (pH>4.5), an increase in negative charge density carried by the solid surface hinders the uptake of the negatively charged anionic arsenic (V) species ($H_2AsO_4^-$ or $HAsO_4^{2-}$). Both the solids showed enhanced percent uptake of arsenic (V) however, compared to these two nanocomposites, the MGO showed significantly higher removal uptake of arsenic (V). Therefore, this inferred that the magnetite solid showed enhanced affinity towards the arsenic (V), and preferentially the arsenic (V) is forming a surface complexation at the solid surface. The interactions of sorbing species with the available functional groups at the solid surface determine the adsorption behavior, in addition to the adsorbent surface's charge properties. The mechanisms of arsenic species sorption by iron oxide-based materials are studied previously and demonstrated that the surface complexation of iron and arsenic occurs in the sorption mechanism (Dixit and Hering, 2003; Jia et al., 2007; Repo et al., 2012). Thus, the adsorption of arsenic species on the surface of MGO is predominantly followed by a mixed effect of electrostatic attraction followed by surface complexation reactions.

Arsenic (III) is highly toxic and more mobile than arsenic (V) in an aqueous medium and is found difficult to remove from waterbodies (Bissen & Frimmel, 2003).

Although the percentage removal of arsenic (III) is slightly lower than that of arsenic (V) using MGO nanocomposite material, however; the material is efficient enough to remove significantly arsenic (III) i.e., around 87% at pH 2.0-5.0.

BN, GO, MGO, and MGOBN@1:2 are used to investigate the pH dependence removal of fluoride and results are shown in Figure 3.9 (b). The uptake of fluoride using the BN and GO is significantly low and an increase in pH further decreases the removal percentage of fluoride. A maximum of *Ca.* 50% of fluoride was removed at pH ~ 2.9 by the BN and GO solids. However, on the other hand, the nanocomposite material MGO and MGOBN@1:2 showed very high de-floridization at a lower pH value (pH ~3.0). A maximum of *Ca.* 81% of fluoride was removed at pH 2.0 using the MGOBN@1:2 nanocomposite and *Ca.* 71% was removed using the MGO at pH 3.0. High uptake of the fluoride at lower pH values is demonstrated with the fact that relatively stronger electrostatic attraction is observed between the partially positively charged solid surface and negatively charged fluoride ions (Sahoo & Hota, 2018). However, higher pH values (pH>5.0) caused for stronger repulsive forces between the solid surface and fluoride ions hence, caused for a significant decrease in the uptake of fluoride by these solids (Mobarak et al., 2018; Sahoo & Hota, 2018). Additionally, at higher pH values the hydroxyl ions compete preferably with the nanocomposite surface active sites hence, caused for a decrease in fluoride removal (Fan et al., 2016; Velazquez-Peña et al., 2017).

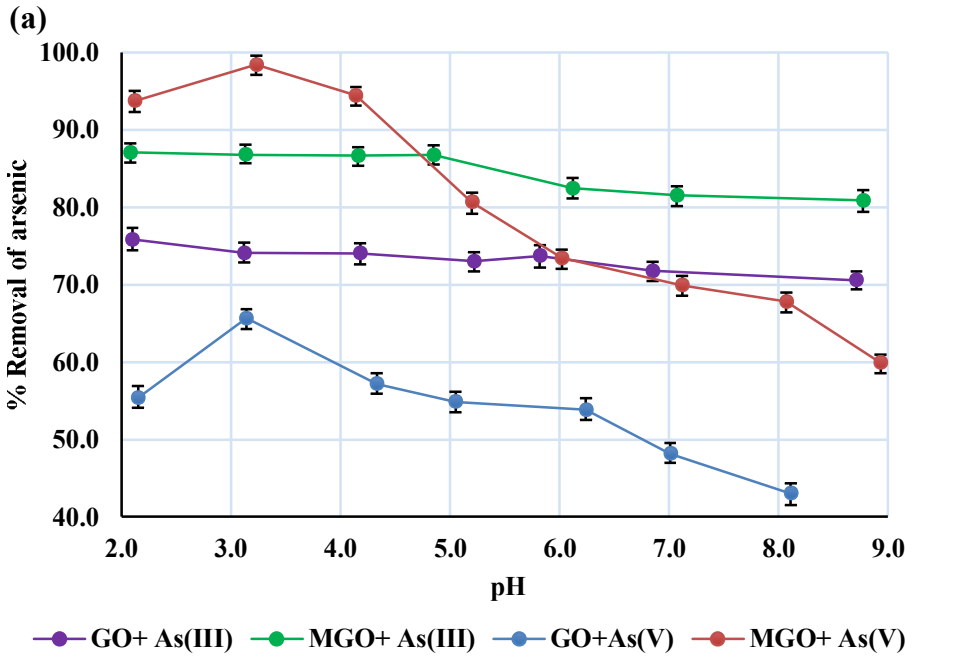
(a)
100.0
90.0
80.0
70.0
60.0
50.0
40.0
% Removal of arsenic
2.0
3.0
4.0
5.0
6.0
7.0
8.0
9.0
pH
GO+ As(III)
MGO+ As(III)
GO+As(V)
MGO+ As(V)

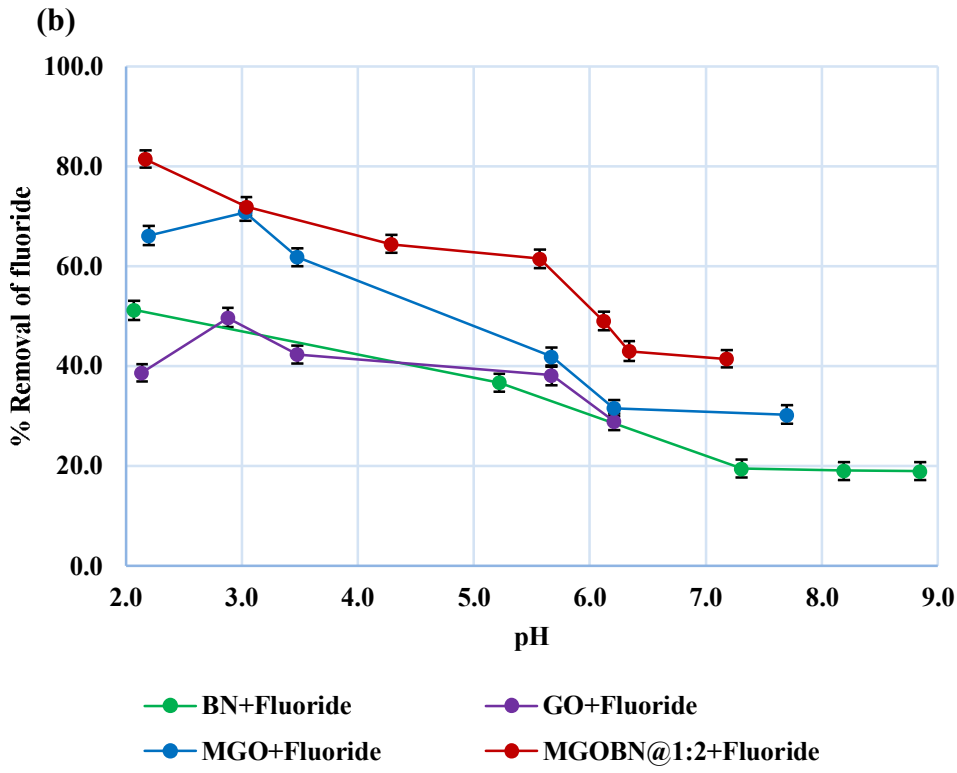
(b)
100.0
80.0
60.0
40.0
20.0
0.0
% Removal of fluoride
2.0
3.0
4.0
5.0
6.0
7.0
8.0
9.0
pH
BN+Fluoride
GO+Fluoride
MGO+Fluoride
MGOBN@1:2+Fluoride

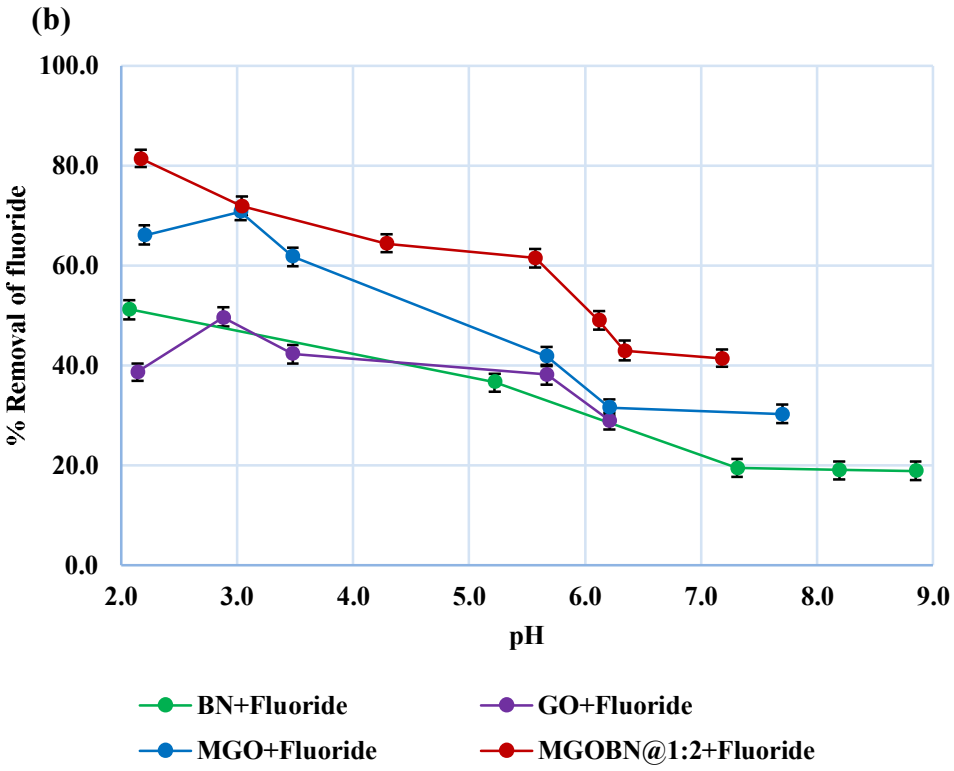

Figure 3.9: Effect of pH in the removal of **(a)** arsenic (III) and arsenic (V); and **(b)** fluoride using the nanocomposite materials ([arsenic (III)/ or arsenic (V)/ or Fluoride ions]: 10.0 mg/L; Solid dose: 2.0 g/L; Temperature: 25±1°C, Agitation speed: 180 rpm).

3.3.2. Effect of sorptive concentration

The removal of arsenic and fluoride is studied for a wide range of initial arsenic or fluoride concentrations (i.e., from 1.0 mg/L to 30.0) at a constant pH (3.0 for arsenic (III) and arsenic (V), and 4.1 for fluoride ions) using the MGO (for arsenic (III) and arsenic (V) and MGOBN@1:2 (for Fluoride ion) nanocomposite materials. The results are shown in figure 3.10. An increase in the concentration of arsenic (III), arsenic (V), and fluoride from 1.0 to 30.0 mg/L causes a decrease in percentage uptake from *Ca.* 98% to 82% and *Ca.* 99% to 87% for arsenic (III) and arsenic (V), respectively using MGO and *Ca.* 66% to 53% for fluoride using MGOBN@1:2 nanocomposite solid. It is evident that an increase in pollutant concentrations caused for an apparent decrease

in the percentage removal of these pollutants from an aqueous medium. This is explicable with the fact that at higher sorbate concentrations the sorbate species are relatively high for the same number of active sites at the solid surface, hence, the percentage removal of these species is decreased increasing the pollutant's concentrations (Sahoo & Hota, 2018). Even at high concentrations, the removal percentage of arsenic and fluoride is seemingly high, which inferred the strong affinity of MGO for arsenic (III) and arsenic (V) and MGOBN@1:2 towards fluoride.

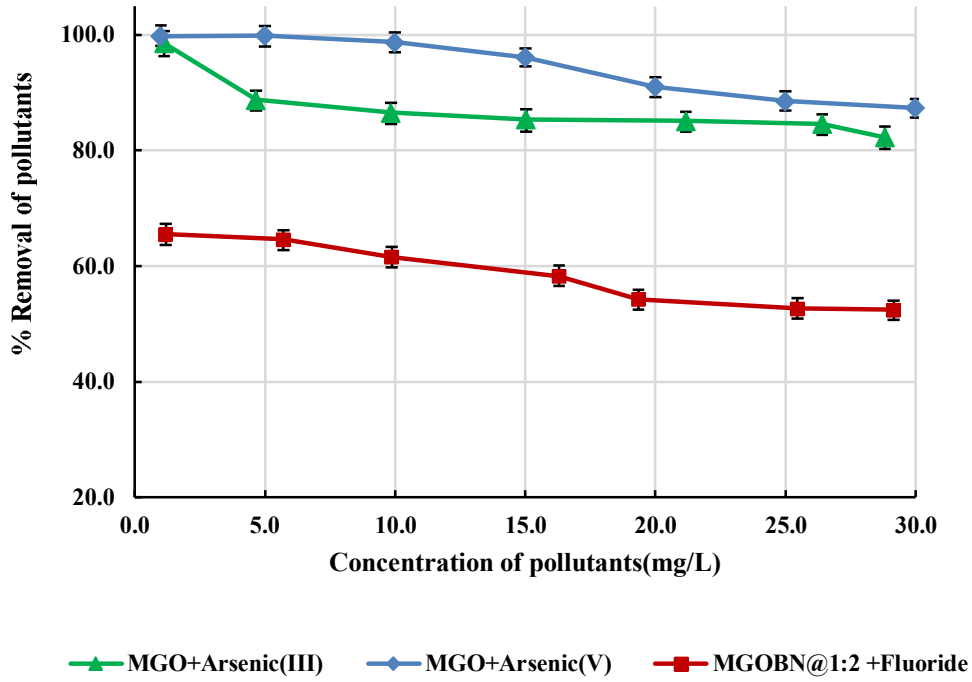

Figure 3.10: Effect of initial sorptive concentration in the removal of arsenic (III), arsenic (V) by MGO, and fluoride by MGOBN@1:2 [pH: 3.0 for arsenic (III) & arsenic (V), 4.1 for fluoride); solid dose: 2.0 g/L: temperature: 25±1°C, agitation speed: 180 rpm].

3.3.2.1.Adsorption isotherm modeling

The concentration dependence removal of arsenic (III), arsenic (V), and fluoride ions are modeled with the known Freundlich, Langmuir, and Sips adsorption isotherms to its non-linear equations as described in Chapter 2, section 2.4 (C*f* Equation (2.2, 2.3 and 2.4)) and simulated results are shown in Figure 3.11 and Table

3.5. The high uptake of arsenic (III) and arsenic (V) is not fitted well with the Langmuir or Freundlich equations. However, the Sips isotherm model is agreed well since the least square sum value is found reasonably low. Further, the removal capacity of arsenic (III), and arsenic (V) was found to be 26.59 mg/g and 35.97 mg/g, respectively using the MGO and 17.81 mg/g for fluoride using the MGOBN@1:2 nanocomposite. These results showed that a very high removal capacity was achieved for the removal of arsenic (III), arsenic (V), and fluoride ions using the novel nanocomposite solids. Further, a closure comparison was presented in Table 3.6 for the removal capacities of arsenic (III), arsenic (V), and fluoride ions using various sorbents employed. It is evident from Table 3.6 that the nanocomposite materials are fairly efficient in removing these pollutants and a comparable removal efficiency was achieved in the removal of arsenic (III), arsenic (V), and fluoride ion from an aqueous medium.

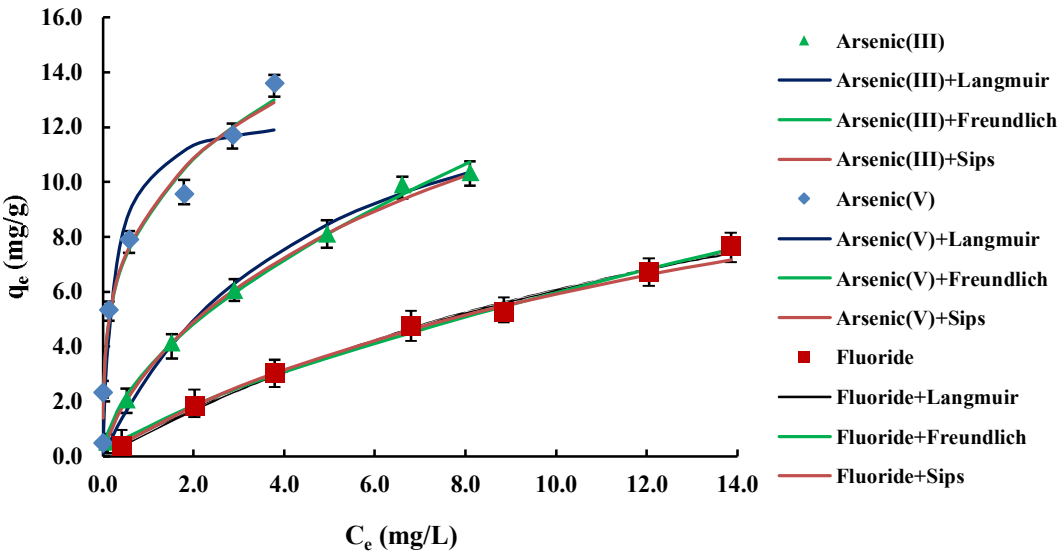

Figure 3.11: Langmuir, Freundlich, and Sips isotherms for the sorption of arsenic (III), arsenic (V) using MGO and fluoride using MGOBN@1:2 [pH: 3.0 for arsenic (III) & arsenic (V), 4.1 for fluoride); solid dose: 2.0 g/L: temperature: 25±1°C, agitation speed:180 rpm].

Table 3.5: Optimized Langmuir, Freundlich, Langmuir, and Sips adsorption models constants along the least square sum for the sorption of arsenic (III), arsenic (V), and fluoride by the nanocomposite solids.

Parameters		Pollutants		
		Arsenic (III)	**Arsenic (V)**	**Fluoride**
		pH		
		3.0	**3.0**	**4.1**
		Material		
		MGO	**MGO**	**MGOBN@1:2**
Langmuir	q_o (mg/g)	16.147 ± 0.831	12.661 ± 0.553	17.32 ± 0.916
	K_L (L/g)	0.221 ± 0.014	4.064 ± 0.211	0.053 ± 0.017
	s^2	0.474	11.823	0.233
Freundlich	1/n	0.574 ± 0.028	0.291 ± 0.011	0.724 ± 0.023
	K_F (mg/g)	3.225 ± 0.391	8.829 ± 1.049	1.123 ± 0.115
	s^2	0.379	2.745	0.172
Sips	q_m (mg/g)	26.59 ± 1.56	35.97 ± 1.87	17.81 ± 0.97
	K_s	0.065 ± 0.029	0.008 ± 0.002	0.046 ± 0.021
	n_s	0.736 ± 0.041	0.292 ± 0.023	0.919 ± 0.045
	s^2	0.004	2.777	0.087

Table 3.6: Adsorption capacity for the removal of arsenic (III), arsenic (V), and fluoride using the variety of materials.

Pollutants	Adsorbent	Adsorption capacity(mg/g)	References
Fluoride	$ZrCl_4$ – graphene supported on vegetal activated carbon composite (G-$ZrCl_4$/VAC)	3.9	(Marin et al., 2016)
	Al_2O_3-Fe_3O_4-expanded graphite nano sandwich (Al_2O_3-Fe_3O_4-EG)	3.4	(Xu et al., 2016)
	Metal ions imprinted graphene oxide/ alginate hybrid biopolymeric beads (GOAlgLa)	6.7	(Pandi and Viswanathan, 2016
	Graphene Oxide (GO)	1.4	(Li et al., 2013)

	Graphene oxide alumina nanocomposites (GO/Al_2O_3)	11.5		Xu et al., 2020)
	Manganese oxide coated graphene oxide (MOGO)	11.9		(Li et al., 2013)
	Activated kaolinite	0.134		(Sarkar et al., 2006)
	Pyrophyllite	2.2		(Goswami and Purkait, 2011)
	Montmorillonite (ANC)	1.324		(Ramdani et al., 2010)
	$Fe3^{+}$- modified bentonite	2.91		(Gitari et al., 2015b)
	Chemically modified bentonite(10%) lanthanum bentonite	4.26		(Kamble et al., 2009)
	Magnesium incorporated bentonite	2.26		(Thakre et al., 2010)
	MGOBN@1:2	**17.81**		**Present Study**
Arsenic (V) and Arsenic (III)	Three dimensional Fe_3O_4 graphene macroscopic composite (3D Fe_3O_4/graphene)	**As(III)** 0.313	**As(V)** 0.385	(Guo et al., 2015)
	Water-Dispersible magnetite reduced graphene oxide composites (Fe_3O_4/rGO)	13.1	5.83	(Chandra et al., 2010b)
	Magnetite graphene oxide (Fe_3O_4GO)		18.8	(Yoon et al., 2016)
	Magnetite reduced graphene oxide (Fe_3O_4/rGO)	29.8	8.42	(Yoon et al., 2016)
	(Graphene oxide/ ferric hydroxide composites) GO/ferric hydroxide		23.78	(Zhang et al., 2010)
	Magnetic graphene nanoplatelet decorated with Fe–Fe_2O_3 nanoparticles (MGNCs)	11.34		(Zhu et al., 2012)
	Graphene oxide (GO)		0.678	(Dubey et al., 2015)
	Reduced graphene oxide (rGO)		1.287	(Dubey et al., 2015)
	Metal doped reduced graphene oxide (Ag–Cu_2O/rGO)		11.51	(Dubey et al., 2015)
	Smart magnetic graphene		3.26	(Gollavelli et al., 2013)
	MGO	**26.59**	**35.97**	**Present study**

3.3.2.2.Competitive adsorption of arsenic (V) and fluoride onto MGO and the expanded sips modeling adsorption isotherms

The concentration dependence sorption of pollutants by MGO solid was modelled with the Sips Equation and the k_s value was obtained for each pollutant, i.e, arsenic (V), and fluoride individually. Further, k_s values are utilized for the simulation of simultaneous sorption of arsenic (V) and fluoride using the MGO solid at pH 3.0. Isotherm modeling for mono-components was performed as described in Chapter 2, section 2.4.2 using the Sips equation (Equation (2.4)). The non-linear fittings of sorption data are shown graphically in Figure 3.12 (a). Further, the isotherm parameters i.e., q_m, K_s, and n_s are optimized for these two pollutants and are tabulated in Table 3.7. The q_m for As(V) and F^- is optimized to 35.97 and 19.12 mg/g, respectively. Moreover, the binary component modeling is conducted using the Sips expanded equation for binary components and for varied molar ratios of the As(V) and F^- (*Cf* Equation (2.5 & 2.6)). The isotherm parameters were optimized for the fitting of sorption data and the K_s values were taken from the mono-component system. The fitting is shown in Figure 3.12(b), and 3.12(c) for the 1:1, 1:2, and 2:1 molar ratio of As (V) to F^-. Similarly, the optimized values are tabulated in Table 3.7. The sorption capacity of As(V) was significantly higher compared to the fluoride in the simultaneous removal of these two pollutants. The maximum sorption capacity of As(V) was 50.091, 95.478, and 53.709 mg/g for 1:1, 1:2, and 2:1 molar ratios of As(V) to F^-. Similarly, the sorption capacity of fluoride was 7.166, 4.552, and 7.579 mg/g for the 1:1, 1:2, and 2:1 molar ratio of As(V) to F^-. These results further indicated that the presence of fluoride ions insignificantly affected the removal capacity of As(V), even for the molar ratios 1:2 and 2:1, the sorption capacity of As(V) was increased significantly.

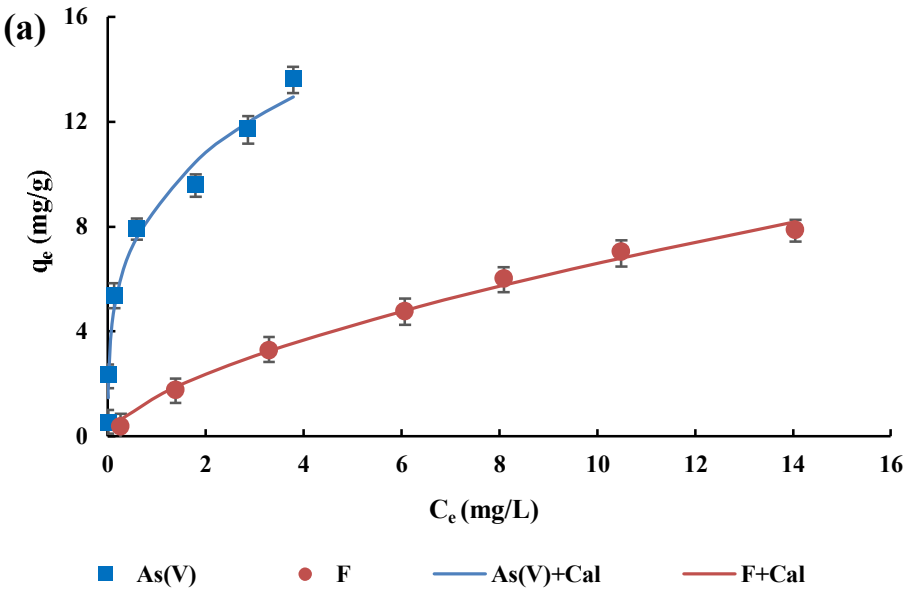
(a)
16
12
8
4
0
q_e (mg/g)
0
2
4
6
8
10
12
14
16
C_e (mg/L)
As(V)
F
As(V)+Cal
F+Cal

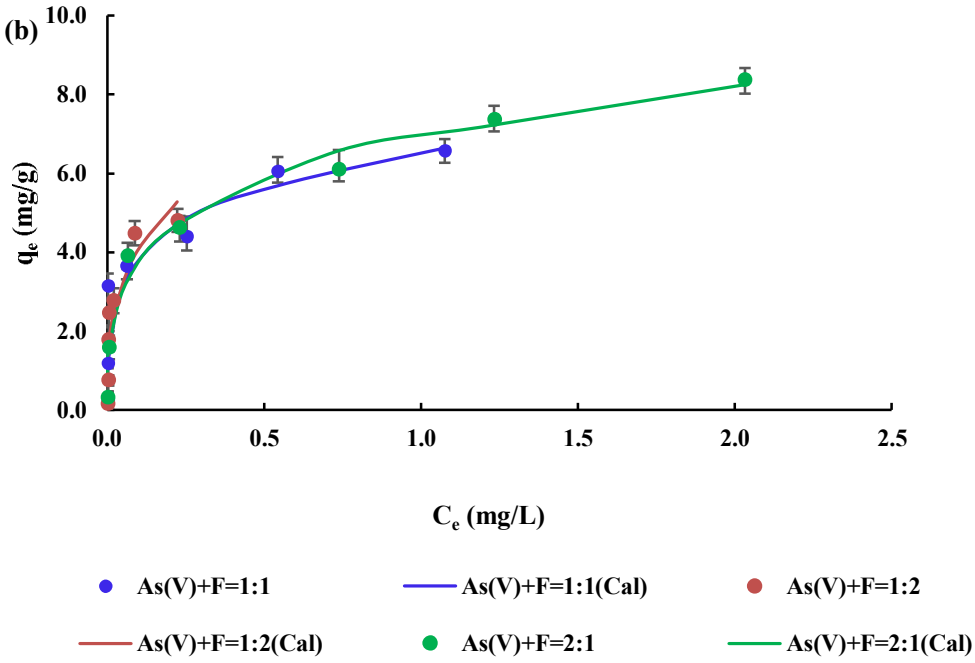
(b)
10.0
8.0
6.0
4.0
2.0
0.0
q_e (mg/g)
0.0
0.5
1.0
1.5
2.0
2.5
C_e (mg/L)
As(V)+F=1:1
As(V)+F=1:1(Cal)
As(V)+F=1:2
As(V)+F=1:2(Cal)
As(V)+F=2:1
As(V)+F=2:1(Cal)

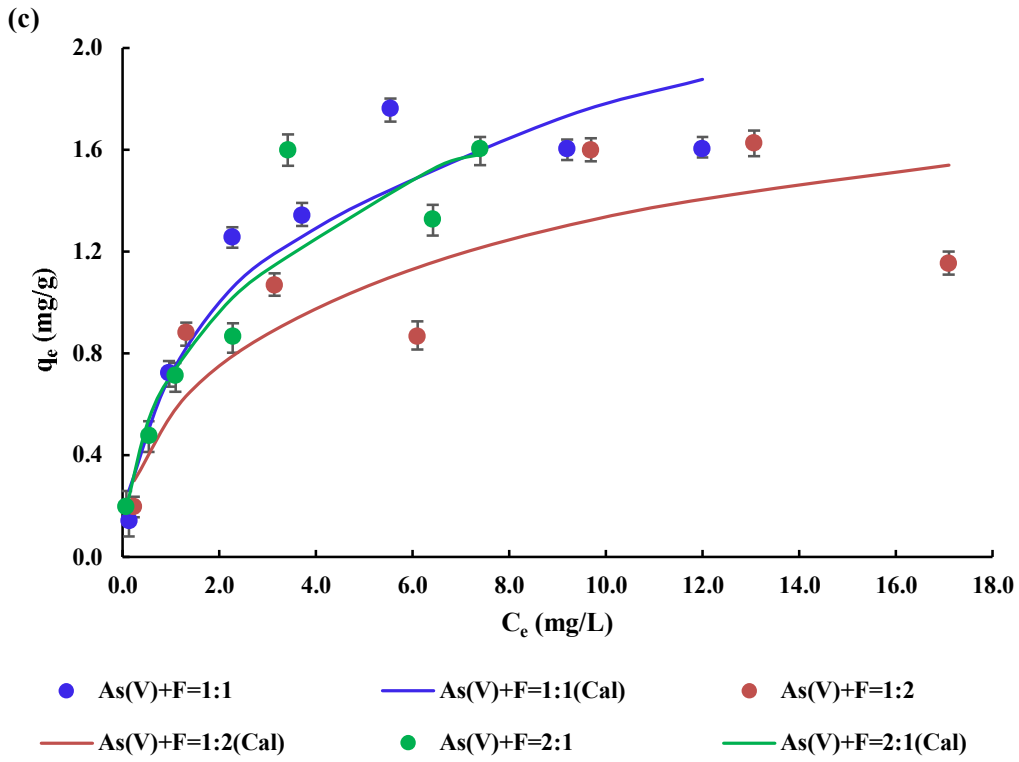

Figure 3.12: (a) Sips isotherm modeling in the sorption of fluoride and arsenic (V) in the single component system; and Sips modelling for the binary systems; **(b)** arsenic (V); and **(c)** fluoride in the simultaneous removal of fluoride and arsenic (V) at varied molar ratios using MGO solid (pH: 3.0; solid dose: 2.0 g/L; temperature: 25±1°C, agitation speed: 180 rpm).

Table 3.7: Isotherm parameters for arsenic (V) and fluoride in mono-components and binary-components systems having varied arsenic (V) and fluoride ratios using expanded Sips equation along with the least square sum value.

Parameters	Pollutants							
	Mono-component system		Binary- components system					
			As(V) As(V)+F			Fluoride As(V)+F		
	As(V)	Fluoride	1:1	1:2	2:1	1:1	1:2	2:1
q_m (mg/g)	35.97 ± 1.23	19.12 ± 0.97	31.88 ± 1.07	54.98 ± 1.92	52.01 ± 1.85	6.56 ± 0.19	4.41 ± 0.13	6.03 ± 0.16
K_s (L/mg)	0.008 ± 0.001	0.017 ± 0.002	0.008 ± 0.001	0.008 ± 0.001	0.008 ± 0.001	0.017 ± 0.002	0.017 ± 0.002	0.017 ± 0.002
n_s	0.292 ± 0.02	0.637 ± 0.015	0.263 ± 0.010	0.235 ± 0.011	0.347 ± 0.029	0.461 ± 0.037	0.408 ± 0.024	0.611 ± 0.041
s^2	2.777	0.314	10.279	30.557	0.964	0.207	0.398	1.073

s^2: least square sum

3.3.3. Effect of time

Time dependence sorption of arsenic (III) and arsenic (V) by MGO and fluoride by MGOBN@1:2 was carried out for longer contact time i.e., from 1 to 1440 mins, and the results are shown in figure 3.13(a). The solids MGO and MGOBN@1:2 quickly adsorb arsenic and fluoride ions during the initial period of time, which attains a constant value within *Ca* 60 mins of contact time. The excess number of accessible active sites on the surface of the adsorbent preferentially occupied by the sorbate ions during the initial period of contact and the saturation of active sites reveals with the saturation of sorption of these pollutants in the latter stage of time by the MGO and MGOBN@1:2. It is evident that even at 5 mins of contact, enabled to remove more than 80% of the arsenic (III) and arsenic (V) by the MGO solid. These results showed that the MGO and MGOBN@1:2 are seemingly efficient in the removal of arsenic and fluoride from an aqueous medium.

The time dependence data is fitted to the pseudo-first-order (PFO) and pseudo-second-order (PSO) kinetic models to its non-linear forms as described previously in Chapter 2, section 2.4 (Equation (2.7, 2.8 and 2.9)) (Lee et al., 2016b). The fitting of data optimized the rate constant values along with the maximum sorption capacity for these pollutants using the MGO and MGOBN@1:2 solids. The results are shown in Figure 3.13 (b) and the optimized parameters along with least square sum is given in Table 3.8. The results showed that the uptake of these pollutants by these solids followed the PSO model than the PFO model. This further indicated that the arsenic (III), arsenic (V), and fluoride are aggregated on the solid surface with relatively stronger chemical forces (Kanrar et al., 2016a). It was reported previously that fluoride is sorption by different sorbents followed the pseudo-second-order model (Bhaumik et al., 2011a; Kameda et al., 2015a).

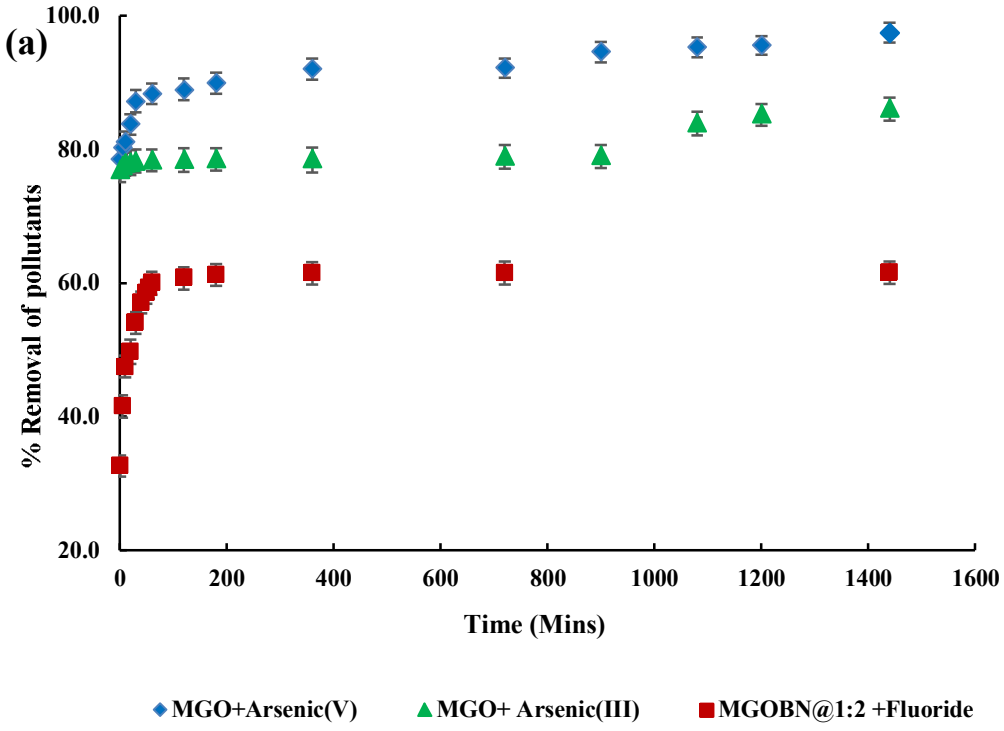

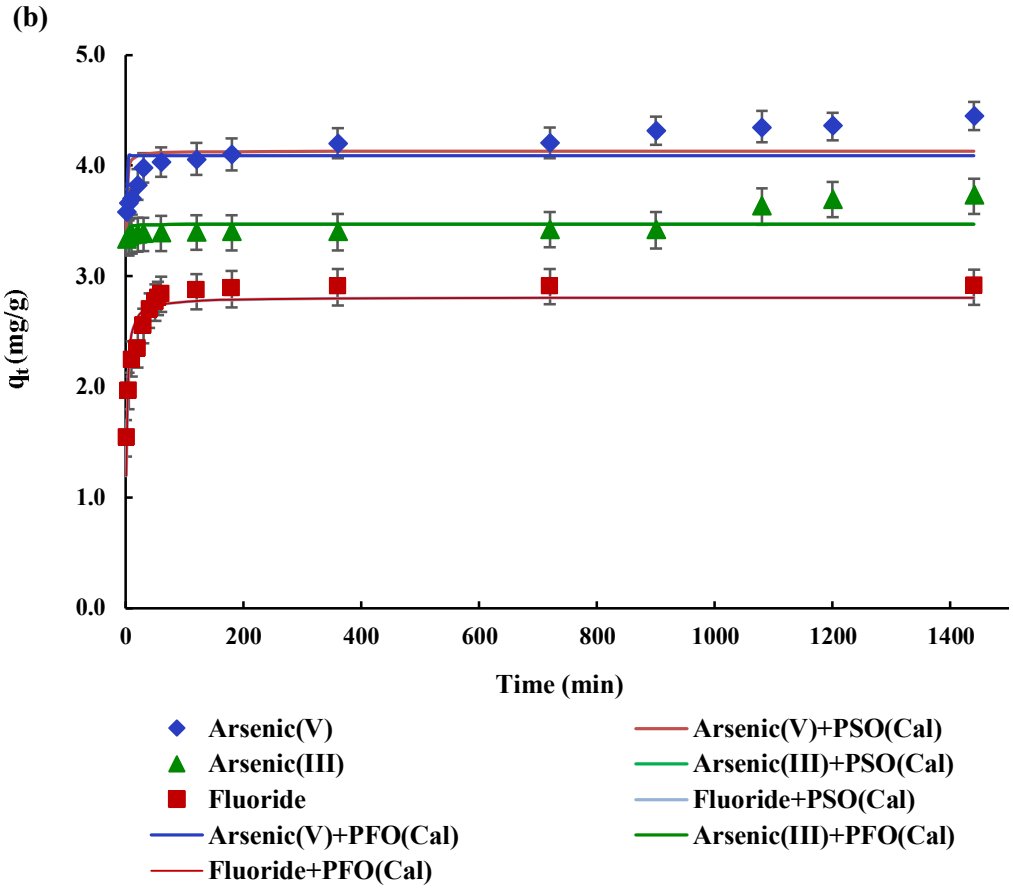

Figure 3.13: (a) Effect of contact time in the removal of arsenic (III), arsenic (V) by MGO, and fluoride by MGOBN@1:2 solids [Pollutant concentrations: 10.0 mg/L; (pH: 3.0 for arsenic (III) & arsenic (V), 4.1 for fluoride); Solid dose: 2.0 g/L; Temperature: 25°C, Agitation speed: 180 rpm]; and **(b)** pseudo-first order and pseudo-second order fitting of kinetic data in the uptake of arsenic (III), arsenic (V) by MGO, and fluoride by MGOBN@1:2 solids.

Table 3.8: Values of q_e, k_1, k_2, and s^2 (Least square sum) obtained for the sorption of arsenic (III) and arsenic (V) by MGO and fluoride by MGOBN@1:2 using the pseudo-first-order and pseudo-second-order kinetic models.

Material	Pollutant	PFO Model			PSO Model		
		k_1 (min^{-1})	q_e (mg/g)	s^2	k_2 (g/mg/min)	q_e (mg/g)	s^2
MGO	Arsenic(V)	2.07 ± 0.11	4.09 ± 0.59	0.767	1.164 ± 0.102	4.13 ± 0.61	0.583
MGO	Arsenic(III)	3.30 ± 0.19	3.46 ± 0.31	0.207	5.573 ± 0.303	3.46 ± 0.37	0.196
MGOBN@1:2	Fluoride	0.67 ± 0.02	2.68 ± 0.27	1.043	0.265 ± 0.021	2.80 ± 0.29	0.400

s^2: least square sum

3.3.4. Effect of background electrolyte

The background electrolyte ionic concentrations in aqueous solutions demonstrate specific and non-specific sorption. The specific sorption in which the sorbate species form the inner-sphere complexes at the solid surface is almost unaffected by an increase in electrolyte concentrations. In contrast, the non-specific sorption is greatly influenced by the background electrolyte concentrations since the sorbate species are aggregated at the solid surface with weaker forces and forming the outer-sphere complexes (Hayes et al., 1988). Figure 3.14 shows the percentage elimination for arsenic (III), arsenic(V), and fluoride with raising the $NaNO_3$ or KCl from 0.001 to 0.5 mol/L concentrations. The outcomes demonstrated that a 500-fold increase in $NaNO_3$ content could not substantially impact arsenic (III) and arsenic (V) elimination using MGO. The outcomes inferred that the arsenic (III) and arsenic (V) species were primarily sorbed by the stronger chemical forces and formed inner-sphere complexes on the surface. The magnetic graphene oxide composites show similar results in removing arsenic (Sheng et al., 2012). On the other hand, an increase in 500 times KCl concentrations causes little influence in removing fluoride. The removal of fluoride was decreased from 51% to 50% by raising the KCl from 0.001 to 0.5 mol/L concentrations. These outcomes inferred that the stronger forces that form 'inner-

sphere' complexes at the surface bind the fluoride at the surface. However, the fewer fluoride ions are attracted by the electrostatic forces and retained at the outer layer forming the outer-sphere complexation and possibly being affected by the changes in electrolyte concentrations.

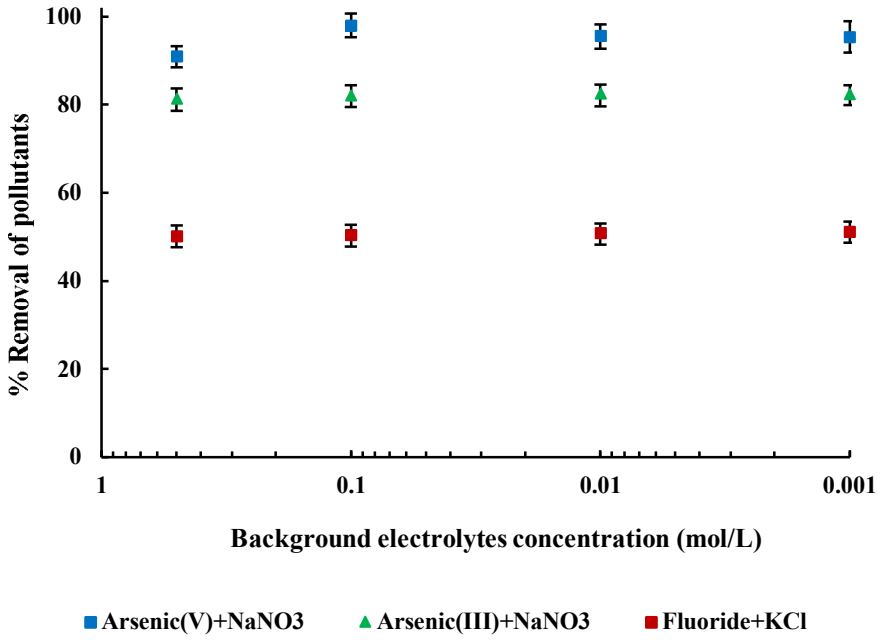

Figure 3.14: Effect of background electrolyte concentrations in the removal of arsenic (III), arsenic (V) by the MGO solid and fluoride by MGOBN@1:2 ([Arsenic (III)/ or arsenic (V), Fluoride]: 10.0 mg/L; pH: 3.0 for arsenic (III) & arsenic (V), and 4.1 for fluoride; solid dose: 2.0 g/L; temperature: 25°C, agitation speed: 180 rpm)

3.3.5. Effect of co-existing ions

In order to study the influence of several cations or anions in the elimination efficiency of these solids for arsenic (III) and arsenic (V) by MGO and fluoride by MGOBN@1:2 and outcomes are represented in Figure 3.15. The elimination efficiency of both arsenic (III) and arsenic (V) by MGO are not significantly afflicted in the existence of cationic ions *viz.*, Ca^{2+}, Mn^{2+}, Mg^{2+}, and Ni^{2+}. These results indicated that the solid has a high affinity towards the arsenic species. Hence, the presence of these cations could not influence the elimination of both arsenic species

employing MGO solid. Similarly, the EDTA, glycine, and oxalic acid showed little influence in eliminating arsenic (III) and arsenic (V) by employing the MGO solid. However, the presence of phosphate slightly hinders the uptake of arsenic (III) and arsenic (V). The phosphate species are preferentially competing with the similar tetrahedral structure of arsenic (V) and arsenic (III) species towards the active sites at the surface; hence, suppresses, to some extent, the elimination of arsenic (III) or arsenic (V) by the MGO surface (Su et al., 2017). Moreover, due to the comparable atomic structure and chemical properties of phosphate with arsenic species, phosphate forms an 'inner-sphere complexes' at the solid surface by a ligand substitution process, hence, sorbed preferentially on the solid surface and hindering the sorption of arsenic species on the MGO surface (Yoon et al., 2017).

The cations or anions have impacted, to varying extents, the removal efficiency of MGOBN@1:2 in eliminating fluoride. The anions are preferentially competing for the solid surface and hence, caused the decrease of fluoride sorption at the MGOBN@1:2 (Lalhmunsiama et al., 2021). The higher amount of negative charges in co-ions led to an increased attraction between the co-ions and the adsorbent, which inhibited the removal of fluoride ion from aqueous media (Xu et al., 2016b).

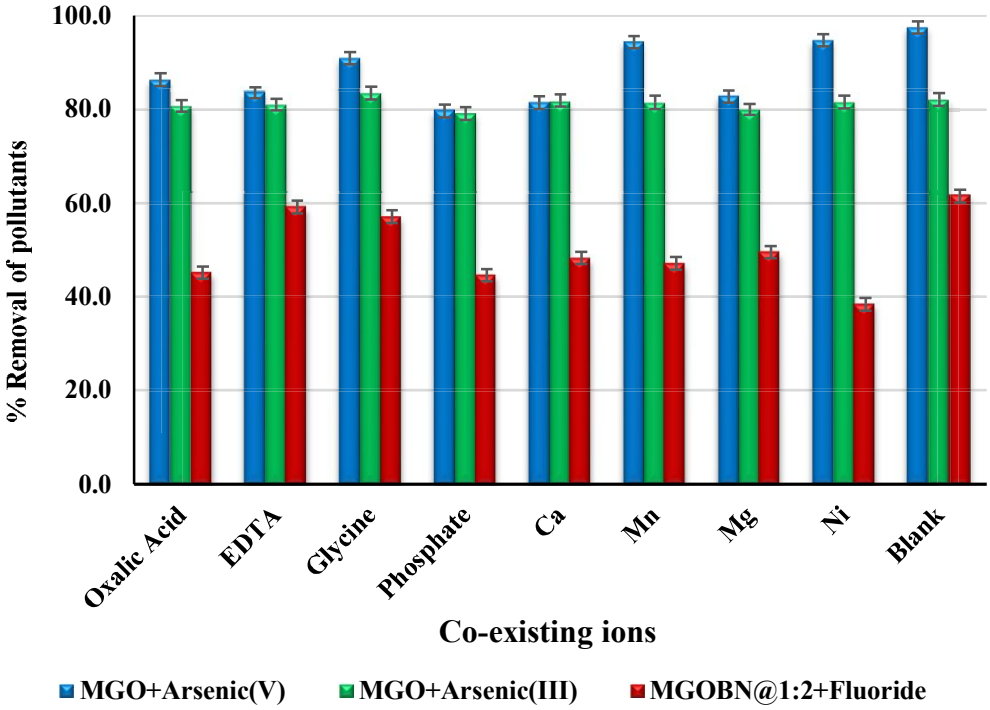

Figure 3.15: Effect of co-existing ions in the removal of arsenic (III) and arsenic (V) by MGO and fluoride by MGOBN@1:2 ([Pollutant concentrations: 10.0 mg/L; cations/anions concentrations: 50.0 mg/L; pH: 3.0 for arsenic (III) & arsenic (V), and 4.1 for fluoride; solid dose: 2.0 g/L; temperature: 25°C, agitation speed: 180 rpm).

3.4. Fixed bed column reactor analysis

A dynamic fixed bed column experiment was performed to obtain the loading capacity and the applicability of MGO-Beads and MGOBN@1:2-Beads in the elimination of these pollutants in an aqueous medium. The elimination of arsenic (III), arsenic (V), and fluoride from aqueous solutions was therefore conducted using column experiments and results are shown in Figure 3.16. These results showed that a complete breakthrough was obtained at the throughput volume of 13.98 L, 19.5 L respectively for arsenic (III) and arsenic (V) by MGO-Beads and 1.46 L for fluoride by MGOBN@1:2-Beads using Thomas equation (*Cf* Equation (2.10)). It is evident from these results that relatively a large throughput volume is obtained for these pollutants, which pointed to greater applicability of materials in the elimination of arsenic (III), arsenic (V), or fluoride even under dynamic conditions. The optimized

parameters along with the least square sum are included in Table 3.8. Results showed that a very high loading capacity of $1.55x10^2$ mg/g and $1.15x10^2$ was obtained for the arsenic (III) and arsenic (V), respectively. These results showed the potential of MGO-Beads solid in the efficient remediation of water contaminated with arsenic species. Similar results showed that the removal of arsenic (V) using the 3-marcaptopropyl trimetoxysilane (CHMS), and trimethoxy-octlysilane (CHTS) solids under the fixed-bed reactor revealed that the breakthrough data demonstrated with Thomas equation and the loading capacity of arsenic (V) was found 8.12 and 5.53 mg/g, employing the CHMS and CHTS solids, respectively (Lalhmunsiama et al., 2016). Chi-APTES, a functionalized hybrid material precursor to chitosan, exhibits a loading capacity of 2.576 mg/g for arsenic (V) (Lalhmunsiama et al., 2016). On the other hand, the loading capacity of fluoride was found 1.54 mg/g using the MGOBN@1:2-Beads.

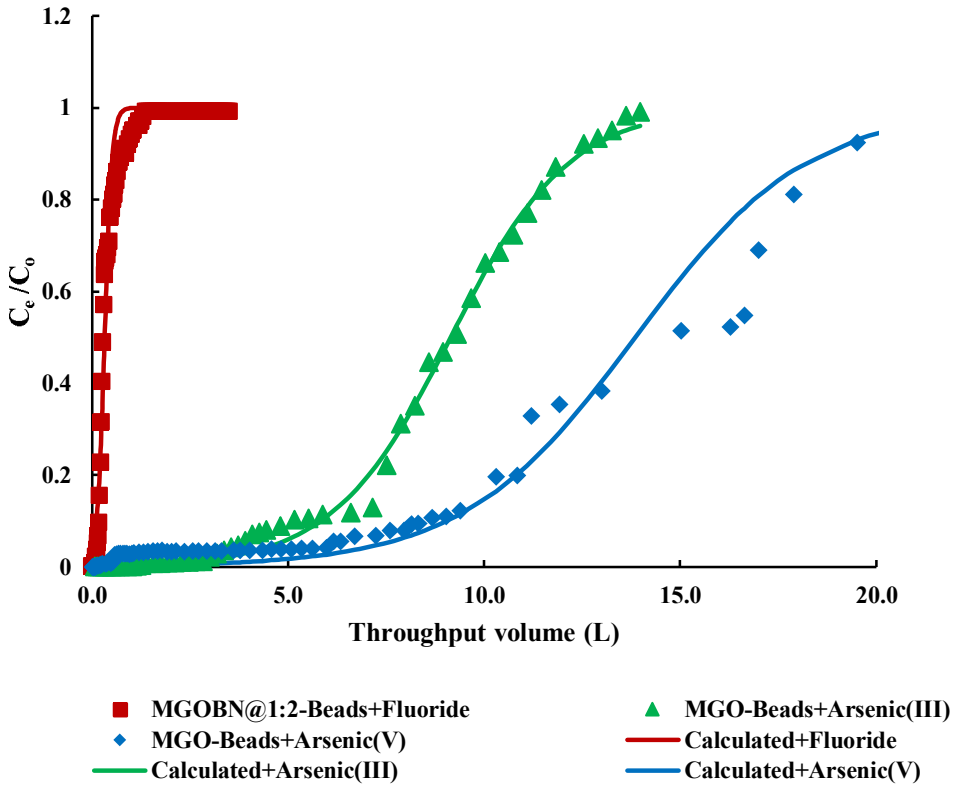

Figure 3.16: Breakthrough curves for the removal of fluoride by MGOBN@1:2-Beads, and arsenic (III) and arsenic (V) by MGO-Beads (Pollutant concentrations: 10.0 mg/L; flow rate: 1.0 mL/min; pH: 4.1 for fluoride, and pH: 3.0 for arsenic (III)/or

arsenic (V); the amount of solid loaded: 2 g for fluoride, 0.5 g for arsenic (III), and 1.0 g for arsenic (V); Temperature: 25°C).

Table 3.9: Thomas constants estimated for the removal of fluoride by MGOBN@1:2-Beads arsenic (III) and arsenic (V) by the MGO- Beads and material.

Material	Pollutants	Amount of solids loaded in column (g)	Thomas constants		Least square sum (s^2)
			q_o (mg/g)	K_T (L/min/mg)	
MGOBN@1:2-Beads	Fluoride	2.0	1.54 ± 0.04	1.11 x10^{-3}± 0.06	1.1x10^{1}
MGO- Beads	Arsenic (III)	0.5	1.55x10^{2}± 0.04	7.81x10^{-5}± 0.04	2.4x10^{-2}
MGO- Beads	Arsenic (V)	1.0	1.15 x10^{2}± 0.13	5.50x10^{-6}± 0.15	2.34x10^{2}

3.5. Application of MGO, and MGOBN@1:2 materials in a natural water system

Natural water samples were collected from the Tlawng river, Chiahpui river, and *tuikhur* (spring) Durtlang N, Aizawl and were used to remove arsenic (III), arsenic (V), and fluoride at various concentrations at pH 3.0 for arsenic and 4.1 for fluoride. The physico-chemical parametric studies of natural water were conducted and displayed in *Cf* Table 3.1. The results revealed that Cu, Pb, Ni, and Al are present at a very low level however, the presence of Ca and Mg is significantly present. Moreover, the total organic carbon analysis showed that these natural water samples are having a high level of inorganic carbon (IC) with a lower extent of NPOC value. Therefore, the presence of high IC with Ca and Mg concentrations showed that the water is having dissolved calcium and magnesium carbonates or bicarbonates. Additionally, the water sample showed a lesser extent of sulphate, phosphate, and nitrates.

Figure 3.17 displays the concentration-dependent removal of arsenic (III) and arsenic (V) by the MGO and fluoride by MGOBN@1:2 solids in a natural water matrix. The percentage removal of these pollutants is compared to the corresponding removal

of these pollutants in distilled water. The findings showed that the removal efficiency of arsenic (III) and arsenic (V) using MGO and fluoride by MGOBN@1:2 in natural water samples was not significantly influenced hence, the solids MGO and MGOBN@1:2 are useful and potential materials in the remediation of water contaminated with these pollutants.

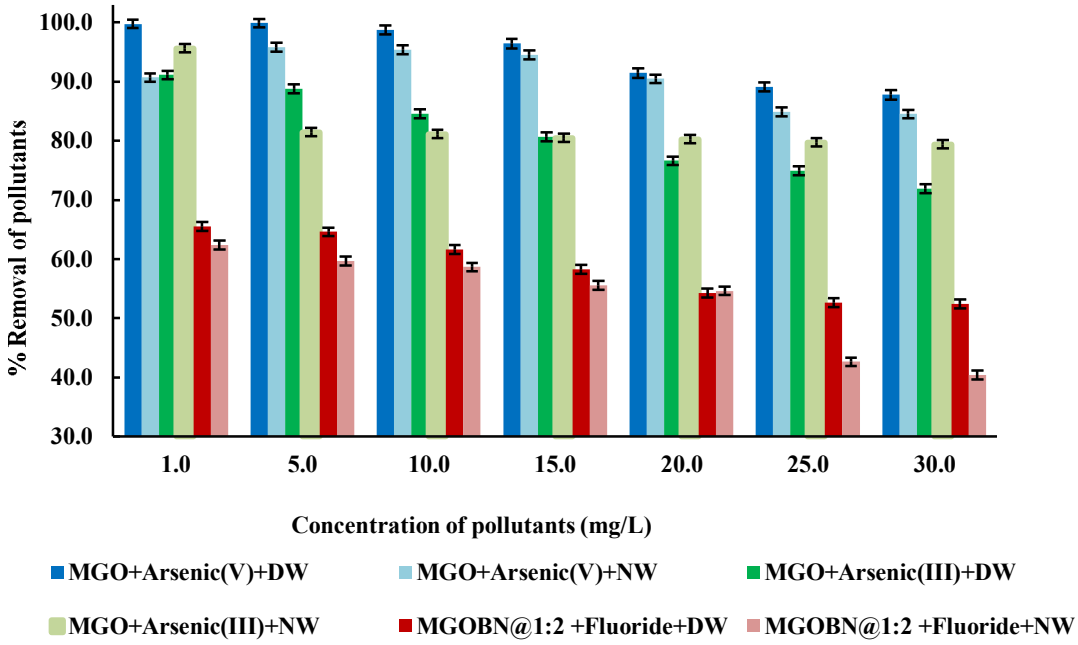

Figure 3.17: Removal of arsenic (III), arsenic (V), and fluoride in distilled water (DW) and natural water (NW) samples using MGO and MGOBN@1:2 materials at varied sorptive concentrations (Pollutants concentration: 10.0 mg/L; pH: 3.0 @ arsenic (III) & arsenic (V), and 4.1 for fluoride, solid dose: 2.0 g/L; temperature: 25±1°C, agitation speed:180 rpm).

3.6. Regeneration and reusability of solid materials

The reusability of adsorbent and preconcentration of pollutant species addresses the issues of disposal of used adsorbents, which protects the environment and saves the input cost, time, and energy to achieve a sustainable solution for wastewater handling.

Phosphate solution was used for the desorption of the preloaded arsenic (III) and arsenic (V) from the MGO solid and acetate solution for fluoride from

MGOBN@1:2 at wide concentrations range from 0.05, 0.01, and 0.1 mol/L. Higher desorption was obtained using the 0.05 M phosphate solution for the pre-adsorbed arsenic (III) and arsenic (V) from MGO solid, whereas 0.01 mol/L of acetate solution show better desorption for fluoride. The phosphate solution (0.05 mol/L) in 120 mins of contact could shows the desorption percentages of 98 and 99 respectively for the arsenic (III) and arsenic (V). Similarly, 97% desorption occurred for fluoride in 120 mins of contact. Further, Figure 3.18 (a&b) shows the reusability of these solids for 5 repeated cycles. Results showed that the efficiency of MGO was only decreased from 82.34 to 77.58% for arsenic (III) and from 98.85% to 96.11% for arsenic (V) from 1^{st} to 5^{th} cycle of operation. On the other hand, the efficiency of MGOBN@1:2 decreased only from 62.23 to 54.86% in removing fluoride at the end of 5^{th} repeated cycle of operation. These results pointed to the wide applicability of solids and solids have shown greater stability in the sorption/desorption operations. Similar results were obtained in the elimination of arsenic (V) by 3-marcaptopropyl trimetoxysilane (CHMS) and trimethoxy-octylsilane (CHTS). A high recovery of pollutant was obtained using the 0.2 mol/L H_3PO_4 solution and the solids were efficiently utilized for several cycles of adsorption/desorption operations (Lalhmunsiama et al., 2016). The removal of fluoride by the zirconium-based metal organic framework (MOF-801) showed that the solid was efficiently regenerated using the 0.1 mol/L NaOH solution. However, the removal efficiency of MOF for fluoride was decreased in the subsequent adsorption/desorption operations (Ling Tan et al., 2020).

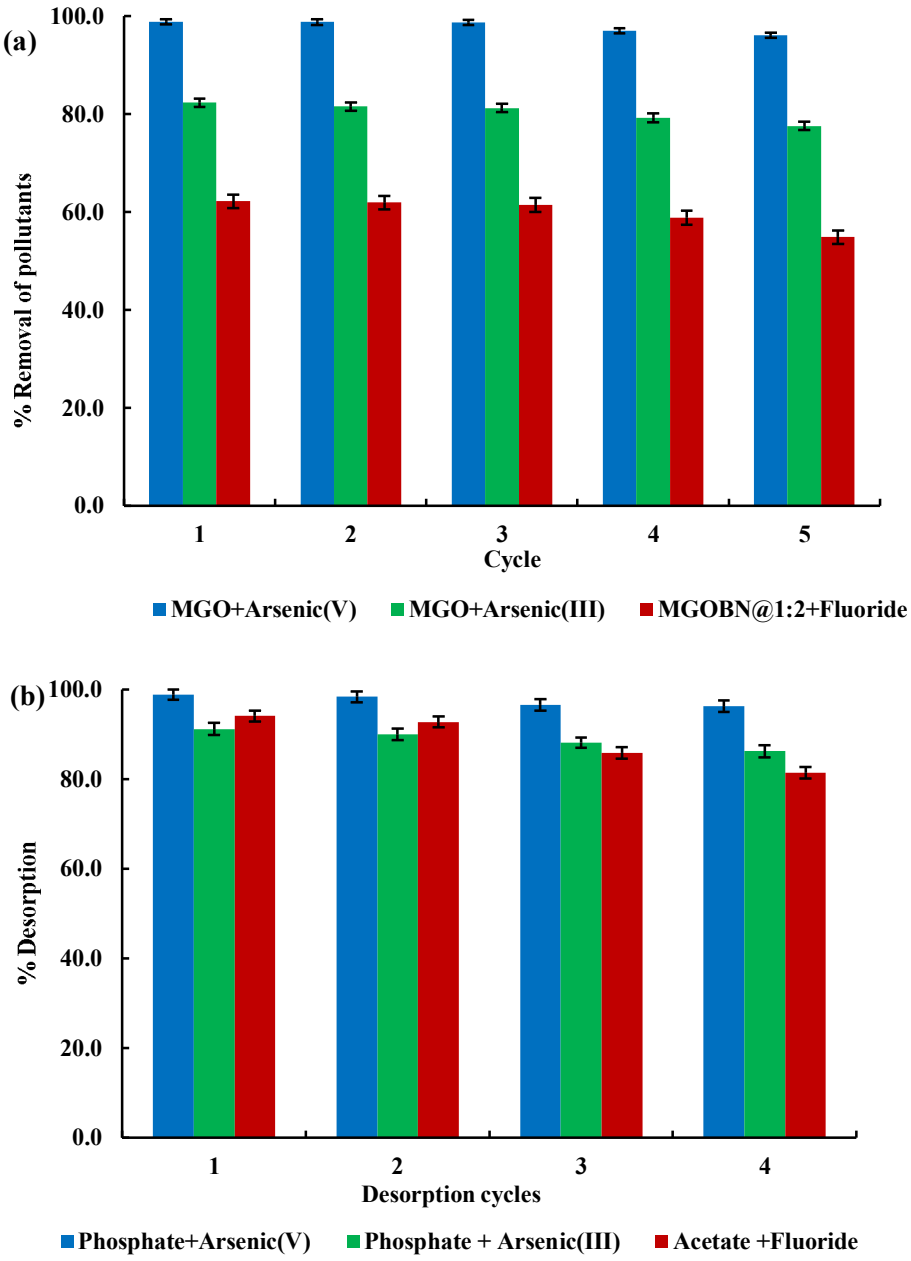

Figure 3.18: (a) Repeated use of MGO, and MGOBN@1:2 materials in the removal of arsenic (III), arsenic (V), and fluoride. (Pollutant concentration: 10.0 mg/L; pH: 3.0 for arsenic (III) & arsenic (V), 4.1 for fluoride, solid dose: 2.0 g/L; temperature: 25°C, agitation speed: 180 rpm; desorptive solution: acetate (0.01M) for fluoride and 0.05M phosphate (0.05M) for arsenic (III) and arsenic (V)); and **(b)** Percentage desorption of pollutants in a repeated cycle of desorptions using acetate (0.01 M) and phosphate solutions (0.05 M).

3.7. Application of MGO in the remediation of CCA

Chromated copper arsenate (CCA) bamboo chips were collected from The Lakher Pioneer Mission,1905, LORRAIN Bungalow, Serkawr, Siaha District, Mizoram, India. The aqueous solutions of the CCA was subjected for the determination of total chromium, arsenic and copper and found to be 1.97 mg/L, 6.07 µg/L, and 0.13 mg/L, respectively. For each 10 mL of CCA solution, 1.0, 2.0, and 5.0 mg of MGO was added and kept in a shaker for 24 hrs. The solution mixture was filtered and again subjected for the concentration of chromium, arsenic, and copper. Hence, the percentage removal of these elements was obtained and shown in Figure 3.19. It is almost 100% of these ions were removed using an optimum dose of 5.0 mg/L of MGO solid. These results inferred that the solid showed reasonably high efficiency in the remediation of water contaminated with multiple pollutants.

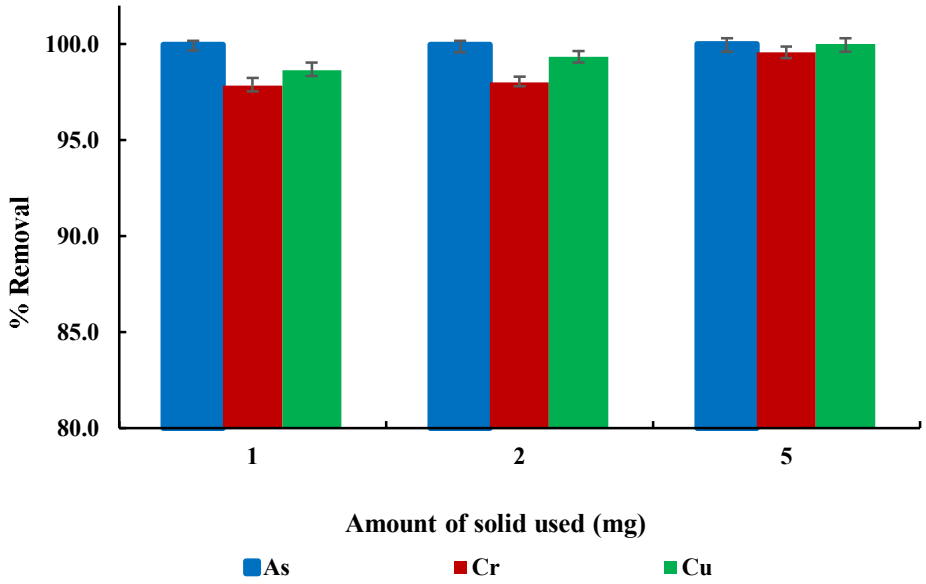

Figure 3.19: Removal of arsenic, copper, and chromium from CCA solution using various doses of MGO nanocomposite [pH of CCA solution: 3.0; contact time: 4 h; temperature: 25±1°C, agitation speed:180 rpm].

3.8. BATCH REACTOR STUDIES FOR LEAD (II) AND CHROMIUM (VI) REMOVAL

3.8.1. Effect of pH

The pH dependence sorption relates the impact on the charges and states of the functional groups both on the sorbent and the sorbate. The sorption of lead (II) by the BN, GO, MGO, and MGOBN materials were determined, and the percent elimination of lead (II) at varied pH is graphically shown in Figures 3.20 (a). The sorption results showed that increasing the pH from 2.0 to 6.0 significantly favored the uptake of lead (II) using these solids. Quantitatively, at pH ~2.0 the uptake of lead (II) was *Ca.* 22% and almost 100% sorption was achieved at pH ~4.0 using the solids GO, MGO, and MGOBN. Further increase in pH>4.0, the high uptake of lead (II) was almost unaffected until pH ~6.0. The sharp increase in lead (II) uptake from pH 2.0 to 4.0 is demonstrated with the speciation of lead (II) and the surface behavior of solids. Previous studies indicated that lead (II) is predominantly present with its ionic species of Pb^{2+} until pH 5.7 and pH>5.7 starts forming the $Pb(OH)_2$ species (D. Tiwari et al., 2007a). On the other hand, the GO, MGO, and MGOBN solids showed the pH_{PZC} values of 6.8, 4.0, 6.5, and 5.3, respectively. This indicated that the surface is positively charged at the pH <pH_{PZC} and negatively charged at pH>pH_{PZC}. The low percentage elimination of lead (II) at lower pH values i.e., pH ~2.0 is explicable due to the strong electrostatic repulsion between the positively charged surface and Pb^{2+} ions, which hindered significantly the elimination of lead (II). Moreover, the GO, MGO, and MGOBN surface active sites are predominantly occupied by hydrogen ions (H^+) at low pH and restricted the sorption of lead (II) by these solids. However, further increase in pH (pH>3.0), a sharp increase in lead (II) elimination is recorded. This showed the affinity of the solid towards the lead (II) ions. Moreover, the carboxyl groups on the surface of GO, MGO, and MGOBN is partially deprotonated with an increase in pH hence, increases the surface negative charge. This enables to attract the Pb^{2+} ions towards the surface and resulted with the complexation at the surface-active sites. A plausible mechanism is demonstrated with the ion-exchange surface complexation of lead (II) at the solid surface (Equation 3.2).

$$\equiv X\text{-}COOH + Pb^{2+} \rightarrow \equiv X\text{-}COO\text{-}Pb^{+} + H^{+} \quad \ldots(3.2)$$

It was also recorded that the final pH values (after adsorption) are found lower than the initial sorptive solution pH. Hence, the 'ion-exchange' process (Equation 3.2) demonstrated the release of H^+ ions and lowered the solution pH with lead (II) sorption. The use of a few layered graphene oxide (FGO) showed an increase in lead (II) sorption, increasing the solution pH (Zhao et al., 2011a).

On the other hand, the percentage elimination of lead (II) by the bentonite solid was only *Ca* 25% at pH ~2.0 and increased to a maximum of 45% at pH ~5.0. This pointed to the potential of nanocomposite materials in the efficient elimination of lead (II) in an aqueous medium at moderate pH values.

Similarly, the sorption efficiency of BN, GO, MGO, and MGOBN solids for chromium (VI) at varied pH values are shown in figure 3.20 (b). It is evident from the graph that with an increase in pH, the removal percentage of chromium (VI) is, in general, decreased using the GO, MGO, and MGOBN solids. The solids GO, MGO, and MGOBN showed almost 100% removal of chromium (VI) at pH ~2.0. However, a further increase in pH>2.0 caused for a gradual decrease in the percentage elimination of chromium (VI) using the MGO, and MGOBN solids. However, increasing the pH from 2.0 to 4.2, the high percentage elimination of chromium (VI) was almost unaffected using the GO solid. This indicated the higher affinity of GO towards chromium (VI). The decrease in percentage uptake of chromium (VI) at pH>2.0 by the solids MGO, and MGOBN is explained by the speciation of chromium ions in solution at varied pH values. It was reported previously that the anionic species *viz.*, CrO_4^{2-}, $HCrO_4^-$, or $Cr_2O_7^{2-}$ of chromium (VI) are predominantly present in aqueous medium within pH region 2-10 (Lee et al., 2016). However, within pH region 2.0 to 5.5, the $HCrO_4^-$ species are dominantly present, and with further increase in pH>5.5, the CrO_4^{2-} predominantly exists. The high uptake of chromium at lower pH values is explicable with the fact that the negatively charged sorbate ions are electrostatically attracted by the positively charged surface resulting in high percentage elimination of chromium (VI). However, a gradual increase in pH resulted with the dissociation of carboxyl and hydroxyl groups present at the solid surface resulted with gradual increase in negative charge at the surface which hindered the uptake of chromium (VI) by these solids. Moreover, at pH ~7.0 the surface carries net negative charge (i.e., $pH>pH_{PZC}$) and chromium (VI) also present with its fully dissociated CrO_4^{2-} species

which caused for strong electrostatic repulsive forces and led to significant decrease in chromium (VI) elimination by these solids. Additionally, at higher pH values, the hydroxyl ions preferentially compete the chromium oxyanions for solid surface and caused for decrease in chromium (VI) sorption by these solids (Lee et al., 2016). The high removal efficacy of magnetic-graphene oxide (MGO) was obtained for chromium (VI) at low pH values. It was demonstrated that a strong electrostatic interactions occurred between the negatively charged $HCrO_4^-$, or $Cr_2O_7^{2-}$ species and positively charged MGO surface which facilitated an enhanced removal efficiency of solid at low pH values (Neolaka et al., 2020).

It is interesting to observe that the sorption of chromium (VI) is significantly low using the pristine bentonite compared to the nanocomposite materials *viz.*, GO, MGO and MGOBN. This again indicated the applicability of nanocomposite solids in the efficient elimination of chromium (VI) from aqueous medium.

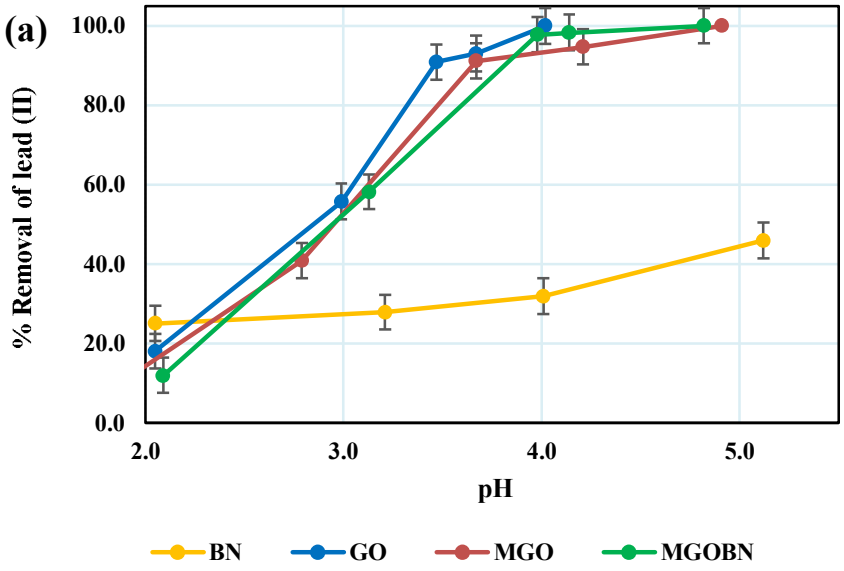

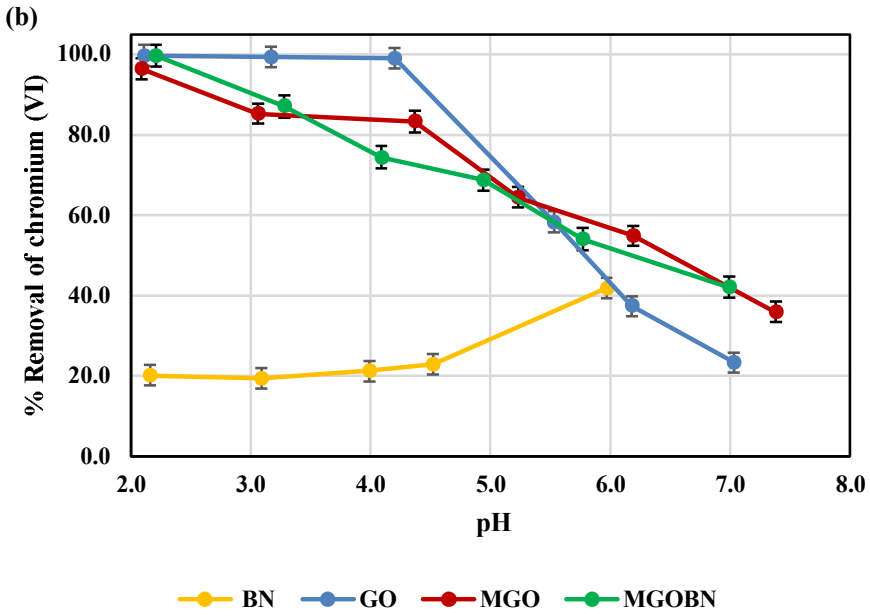

Figure 3.20: Effect of pH in the removal of **(a)** lead (II); and **(b)** chromium (VI) by BN, GO, MGO, and MGOBN solids ([Pollutants]: 10.0 mg/L; Solids dose: 2.0 g/L).

3.8.2. Effect of sorptive concentration

The sorption of lead (II) and chromium (VI) by the nanocomposite solid MGOBN was studied by varying the initial pollutant's concentrations from 1.0 to 30.0 mg/L at a constant equilibrium pH of 4.0 for lead (II), and 3.6 for chromium (VI). Figure 3.21 displays the equilibrium stage percent elimination and equilibrium extent of pollutant removal (q_e) against the initial concentration of the pollutants. The concentration dependence results clearly showed that increasing the lead (II) and chromium (VI) concentrations from 1.0 to 30.0 mg/L had caused an apparent decrease in the percentage removal of these two ions. However, a similar increase in pollutant concentrations favored the extent of removal of these two ions i.e., lead (II) and chromium (VI) utilizing the MGOBN. Quantitatively, increasing the pollutant concentration from 1.0 to 30.0 mg/L the percentage elimination was decreased from 100 to 85% (for lead (II)) and from 97 to 33% for chromium (VI), respectively. Similarly, the extent of removal was increased from 0.493 to 12.755 mg/g (for lead (II)) and 0.50 to 4.987 mg/g (for chromium (VI)) respectively for the increase in

respective pollutant's concentrations from 1.0 to 30.0 mg/L. The high removal extent at high initial concentration is explicable due to the reason that at higher sorbate concentrations propelling force is high which breaks the mass transfer barriers at the interface, leading to a greater extent of lead (II) and chromium (VI) removal (Tiwari et al., 1999; Lee et al., 2010). It is further noted that the percentage removal of lead (II) is less affected with an increase in lead (II) concentration which demonstrated the high affinity of lead (II) towards the nanocomposite solid (Dang et al., 2009). On the other hand, the percentage removal of chromium (VI) is significantly decreased with an increase in chromium (VI) concentrations. This is explicable with the reason that at higher sorbate concentrations relatively lesser number of active sites are available for large number of sorbate ions, resulting in decrease in the percentage elimination of chromium (VI). Similar results were obtained using several functionalized chitosan biomaterials in the removal of chromium (VI) (Lee et al., 2016b).

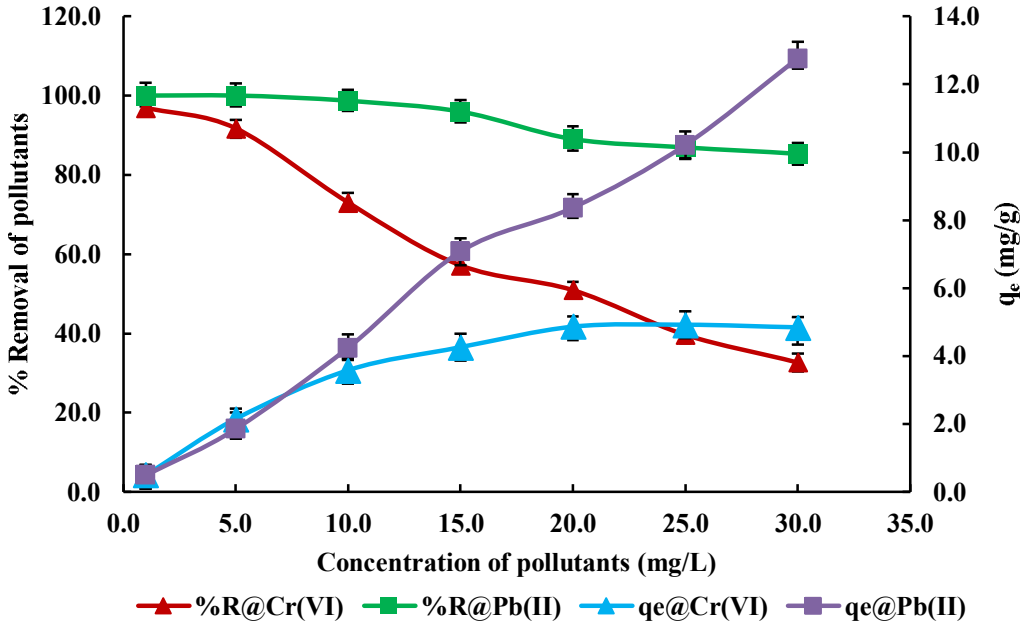

Figure 3.21: Effect of sorptive concentrations in the removal of lead (II) and chromium (VI) using MGOBN [pH: 4.0 for lead (II), 3.6 for chromium (VI); Solid dose: 2.0 g/L].

3.8.2.1. Adsorption isotherm modeling

The equilibrium state sorption results are utilized to model with the known adsorption isotherms *viz.*, Freundlich, Langmuir, and Sips to their non-linear forms as shown in Chapter 2, section 2.4 (Equation (2.2, 2.3, and 2.4)). The modeling results are represented in Figure 3.22. The optimized isotherm parameters along with the least square sums are included in Table 3.10. The results showed that the equilibrium state lead (II) sorption is not fitted well with the Langmuir or Freundlich isotherms however, agreed well with the Sips isotherm since the least square sum is relatively low and the removal capacity was 32.484 mg/g. On the other hand, the chromium (VI) sorption data is fitted well to the Langmuir ($s^2 = 0.485$) as well as Sips isotherms ($s^2 = 0.829$) with the removal capacity of 5.17 mg/g by Sips isotherm. Higher value of the Langmuir constant (K_L) showed the affinity of MGOBN towards the sorbate species, and the fractional value of the Freundlich constant (1/n); ($0 < 1/n > 1$) implied the heterogeneous surface structure of MGOBN with an exponential distribution of active sites (Lalhmunsiama, Lalchhingpuii, et al., 2016c). The maximum elimination capacity of MGOBN for lead (II), and chromium (VI) is compared with several other materials and summarized in Table 3.11. It is evident from the table that the nanocomposite MGOBN material possessed a relatively high elimination capacity for these ions compared to several other materials, hence, showed potential in the remediation of water contaminated with these pollutant ions.

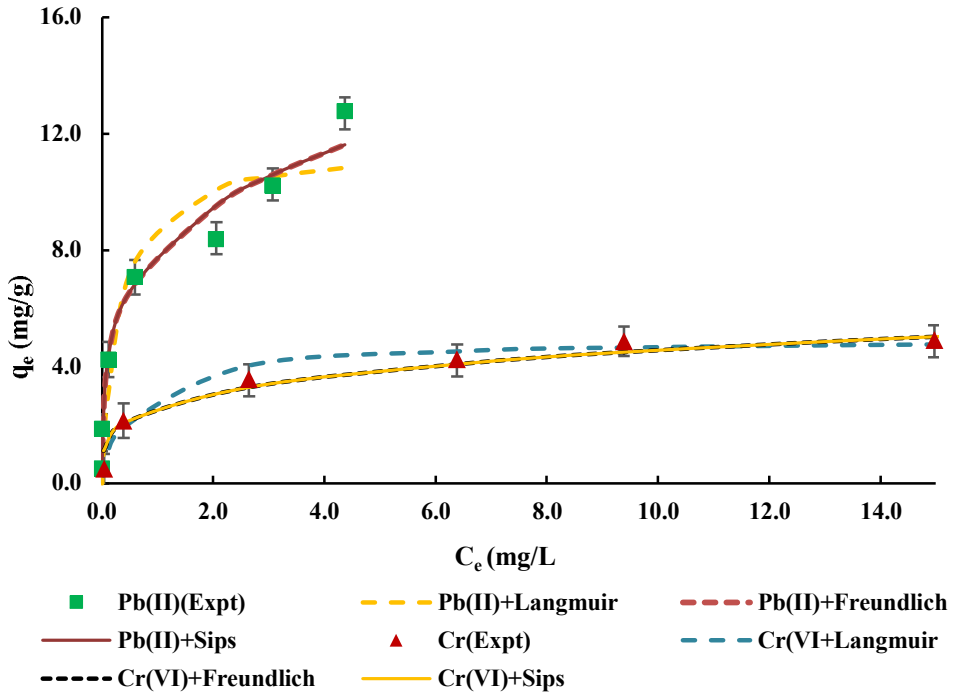

Figure 3.22: Langmuir, Freundlich and Sips isotherms for the sorption of lead (II), and chromium (VI) using MGOBN [pH: 4.0 for lead (II), 3.6 for chromium (VI); Solid dose: 2.0 g/L].

Table 3.10: Isotherm parameters of Langmuir, Freundlich, and Sips for the sorption of lead (II), and chromium (VI) by MGOBN along with its least sum square value.

Material	Parameters		Pollutants	
			Lead (II)	Chromium (VI)
			pH	
			4.0	3.6
MGOBN	Langmuir	q_o (mg/g)	11.58 ± 0.93	4.96 ± 0.32
		K_L (L/g)	3.22 ± 0.31	1.61 ± 0.12
		s^2	11.90	0.45
	Freundlich	1/n	0.26 ± 0.01	0.24 ± 0.02
		K_F (mg/g)	7.85 ± 1.05	2.59 ± 0.44
		s^2	4.24	0.82
	Sips	q_m (mg/g)	32.84 ± 1.91	5.17 ± 0.72
		K_s	0.004 ± 0.001	0.029 ± 0.010
		n_s	0.26 ± 0.01	0.24 ± 0.01
		s^2	4.30	0.82

Table 3.11: Sorption capacity of MGOBN and several other materials in the elimination of lead (II), and chromium (VI).

Pollutants	Adsorbent	pH	q_m (mg/g)	References
Lead (II)	Graphene Nanosheets (GNS)	4.0	22.42	(Huang et al., 2011)
	Organo-mineral complexes (OMC)	7.0	1.587	(Fan et al., 2017)
	Raw multi-walled carbon nanotubes (MWCNTs)	5.7-6	6.7	(Tehrani et al., 2014)
	Oxidized multi-walled carbon nanotubes (MWCNTs)		27.8	
	Mesoporous silica (AMS)	5	4.57	(Lalchhingpuii et al., 2017b)
	Sericite	5.5	4.69	(Tiwari et al., 2007a)
	Magnetite graphene oxide clay nanocomposite (MGOBN)	**4.0**	**32.848**	**Present study**
Chromium (VI)	Rice husk ash(RHA)	2	0.49	(Wongjunda and Saueprasea, 2010)
	Modified rice husk ash(MRHA)		0.84	
	Granular activated carbon - Filtrasorb 400 (GAC-F400)	-	0.18	(Han et al., 2000)
	Granular activated carbon - LB 830 (GAC-LB830)	-	0.13	
	Dust coal	3.0-4.0	4.4	(Selomulya et al., 1999)
	Wood	2.0	5.1	
	Saw dust (SD)	5	1	(Ansari and Fahim, 2007)
	Polypyrrole coated saw dust (PPY/SD)		3.4	
	Magnetite graphene oxide clay nanocomposites (MGOBN)	**3.6**	**5.171**	**Present Study**

s^2: Least square sum

3.8.2.2. Simultaneous elimination of lead (II) & chromium (VI) using MGOBN and arsenic (V) & lead, arsenic (V) & chromium (VI) using MGO

The concentration dependence sorption of pollutants by the MGOBN and MGO solids was modelled with the Sips Equation. The simultaneous sorption of lead (II) and chromium (VI) at pH 3.7 was performed using the MGOBN, whereas arsenic (V) and lead (II) at pH 4.0, and arsenic (V) and chromium (VI) at pH 3.0 were carried out using the MGO solid material to expand and study the applicability of prepared MGO solid material towards the simultaneous removal of these pollutants. Figure 3.23 (a) displays graphically the non-linear fits of the sorption data to the Sips equation (Equation (2.4)). Further, the Sips isotherm parameters, *viz*., q_m, K_S, and n_s, were optimized for these pollutants individually and tabulated in Table 3.12. The adsorption capacity of lead (II) (32.128 mg/g) was found relatively high compared to the chromium (VI) (4.562 mg/g) at pH 3.7 with the K_s value of 0.002 and 0.011 for lead (II) and chromium (VI), respectively. The K_s values obtained for the individual ions were further used for the simulation studies in binary systems. Arsenic (V) and lead (II) at pH 4.0 shows a sorption capacity of 87.543 mg/g and 36.157 mg/g, respectively. Additionally, the removal of arsenic (V) and chromium (VI) at pH 3.0 was conducted and the sorption capacity was found to be 40.082 mg/g and 18.179 mg/g for arsenic (V) and chromium (VI), respectively. The Sips fitting agrees well to demonstrate the sorption results in these systems.

Furthermore, the expanded Sips equation is used for the binary component systems in the simultaneous removal of several systems. The K_s values obtained for the single component systems were used in the Sips equation simulation. The lead (II) and chromium (VI) simultaneous sorption results along with the Sips modelled graphs are shown in Figure 3.23 (b). The quantitative simulated data is shown in Table 3.13. The derived parameters indicated that the sorption capacities of lead (II), and chromium (VI) at pH 3.7 was found to be 27.53 mg/g and 25.15 mg/g, respectively for the lead (II) and chromium (VI) molar ratios of 1:1. It is interesting to observe that relatively higher removal capacity of lead (II) and chromium (VI) was achieved at the 2:1 ratio of lead (II) to chromium (VI) with the adsorption capacity of 77.42 mg/g and 28.18 mg/g respectively. However, for the molar ratio 1:2, apparently, the sorption

capacity of both the pollutants were decreased i.e., 24.12 mg/g and 19.19 mg/g for lead (II) and chromium (VI) compared to the 1:1 and 2:1 ratios of lead (II) to chromium (VI). Similarly, the simultaneous removal of arsenic (V) and lead (II) and the arsenic (V) and chromium (VI) were studied and graphically represented in Figure 3.23 (c&d). The sorption was carried out using the MGO nanomaterial. Arsenic (V), and lead (II) removal efficacy for the 1:1 ratio was found to be 52.71, and 88.05 mg/g, respectively. However, the 1:2 ratio of arsenic (V) to lead (II) showed a significant decrease in the sorption capacities with 47.57 and 39.42 mg/g, respectively for arsenic (V) to lead (II). However, the 2:1 ratio caused a significant increase in elimination capacity of 104.78 and 43.597 mg/g, respectively for arsenic (V) to lead (II). Likewise, the removal efficiency of arsenic (V) and chromium (VI) was observed in the binary system of arsenic (V) and chromium (VI) and found to be 75.86 mg/g and 22.18 mg/g for 1:1 molar ratio of arsenic (V) to chromium (VI), which further increased for the 2:1 ratio with the removal capacities of 107.06 mg/g and 26.38 mg/g. The decrease and increase in the removal capacity are explained by the availability of surface-active sites and preferential sorption for sorbate ions (Thanhmingliana et al., 2016).

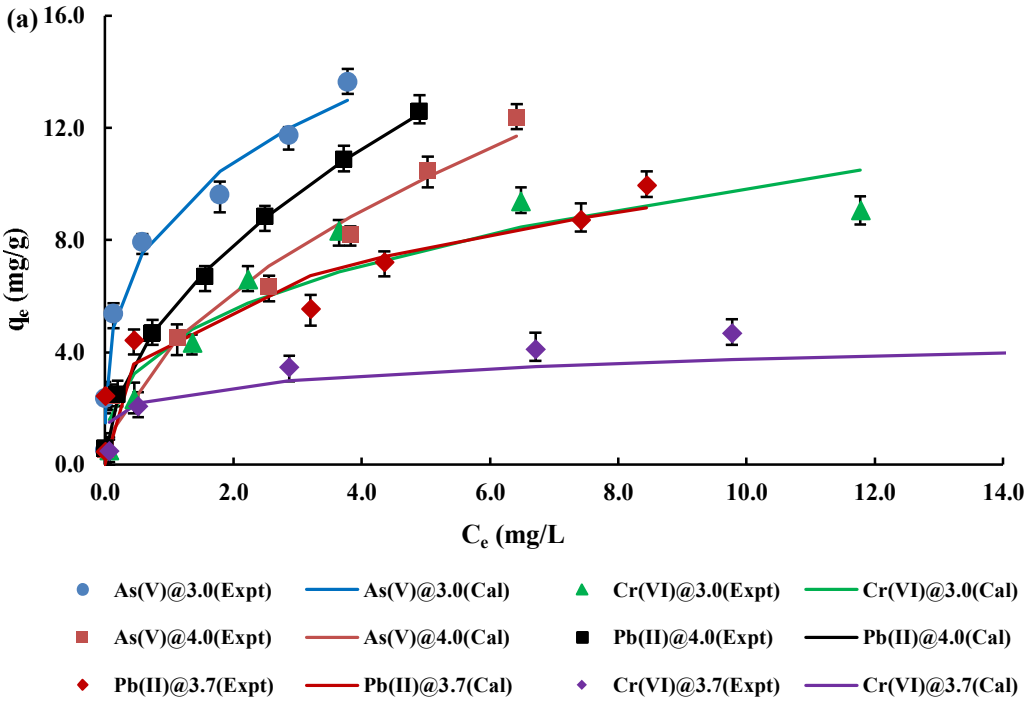

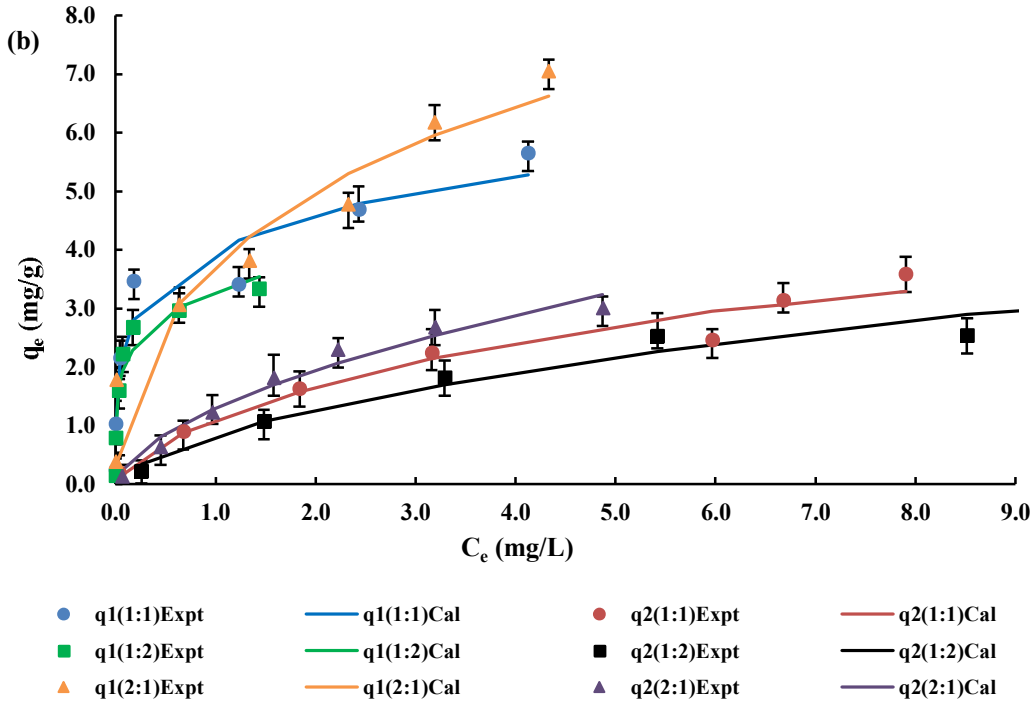
(b)
8.0
7.0
6.0
5.0
4.0
3.0
2.0
1.0
0.0
q_e (mg/g)
0.0
1.0
2.0
3.0
4.0
5.0
6.0
7.0
8.0
9.0
C_e (mg/L)
q1(1:1)Expt
q1(1:1)Cal
q2(1:1)Expt
q2(1:1)Cal
q1(1:2)Expt
q1(1:2)Cal
q2(1:2)Expt
q2(1:2)Cal
q1(2:1)Expt
q1(2:1)Cal
q2(2:1)Expt
q2(2:1)Cal

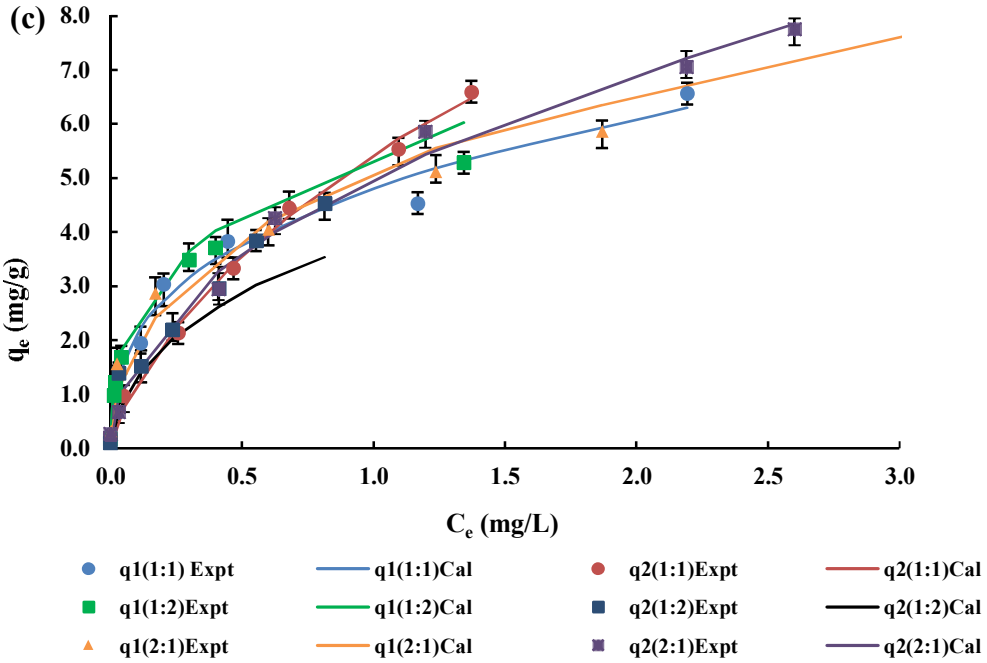
(c)
8.0
7.0
6.0
5.0
4.0
3.0
2.0
1.0
0.0
q_e (mg/g)
0.0
0.5
1.0
1.5
2.0
2.5
3.0
C_e (mg/L)
q1(1:1) Expt
q1(1:1)Cal
q2(1:1)Expt
q2(1:1)Cal
q1(1:2)Expt
q1(1:2)Cal
q2(1:2)Expt
q2(1:2)Cal
q1(2:1)Expt
q1(2:1)Cal
q2(2:1)Expt
q2(2:1)Cal

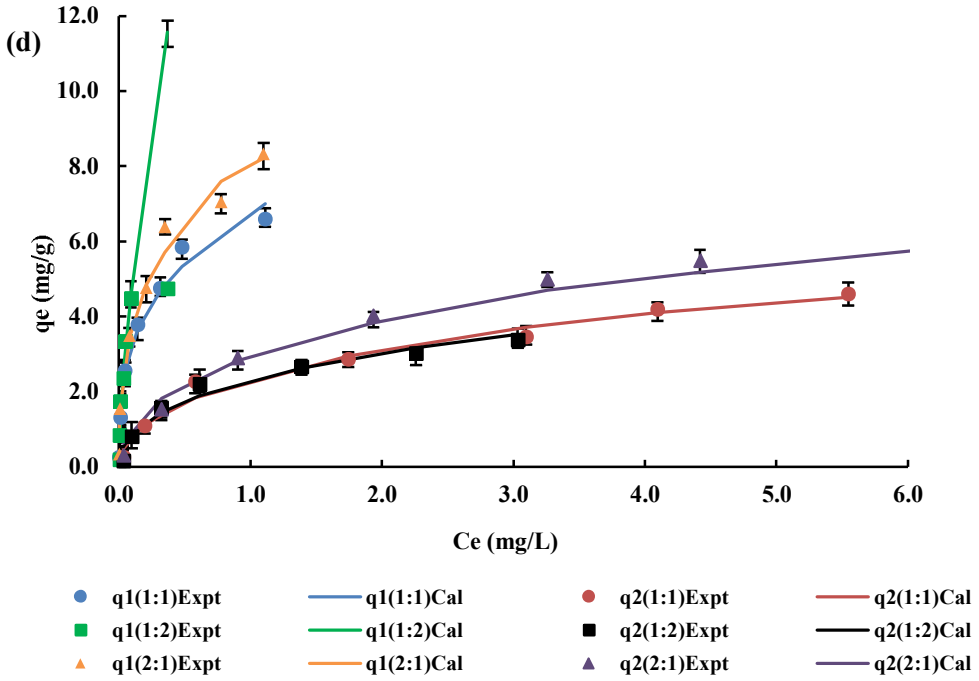

Figure 3.23: (a) Sips isotherm modeling for the sorption of lead (II) (pH: 3.7 and 4.0), Cr (VI) (pH: 3.7 and 3.0), and As (V) (pH: 3.0 and 4.0) in the single component system; expanded Sips modelling for the binary systems for the simultaneous removal at varied molar ratios of **(b)** lead (II) and chromium (VI) (pH: 3.7) where q1: adsorption capacity of Pb (II) in Pb:Cr, q2: adsorption capacity of Cr (VI) in Pb:Cr using MGOBN; **(c)** arsenic (V) and lead (II) (pH: 4.0) where q1: adsorption capacity of As (V) in As:Pb, q2: adsorption capacity of Pb (II) in As:Pb using MGO; and **(d)** arsenic (V) and chromium (VI)) (pH: 3.0) using MGO solid where q1: adsorption capacity of As (V) in As:Cr, q2: adsorption capacity of Cr (VI) in As:Cr

Table 3.12: Sips Isotherm parameters for lead (II), chromium (VI), and arsenic (V) along with the least square sum value.

Pollutants	pH	Materials	Sips			
			q_m (mg/g)	K_s	n_s	s^2
Lead (II)	3.7	MGOBN	32.12 ± 1.03	0.002 ± 0.001	0.32 ± 0.02	8.913
	4.0	MGO	36.15 ± 1.02	0.025 ± 0.002	0.52 ± 0.02	0.115
Chromium (VI)	3.0	MGO	18.17 ± 0.92	0.015 ± 0.001	0.36 ± 0.01	7.977
	3.7	MGOBN	4.56 ± 0.13	0.011 ± 0.001	0.18 ± 0.01	5.697
Arsenic (V)	3.0	MGO	40.08 ± 1.72	0.005 ± 0.002	0.29 ± 0.02	2.766
	4.0	MGO	87.54 ± 2.11	0.004 ± 0.003	0.55 ± 0.03	3.190

s^2: Least square sum

Table 3.13: Isotherm parameters for lead (II) and chromium (VI), arsenic (V) and lead (II), and arsenic (V) and chromium (VI) dual-components system using binary sips equation along with the least square sum value.

pH	Adsorbent	Pollutants			Parameters		
					q_m (mg/g)	n_s	s^2
3.7	MGOBN	Pb(II): Cr(VI	Pb(II) Pb(II)+Cr(VI)	1:1	27.53 ± 1.91	0.26 ± 0.02	1.91
				1:2	24.12 ± 1.02	0.26 ± 0.01	0.93
				2:1	77.42 ± 2.33	0.47 ± 0.11	2.99
			Cr(VI) Pb(II)+Cr(VI)	1:1	25.15 ± 1.42	0.67 ± 0.05	1.91
				1:2	19.19 ± 1.02	0.68 ± 0.04	0.93
				2:1	28.18 ± 2.01	0.66 ± 0.03	2.99
4.0	MGO	As(V): Pb(II)	As (V) As(V):Pb(II)	1:1	52.71 ± 3.02	0.40 ± 0.02	0.77
				1:2	47.57 ± 2.11	0.37 ± 0.01	2.38
				2:1	87.32 ± 3.03	0.47 ± 0.02	1.80
			Pb(II) As(V):Pb(II)	1:1	88.05 ± 3.02	0.71± 0.05	0.77
				1:2	39.42 ± 2.21	0.56 ± 0.04	2.38
				2:1	26.90 ± 1.93	0.47 ± 0.01	1.80
3.0	MGO	As(V): Cr(VI)	As (V) As(V):Cr(VI)	1:1	75.86 ± 3.33	0.39 ± 0.04	1.20
				1:2	112.35 ± 4.02	0.69 ± 0.06	0.88
				2:1	107.06 ± 4.04	0.42 ± 0.02	1.74
			Cr (VI) As(V):Cr(VI)	1:1	22.18 ± 2.01	0.49 ± 0.03	1.20
				1:2	18.40 ± 1.94	0.46 ± 0.01	0.88
				2:1	26.38 ± 2.01	0.48 ± 0.01	1.74

s^2: Least square sum

3.8.3. Effect of contact time

The time dependence sorption of lead (II) and chromium (VI) by MGOBN composites was conducted at pH 4.0 for lead (II) and 3.6 for chromium (VI) by varying the contact time from 1 to 1080 mins while keeping the initial pollutant's concentrations 10.0 mg/L. The sorption results are represented in Figure 3.24 (a). Results inferred that during the initial period of contact, a fast and rapid sorption of

these two ions took place and almost 90% of lead (II) was sorbed within 10 mins of contact, whereas within 60 mins of contact, almost 53% of chromium (VI) was sorbed. This inferred that the sorbate ions quickly occupied the active sites available at the surface of solid. Further, an apparent solid/solution equilibrium was obtained within *Ca.* 720 minutes of contact.

The kinetic data for the sorption of lead (II) and chromium (VI) by the MGOBN is utilized to fit with the known pseudo-first-order (PFO), pseudo-second-order (PSO), and fractal-like pseudo-second-order (FL-PSO) models as shown in Chapter 2, section 2.4 (Equation (2.2, 2.3, and 2.4)) (Thanhmingliana & Tiwari, 2015a) and results are represented in Figure 3.24 (b). The least-square fitting was conducted to optimize the kinetic parameters and the optimized parameters are included in Table 3.14. The fitting results showed that the kinetic data is well fitted to the pseudo-second-order model and fractal-like pseudo-second-order models compared to the pseudo-first-order equation for both leads (II), and chromium (VI). The fitting of PSO or FL-PSO indicated that the sorbate species are bound relatively with stronger forces at the MGOBN surface (Zhang et al., 2016). The sorption of lead (II) by the magnetic graphene oxide-EDTA functionalized material followed pseudo-second-order kinetics with the k_2 value of 0.0014 (g/mg/min), and q_e value of 476.2 (mg/g) (Cui et al., 2015).

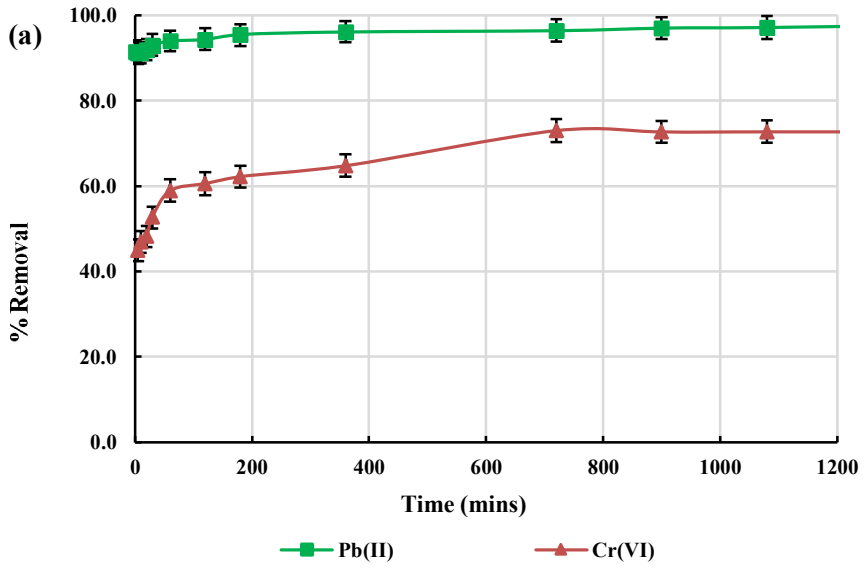

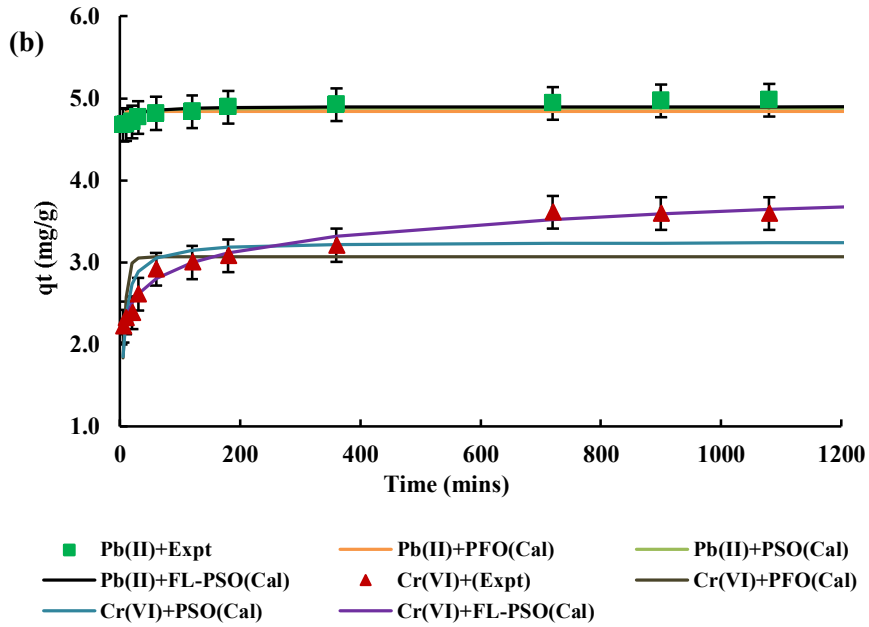

Figure 3.24: (a) Effect of contact time in the removal of lead (II), and chromium (VI) by MGOBN; **(b)** Pseudo-first-order, pseudo-second-order, and fractal-like pseudo-second-order kinetic fitting for the sorption of lead (II), and chromium (VI) using MGOBN [Pollutants]: 10.0 mg/L; pH: 4.0 @ lead (II), 3.6 @ chromium (VI); Solid dose: 2.0 g/L).

Table 3.14: Kinetics parameters for the sorption of lead (II), and chromium (VI) by MGOBN nanocomposite using PFO, PSO and FL-PSO kinetics models.

Pollutants	PFO			PSO			FL-PSO			
	k_1 (min^-)	q_e (mg/g)	s^2	k_2 (g/mg/min)	q_e (mg/g)	s^2	k (g/mg/min)	q_e (mg/g)	α	s^2
Pb (II)	0.65± 0.03	4.83 ± 0.62	0.08	0.66 ± 0.020	4.88 ± 0.63	0.03	0.78 ± 0.01	4.90 ± 0.51	0.81 ± 0.02	0.03
Cr (VI)	0.18 ± 0.01	3.06 ± 0.32	1.39	0.08 ± 0.002	3.25 ± 0.21	0.66	0.03 ± 0.001	7.89 ± 0.62	0.15 ± 0.01	0.05

s^2 : Least square sum

3.8.4. Effect of background electrolyte

The interaction of lead (II) and chromium (VI) at the surface of MGOBN was investigated by extending the studies for background electrolyte concentrations. The sodium chloride concentration was varied from 0.001 to 0.5 mol/L in the sorption of these two ions using MGOBN nanocomposites and results are shown in Figure 3.25. The results showed that a 500-fold increase in sodium chloride concentrations could not affect significantly the removal efficiency of lead (II). This indicated that the lead (II) ions are sorbed specifically on the solid surface and forming inner-sphere complexes at the surface (Lalhmunsiama et al., 2016). Similar results showed that the 1000 times increase in $NaNO_3$ concentrations could not affect significantly the sorption of lead (II) by the sericite (Tiwari et al., 2007a). On the other hand, the elimination of chromium (VI) was affected to some extent. Increasing the sodium chloride concentrations from 0.001 to 0.5 mol/L, the corresponding decrease in percentage elimination of chromium was from 68.6 to 51.1%. This indicated that the chromium (VI) is not predominantly sorbed with strong forces, but partly attached with the electrostatic and weaker forces at the MGOBN surface. The results are in line with the pH dependence studies demonstrated previously. In a study, increasing the NaCl concentrations from 0.001 mol/L to 0.1 mol/L caused for a decrease in sorption capacity from 20.8 mg/g to 8.5 mg/g, respectively in the elimination of chromium (VI) by modified hydrochar (MCH). This was suggested that the positively charged adsorbent sites and Na^+ ions compete for the negatively charged chromium (VI) ions, hence causing for a decrease in the sorption capacity of chromium (VI) (Ghanim et al., 2022).

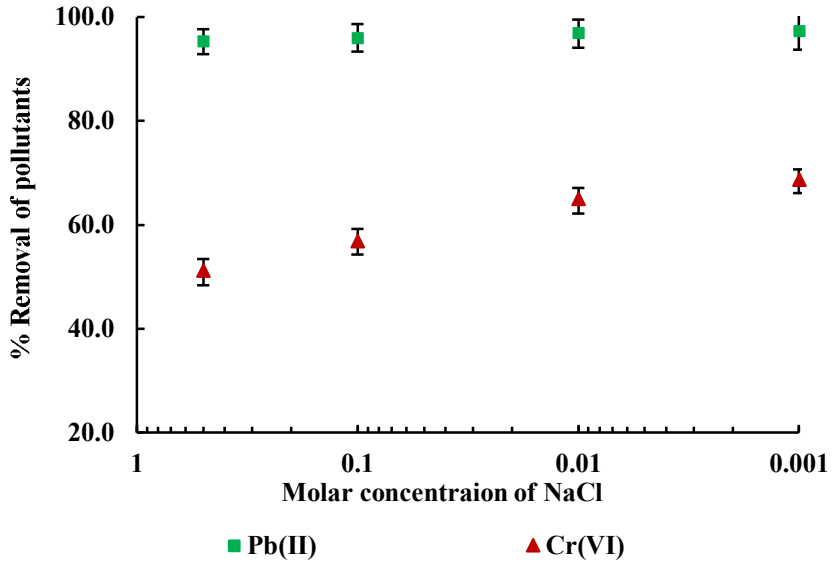

Figure 3.25: Effect of background electrolyte in the removal of lead (II), and chromium (VI). (Lead (II) and chromium (VI): 10.0 mg/L; NaCl concentrations: 0.001 to 0.5 mg/L; pH: 4.0 for lead (II) and 3.6 for chromium (VI); solid dose: 2.0 g/L).

3.8.5. Effect of co-existing ions

The sorption of lead (II) and chromium (VI) by MGOBN was performed in the presence of various cations and anions. The results are shown graphically in Figure 3.26. It is evident from the figure that the percentage elimination of lead (II) is suppressed to a greater extent in presence of cations *viz.*, Mg(II), Ca(II), Ni(II), and Mn(II). This decrease in removal percentage is primarily due to the competition between co-existing cations and lead (II) for the available active sites. It was reported previously that the metals' molecular mass, ion charges, hydrated ionic radius, and hydration energy, are the factors influencing the competitive sorption ability (Lv et al., 2005). On the other hand, the anions *viz.*, oxalic acid, phosphate, EDTA, and glycine are not significantly affected the sorption of lead (II) by the MGOBN. This showed greater affinity and selectivity of the solid towards the lead (II) sorption.

The percentage uptake of chromium (VI) is not significantly affected in the presence of cations however, the presence of anions (oxalic acid, phosphate, and EDTA) significantly suppressed the elimination of chromium (VI) using the MGOBN

nanocomposite. The oxalic acid, EDTA, and phosphate anions are possessed with larger charge densities than $HCrO_4^-$ anions hence, competes for the solid surface and suppressed the percentage elimination of chromium (VI). However, the presence of glycine did not hamper the removal of chromium (VI). The removal of chromium (VI) by the activated carbon showed a similar decrease in the presence of several anions, and explained that the increased charge density of the co-existing anions caused for a decrease in chromium sorption (Duranoğlu et al., 2012).

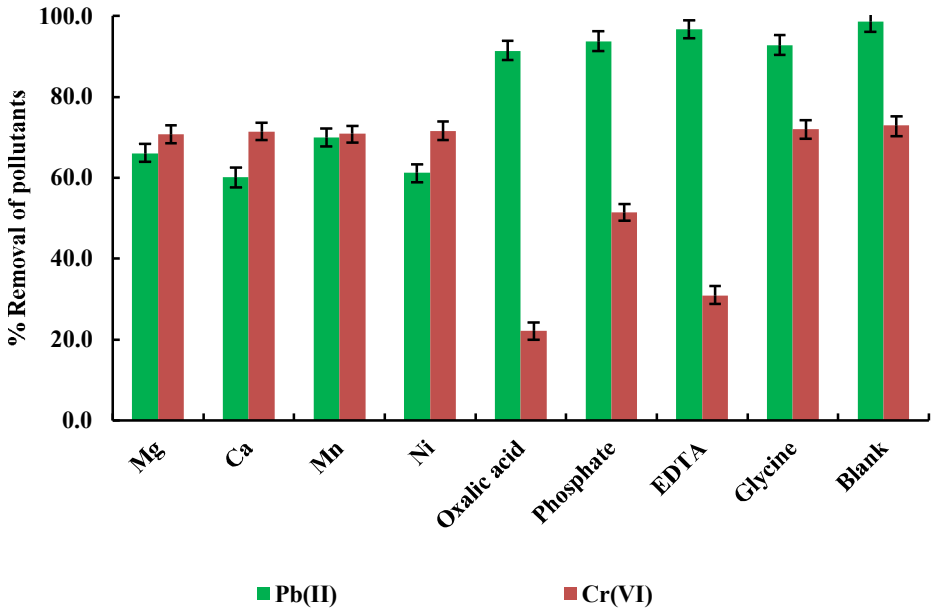

Figure 3.26: Effect of co-existing ions in the removal of lead (II) and chromium (VI) by MGOBN (Lead (II) and chromium (VI): 10.0 mg/L; co-ions concentrations: 50.0 mg/L; pH: 4.0 for lead (II) and 3.6 for chromium (VI); solid dose: 2.0 g/L).

3.9. The potential of MGOBN in a natural water matrix

A natural water sample was obtained from Pukpui waterfall in Aizawl and spiked with varied concentrations of lead (II) and chromium (VI) at different

concentrations of pH 4.0 for lead (II) and 3.6 for chromium (VI). The removal efficiency of nanocomposite solid in the removal of lead (II) and chromium (VI) was assessed in natural matrix samples and compared with similar results obtained with purified water. Prior to conduct the sorption experiments, the natural water was subjected for various physico-chemical parametric analyses and results are tabulated in *Cf* Table 3.1. The water sample contained with insignificant concentrations of Cu, Pb, Ni, and Al. However, relatively higher content of Ca and Mg were detected in water sample. The Ca and Mg contents were 37.0 and 4.0 mg/L, respectively. Similarly, a significant extent of inorganic carbon (16.396 mg/L) is present with lesser extent of non-purgeable organic carbon (NPOC) (1.434 mg/L) in the natural water sample. The phosphate (0.3 mg/L), and sulphates (4.0 mg/L) are present at very low levels. Figure 3.27 shows the sorption efficiency of MGOBN for lead (II) and chromium (VI) at varied pollutants' concentrations in natural water matrix along with the purified water sample. The results demonstrated that the removal efficiency of MGOBN for lead (II) and chromium (VI) elimination in a natural water sample is not considerably impacted as compared to the purified water. This pointed that the MGOBN displayed fair applicability and selectivity for attenuating the lead (II) and chromium (VI) in natural water samples.

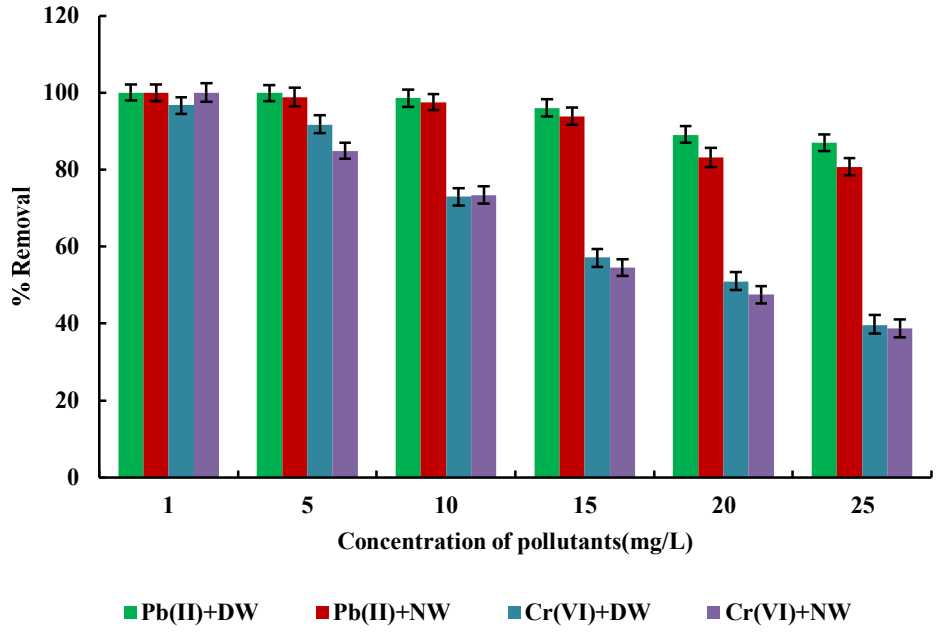

Figure 3.27: Removal of lead (II) and chromium (VI) in distilled water (DW) and natural water (NW) samples using MGOBN nanocomposite at varied sorptive concentrations (Pollutants concentration: 10.0 mg/L; pH: 4.0 for lead (II), and 3.6 for chromium (VI), solid dose: 2.0 g/L; temperature: 25±1°C, agitation speed:180 rpm).

3.10. Desorption and reusability studies

The reuse of an adsorbent is useful for sustainable implications of the materials in unit operations. The desorption studies were conducted using varied concentrations of HCl and H_2SO_4 (0.05 M, 0.01 M, and 0.1 M) to optimize the efficient desorption of pre-adsorbed metal ions at the nanocomposite solid.

The pre-adsorbed lead (II) and chromium (VI) from the MGOBN nanocomposite showed efficient desorption by using the 0.1 M HCl and 0.1 M H_2SO_4 solutions, respectively for the desorption of lead (II) and chromium (VI). It was noted that 99.3% of lead (II) was desorbed within 120 mins of contact using 0.1 M HCl solution, whereas 0.1 M H_2SO_4 solution desorbs 98.7% of chromium (VI) within 120 mins of contact. The material was employed for the successive cycles and results are shown in Figure 3.28, where the primary Y-axis represents the recovery percentage of these ions whereas the secondary Y-axis represents the sorption percentages at the successive cycles. Results indicated that a very high recovery percentage (99.3 to

96.8% for lead (II)) and (98.7 to 94.1% for chromium (VI)) was achieved using the 0.1 mol/L acid solutions in the five successive cycles. Similarly, the removal efficiency of nanocomposite is also not decreased significantly in the five successive operations. The removal percentage was decreased from 98.2 to 96.2 % for lead (II) and from 74.1 to 70.0 % for chromium (VI) for the five repeated use of solid. These results implied that synthesized MGOBN showed high stability for repeated treatment operations, hence sustainable in possible unit operation. Similar results were obtained using mesoporous silica (AMS), a precursor material to the 3-aminopropyltriethoxysilane (APTES) and chitosan. The desorption studies revealed that 0.05 mol/L HCl could desorb *Ca.* 95 % of pre-adsorbed lead (II) from AMS solid within 60 mins (Lalchhingpuii et al., 2017c). Furthermore, with the utilization of 1 mM HNO_3 could efficiently desorb the lead (II) with only 6% efficiency was lost at the end of fifth repeated cycle of operations using the clay-/poly(methoxyethyl)acrylamide (PMEA) solid (Şölener et al., 2008b).

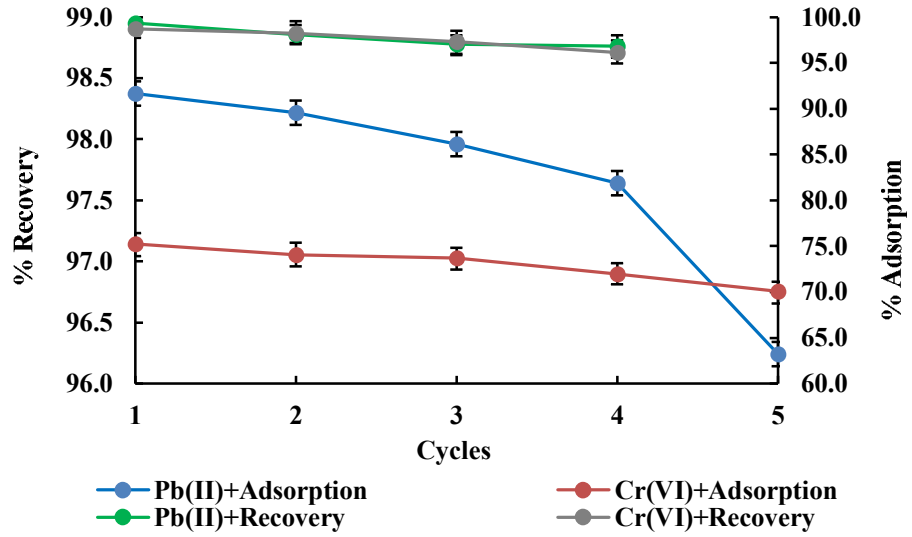

Figure 3.28: Percentage recovery and percentage adsorption of lead (II) and chromium (VI) in the repeated use of MGOBN nanocomposite; (Pollutant concentration: 10.0 mg/L; pH: 4.0 for lead (II) and 3.6 chromium (VI), solid dose: 2.0 g/L; temperature: 25°C, agitation speed: 180 rpm; desorption solution: 0.1 M HCl for lead (II) and 0.1 M H_2SO_4 for chromium (VI).

3.11. BATCH REACTOR STUDIES FOR REMOVAL OF DICLOFENAC SODIUM AND RHODAMINE B

3.11.1. Effect of pH

One crucial physicochemical characteristic that helps to determine the mechanism that occurred at the solid solution interface is the pH dependence sorption of pollutants at the solid surface. The pH dependence sorption of diclofenac sodium is investigated by altering the pH from 2.0 to 10.0 and the percentage removal of diclofenac sodium at different pH values are shown in Figure 3.29(a). The figure shows that diclofenac sodium uptake is slightly lower at low pH value i.e., pH 2.0 i.e., *Ca* 90 % using GO, MGO, and MGOBN and *Ca* 64 % using BN. However, a within pH region ~3.0 to 4.0 a maximum of *Ca* 97% of diclofenac was removed using the GO and MGO and *Ca* 90% using the MGOBN. Further increase in pH pH ~4.0 to 7.0 caused for a gradual decrease in percentage uptake of diclofenac sodium using these nanocomposite solids. Quantitatively, increasing the pH from 4.0 to 6.8 caused for a decrease in the percentage removal of diclofenac sodium from 98.7 to 91.3% for (GO), and from 97.0 to 56.0 (for MGO), respectively. Similarly, increasing the pH from 4.0 to 6.2 caused for a sharp decrease in the percentage removal of diclofenac sodium i.e., from 87.5 to 33.6%, respectively. The results are demonstrated based on the surface properties and speciation of diclofenac sodium in an aqueous medium. The solids BN, GO, MGO, and MGOBN showed pH_{PZC} values of 6.8, 4.0, 6.5, and 5.3 respectively. On the other hand, diclofenac sodium possesses a low dipole moment and the pk_a value of diclofenac sodium is 4.21 (Meloun et al., 2007). Therefore, the diclofenac sodium is predominantly possessed with an anionic species with a pH>4.2. A very high uptake occurred within the pH region 2.0 to 5.0 by these nanocomposite solids is explicable with the fact that these solids are predominantly contained with GO which provides strong organophilic active sites for the diclofenac sodium. In addition, the various functional groups present in graphene oxides *viz.*, the hydroxyl, carboxyl, and epoxy groups that could form the hydrogen bond with the oxygen (O), and nitrogen (N) of diclofenac sodium, which increases the uptake of diclofenac sodium by the solids at lower pH values (Bhadra et al., 2016). Also,

relatively a strong van der Waals interaction occurred between the diclofenac sodium and nanocomposite solids led to the higher uptake of diclofenac (Guerra et al., 2021). Additionally, the π-π interaction between the diclofenac sodium and solid synergizes the uptake of diclofenac by these solids (Nam et al., 2015). Moreover, the GO showed relatively very high uptake which was not significantly affected throughout the studied pH region (~2.0-6.0) inferred that the diclofenac sodium is dominantly bound with the organophilic interactions at the solid surface. On the other hand, the decrease in uptake of diclofenac at higher pH values i.e., pH 4~7, is due to the two reasons that the surface possessed with less hydrophobicity and the acidic dissociation of diclofenac sodium species are not attracted by the surface and caused for a decrease in percentage uptake of diclofenac. At very low pH value i.e., pH 2.0, slightly a less uptake of the diclofenac sodium is attributed due to the reason that the diclofenac sodium is not a very strong organophilic compound and the excess of H^+ ions are occupied the solid surface and hindered slightly the sorption of diclofenac by these nanocomposite solids (Tiwari et al., 2015).

Similarly, the elimination of Rhodamine B at an initial concentration of 10.0 mg/L, an adsorbent dose of 2g/L with a pH range from 2.0 to 10.0 was studied using BN, GO, MGO, and MGOBN solid materials. Figure 3.29 (b) shows that the high removal percentage of Rhodamine B by the GO and MGOBN was almost unaffected within the pH region ~2.0 to 4.0. Further increase in pH (pH>5.0) caused for the sharp decrease in percentage uptake of Rhodamine B by these solids i.e., GO and MGOBN. On the other hand, the MGO showed slightly different removal behavior for Rhodamine B. The low initial uptake of Rhodamine B at pH ~2.0 was increased gradually up until pH 6.2 and pH>6.2 had caused for the sharp decrease in the percentage removal of rhodamine B. Rhodamine B is having dissociable hydrogen with a pk_a value of 4.2 (Maurya et al., 2006). Therefore, the speciation studies indicated that the negatively charged species of RhB^- is gradually increasing with an increase in the pH (pH>4.2). However, with pH<4.2 it possesses the zwitterionic species ($RhB^{\pm}$) (Hou et al., 2011). On the other hand, the pH_{PZC} of these solids are 4.0, 6.5, and 5.3 respectively for the GO, MGO, and MGOBN. The higher uptake of Rhodamine B by the GO and MGOBN at lower pH values is due to the high affinity of solids towards the zwitterionic species of Rhodamine B by these solids. Moreover,

the enhanced organophilic nature of these solids attracted Rhodamine B. However, the decrease in the sorption of Rhodamine B at pH>5.0 is due to the strong repulsion between the negatively charged surface and anionic species of Rhodamine B. Similarly, the solid MGO showed lower uptake at lower pH (pH~2.0) showed less affinity of solid towards the neutral species of Rhodamine B. However, the uptake was gradually increased with increase in pH (pH 2.0~6.2) due to the acidic dissociation of Rhodamine B is partly attracted by the positively charged surface of MGO (pH_{PZC} = 6.5) and attains maximum sorption at around pH 6.2. However, a further increase in pH (pH>6.2), because of stronger repulsive forces between the anionic species of Rhodamine B and the negative surface of MGO caused for a gradual decrease in the sorption of Rhodamine B. Similar results were found in the removal of Rhodamine B using the functional hybrid of Fe_3O_4 magnetic nanoparticles and graphene oxide (MNPs-GO). The ionic interaction between the graphene oxide and Rhodamine B were the driving forces involved in the sorption process (Junyong et al., 2013). Furthermore, the adsorption of Rhodamine B from an aqueous solution onto activated rice husk ash (ARHA) exhibits similar sorptive behavior (Suc and Kim , 2017).

On the other hand, the pristine bentonite showed significantly less sorption of diclofenac sodium and Rhodamine B compared to the GO, MGO and MGOBN solids. Moreover, an increase in pH (pH>4.0) further diminishes the sorption of these two pollutants by the BN solid. The lower uptake of diclofenac sodium and Rhodamine B by the pristine BN pointed to the less affinity of BN towards these pollutants in an aqueous medium. These results further indicated the potential of GO or nanocomposite solids in the efficient remediation of water contaminated with diclofenac sodium or Rhodamine B.

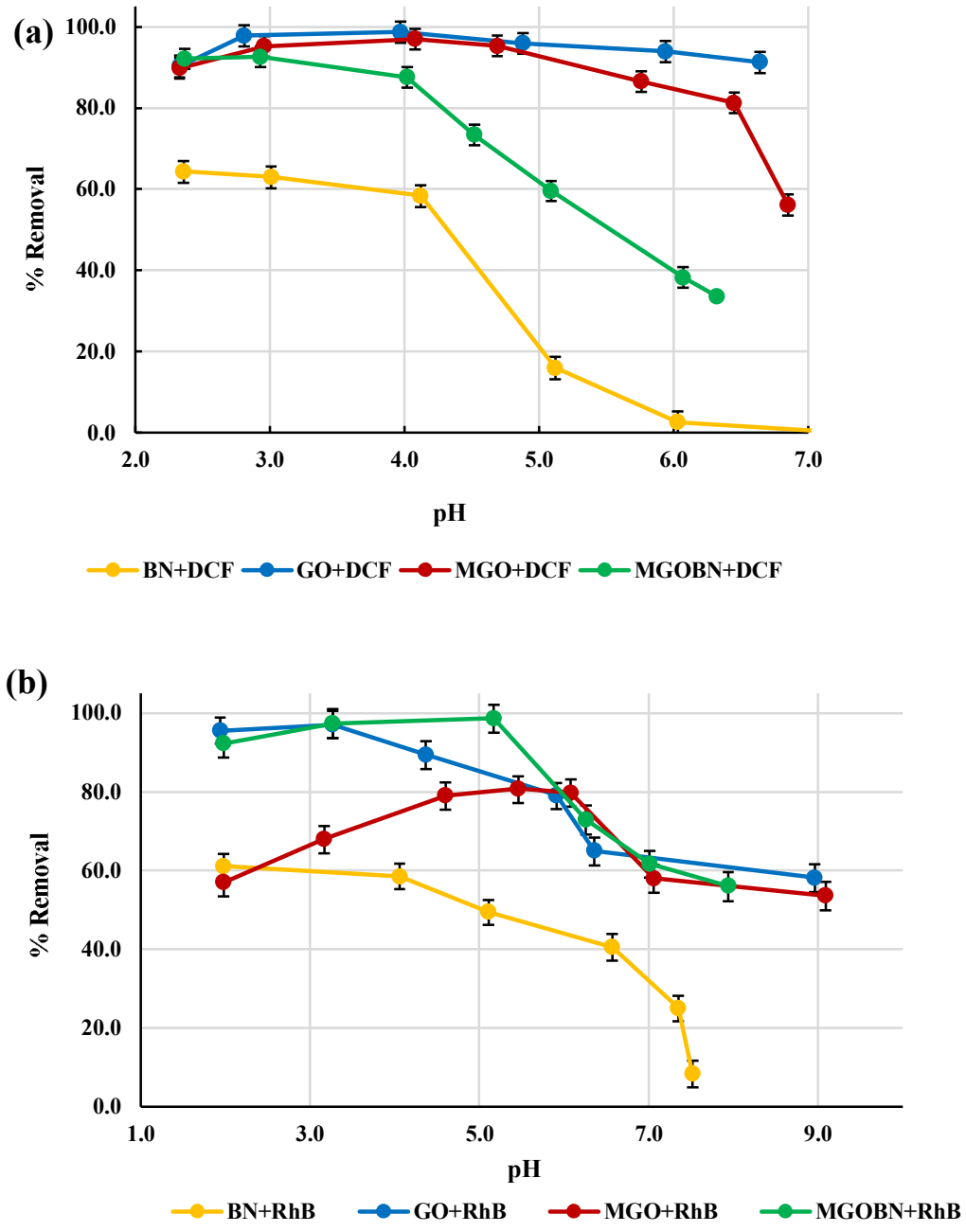

Figure 3.29: Effect of pH in the removal of **(a)** diclofenac sodium; **(b)** Rhodamine B by the BN, GO, MGO, and MGOBN solids ([Pollutants]: 10.0 mg/L; Solid dose: 2.0 g/L; Temperature: 25°C, Agitation speed: 180 rpm).

3.11.2. Effect of sorptive concentrations

The sorption of diclofenac sodium and Rhodamine B by the MGOBN nanocomposite was investigated in a wide range of initial pollutant concentrations from 1.0 to 30.0 mg/L at a constant equilibrium pH of 3.7 and 4.0 respectively for diclofenac sodium and Rhodamine B and at temperature 25.±01°C. Diclofenac sodium and Rhodamine B equilibrium stage percent elimination and extent of removal are obtained at varied initial concentrations and results are shown graphically in Figure 3.30. The percentage uptake of these two pollutants is increased with the dilution of pollutant concentrations (*Cf* Figure 3.30 (Primary Y-Axis)). Quantitatively, decreasing the sorbate concentration from 30.0 to 1.0 mg/L caused for an increase in percentage uptake from 59.8 to 86.5% (for diclofenac sodium) and from 45.7 to 98.9 % (for Rhodamine B), respectively. The decrease in the percentage removal of these pollutants at higher initial sorbate concentrations is explicable by the fact that at lower concentrations of diclofenac sodium and Rhodamine B, a relatively large number of active sites are available on the nanocomposite surface for a lesser number of sorbing ions hence, higher percentage uptake is recorded. Further, at higher initial concentrations of sorbate species, a fair possibility of saturating the surface-active sites of the MGOBN, which saturates the percentage uptake of diclofenac sodium and Rhodamine B. A similar finding was observed in the removal of diclofenac sodium by potassium ferrate-activated porous graphitic biochar (Fe@BC), where the percentage removal of diclofenac sodium was decreased with an increase in the initial concentrations of diclofenac. This was attributed that at higher concentrations of sorbate species, an apparent saturation of surface active sites caused for the decrease in the percentage removal of diclofenac sodium (Tam et al., 2020). However, the equilibrium state extent of sorbate removal is increased with an apparent increase in sorbate initial concentrations (*Cf* Figure 3.30 (Secondary Y-Axis)). Quantitatively, increasing the pollutant concentrations from 1.0 to 30.0 mg/L caused for an increase in extent removal from 0.52 to 8.94 mg/g (for diclofenac sodium) and 0.49 to 6.77 mg/g (for Rhodamine B), respectively. Furthermore, in the use of *Casuarina equisetifolia* needles (CEN) in the uptake of Rhodamine B, the adsorption capacity was increased

from 7.3 mg/g to 68.1 mg/g for the increase of Rhodamine B initial concentration from 20 to 300 mg/L (Kooh et al., 2016).

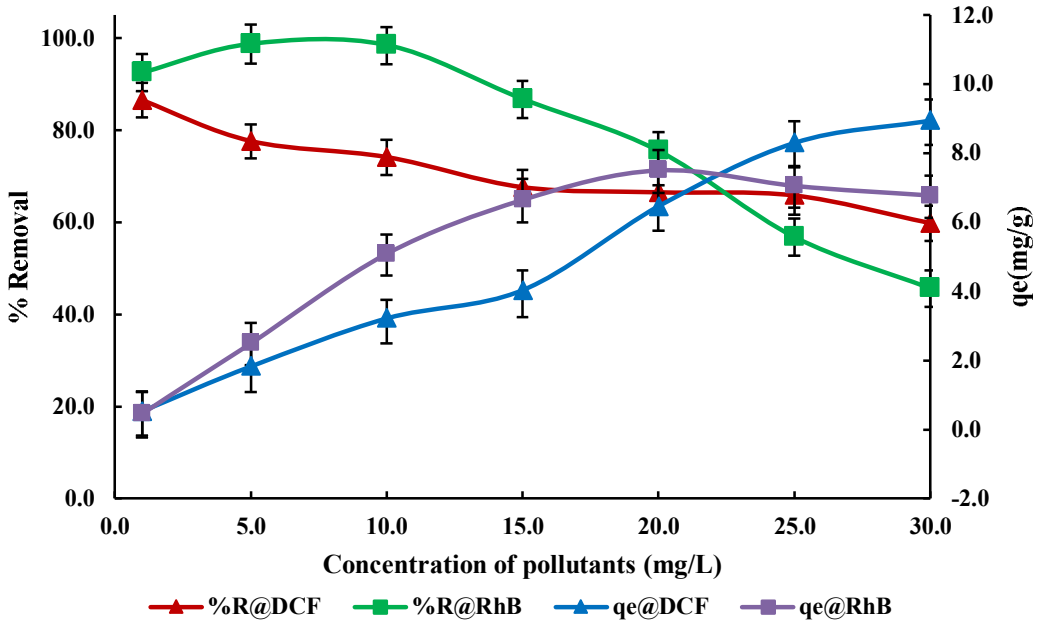

Figure 3.30: Effect of initial sorptive concentrations in the removal of diclofenac sodium and Rhodamine B onto MGOBN [pH: 3.6 for DCF and 4.0 for RhB; Solid dose: 2.0 g/L: Temperature: 25°C, Agitation speed: 180 rpm].

3.11.2.1. Adsorption isotherm modeling

Langmuir, Freundlich, and Sips adsorption isotherms to its non-linear form (*Cf* Equation (2.2, 2.3, and 2.4)) are utilized to simulate the equilibrium state sorption data obtained for varied concentrations of diclofenac sodium and Rhodamine B using MGOBN solid. The isotherm modeling results are represented graphically in Figure 3.31 and the optimized parameters along with the least square sums are included in Table 3.15. Results showed that the equilibrium sorption data is reasonably fitted well to the Langmuir and Sips adsorption isotherms for the sorption of diclofenac sodium by MGOBN whereas the sorption of Rhodamine B by MGOBN is fitted well to the Langmuir adsorption isotherm since the least square sum is reasonably low for these isotherms, which represent chemisorption with monolayer coverage (Swain et al.,

2011) and the Sips isotherm, on the other hand, anticipate the sorption on the surfaces and overcomes the Freundlich isotherm's restriction at high adsorbate concentrations which predicts monolayer adsorption similarly to the Langmuir isotherm at higher adsorbate concentrations. Moreover, the sorption is related to the Freundlich isotherm at low adsorbate concentrations. Consequently, only monolayer sorption is described using the Sips isotherm (Tzabar and Ter, 2016).

Further, the maximum monolayer coverage of diclofenac sodium and Rhodamine B (q_o) was found to be 17.33 mg/g and 8.00 mg/g, respectively optimized with the Langmuir isotherm model. Similarly, the Sips model optimized the sorption capacities of 55.02 mg/g and 12.68 mg/g for the diclofenac sodium and Rhodamine B using the MGOBN. The high value of the sorption capacity indicated the potential of MGOBN in the efficient removal of diclofenac sodium and Rhodamine B from an aqueous medium.

The removal of diclofenac sodium using the porous carbon carbonized at 1000°C (PC1000) showed the monolayer-layer chemisorption compared to the Freundlich (Mao et al., 2019). Similarly, modified carbon xerogels are used to remove Rhodamine B from aqueous solutions. A monomolecular layer of adsorbate is formed on the adsorbent surface and agreed well with the Langmuir equation (Ptaszkowska-Koniarz et al., 2018).

Furthermore, Table 3.16 compares the efficiency of MGOBN' in the elimination of diclofenac sodium and Rhodamine B with several other materials used in the literature. It is evident from Table 3.16 that the nanocomposite MGOBN material demonstrated ability in the treatment of water contaminated with these potential water contaminants due to its extremely high removal capacity in comparison to many other materials employed.

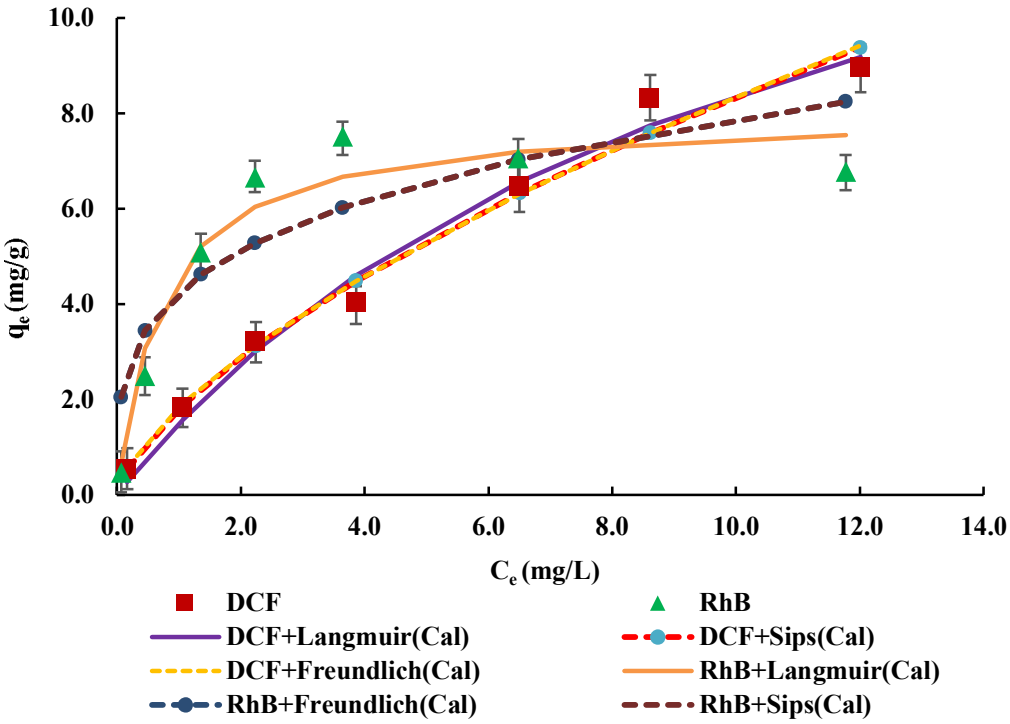

Figure 3.31: Langmuir, Freundlich, and Sips isotherms for the sorption of diclofenac sodium, and Rhodamine B using MGOBN [pH: 3.7 for diclofenac sodium, 4.0 for Rhodamine B; Solid dose: 2.0 g/L].

Table 3.15: Isotherm parameters of Langmuir, Freundlich, and Sips for the sorption of diclofenac sodium and Rhodamine B by MGOBN along with its least sum square value.

Material	Parameters		Pollutants	
			Diclofenac sodium	Rhodamine B
			pH	
			3.6	4.0
MGOBN	Langmuir	q_o (mg/g)	17.33 ± 1.02	8.004 ± 0.871
		K_L (L/g)	0.093 ± 0.031	1.371 ± 0.127
		s^2	0.900	2.061
	Freundlich	1/n	0.65 ± 0.07	0.26 ± 0.02
		K_F (mg/g)	1.85 ± 0.62	4.25 ± 0.85
		s^2	0.994	9.867
	Sips	q_m (mg/g)	55.01 ± 2.47	12.86 ± 1.09
		K_s	0.68 ± 0.07	0.26 ± 0.03
		n_s	0.93 ± 0.09	0.01 ± 0.01
		s^2	4.30	9.867

s^2: Least square sum

Table 3.16: Adsorption capacities for the removal of diclofenac sodium and Rhodamine B using a variety of materials.

Pollutants	Material	Adsorption capacity (mg/g)	Isotherm	Reference
Diclofenac sodium	Pine wood biochar	0.52	Langmuir	(Lonappan et al., 2018)
	Pig manure biochar	12.50	Langmuir	
	Regenerable granular carbon nanotubes/ alumina hybrid	31.54	Langmuir	(Wei et al., 2013)
	Multi walled carbon nanotubes	19.90	Langmuir	(Hu et al., 2017)
	Activated carbon derived from pine tree	54.67	Langmuir	(Naghipour et al., 2018)

	Magnetite graphene oxide clay nanocomposite (MGOBN)	**55.01**	**Sips**	**Present study**
Rhodamine B	Red mud	5.56	Langmuir	(Gupta et al., 2004)
	Fly ash	10	Langmuir	(Chang et al., 2009)
	Water chest nut peel waste (WCPW)	3	Langmuir	(Khan et al., 2013)
	Mango leaf powder	3.31	Langmuir	(Khan et al.,2013)
	Cedar cone (CC)	4.44		(Hamdaoui and Zamouche, 2012)
	Walnut shells (WS)	2.29	Langmuir	(Shah et al., 2013)
	Acid modified banana peels	9.5	Langmuir	(Adeleke et al., 2019)
	Magnetite graphene oxide clay nanocomposite (MGOBN)	**12.86**	**Sips**	**Present study**

3.11.3. Effect of time

The time dependence sorption of diclofenac sodium and Rhodamine B by the MGOBN is conducted by varying the contact time from 1 to 960 mins at pH 3.7 (diclofenac sodium0 and at pH 4.0 (for Rhodamine B (pH 4.0) using the initial concentration of 10.0 mg/L for both pollutant solutions Figure 3.32 (a) graphically depicts the percentage uptake of diclofenac sodium and Rhodamine B by MGOBN as a function of time. The result demonstrates that during the early stage of interaction (i.e., just in 1 min), MGOBN quickly adsorbs the diclofenac sodium and Rhodamine B. Moreover, almost an apparent sorption equilibrium was attained within 5-10 mins of contact for diclofenac sodium and Ca 30 mins for Rhodamine B using the MGOBN. This indicated that the MGOBN is reasonably efficient in the removal of diclofenac sodium and Rhodamine B from an aqueous medium. Moreover, this demonstrated that the MGOBN possessed high affinity towards these pollutants. Similarly, kinetic data for the sorption of diclofenac sodium using the hexadecyltrimethyammonium bromide

modified bentonite (BH) and aluminum hexadecyltrimethyammonium bromide modified bentonite (BAH) showed that an apparent sorption equilibrium was achieved within 2-3 minutes of the contact (Thanhmingliana & Tiwari, 2015). The effect of time on the ability of activated carbon made from sago waste to adsorb rhodamine-B from an aqueous solution showed that the sorption equilibrium was attained in 120 mins of contact (Kadirvelu et al., 2005).

Further, the kinetic data collected for the sorption of diclofenac sodium and Rhodamine B by the MGOBN is utilized to study the kinetics of sorption. The modelling with known kinetics could lead to a better understanding of the sorption mechanism at solid/solution interfaces. The known kinetic models i.e., PFO, PSO, and FL-PSO are employed in its non-linear forms (*Cf* Equations (2.7, 2.8, and 2.9)) and results are shown graphically in Figure 3.32 (b) and the optimized parameters along with the least square sums are included in Table 3.17. These results indicated that the sorption of diclofenac sodium and Rhodamine B on the MGOBN agreed well with the FL-PSO and PSO models than the PFO model since the modelling resulted with reasonably low least square sum. Further, the rate constant values along with the sorption capacities are optimized and included in Table 3.17. The results showed that reasonably a sorption capacity is obtained for the removal of diclofenac sodium and Rhodamine B using the MGOBN solid. Moreover, the applicability of the PSO and FL-PSO models implies that the sorbate species are attached to the solid surface by strong chemical forces. In the study of *Chlorella pyrenoidosa* microalgae were tested for their removal capacity to remove the Rhodamine B from dyeing stone effluents. The pseudo-second-order model was followed by the biosorption kinetics (da Rosa et al., 2018). The sorption of diclofenac sodium onto Isabel grape bagasse also complies with the pseudo-second-order rate kinetic model (Antunes et al., 2012).

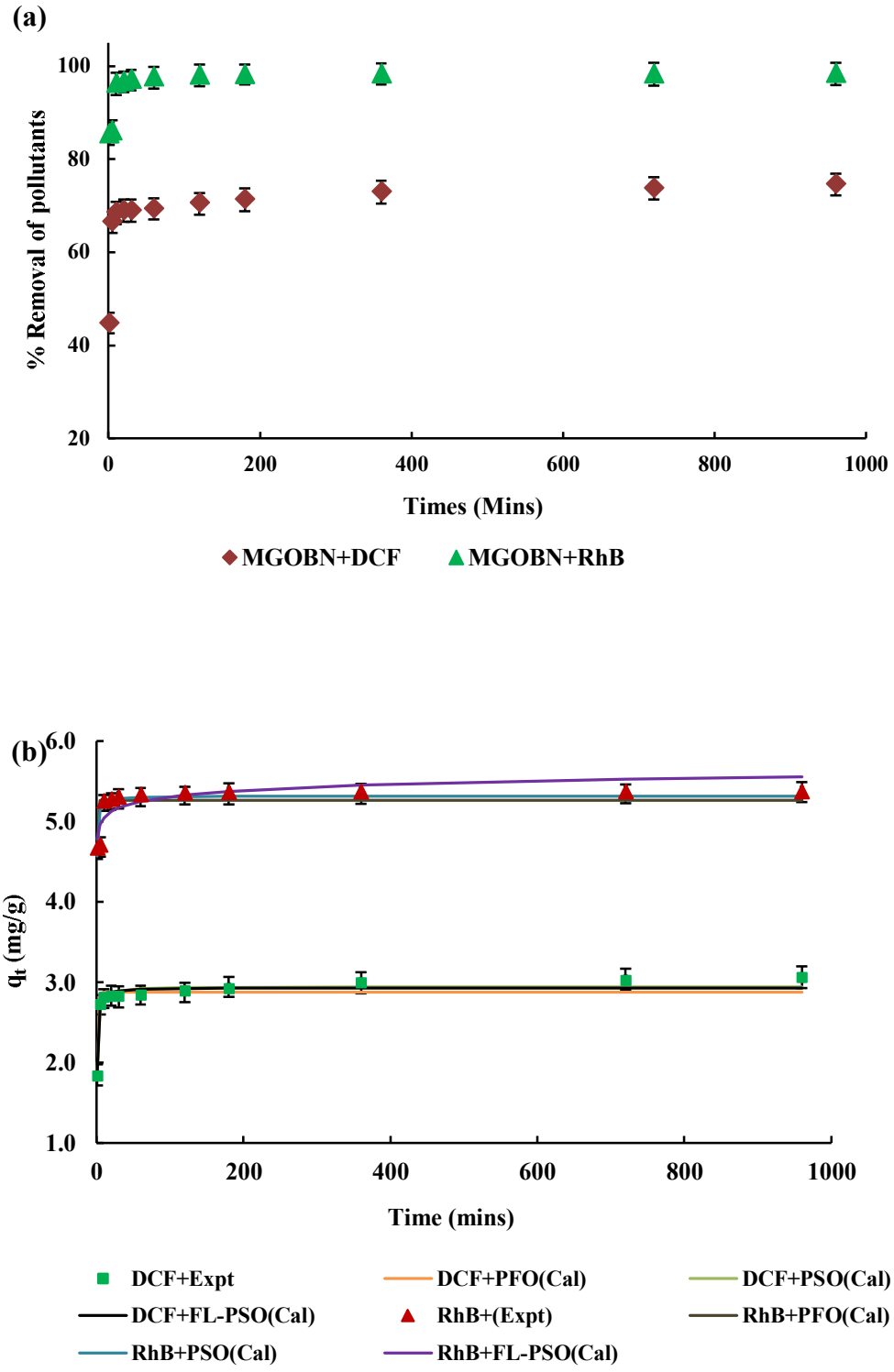

Figure 3.32: (a) Effect of contact time in the removal of diclofenac sodium, and Rhodamine B by MGOBN; **(b)** Pseudo-first-order, pseudo-second-order, and fractal-like pseudo-second-order kinetic fitting for the sorption of diclofenac sodium and

Rhodamine B using MGOBN [Pollutants]: 10.0 mg/L; pH: 3.7 for diclofenac sodium, 4.0 for Rhodamine B; Solid dose: 2.0 g/L).

Table 3.17: Kinetic parameters for the sorption of diclofenac sodium, and Rhodamine B by MGOBN nanocomposite using PFO, PSO, and FL-PSO kinetics models.

Pollutants	PFO			PSO			FL-PSO			
	k_1 (min^-)	q_e (mg/g)	s^2	k_2 (g/mg/min)	q_e (mg/g)	s^2	K (g/mg/min)	q_e (mg/g)	α	s^2
DCF	1.00 ± 0.12	2.88 ± 0.44	0.06	0.58 ± 0.02	2.94 ± 0.19	0.03	0.58 ± 0.01	2.93 ± 0.49	1.13 ± 0.17	0.02
RhB	2.28 ± 0.23	5.26 ± 0.72	0.36	1.14 ± 0.09	5.31 ± 0.67	0.21	0.15 ± 0.01	8.36 ± 0.81	0.05 ± 0.02	0.20

s^2: Least square sum

3.11.4. Effect of background electrolyte

The background electrolyte concentration dependence sorption is typically demonstrating the specific and non-specific sorption process. Non-specific adsorption is characterized by relatively weaker forces forming outer-sphere complexes, whereas specific adsorption proceeds through the stronger chemical forces, and adsorbed molecules are forming inner-sphere complexes at the surface and found irreversible (Bradl, 2004). Thus, to understand the process of interaction at the solid/solution interface the sorption of diclofenac sodium and Rhodamine B by the MGOBN was studied varying the NaCl concentrations from 0.001 to 0.5 mol/L. The initial concentration of diclofenac sodium and Rhodamine B was 10.0 mg/L at pH 3.7 (for diclofenac sodium) and pH 4.0 (for Rhodamine B). Figure 3.33 graphically displays the percentage elimination of diclofenac sodium and Rhodamine B as a function of background electrolyte concentrations. Quantitatively, an increase in 500 times of NaCl concentration caused for a very insignificant decrease in the sorption percentage of these two pollutants in an aqueous medium. Increasing the background electrolyte

concentration from 0.001 to 0.5 mol/L caused to decrease the percentage removal of diclofenac sodium from 74.1 to 70.6% and Rhodamine B from 93.1 to 88.9, respectively. These findings suggest that the diclofenac sodium and Rhodamine B are aggregated at the surface of MGOBN with relatively stronger forces and forming "inner-sphere" complexes at the solid surface.

The sorption of Rhodamine B using the activated rice husk ash (ARHA) showed a negative impact with an increase of NaCl from 0.0 to 0.3 mol/L. The extent of removal percentage was decreased from 90 % to 65.3 % and the results inferred that sodium ions compete for the active sites at the solid surface and caused for a significant decrease in the removal of Rhodamine B (Suc and Kim , 2017). Similarly, the removal of diclofenac sodium using the calcined ZnAl- layered double hydroxides (ZnAl-C LDH), and K10 montmorillonite (K10Mt) intercalated with cetyltrimethyl- ammonium bromide cation (K10Mt-C16) was influenced significantly in the presence of NaCl concentrations. Increasing the NaCl concentrations from 0.005 to 0.1 mol/L, the extent removal of diclofenac sodium was decreased from 42.9 to 27 mg/g (using ZnAl-C LDH) and from 48.6 to 36.9 mg/g (using K10Mt-C16), respectively. These results revealed that the sodium ions compete for the surface compared to the diclofenac sodium (Boukhalfa et al., 2017)

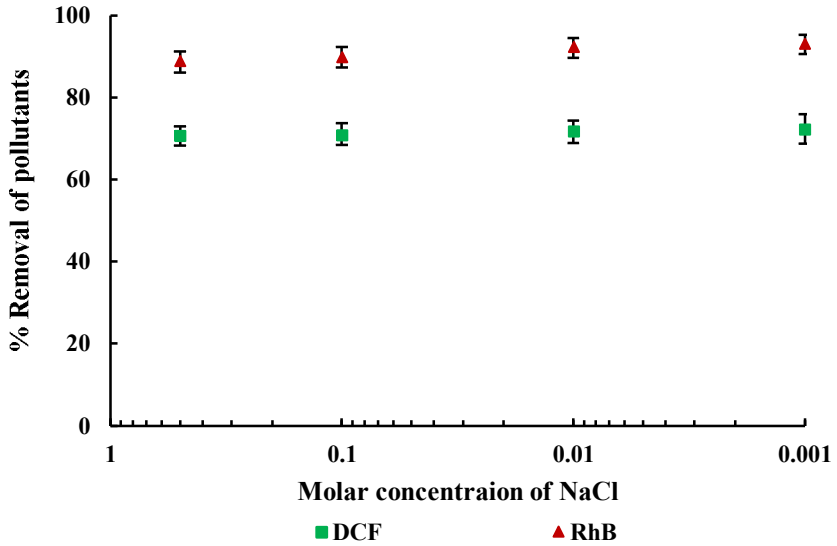

Figure 3.33: Effect of background electrolyte in the removal of diclofenac sodium and Rhodamine B by MGOBN; [Pollutants]: 10.0 mg/L; pH: 3.7 for diclofenac sodium and

4.0 for Rhodamine B; Solid dose: 2.0 g/L; Temperature: 25°C, Agitation speed:180rpm.

3.11.5. Effect of co-existing ions

The presence of several co-existing ions was studied in the elimination of diclofenac sodium and Rhodamine B removal by MGOBN. The cations *viz.*, magnesium (II), calcium (II), manganese (II), and nickel (II), and the anions *viz.*, ethylenediaminetetraacetic acid (EDTA), phosphate, oxalic acid, and glycine were chosen for the studies and the concentrations of diclofenac sodium or Rhodamine B was taken 10.0 mg/L at pH 3.7 (for diclofenac sodium) and pH 4.0 (for Rhodamine B) with a solid dose of 2.0 g/L and the co-ions concentration was 50.0 mg/L. Figure 3.34 shows the removal percentage of diclofenac sodium and Rhodamine B by MGOBN in the presence of these cations or anions. The removal of diclofenac sodium by MGOBN was not hampered significantly in the presence of cations or anions whereas the removal of Rhodamine B was slightly suppressed in the presence of phosphate, oxalic acid, and EDTA. These results indicated that the anions (EDTA, oxalic acid, and phosphate) compete for the solid surface more than the Rhodamine B which caused the decrease in adsorption of Rhodamine B by MGOBN. On the other hand, the presence of cations did not affect the sorption of Rhodamine B by the MGOBN. Therefore, the results indicated that the MGOBN is reasonably selective for the removal of diclofenac sodium and Rhodamine B in an aqueous medium. It was reported previously that the removal of Rhodamine B by exhausted coffee ground powder (CGP) showed similar results. The presence of hydrogen phosphate affected the removal percentage of Rhodamine (Shen and Gondal, 2017).

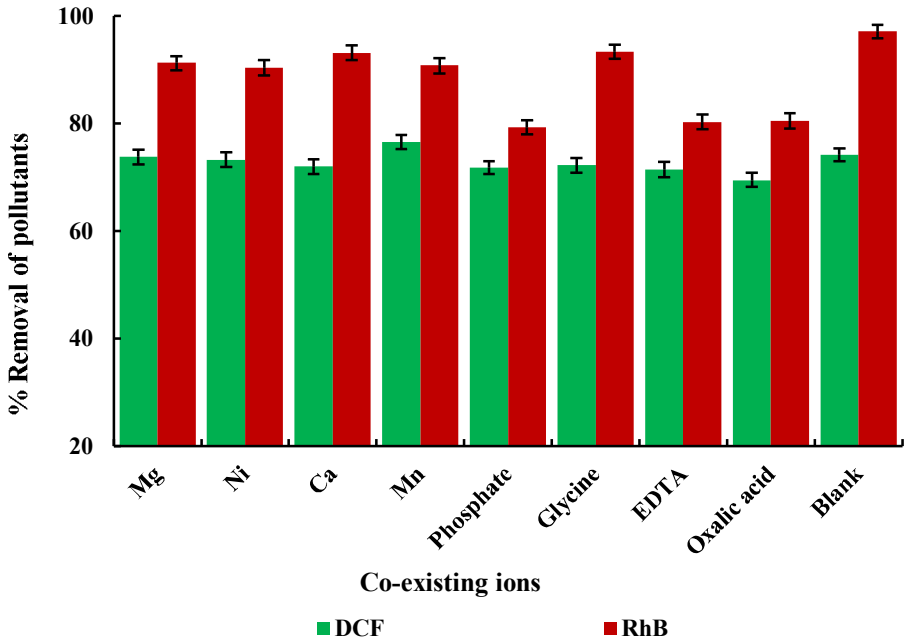

Figure 3.34: Effect of co-existing ions in the removal of diclofenac sodium and Rhodamine B by MGOBN(Pollutants]: 10.0 mg/L; [ions: 50.0 mg/L; pH: 3.7 for diclofenac sodium and 4.0 for Rhodamine B; Solid dose: 2.0 g/L; Temperature: 25°C, Agitation speed:180 rpm).

3.11.6. Application of MGOBN in a natural water sample

A natural water sample was collected from the Lengpui river stream (Tlwang River) and employed in the removal of diclofenac sodium and Rhodamine B using MGOBN to simulate the studies for real matrix treatment. The water sample was studied for various physico-chemical parametric analyses and the results are returned in Table 3.1. The analyses revealed that the Cu, Pb, Ni, and Al level in the river water was significantly low. However, the content of Ca and Mg were relatively high as 35.0 and 4.5 mg/L, respectively. Similarly, the TOC analysis of the stream water showed high inorganic carbon (16.004 mg/L) and with moderate non-purgeable organic carbon (NPOC: 1.043 mg/L). Additionally, the water sample contained with sulphate (4.0 mg/L), phosphate (0.4 mg/L), and nitrates (4.0 µ/L). The river water was spiked with known concentrations of diclofenac sodium and Rhodamine B at pH 3.7 (for diclofenac sodium) and 4.0 (for Rhodamine B). Figure 3.35 displays the concentration-dependent MGOBN removal efficiency for diclofenac sodium and Rhodamine B in a natural

water matrix. Figure 3.35 also compares the percentage removal of these pollutants in river water with the purified water as well. The findings showed that, in comparison to purified water, the removal efficiency of MGOBN is not significantly affected at least in the removal of diclofenac sodium and Rhodamine B in natural water samples. Therefore, the MGOBN exhibits good selectivity and applicability in attenuating the diclofenac sodium and Rhodamine B in real water samples.

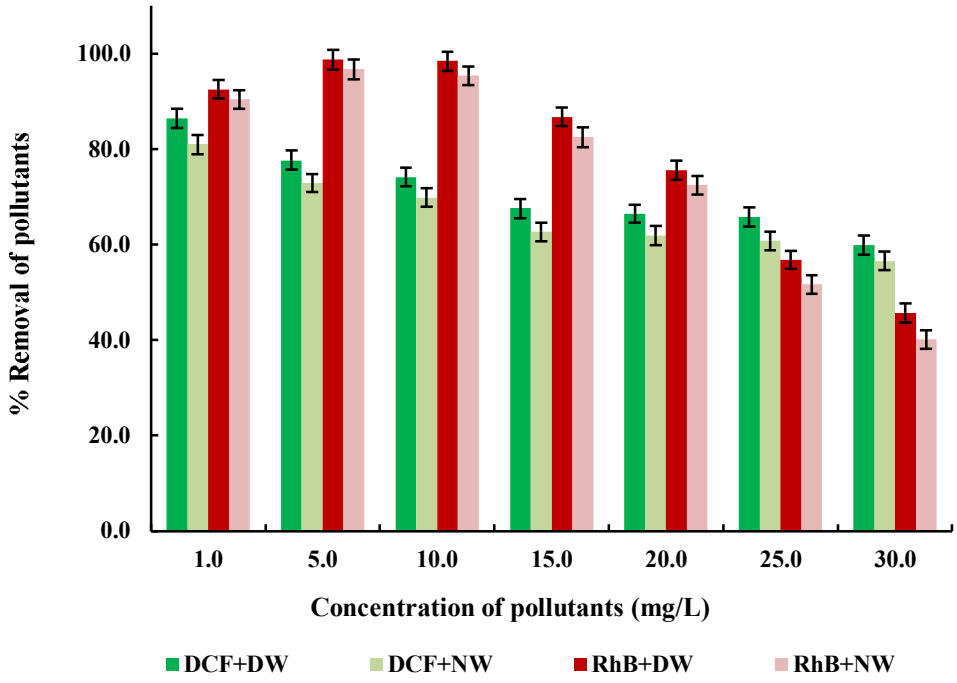

Figure 3.35: Removal of diclofenac sodium and Rhodamine B in distilled water (DW) and natural water (NW) samples using MGOBN composite at varied sorptive concentrations (Pollutants concentration: 10.0 mg/L; pH: 3.7 (for diclofenac sodium), and 4.0 (for Rhodamine B), solid dose: 2.0 g/L; temperature: 25±1°C, agitation speed:180 rpm).

3.11.7. Regeneration and reusability of MGOBN

To assess the stability and reuse of MGOBN adsorbent in a repeated cycle of sorption/desorption operations, it is necessary to consider the material's potential for

its reuse. To obtain a suitable molar concentration of HCl to desorb efficiently the pre-adsorbed diclofenac sodium and Rhodamine B from the MGOBN nanocomposite, the regeneration experiments were conducted using varied molar concentrations of HCl (0.1 M, 0.01 M, and 0.05 M). The results indicated that the 0.1 M HCl is effective in removing efficiently the pre-sorbed diclofenac sodium or Rhodamine B from the MGOBN solid. Therefore, the recovery percentage and the adsorption percentage for the successive cycle of operations are represented in Figure 3.36 where the primary Y-axis and secondary Y-axis are intended for the percentage recovery and percentage sorption, respectively for these pollutants. The desorption was conducted in equilibrating the pre-sorbed MGOBN with the desorptive solutions for 2 hrs of contact. The results revealed that from the percentage recovery of diclofenac sodium and Rhodamine B was achieved *Ca.* 99% for four successive cycles of operations. On the other hand, the percentage removal of diclofenac sodium decreased from 74.9 to 69.3% from the 1^{st} to the 5^{th} cycle of operation. Similarly, from the 1^{st} to the 5^{th} cycle of sorption/desorption experiments showed that the Rhodamine B percentage removal decreased from 98.4 to 94.0%, respectively. These results indicated that a high percentage recovery of diclofenac sodium and Rhodamine B from the pre-sorbed MGOBN was achieved using 0.1 M HCl. Similarly, the MGOBN nanocomposite showed relatively higher stability for successive sorption/desorption of these pollutants since the sorption percentage was not affected significantly even for five successive sorption/desorption studies. The desorption and reusability of phosphotungstic acid (PTA) encapsulated material institut Lavoisier (MIL101(Cr) i.e., PTA@MIL101(Cr) was employed for the removal of diclofenac sodium. The regeneration of the adsorbent was performed using 0.1 M NaOH, 0.1 M HCl, 0.1 M HCl/EtOH (20/80,v/v), and 0.1 M NaOH/EtOH (20/80,v/v) for the desorption experiments. Results revealed that 0.1 HCl/EtOH (20/80,v/v) showed a maximum desorption percentage. Moreover, the efficiency of solid was decreased only 12 % at the end of five repeated sorption/desorption cycles (Sharifian et al., 2022). Similarly, the sodium dodecyl sulphate (SDS) – modified nano α-Al_2O_3 used for the Rhodamine B removal. The regeneration and reusability of the adsorbent was studied using a 0.1 M NaOH desorptive solution. The sorption/desorption results showed that the removal efficiency

was not significantly affected even at the fourth cycle of the use since *Ca* 98% of removal efficiency was achieved (Yen et al., 2020).

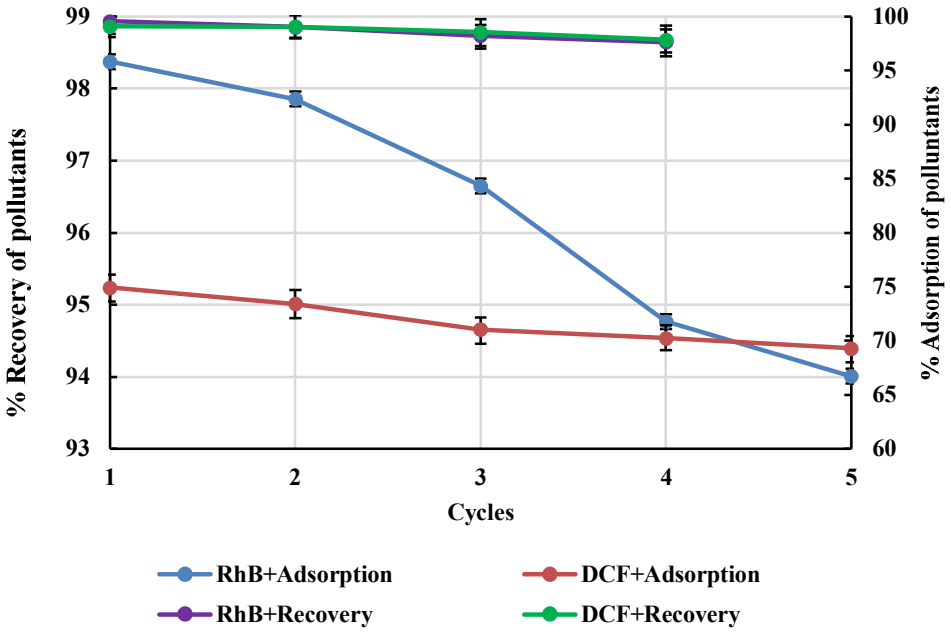

Figure 3.36: Percentage recovery and percentage adsorption of diclofenac sodium and Rhodamine B in the repeated use of MGOBN nanocomposite; (Pollutant concentration: 10.0 mg/L; pH: 3.6 for diclofenac sodium and 4.0 for Rhodamine B, solid dose: 2.0 g/L; temperature: 25°C, agitation speed: 180 rpm; desorptive solution: 0.1 M HCl.

CHAPTER 4
CONCLUSION

4. CONCLUSION

A facile and environmentally benign process allowed to synthesize the novel magnetite graphene oxide clay nanocomposite (MGOBN) material precursors to the graphene oxide and naturally occurring bentonite clay. Naturally available sugarcane juice was fully exploited for the preparation of graphene oxide (GO) using an expanded dehydration process, which was further magnetite with Fe_3O_4 by *in situ* co-precipitation method for the formation of magnetite graphene oxide (MGO). The nanocomposite MGOBN was obtained by a simple facile process. Further, these composite materials were employed for the remediation of aquatic environments contaminated with arsenic (III), arsenic (V), fluoride, lead (II), chromium (VI), diclofenac sodium, and Rhodamine B.

The SEM/EDX and TEM analyses demonstrated the surface morphology and elemental composition of the BN, GO, MGO, and MGOBN solids. The micrographic images revealed the heterogeneous morphology of nanocomposite materials and the nanoparticles possessed an average particle size of 11.88 nm and 12.44 nm for MGO and MGOBN, respectively. Moreover, the d-spacing was found 0.296 nm assigned to the characteristics (220) plane of Fe_3O_4. Graphene oxide contained with C and O elements, and an additional EDX peak of Fe validated the existence of Fe_3O_4 in MGO. Si, Al, Na, Ti, and K elements EDX peaks present with the MGOBN confirmed the presence of bentonite in the nanocomposite solid. The FT-IR results showed oxygen-containing functional groups in GO, symmetric and asymmetric Fe-O vibrations in MGO, and Si-O-Si-O-Al stretching in BN were identified. X-ray diffraction result showed the presence of graphene oxide which exhibits a broad characteristics diffraction peak at the 2θ value of 26.04° and 43.09°. Moreover, the MGO reveals the diffraction peaks at the 2θ values of 30.18°, 35.56°, 43.18°, 53.55°, 57.19°, and 62.86° due to the face centered cubic (fcc) magnetite nanoparticles. The saturation magnetization of both MGO and MGOBN was found 35 emu/g and 17 emu/g, respectively, which reveals the paramagnetic property of the materials. The Brunauer-Emmett-Teller (BET) N2 adsorption/desorption results showed that all these four solids materials *viz.*, BN, GO, MGO, and MGOBN displayed type IV isotherms demonstrating that the solid materials had mesoporous surface structures. Adsorption

hysteresis of H3 type loop was observed for the BN, GO, and MGOBN solids which are indicative of plate-like particles forming slit-shaped pores whereas MGO exhibits H1 type hysteresis loop referred to the porous materials having narrow pore size distributions. The BET-specific surface areas of BN, GO, MGO, and MGOBN were 164.01, 428.55, 238.64, and 195.84 m^2/g, respectively. Furthermore, the pore size distribution revealed that all the solid materials exhibited mesoporous structure. From the Zeta potential measurements, all these solid materials possess negative charges on their surface. Further, the BN, GO, MGO, and MGOBN had pH_{PZC} values of 6.8, 4.0, 6.5, and 5.3 respectively.

The batch and column reactor operations revealed the efficiency of MGO and MGOBN@1:2 in the removal of arsenic (III), arsenic (V), and fluoride ions. The parametric studies further reveal the mechanism involved at solid/solution interface in the removal of these pollutants by the solids. Arsenic (III) and arsenic (V) showed very high removal efficiency throughout the studied pH (2~10) using the MGO and pH *Ca* 3.0-4.0 favored greatly the elimination of these pollutants with 86.75% removal of arsenic (III) and 98.38% for arsenic (V) by MGO. The adsorption of arsenic species on the surface of MGO is due to a mixed effect of electrostatic attraction followed by the surface complexation reactions. MGOBN@1:2 shows 64.41% removal efficiency of fluoride at *Ca* pH 4.0 and a maximum of *Ca.* 81% of fluoride was removed at pH 2.0 and further the removal percentage decreases with an increased in pH, as the fluoride uptake is driven predominantly by the electrostatic attraction at low pH and electrostatic repulsion at higher pH values. An increase in pollutant concentrations (1.0 to 30.0 mg/L) did not impact significantly the elimination efficiency of MGO and MGOBN@1:2 in the elimination of arsenic (III), arsenic (V), and fluoride ions. The isotherm studies fitted well to the Sips isotherm and the sorption capacities estimated by the Sips fitting were 26.59 mg/g, and 35.97 mg/g for arsenic (III) and arsenic (V), respectively using the MGO whereas the fluoride ions removal efficiency estimated by Sips model was 17.81 mg/g using the MGOBN@1:2 nanocomposite. The simultaneous removal of arsenic (V) and fluoride ions was modeled with the expanded Sips equation and the optimized capacities were 31.88 and 6.57 mg/g, respectively for arsenic (V) and fluoride ions using the MGO solid. The kinetics showed that the uptake of arsenic (III), arsenic (V), and fluoride ions followed the pseudo-second-order rate

kinetics. Moreover, the 500 times increase in background electrolytes did not effect significantly the sorption of arsenic (III) and arsenic (V) species which infers that the sorbate species forming the 'inner-sphere complexes' at the solid surface. On the other hand, in the case of fluoride ions, fewer fluoride ions are attracted by the electrostatic forces and retained at the outer layer forming the outer-sphere complexes and affected by the increase in electrolyte concentrations. The elimination efficiency of both arsenic (III) and arsenic (V) by MGO are not significantly afflicted in the existence of cationic ions *viz.*, Ca^{2+}, Mn^{2+}, Mg^{2+}, and Ni^{2+}. Similarly, the EDTA, glycine, and oxalic acid showed insignificant influence in the removal of arsenic species. However, the presence of phosphate slightly hinders the uptake of arsenic (III) and arsenic (V) as the phosphate species are preferentially competing with the arsenic (V) and arsenic (III) species towards the active sites at the surface. On the other hand, the elimination of fluoride ions are affected to a varied extent in the presence of cations or anions using the MGOBN@1:2. The anions are preferentially competing for the solid surface and hence, caused for decrease in fluoride sorption by the MGOBN@1:2. The nanocomposite beads showed high loading capacities i.e., 1.54 mg/g for fluoride ions using MGOBN@1:2-beads, 1.55×10^2 and 1.15×10^2 mg/L for arsenic (III) and arsenic (V), respectively using the MGO-beads under the column studies. The materials were tested for real matrix implications and showed promising in eliminating these pollutants with the removal efficiencies of 95.61 % to 79.35%, 90.71% to 84.54% respectively for arsenic (III), and arsenic (V) by MGO with the increase in initial sorptive concentrations from 1.0 to 30.0 mg/L. Similarly, the percentage removal of fluoride was decreased from 52.46% to 40.41% with an increase in sorptive concentrations from 1.0 to 30.0 mg/L using the MGOBN@1:2 solid. Moreover, the solids were regenerated using the phosphate solution (0.05 M) for arsenic (III), arsenic (V), and acetate solution (0.01 M) for fluoride ions and the sorbed pollutants were fully recovered for 4 repeated cycles with the recovery percentage of *Ca* 98-96 % for arsenic (V), *Ca* 91-86% for arsenic (III), and *Ca* 94 to 84% in the case of fluoride and the regenerated solid showed only insignificant decrease in percentage removal of these pollutants in these repeated cycle of operations. The MGO material showed efficiency in the removal of arsenic, chromium, and copper simultaneously using an archeological bamboo chip sample. The nanocomposite materials are promising in

large scale implications for the remediation of water contaminated with arsenic and fluoride.

Furthermore, MGOBN solid was efficiently applied in the removal of lead (II) and chromium (VI) from aqueous solutions under the batch reactor operation. The removal efficiency of MGOBN for lead (II) was favored with an increase in pH and almost 100% sorption was achieved at pH ~4.0 and electrostatic interaction and ion-exchange surface complexation are the driving force involved in the removal of lead (II), however, the lower pH favored the elimination of chromium (VI) with *Ca* 99.6% at 2.0 pH and a strong electrostatic interaction controls the removal efficiencies of chromium (VI). The extent of adsorption capacity was increased from 0.493 to 12.755 mg/g for lead (II) and 0.50 to 4.987 mg/g for chromium (VI) respectively for the increase in pollutant's concentrations from 1.0 to 30.0 mg/L. The isotherm modelling fitted well to the Sips isotherm and the adsorption capacity was 32.484 mg/g for lead (II). On the other hand, the chromium (VI) sorption data is fitted well to the Langmuir as well as Sips isotherms with the adsorption capacity of 5.17 mg/g using the Sips isotherm modeling. The theoretical modelling using the Sips expanded equation revealed the removal efficiency of nanocomposite solid MGOBN for lead (II) and chromium (VI) was 27.5 mg/g and 25.15 mg/g, respectively in the 1:1 molar ratio of lead (II) and chromium (VI). Similarly, adsorption efficiency of MGO (magnetite graphene oxide) was 52.7 mg/g and 88.0 mg/g, respectively for the arsenic (V) and lead (II), and 60.5 mg/g and 19.2 mg/g for arsenic (V) and chromium (VI), respectively for their 1:1 molar ratio. The lead (II), and chromium (VI) are rapidly sorbed at the MGOBN solid with *Ca* 90% of lead (II) was sorbed in 10 mins of contact time, whereas within 60 mins of contact *Ca* 53% of chromium (VI) was sorbed and kinetic data agreed well to the pseudo-second-order and fractal-like-pseudo-second-order rate kinetics. The lead (II) sorption proceeds with an 'ion-exchange' process and forming an 'inner-sphere surface complexation' at the solid surface, whereas chromium (VI) is predominantly sorbed with relatively weaker forces and forming predominantly the 'outer-sphere complexes' at the surface. The percentage elimination of lead (II) is suppressed to a greater extent in the presence of cations *viz.*, Mg(II), Ca(II), Ni(II), and Mn(II) which is primarily due to the competition between the co-existing cations and lead (II) for the available active sites. On the other hand, the anions *viz.*, oxalic acid,

phosphate, EDTA, and glycine are not significantly affected the sorption of lead (II) by the MGOBN. The percentage uptake of chromium (VI) is not significantly affected in the presence of cations however, the presence of anions (oxalic acid, phosphate, and EDTA) significantly suppressed the elimination of chromium (VI) using the MGOBN nanocomposite. The nanocomposite solid showed high selectivity in the removal of lead (II) and chromium (VI) in the spiked natural water sample. Fairly a high percentage recovery (>95%) of pre-sorbed lead (II) and chromium (VI) from solid surface for four successive batch operations using the 0.1 mol/L of HCl and H_2SO_4 was achieved for four successive cycles and the removal percentage was decreased from 98.2 to 96.2 % for lead (II) and from 74.1 to 70.0 % for chromium (VI) for the five repeated use of solid material. The repeated use of nanocomposite solid pointed the potential of nanocomposite solid in the sustainable unit operations.

Furthermore, diclofenac sodium and Rhodamine B removal were studied by the use of MGOBN nanocomposite solid. Diclofenac sodium uptake show very high removal efficiency within the pH region ~3.0 to 4.0 with a maximum of *Ca* 97% was removed using the GO and MGO and *Ca* 90% using the MGOBN and further increase in pH ~4.0 to 7.0 caused for gradual decrease in percentage uptake of diclofenac sodium using these nanocomposite solids. Rhodamine B removal by the GO and MGOBN showed the high removal percentage which was almost unaffected within the pH region of ~2.0 to 4.0. Further increase in pH (pH>5.0) caused for sharp decrease in percentage uptake of Rhodamine B by these solids i.e., GO and MGOBN. The sorption of diclofenac sodium is dominated by organophilic interactions. The π- π and van der Waals interaction is the driving forces in the sorption of diclofenac sodium. Similarly, the strong organophilic interaction lead the sorption of Rhodamine B along with the electrostatic attraction, to some extent, for the sorption of Rhodamine B by this solid. The isotherm modeling for diclofenac sodium agrees well to the Langmuir as well as the Sips isotherm models whereas Rhodamine B follows the Langmuir isotherm model. The adsorption capacity was found to be 55.02 mg/g and 12.68 mg/g respectively for diclofenac sodium and Rhodamine B by the Sips equation fitting. The kinetic data reveals that the uptake of diclofenac sodium and Rhodamine B uptake is rapid and fast during the initial period of contact and an apparent sorption equilibrium is attained within 5-10 mins of contact for diclofenac sodium and *Ca* 30 mins for

Rhodamine B using the MGOBN solid. Diclofenac sodium and Rhodamine B uptake followed pseudo-second-order rate kinetics and fractal-like pseudo-second-order rate kinetics. At the solid surface, diclofenac sodium and Rhodamine B are forming "inner-sphere-complexes" and proceeded with relatively stronger forces. The removal of diclofenac sodium by MGOBN was not hampered significantly in the presence of cations or anions whereas the removal of Rhodamine B was slightly suppressed in the presence of phosphate, oxalic acid, and EDTA. The MGOBN showed potential in removing diclofenac sodium and Rhodamine B even in spiked natural water samples with an insignificant decrease in the percentage removal of these two pollutants compared to the pollutant's solution prepared in purified water. The pre-adsorbed diclofenac sodium and Rhodamine B were fully desorbed for four consecutive cycles using the 0.1 M HCl solution from pre-adsorbed MGOBN solid. Moreover, the removal efficiency of MGOBN is not significantly affected in the repeated sorption/desorption cycles at least for 5 repeated cycles.

Overall, the studies inferred that magnetite graphene oxide (MGO), and magnetite graphene oxide clay nanocomposite (MGOBN) are efficient in the removal of several potential water contaminants *viz* : arsenic (III), arsenic (V), fluoride ion, lead (II), chromium (VI), diclofenac sodium and Rhodamine B. Further, the input laboratory data from batch and column reactor operations could be employed for the large-scale or even Pilot Scale Unit Operations to decontaminate the water contaminated with these emerging water contaminants.

REFERENCES

Abbas, Z., Ali, S., Rizwan, M., Zaheer, I. E., Malik, A., Riaz, M. A., Shahid, M. R., Rehman, M. Z. ur, and Al-Wabel, M. I. (2018). Acritical review of mechanisms involved in the adsorption of organic and inorganic contaminants through biochar. *Arab. J. Geosci.*, **11(16)**: 448. https://doi.org/10.1007/s12517-018-3790-1

Acuña, V., Ginebreda, A., Mor, J. R., Petrovic, M., Sabater, S., Sumpter, J., and Barceló, D. (2015). Balancing the health benefits and environmental risks of pharmaceuticals: Diclofenac as an example. *Environ Int.*, **85**: 327–333. https://doi.org/10.1016/j.envint.2015.09.023

Adeleke, A., Ahmad, A., Hossain, K., and Rafatullah, M. (2019). Adsorption of Rhodamine B dye from aqueous solution onto acid treated banana peel: Response surface methodology, kinetics and isotherm studies. *PLOS ONE.*, **14**: e0216878. https://doi.org/10.1371/journal.pone.0216878

Ahmaruzzaman, Md. (2008). Adsorption of phenolic compounds on low-cost adsorbents: A review. *Adv. Colloid Interface Sci.*, **143(1)**: 48–67. https://doi.org/10.1016/j.cis.2008.07.002

Ai, L., Zhang, C., Liao, F., Wang, Y., Li, M., Meng, L., and Jiang, J. (2011). Removal of methylene blue from aqueous solution with magnetite loaded multi-wall carbon nanotube: Kinetic, isotherm and mechanism analysis. *J. Hazard Mater.*, **198**: 282–290. https://doi.org/10.1016/j.jhazmat.2011.10.041

Ajayan, P. M. (1999). Nanotubes from Carbon. *Chem. Rev.*, **99(7)**: 1787–1800. https://doi.org/10.1021/cr970102g

Ali, I., Asim, Mohd., and Khan, T. A. (2012). Low cost adsorbents for the removal of organic pollutants from wastewater. *J. Environ Manage.*, **113**: 170–183. https://doi.org/10.1016/j.jenvman.2012.08.028

Alizadeh, A., Abdi, G., Khodaei, M. M., Ashokkumar, M., and Amirian, J. (2017). Graphene oxide/Fe_3O_4/SO_3H nanohybrid: A new adsorbent for adsorption and reduction of Cr(VI) from aqueous solutions. *RSC Adv.*, **7(24)**: 14876–14887. https://doi.org/10.1039/C7RA01536D

Al-Khaldi, F. A., Abu-Sharkh, B., Abulkibash, A. M., and Atieh, M. A. (2013). Cadmium removal by activated carbon, carbon nanotubes, carbon nanofibers, and carbon fly ash: A comparative study. *Desalin. Water Treat.*, 1–13. https://doi.org/10.1080/19443994.2013.847805

Alkorta, I., Hernández-Allica, J., Becerril, J. M., Amezaga, I., Albizu, I., and Garbisu, C. (2004). Recent Findings on the Phytoremediation of Soils Contaminated with Environmentally Toxic Heavy Metals and Metalloids Such as Zinc, Cadmium, Lead, and Arsenic. *Rev. Environ. Sci. Biotechnol.*, **3(1)**: 71–90. https://doi.org/10.1023/B:RESB.0000040059.70899.3d

Altman, R., Bosch, B., Brune, K., Patrignani, P., and Young, C. (2015). Advances in NSAID Development: Evolution of Diclofenac Products Using Pharmaceutical Technology. *Drugs*, **75(8)**: 859–877. https://doi.org/10.1007/s40265-015-0392-z

Altundoğan, H. S., Altundoğan, S., Tümen, F., and Bildik, M. (2002). Arsenic adsorption from aqueous solutions by activated red mud. *Waste Manag.*, **22(3)**: 357–363. https://doi.org/10.1016/S0956-053X(01)00041-1

Alwan, S. H., Alshamsi, H. A. H., and Jasim, L. S. (2018). Rhodamine B removal on A-rGO/cobalt oxide nanoparticles composite by adsorption from contaminated water. *J. Mol. Struct.*, **1161**: 356–365. https://doi.org/10.1016/j.molstruc.2017.11.127

Ambient Water Quality Criteria for Fluoride". Government of British Columbia . Archived from the original on 24th September 2015. Retrieved 8 October 2014.WHO/UNICEF Joint Monitoring Programme for Water Supply, Sanitation and Hygiene (JMP).2020 Annual Report

Ansari, R., and Fahim, N. K. (2007). Application of polypyrrole coated on wood sawdust for removal of Cr(VI) ion from aqueous solutions. *React. Funct. Polym.*, **67(4)**: 367–374. https://doi.org/10.1016/j.reactfunctpolym.2007.02.001

Antunes, M., Esteves, V. I., Guégan, R., Crespo, J. S., Fernandes, A. N., and Giovanela, M. (2012). Removal of diclofenac sodium from aqueous solution by Isabel grape bagasse. *J. Chem. Eng.* **192**: 114–121. https://doi.org/10.1016/j.cej.2012.03.062

Aprile, A., and De Bellis, L. (2020). Editorial for Special Issue "Heavy Metals Accumulation, Toxicity, and Detoxification in Plants." *Int. J. Mol. Sci.*, **21(11)**: 4103. https://doi.org/10.3390/ijms21114103

Arsenic Exposure and Health Effects IV - 1st Edition. (n.d.). Retrieved November 11, 2022, from https://www.elsevier.com/books/arsenic-exposure-and-health-effects-iv/chappell/978-0-08-044067-5

Assunção, A. G. L., Schat, H., and Aarts, M. G. M. (2003). Thlaspi caerulescens, an attractive model species to study heavy metal hyperaccumulation in plants. *New Phytol.*, **159(2)**: 351–360. https://doi.org/10.1046/j.1469-8137.2003.00820.x

Azeh Engwa, G., Udoka Ferdinand, P., Nweke Nwalo, F., and N. Unachukwu, M. (2019). Mechanism and Health Effects of Heavy Metal Toxicity in Humans. In O. Karcioglu & B. Arslan (Eds.), *Poisoning in the Modern World—New Tricks for an Old Dog?* IntechOpen. https://doi.org/10.5772/intechopen.8251

Azizian, S. (2004). Kinetic models of sorption: A theoretical analysis. *J. Colloid Interface Sci.*, **276(1)**: 47–52. https://doi.org/10.1016/j.jcis.2004.03.048

Baig, N., Ihsanullah, Sajid, M., and Saleh, T. A. (2019). Graphene-based adsorbents for the removal of toxic organic pollutants: Areview. *J. Environ. Mangne.*, **244**: 370–382. https://doi.org/10.1016/j.jenvman.2019.05.047

Bailey, S.E., Olin, T.J., Bricka, R.M., Adrian, D.D., (1999). A review of potentially low–cost sorbents for heavy metals. *Water Res.*, **33**: 2469–2479.

Bain, R., Cronk, R., Hossain, R., Bonjour, S., Onda, K., Wright, J., Yang, H., kSlaymaker, T., Hunter, P., Prüss-Ustün, A., and Bartram, J. (2014). Global assessment of exposure to faecal contamination through drinking water based on a systematic review. *Trop Med. Int. Health.*, **19(8)**: 917–927. https://doi.org/10.1111/tmi.12334

Baltpurvins, K. (1997). Effect of electrolyte composition on zinc hydroxide precipitation by lime. *Water Res.*, **31(5)**: 973–980. https://doi.org/10.1016/S0043-1354(96)00327-2

Banerjee, S., and Chattopadhyaya, M. C. (2017). Adsorption characteristics for the removal of a toxic dye, tartrazine from aqueous solutions by a low cost agricultural by-product. *Arab. J. Chem.*, **10**: S1629–S1638. https://doi.org/10.1016/j.arabjc.2013.06.005

Barbier, O., Arreola-Mendoza, L., and Del Razo, L. M. (2010). Molecular mechanisms of fluoride toxicity. *Chemico-Biol. Interact.*, **188(2)**: 319–333. https://doi.org/10.1016/j.cbi.2010.07.011

Barceló, D. (2003). Emerging pollutants in water analysis. *TrAC Trends Anal. Chem.*, **22(10)**: 14–16. https://doi.org/10.1016/S0165-9936(03)01106-3

Barnhart, J. (1997). Chromium chemistry and implications for environmental fate and toxicity. *J. Soil Contam.*, **6(6)**: 561–568. https://doi.org/10.1080/15320389709383589

Barraqué, F., Montes, M. L., Fernández, M. A., Candal, R., Torres Sánchez, R. M., and Marco-Brown, J. L. (2021). Arsenate removal from aqueous solution by montmorillonite and organo-montmorillonite magnetic materials. *Environ. Res.*, **192**: 110247. https://doi.org/10.1016/j.envres.2020.110247

Bartolomeu, M., Neves, M. G. P. M. S., Faustino, M. A. F., and Almeida, A. (2018). Wastewater chemical contaminants: Remediation by advanced oxidation processes. *Photochem. Photobiol. Sci.*, **17(11)**: 1573–1598. https://doi.org/10.1039/c8pp00249e

Bcee, M. L. D. P. D. P. E. (2020). *Water and Wastewater Engineering: Design Principles and Practice*. McGraw-Hill Education. https://www.accessengineeringlibrary.com/content/book/9781260132274

Belachew, N., and Bekele, G. (2020). Synergy of Magnetite Intercalated Bentonite for Enhanced Adsorption of Congo Red Dye. *Silicon.*, **12(3)**: 603–612. https://doi.org/10.1007/s12633-019-00152-2

Bergeson, L. L. (2008). The proposed lead NAAQS: Is consideration of cost in the clean air act's future? *Environ. Qual. Manag.*, **18(1)**: 79–84. https://doi.org/10.1002/tqem.20197

Bhadra, B. N., Seo, P. W., and Jhung, S. H. (2016). Adsorption of diclofenac sodium from water using oxidized activated carbon. *J. Chem. Eng.*, **301**: 27–34. https://doi.org/10.1016/j.cej.2016.04.143

Bharati, R., Sundaramurthy, S., and Thakur, C. (2017). 14—Nanomaterials and food-processing wastewater. In A. M. Grumezescu (Ed), *Water Purification* (479–516). Academic Press. https://doi.org/10.1016/B978-0-12-804300-4.00014-9

Bhatnagar, A., Kumar, E., and Sillanpää, M. (2011). Fluoride removal from water by adsorption—A review. *J. Chem. Eng.,* **171(3)** : 811–840. https://doi.org/10.1016/j.cej.2011.05.028

Bhatnagar, A., and Sillanpää, M. (2010). Utilization of agro-industrial and municipal waste materials as potential adsorbents for water treatment—A review. *J. Chem. Eng.* **157(2)**: 277–296. https://doi.org/10.1016/j.cej.2010.01.007

Bhattacharya, P., Chatterjee, D., and Jacks, G. (1997). Occurrence of Arsenic-contaminatedGroundwater in Alluvial Aquifers from Delta Plains, Eastern India: Options for Safe Drinking Water Supply. *Int. J. Water Resour. Dev.*, **13(1)**: 79–92. https://doi.org/10.1080/07900629749944

Bhaumik, M., Leswifi, T. Y., Maity, A., Srinivasu, V. V., and Onyango, M. S. (2011a). Removal of fluoride from aqueous solution by polypyrrole/Fe3O4 magnetic nanocomposite. *J. Hazard. Mater.*, **186(1)**: 150–159. https://doi.org/10.1016/j.jhazmat.2010.10.098

Bian, Y., Bian, Z.-Y., Zhang, J.-X., Ding, A.-Z., Liu, S.-L., and Wang, H. (2015). Effect of the oxygen-containing functional group of graphene oxide on the aqueous cadmium ions removal. *Appl. Surf. Sci.*, **329**: 269–275. https://doi.org/10.1016/j.apsusc.2014.12.090

Bissen, M., and Frimmel, F. H. (2003). Arsenic — a Review. Part I: Occurrence, Toxicity, Speciation, Mobility. *Acta Hydroch. Hydrob.*, **31(1)**: 9–18. https://doi.org/10.1002/aheh.200390025

Bitten by witch fever: Wallpaper & arsenic in the Victorian home | WorldCat.org. (2023). https://www.worldcat.org/title/bitten-by-witch-fever-wallpaper-arsenic-in-the-victorian-home/oclc/958378017

Blackburn, R. S. (2004). Natural Polysaccharides and Their Interactions with Dye Molecules: Applications in Effluent Treatment. *Environ. Sci. Technol.*, **38(18)**: 4905–4909. https://doi.org/10.1021/es049972n

Bolong, N., Ismail, A. F., Salim, M. R., and Matsuura, T. (2009). Areview of the effects of emerging contaminants in wastewater and options for their removal. *Desalination.*, **239(1–3)**: 229–246. https://doi.org/10.1016/j.desal.2008.03.020

Borah, P., Kumar, M., and Devi, P. (2020). Types of inorganic pollutants: Metals/metalloids, acids, and organic forms. In *Inorganic Pollutants in Water* (17–31). Elsevier. https://doi.org/10.1016/B978-0-12-818965-8.00002-0

Boruah, S. (2012). Synthesis of graphene oxide nanosheets from pencil lead and in-situ synthesis of gold nanoparticles on graphene oxide nanosheets. *Int. J. Innov. Res. Dev.*,**1**: 146–154.

Boukhalfa, N., Boutahala, M., and Djebri, N. (2017). Synthesis and characterization of ZnAl-layered double hydroxide and organo-K10 montmorillonite for the removal of diclofenac from aqueous solution. *Adsorpt Sci Technol.*, **35(1–2)**: 20–36. https://doi.org/10.1177/0263617416666548

Bradl, H. B. (2004). Adsorption of heavy metal ions on soils and soils constituents. *J. Colloid Interface Sci.*, **277(1)**: 1–18. https://doi.org/10.1016/j.jcis.2004.04.005

Brahman, K. D., Kazi, T. G., Baig, J. A., Afridi, H. I., Khan, A., Arain, S. S., and Arain, M. B. (2014). Fluoride and arsenic exposure through water and grain crops in Nagarparkar, Pakistan. *Chemosphere.*, **100**: 182–189. https://doi.org/10.1016/j.chemosphere.2013.11.035

Brierley, C. L. (1990). Bioremediation of metal-contaminated surface and groundwaters. *Geomicrobiology J.*, **8(3–4)**: 201–223. https://doi.org/10.1080/01490459009377894

Bustingorri, C., and Lavado, R. S. (2014). Soybean as affected by high concentrations of arsenic and fluoride in irrigation water in controlled conditions. *Agric. Water Manag.*, **144**: 134–139. https://doi.org/10.1016/j.agwat.2014.06.004

Butt, H.-J., Graf, K., & Kappl, M. (2013). *Physics and Chemistry of Interfaces*.

Cao, L., Li, Z., Su, K., and Cheng, B. (2016). Hydrophilic Graphene Preparation from Gallic Acid Modified Graphene Oxide in Magnesium Self-Propagating High Temperature Synthesis Process. *Sci. Rep.*, **6(1)**: Article 1. https://doi.org/10.1038/srep35184

Carolin, C. F., Kumar, P. S., Saravanan, A., Joshiba, G. J., and Naushad, Mu. (2017). Efficient techniques for the removal of toxic heavy metals from aquatic environment: A review. *J. Environ. Chem. Eng.*, **5(3)**: 2782–2799. https://doi.org/10.1016/j.jece.2017.05.029

CGWA, (2018). Ground water quality in shallow quifiers of India. Central Ground Water Board Ministry of Water Resources. Government of India.

Chai, L., Wang, Y., Zhao, N., Yang, W., and You, X. (2013). Sulfate-doped Fe3O4/Al2O3 nanoparticles as a novel adsorbent for fluoride removal from drinking water. *Water Res*, **47(12)**: 4040–4049. https://doi.org/10.1016/j.watres.2013.02.057

Chandra, V., Park, J., Chun, Y., Lee, J. W., Hwang, I.-C., and Kim, K. S. (2010a). Water-Dispersible Magnetite-Reduced Graphene Oxide Composites for Arsenic Removal. *ACS Nano*, **4(7)**: 3979–3986. https://doi.org/10.1021/nn1008897

Chang, S.-H., Wang, K.-S., Li, H.-C., Wey, M.-Y., and Chou, J.-D. (2009). Enhancement of Rhodamine B removal by low-cost fly ash sorption with Fenton pre-oxidation. *J. Hazard Mater.*, **172(2–3)**: 1131–1136. https://doi.org/10.1016/j.jhazmat.2009.07.106

Chantawong, V., Harvey, N.W., Bashkin, V.N., (2001). Adsorption of lead nitrate on Thai kaolin and ballclay. *Asian J. Energy Environ*., **2**: 33–48

Chappell, W. R., Abernathy, C. O., Calderon, R. L., and Thomas, D. J. (2003). List of Contributors. In *Arsenic Exposure and Health Effects V*. Elsevier Science B.V. https://doi.org/10.1016/B978-044451441-7/50001-4

Chen, C.-C., and Chung, Y.-C. (2006). Arsenic Removal Using a Biopolymer Chitosan Sorbent. *J. Environ. Sci. Health A.*, **41(4)**: 645–658. https://doi.org/10.1080/10934520600575044

Chi, Z., Hao, L., Dong, H., Yu, H., Liu, H., Wang, Z., and Yu, H. (2020). The innovative application of organosolv lignin for nanomaterial modification to boost its heavy metal detoxification performance in the aquatic environment. *J. Chem. Eng.*, **382**: 122789. https://doi.org/10.1016/j.cej.2019.122789

(CSEM) 2010. "Case Studies in Environmental Medicine ".Arsenic Toxicity Exposure Pathways" Agency for Toxic Substances and disease registry. Retrived 15 May.

Cui, L., Wang, Y., Gao, L., Hu, L., Yan, L., Wei, Q., and Du, B. (2015). EDTA functionalized magnetic graphene oxide for removal of Pb(II), Hg(II) and Cu(II) in water treatment: Adsorption mechanism and separation property. *J. Chem. Eng.*, **281**: 1–10. https://doi.org/10.1016/j.cej.2015.06.043

da Rosa, A. L. D., Carissimi, E., Dotto, G. L., Sander, H., and Feris, L. A. (2018). Biosorption of rhodamine B dye from dyeing stones effluents using the green

microalgae Chlorella pyrenoidosa. *J. Clean. Prod.*, **198**: 1302–1310. https://doi.org/10.1016/j.jclepro.2018.07.128

Dang, V. B. H., Doan, H. D., Dang-Vu, T., and Lohi, A. (2009a). Equilibrium and kinetics of biosorption of cadmium(II) and copper(II) ions by wheat straw. *Bioresour. Technol.*, **100(1)**: 211–219. https://doi.org/10.1016/j.biortech.2008.05.031

Das, A., and Singh, S. (2011). Occupational health assessment of chromite toxicity among Indian miners. *Indian J. Occup. Environ. Med.*, **15(1)**: 6. https://doi.org/10.4103/0019-5278.82998

Dawodu, F., and Akpomie, K. (2014). Kinetic, Equilibrium and Thermodynamic Studies on the Adsorption of Cadmium (II) ions using Aloji Kaolinite Mineral. *Pac. J. Sci. Technol.*, **15**., 268–276.

Deng, F., Luo, X.-B., Ding, L., and Luo, S.-L. (2019). Application of Nanomaterials and Nanotechnology in the Reutilization of Metal Ion From Wastewater. In *Nanomaterials for the Removal of Pollutants and Resource Reutilization* (149–178). Elsevier. https://doi.org/10.1016/B978-0-12-814837-2.00005-6

Dhamodharan, D., Senthil, T., Wu, L., Mubarak, S., Kale, M. B., Divakaran, N., Zheng, L., and Zhang, X. (2019). Water dispersible magnetite graphene oxide anchored sulfonic acid hybrid for mechanical enhancement of waterborne epoxy nanocomposites. *Compos. B. Eng.*, **171**: 119–129. https://doi.org/10.1016/j.compositesb.2019.04.039

Dhir, B. (2013). *Phytoremediation: Role of Aquatic Plants in Environmental Clean-Up*. Springer. https://doi.org/10.1007/978-81-322-1307-9

Dixit, S., and Hering, J. G. (2003). Comparison of Arsenic(V) and Arsenic(III) Sorption onto Iron Oxide Minerals: Implications for Arsenic Mobility. *Environ Sci. Technol.,* **37(18)**: 4182–4189. https://doi.org/10.1021/es030309t

Domínguez-González, R., González Varela, L., and Bermejo-Barrera, P. (2014). Functionalized gold nanoparticles for the detection of arsenic in water. *Talanta*, **118**: 262–269. https://doi.org/10.1016/j.talanta.2013.10.029

Done, A. K., and Peart, A. J. (1971). Acute Toxicities of Arsenical Herbicides. *Clin. Toxicol.*, **4(3)**: 343–355. https://doi.org/10.3109/15563657108990485

Dubey, S. P., Nguyen, T. T. M., Kwon, Y.-N., and Lee, C. (2015). Synthesis and characterization of metal-doped reduced graphene oxide composites, and their application in removal of Escherichia coli, arsenic and 4-nitrophenol. *J. Ind. Eng. Chem.*, **29**: 282–288. https://doi.org/10.1016/j.jiec.2015.04.008

Duranoğlu, D., Trochimczuk, A. W., and Beker, U. (2012). Kinetics and thermodynamics of hexavalent chromium adsorption onto activated carbon derived from acrylonitrile-divinylbenzene copolymer. *J. Chem. Eng.*, **187**: 193–202. https://doi.org/10.1016/j.cej.2012.01.120

Ebele, A. J., Abou-Elwafa Abdallah, M., and Harrad, S. (2017). Pharmaceuticals and personal care products (PPCPs) in the freshwater aquatic environment. *Emerg. Contam.*, **3(1)**: 1–16. https://doi.org/10.1016/j.emcon.2016.12.004

Eckenfelder, W. W., and O'Connor, D. J. (2013). *Biological Waste Treatment*. Elsevier.

Edmunds,W. M., Ahmed, K. M., and Whitehead, P. G. (2015). A review of arsenic and its impacts in groundwater of the Ganges–Brahmaputra–Meghna delta, Bangladesh. *Environ. Sci.: Processes and Impacts*, **17(6)**: 1032–1046. https://doi.org/10.1039/C4EM00673A

El-Maghrabi, N., el Borady, O., Hosny, M., and Fawzy, M. (2021). Catalytic and Medical Potential of a Phyto-Functionalized Reduced Graphene Oxide–Gold Nanocomposite Using Willow-Leaved Knotgrass. *ACS Omega*. https://doi.org/10.1021/acsomega.1c05596

Fan, C., Du, B., Zhang, Y., Ding, S., Gao, Y., and Chang, M. (2017). Adsorption of lead on organo-mineral complexes isolated from loess in Northwestern China. *J. Geochem. Explor.*, **176**: 50–56. https://doi.org/10.1016/j.gexplo.2016.02.012

Fan, L., Luo, C., Sun, M., and Qiu, H. (2012a). Synthesis of graphene oxide decorated with magnetic cyclodextrin for fast chromium removal. *J. Mater. Chem.*, **22(47)**: 24577. https://doi.org/10.1039/c2jm35378d

Fan, Y., Fu, D., Zhou, S., Lu, Y., Zhao, X., Jin, W., and Zhao, Y. (2016). Facile synthesis of goethite anchored regenerated graphene oxide nanocomposite and its application in the removal of fluoride from drinking water. *Desalin. Water Treat.*, **57(58)**: 28393–28404. https://doi.org/10.1080/19443994.2016.1179222

Fiyadh, S. S., AlSaadi, M. A., Jaafar, W. Z., AlOmar, M. K., Fayaed, S. S., Mohd, N. S., Hin, L. S., and El-Shafie, A. (2019). Review on heavy metal adsorption processes by carbon nanotubes. *J. Clean Prod.*, **230**: 783–793. https://doi.org/10.1016/j.jclepro.2019.05.154

Foo, K. Y., and Hameed, B. H. (2010). Insights into the modeling of adsorption isotherm systems. *J. Chem. Eng.*, **156(1).**, 2–10. https://doi.org/10.1016/j.cej.2009.09.013

Fosshage, M. (2014). A new wastewater treatment technology for developing countries. *Filtr. Sep.*, **51(5)**: 14–17. https://doi.org/10.1016/S0015-1882(14)70180-6

Fu, F., and Wang, Q. (2011). Removal of heavy metal ions from wastewaters: Areview. *J. Environ. Manage.*, **92(3)**: 407–418. https://doi.org/10.1016/j.jenvman.2010.11.011

Fu, R., and Zhu, M. (2016). Synthesis and Characterization of Structure of Fe3O4@Graphene Oxide Nanocomposites. *Adv. Compos. Lett.*, **25(6)**: 096369351602500604. https://doi.org/10.1177/096369351602500604

Fuller, S. J., Burke, I. T., McMillan, D. G. G., Ding, W., and Stewart, D. I. (2015). Population Changes in a Community of Alkaliphilic Iron-Reducing Bacteria Due to Changes in the Electron Acceptor: Implications for Bioremediation at Alkaline Cr(VI)-Contaminated Sites. *Wat. Air, and Soil Poll.*, **226(6)**; 180. https://doi.org/10.1007/s11270-015-2437-z

Ganesan, V., Louis, C., and Damodaran, S. P. (2018). Graphene oxide-wrapped magnetite nanoclusters: A recyclable functional hybrid for fast and highly efficient removal of organic dyes from wastewater. *J. Environ. Chem. Eng.*, **6(2)**: 2176–2190. https://doi.org/10.1016/j.jece.2018.03.026

Gao, W. (2015). The Chemistry of Graphene Oxide. In W. Gao (Ed.), *Graphene Oxide* (61–95). Springer International Publishing. https://doi.org/10.1007/978-3-319-15500-5_3

Ghanim, B., Leahy, J. J., O'Dwyer, T. F., Kwapinski, W., Pembroke, J. T., and Murnane, J. G. (2022). Removal of hexavalent chromium (Cr(VI)) from aqueous solution using acid-modified poultry litter-derived hydrochar: Adsorption, regeneration and reuse. *J. Chem Technol Biotechnol.*, **97(1)**: 55–66. https://doi.org/10.1002/jctb.6904

Ghasemi, Z., Sourinejad, I., Kazemian, H., and Rohani, S. (2018). Application of zeolites in aquaculture industry: A review. *Rev. Aquac.*, **10(1)**: 75–95. https://doi.org/10.1111/raq.12148

Gitari, W. M., Ngulube, T., Masindi, V., and Gumbo, J. R. (2015a). Defluoridation of groundwater using Fe^{3+} -modified bentonite clay: Optimization of adsorption

conditions. *Desalin. Water Treat.*, **53(6)**: 1578–1590. https://doi.org/10.1080/19443994.2013.855669

Gleeson, T., Wada, Y., Bierkens, M. F. P., and van Beek, L. P. H. (2012). Water balance of global aquifers revealed by groundwater footprint. *Nature*, **488(7410)**: Article 7410. https://doi.org/10.1038/nature11295

Gode, F., and Pehlivan, E. (2005). Removal of Cr(VI) from aqueous solution by two Lewatit-anion exchange resins. *J. Hazard. Mater.*, **119(1–3)**: 175–182. https://doi.org/10.1016/j.jhazmat.2004.12.004

Gogoi, P. K., and Baruah, R. (2008). Fluoride removal from water by adsorption on acid activated kaolinite clay. *IJCT* **15(5)**: http://nopr.niscpr.res.in/handle/123456789/2845

Gollavelli, G., Chang, C.-C., and Ling, Y.-C. (2013). Facile Synthesis of Smart Magnetic Graphene for Safe Drinking Water: Heavy Metal Removal and Disinfection Control. *ACS Sustain. Chem. Eng.*, **1(5).**, 462–472. https://doi.org/10.1021/sc300112z

Goswami, A., and Purkait, M. K. (2011). Kinetic and Equilibrium Study for the Fluoride Adsorption using Pyrophyllite. *Sep Sci Technol.*, **46(11)**: 1797–1807. https://doi.org/10.1080/01496395.2011.572327

Grassi, M., Rizzo, L., and Farina, A. (2013). Endocrine disruptors compounds, pharmaceuticals and personal care products in urban wastewater: Implications for agricultural reuse and their removal by adsorption process. *Environ. Sci. Pollut. Res.*, **20(6)**: 3616–3628. https://doi.org/10.1007/s11356-013-1636-7

Guerra, A. C. S., de Andrade, M. B., Tonial dos Santos, T. R., and Bergamasco, R. (2021). Adsorption of sodium diclofenac in aqueous medium using graphene oxide nanosheets. *Environ. Technol.,* **42(16)**: 2599–2609. https://doi.org/10.1080/09593330.2019.1707882

Guertin, J., Jacobs, J. A., and Avakian, C. P. (2004). *Chromium(VI) Handbook*. CRC Press.

Guggenheim, S. (1995). Definition of Clay and Clay Mineral: Joint Report of the AIPEA Nomenclature and CMS Nomenclature Committees. *Clays clay Miner.*, **43(2)**: 255–256. https://doi.org/10.1346/CCMN.1995.0430213

Guleria, A., Kumari, G., Lima, E. C., Ashish, D. K., Thakur, V., and Singh, K. (2022). Removal of inorganic toxic contaminants from wastewater using sustainable biomass: A review. *Sci. Total Environ.*, *823*, 153689. https://doi.org/10.1016/j.scitotenv.2022.153689

Gulson, B. (2008). Stable lead isotopes in environmental health with emphasis on human investigations. *Science of The Total Environment*, **400(1–3)**: 75–92. https://doi.org/10.1016/j.scitotenv.2008.06.059

Guo, L., Ye, P., Wang, J., Fu, F., and Wu, Z. (2015). Three-dimensional Fe3O4-graphene macroscopic composites for arsenic and arsenate removal. *J. Hazar. Mater.*, **298**: 28–35. https://doi.org/10.1016/j.jhazmat.2015.05.011

Gupta, T., Singh, S. P., Rajput, P., and Agarwal, A. K. (Eds.). (2020). *Measurement, Analysis and Remediation of Environmental Pollutants*. Springer Singapore. https://doi.org/10.1007/978-981-15-0540-9

Gupta, V. K., Suhas, Ali, I., and Saini, V. K. (2004). Removal of Rhodamine B, Fast Green, and Methylene Blue from Wastewater Using Red Mud, an Aluminum Industry Waste. *Ind. Eng. Chem. Res.*, **43(7)**: 1740–1747. https://doi.org/10.1021/ie034218g

Gürel, L., Altaş, L., and Büyükgüngör, H. (2005). Removal of Lead from Wastewater Using Emulsion Liquid Membrane Technique. *Environ. Eng. Sci.*, **22(4)**: 411–420. https://doi.org/10.1089/ees.2005.22.411

Haerifar, M., and Azizian, S. (2012). Fractal-Like Adsorption Kinetics at the Solid/Solution Interface. *J. Phys. Chem. C*, **116(24)**: 13111–13119. https://doi.org/10.1021/jp301261h

Hamdaoui, O., and Zamouche, M. (2012). Sorption of Rhodamine B by Cedar Cone: Effect of Ph and Ionic Strength. *Energy Procedia.*, **18**: 1228–1239. https://doi.org/10.1016/j.egypro.2012.05.119

Hamdi, N., and Srasra, E. (2007). Removal of fluoride from acidic wastewater by clay mineral: Effect of solid–liquid ratios. *Desalination*, **206(1–3)**: 238–244. https://doi.org/10.1016/j.desal.2006.04.054

Han, B., Weatherley, A. J., Mumford, K., Bolan, N., He, J.-Z., Stevens, G. W., and Chen, D. (2022). Modification of naturally abundant resources for remediation of potentially toxic elements: A review. *J. Hazard. Mater.*, **421**: 126755. https://doi.org/10.1016/j.jhazmat.2021.126755

Han, I., Schlautman, M. A., and Batchelor, B. (2000). Removal of Hexavalent Chromium from Groundwater by Granular Activated Carbon. *Water Environ. Res.*, **72(1)**: 29–39.

Hawksley and Lucinda (2016). Bitten by Witch Fever: Wallpaper & Arsenic in the Victorian Home. New York: Thames & Hudson

Hayes, K. F., Papelis, C., and Leckie, J. O. (1988). Modeling ionic strength effects on anion adsorption at hydrous oxide/solution interfaces. *J Colloid Interface Sci.*, **125(2)**: 717–726. https://doi.org/10.1016/0021-9797(88)90039-2

He, Z. L., Yang, X. E., and Stoffella, P. J. (2005). Trace elements in agroecosystems and impacts on the environment. *J. Trace Elem. Med. Biol.*, **19(2)**: 125–140. https://doi.org/10.1016/j.jtemb.2005.02.010

Heberer, T. (2002). Occurrence, fate, and removal of pharmaceutical residues in the aquatic environment: A review of recent research data. *Toxicol Lett.*, **131(1–2)**: 5–17. https://doi.org/10.1016/S0378-4274(02)00041-3

Hiew, B. Y. Z., Lee, L. Y., Lee, X. J., Gan, S., Thangalazhy-Gopakumar, S., Lim, S. S., Pan, G.-T., and Yang, T. C.-K. (2019). Adsorptive removal of diclofenac by graphene oxide: Optimization, equilibrium, kinetic and thermodynamic studies. *J. Taiwan Inst. Chem. Eng.*, **98**: 150–162. https://doi.org/10.1016/j.jtice.2018.07.034

Ho, Y. S., and McKay, G. (1999). Pseudo-second order model for sorption processes. *Process Biochem.*, **34(5)**: 451–465. https://doi.org/10.1016/S0032-9592(98)00112-5

Ho, Y.-S. (2006). Review of second-order models for adsorption systems. *J. Hazard. Mater.*,**136(3)**: 681–689. https://doi.org/10.1016/j.jhazmat.2005.12.043

Hou, M.-F., Ma, C.-X., Zhang, W.-D., Tang, X.-Y., Fan, Y.-N., and Wan, H.-F. (2011). Removal of rhodamine B using iron-pillared bentonite. *J. Hazard. Mater.*, **186(2–3)**: 1118–1123. https://doi.org/10.1016/j.jhazmat.2010.11.110

Hu, H., and Xu, K. (2020). Chapter 8—Physicochemical technologies for HRPs and risk control. In H. Ren & X. Zhang (Eds.), *High-Risk Pollutants in Wastewater* (169–207). Elsevier. https://doi.org/10.1016/B978-0-12-816448-8.00008-3

Hu, X., Cheng, Z., Sun, Z., and Zhu, H. (2017). Adsorption of Diclofenac and Triclosan in Aqueous Solution by Purified Multi-Walled Carbon Nanotubes. *Pol. J. Environ. Stud.*, **26(1)**: 87–95. https://doi.org/10.15244/pjoes/63885

Hu, X., Li, Y., Wang, Y., Li, X., Li, H., Liu, X., and Zhang, P. (2010). Adsorption kinetics, thermodynamics and isotherm of thiacalix[4]arene-loaded resin to heavy metal ions. *Desalination*, **259(1)**: 76–83. https://doi.org/10.1016/j.desal.2010.04.032

Huang, C. P., Dong, C., and Tang, Z. (1993). Advanced chemical oxidation: Its present role and potential future in hazardous waste treatment. *Waste Manage.*, **13(5)**: 361–377. https://doi.org/10.1016/0956-053X(93)90070-D

Huang, D., Li, B., Wu, M., Kuga, S., and Huang, Y. (2018). Graphene Oxide-Based Fe–Mg (Hydr)oxide Nanocomposite as Heavy Metals Adsorbent. *J. Chem. Eng. Data*, **63(6)**: 2097–2105. https://doi.org/10.1021/acs.jced.8b00100

Huang, Z.-H., Zheng, X., Lv, W., Wang, M., Yang, Q.-H., and Kang, F. (2011). Adsorption of Lead(II) Ions from Aqueous Solution on Low-Temperature Exfoliated Graphene Nanosheets. *Langmui.r*, **27(12)**: 7558–7562. https://doi.org/10.1021/la200606r

Huq, Md. E., Fahad, S., Shao, Z., Sarven, M. S., Khan, I. A., Alam, M., Saeed, M., Ullah, H., Adnan, M., Saud, S., Cheng, Q., Ali, S., Wahid, F., Zamin, M., Raza, M. A., Saeed, B., Riaz, M., and Khan, W. U. (2020). Arsenic in a groundwater environment in Bangladesh: Occurrence and mobilization. *J. Environ. Manage.*, **262**: 110318. https://doi.org/10.1016/j.jenvman.2020.110318

IARC (1982) *IARC Monographs on the Evaluation of the Carcinogenic Risk of Chemicals to Humans*, Suppl. 4, *Chemicals, Industrial Processes and Industries Associated with Cancer in Humans*. IARC Monographs *Volumes 1 to 29*, Lyon, pp. 91–93.

Iiu, Y., Lv, J., Jin, W., and Zhao, Y. (2016a). Defluoridation by rice spike-like akaganeite anchored graphene oxide. *RSC Adv.*, **6(14)**: 11240–11249. https://doi.org/10.1039/C5RA24565F

Jabeen, H., Chandra, V., Jung, S., Lee, J. W., Kim, K. S., and Kim, S. B. (2011). Enhanced Cr(VI) removal using iron nanoparticle decorated graphene. *Nanoscale*, **3(9)**: 3583–3585. https://doi.org/10.1039/C1NR10549C

Jabeen, H., Kemp, K. C., and Chandra, V. (2013). Synthesis of nano zerovalent iron nanoparticles – Graphene composite for the treatment of lead contaminated water. *J. Environ. Manage.*, **130**: 429–435. https://doi.org/10.1016/j.jenvman.2013.08.022

Jadhav, S. V., Bringas, E., Yadav, G. D., Rathod, V. K., Ortiz, I., and Marathe, K. V. (2015). Arsenic and fluoride contaminated groundwaters: A review of current technologies for contaminants removal. *J. Environ. Manage.*, **162**: 306–325. https://doi.org/10.1016/j.jenvman.2015.07.020

Jauris, I. M., Matos, C. F., Saucier, C., Lima, E. C., Zarbin, A. J. G., Fagan, S. B., Machado, F. M., and Zanella, I. (2016). Adsorption of sodium diclofenac on graphene: A combined experimental and theoretical study. *Phys. Chem. Chem. Phys.*, **18(3)**: 1526–1536. https://doi.org/10.1039/C5CP05940B

Jia, Y., Xu, L., Wang, X., and Demopoulos, G. P. (2007). Infrared spectroscopic and X-ray diffraction characterization of the nature of adsorbed arsenate on ferrihydrite. *Geochim. Cosmochim. Acta.*, **71(7)**: 1643–1654. https://doi.org/10.1016/j.gca.2006.12.021

JMP (2017). Joint Monitoring Programme for Water Supply, Sanitation and Hygiene . ANNUAL REPORT WHO/UNICEF

Johnson, A. C., and Sumpter, J. P. (2001). Removal of Endocrine-Disrupting Chemicals in Activated Sludge Treatment Works. *Environ. Sci. Technol.*, **35(24)**: 4697–4703. https://doi.org/10.1021/es010171j

Johnston, R. B., Berg, M., Johnson, C. A., Tilley, E., & Hering, J. G. (2011). Water and Sanitation in Developing Countries: Geochemical Aspects of Quality and Treatment. *Elements*, *7*(3), 163–168. https://doi.org/10.2113/gselements.7.3.163

Junyong, C., Yongmei, H., Yan, L., and Jiajia, G. (2013). Magnetic graphene oxides as highly effective adsorbents for rapid removal of a cationic dye rhodamine B from aqueous solutions. *RSC Adv.*, **3(20)**: 7254. https://doi.org/10.1039/c3ra22599b

Jurdziak, M., Gać, P., Martynowicz, H., and Poręba, R. (2015). Function of respiratory system evaluated using selected spirometry parameters in persons occupationally exposed to lead without evident health problems. *Environ. Toxicol. Pharmacol.*, **39(3)**: 1034–1040. https://doi.org/10.1016/j.etap.2015.03.009

Kadirvelu, K., Karthika, C., Vennilamani, N., and Pattabhi, S. (2005). Activated carbon from industrial solid waste as an adsorbent for the removal of Rhodamine-B from aqueous solution: Kinetic and equilibrium studies. *Chemosphere*, **60(8)**: 1009–1017. https://doi.org/10.1016/j.chemosphere.2005.01.047

Kahsay, M. H., Belachew, N., Tadesse, A., and Basavaiah, K. (2020). Magnetite nanoparticle decorated reduced graphene oxide for adsorptive removal of crystal violet and antifungal activities. *RSC Adv.*, **10(57):** 34916–34927. https://doi.org/10.1039/D0RA07061

Kamble, S. P., Dixit, P., Rayalu, S. S., and Labhsetwar, N. K. (2009). Defluoridation of drinking water using chemically modified bentonite clay. *Desalination*, **249(2)**: 687–693. https://doi.org/10.1016/j.desal.2009.01.031

Kameda, T., Oba, J., and Yoshioka, T. (2015). Recyclable Mg–Al layered double hydroxides for fluoride removal: Kinetic and equilibrium studies. *J. Hazard. Mater.*, **300**: 475–482. https://doi.org/10.1016/j.jhazmat.2015.07.023

Kang, B. K., Lim, B. S., Yoon, Y., Kwag, S. H., Park, W. K., Song, Y. H., Yang, W. S., Ahn, Y.-T., Kang, J.-W., and Yoon, D. H. (2017). Efficient removal of arsenic

by strategically designed and layer-by-layer assembled PS@+rGO@GO@Fe3O4 composites. *J. Environ. Manage.*, **201**: 286–293. https://doi.org/10.1016/j.jenvman.2017.05.066

Kanrar, S., Debnath, S., De, P., Parashar, K., Pillay, K., Sasikumar, P., and Ghosh, U. C. (2016b). Preparation, characterization and evaluation of fluoride adsorption efficiency from water of iron-aluminium oxide-graphene oxide composite material. *J. Chem. Eng.*, **306**: 269–279. https://doi.org/10.1016/j.cej.2016.07.037

Karimi-Maleh, H., Shafieizadeh, M., Taher, M. A., Opoku, F., Kiarii, E. M., Govender, P. P., Ranjbari, S., Rezapour, M., and Orooji, Y. (2020). The role of magnetite/graphene oxide nano-composite as a high-efficiency adsorbent for removal of phenazopyridine residues from water samples, an experimental/theoretical investigation. *J. Mol. Liq.*, **298**: 112040. https://doi.org/10.1016/j.molliq.2019.112040

Katsoyiannis, I. A., and Zouboulis, A. I. (2006). Comparative Evaluation of Conventional and Alternative Methods for the Removal of Arsenic from Contaminated Groundwaters. *Rev. Environ. Health.*, **21(1)**: https://doi.org/10.1515/REVEH.2006.21.1.25

Khan, S., Achazhiyath Edathil, A., and Banat, F. (2019). Sustainable synthesis of graphene-based adsorbent using date syrup. *Sci Rep.*, **9(1)**: 18106. https://doi.org/10.1038/s41598-019-54597-x

Khan, T. A., Nazir, M., and Khan, E. A. (2013). Adsorptive removal of rhodamine B from textile wastewater using water chestnut (Trapa natans L.) peel: Adsorption dynamics and kinetic studies. *Toxicol. Environ. Chem.*, **95(6)**: 919–931. https://doi.org/10.1080/02772248.2013.840369

Khan, T. A., Sharma, S., and Ali, I. (n.d.). *Adsorption of Rhodamine B dye from aqueous solution onto acid activated mango (Magnifera indica) leaf powder: Equilibrium, kinetic and thermodynamic studies*.

Kimambo, V., Bhattacharya, P., Mtalo, F., Mtamba, J., and Ahmad, A. (2019). Fluoride occurrence in groundwater systems at global scale and status of defluoridation – State of the art. *Groundwater for Sustainable Development*, **9**: 100223. https://doi.org/10.1016/j.gsd.2019.100223

King, W. G., Rodriguez, J. M., and Wai, C. M. (1974). Losses of trace concentrations of cadmium from aqueous solution during storage in glass containers. *Anal. Chem.*, **46(6)**: 771–773. https://doi.org/10.1021/ac60342a024

Knepper, T. P. (2003). Synthetic chelating agents and compounds exhibiting complexing properties in the aquatic environment. *Trends Analyt. Chem.*, **10(22)**: 708–724. https://doi.org/10.1016/S0165-9936(03)01008-2

Konta, J. (1995). Clay and man: Clay raw materials in the service of man. *Appl. Clay Sci.*, **10(4)**: 275–335. https://doi.org/10.1016/0169-1317(95)00029-4

Kooh, M. R. R., Dahri, M. K., and Lim, L. B. L. (2016). The removal of rhodamine B dye from aqueous solution using *Casuarina equisetifolia* needles as adsorbent. *Cogent Environ. Sci.*, **2(1)**: 1140553. https://doi.org/10.1080/23311843.2016.1140553

Kosnett, M. J., Wedeen, R. P., Rothenberg, S. J., Hipkins, K. L., Materna, B. L., Schwartz, B. S., Hu, H., and Woolf, A. (2007). Recommendations for Medical Management of Adult Lead Exposure. *Environ. Health Perspect.*, **115(3)**: 463–471. https://doi.org/10.1289/ehp.9784

Krzmarzick, M. J., and Novak, P. J. (2014). Removal of chlorinated organic compounds during wastewater treatment: Achievements and limits. *Appl.*

Microbiol. Biotechnol., **98(14)**: 6233–6242. https://doi.org/10.1007/s00253-014-5800-x

Kumar, A. S. K., and Jiang, S.-J. (2016). Chitosan-functionalized graphene oxide: A novel adsorbent an efficient adsorption of arsenic from aqueous solution. *J. Environ. Chem. Eng.*, **4(2)**: 1698–1713. https://doi.org/10.1016/j.jece.2016.02.035

Kumar, V., Kim, K.-H., Park, J.-W., Hong, J., and Kumar, S. (2017). Graphene and its nanocomposites as a platform for environmental applications. *J. Chem. Eng.*, **315**: 210–232. https://doi.org/10.1016/j.cej.2017.01.008

Lalchhingpuii, Tiwari, D., Lalhmunsiama, and Lee, S. M. (2017a). Chitosan templated synthesis of mesoporous silica and its application in the treatment of aqueous solutions contaminated with cadmium(II) and lead(II). *J. Chem. Eng.*, **328**: 434–444. https://doi.org/10.1016/j.cej.2017.07.053

Lalhmunsiama, L., Ngainunsiami, N., Kim, D.-J., and Tiwari, D. (2021). Graphene based advanced materials in the remediation of aquatic environment contaminated with fluoride: Newer insights and applicability. *Chem. Eng. Process.:Process Intensif*, **165**: 108428. https://doi.org/10.1016/j.cep.2021.108428

Lalhmunsiama, L., Tiwari, D., and Lee, S. (2012a). Activated carbon and manganese coated activated carbon precursor to dead biomass in the remediation of arsenic contaminated water. *Environ. Eng. Res.*, **17**: 41–48. https://doi.org/10.4491/eer.2012.17.S1.S41

Lalhmunsiama, Lalchhingpuii, Nautiyal, B. P., Tiwari, D., Choi, S. I., Kong, S.-H., and Lee, S.-M. (2016a). Silane grafted chitosan for the efficient remediation of aquatic environment contaminated with arsenic(V). *J. Colloid Interface Sci.*, **467**: 203–212. https://doi.org/10.1016/j.jcis.2016.01.019

Lalhmunsiama, Lee, S. M., and Tiwari, D. (2013). Manganese oxide immobilized activated carbons in the remediation of aqueous wastes contaminated with copper(II) and lead(II). *J. Chem. Eng.* **225**: 128–137. https://doi.org/10.1016/j.cej.2013.03.083

Lalhmunsiama, Lee, S.-M., Lalchhingpuii, and Tiwari, D. (2016). Functionalized hybrid material precursor to chitosan in the efficient remediation of aqueous solutions contaminated with As(V). *J. Environ. Chem. Eng.*, **4(2)**: 1537–1544. https://doi.org/10.1016/j.jece.2016.02.015

Lata, S., and Samadder, S. R. (2016). Removal of arsenic from water using nano adsorbents and challenges: A review. *J. Environ. Manage.*, **166**: 387–406. https://doi.org/10.1016/j.jenvman.2015.10.039

Lee, S. M., Lalchhingpuii, Lalhmunsiama, and Tiwari, D. (2016a). Synthesis of functionalized biomaterials and its application in the efficient remediation of aquatic environment contaminated with Cr(VI). *J. Chem. Eng.*, **296**: 35–44. https://doi.org/10.1016/j.cej.2016.03.077

Lee, S. M., Lalhmunsiama, Thanhmingliana, and Tiwari, D. (2015). Porous hybrid materials in the remediation of water contaminated with As(III) and As(V). *J. Chem. Eng.,* **270**: 496–507. https://doi.org/10.1016/j.cej.2015.02.053

Lee, S. M., and Tiwari, D. (2012). Organo and inorgano-organo-modified clays in the remediation of aqueous solutions: An overview. *Appl. Clay Sci.*, **59–60**: 84–102. https://doi.org/10.1016/j.clay.2012.02.006

Lee, S.-M., Kim, W.-G., Laldawngliana, C., and Tiwari, D. (2010). Removal Behavior of Surface Modified Sand for Cd(II) and Cr(VI) from Aqueous Solutions. *J. Chem Eng. Data.*, **55(9)**: 3089–3094. https://doi.org/10.1021/je901094h

Li, J., Hu, J., Sheng, G., Zhao, G., and Huang, Q. (2009). Effect of pH, ionic strength, foreign ions and temperature on the adsorption of Cu(II) from aqueous solution to GMZ bentonite. *Colloids Surf A: Physicochem. Eng. Asp.*, **349(1)**: 195–201. https://doi.org/10.1016/j.colsurfa.2009.08.018

Li, Y., Du, Q., Wang, J., Liu, T., Sun, J., Wang, Y., Wang, Z., Xia, Y., and Xia, L. (2013). Defluoridation from aqueous solution by manganese oxide coated graphene oxide. *J. Fluor. Chem.*, **148**: 67–73. https://doi.org/10.1016/j.jfluchem.2013.01.028

Li, Y., Zhang, F.-S., & Xiu, F.-R. (2009). Arsenic (V) removal from aqueous system using adsorbent developed from a high iron-containing fly ash. *The Science of the Total Environment*, *407*(21), 5780–5786. https://doi.org/10.1016/j.scitotenv.2009.07.017

Li, Y.-H., Wang, S., Wei, J., Zhang, X., Xu, C., Luan, Z., Wu, D., and Wei, B. (2002). Lead adsorption on carbon nanotubes. *Chem. Phys. Lett.*, **357(3–4)**: 263–266. https://doi.org/10.1016/S0009-2614(02)00502-X

Ling Tan, T., A/P Krusnamurthy, P., Nakajima, H., and Abdul Rashid, S. (2020). Adsorptive, kinetics and regeneration studies of fluoride removal from water using zirconium-based metal organic frameworks. *RSC Adv.*, **10(32).**, 18740–18752. https://doi.org/10.1039/D0RA01268H

Liu, C.-H., Chuang, Y.-H., Chen, T.-Y., Tian, Y., Li, H., Wang, M.-K., and Zhang, W. (2015). Mechanism of Arsenic Adsorption on Magnetite Nanoparticles from Water: Thermodynamic and Spectroscopic Studies. *Environ. Sci. Technol.*, **49(13)**, 7726–7734. https://doi.org/10.1021/acs.est.5b00381

Liu, L., Zhang, Y., He, Y., Xie, Y., Huang, L., Tan, S., and Cai, X. (2015). Preparation of montmorillonite-pillared graphene oxide with increased single- and co-

adsorption towards lead ions and methylene blue. *RSC Adv.*, **5(6):** 3965–3973. https://doi.org/10.1039/C4RA13008A

Liu, S., Zeng, T. H., Hofmann, M., Burcombe, E., Wei, J., Jiang, R., Kong, J., and Chen, Y. (2011). Antibacterial Activity of Graphite, Graphite Oxide, Graphene Oxide, and Reduced Graphene Oxide: Membrane and Oxidative Stress. *ACS Nano*, **5(9)**: 6971–6980. https://doi.org/10.1021/nn202451x

Liu, Z., Kanjo, Y., and Mizutani, S. (2009). Removal mechanisms for endocrine disrupting compounds (EDCs) in wastewater treatment — physical means, biodegradation, and chemical advanced oxidation: A review. *Sci. Total Environ.*, **407(2)**: 731–748. https://doi.org/10.1016/j.scitotenv.2008.08.039

Lonappan, L., Brar, S. K., Das, R. K., Verma, M., and Surampalli, R. Y. (2016). Diclofenac and its transformation products: Environmental occurrence and toxicity - A review. *Environ. Int.*, **96**: 127–138. https://doi.org/10.1016/j.envint.2016.09.014

Lonappan, L., Pulicharla, R., Rouissi, T., Brar, S. K., Verma, M., Surampalli, R. Y., and Valero, J. R. (2016). Diclofenac in municipal wastewater treatment plant: Quantification using laser diode thermal desorption—atmospheric pressure chemical ionization—tandem mass spectrometry approach in comparison with an established liquid chromatography-electrospray ionization–tandem mass spectrometry method. *J. Chromatogr. A*, **1433**: 106–113. https://doi.org/10.1016/j.chroma.2016.01.030

Lonappan, L., Rouissi, T., Kaur Brar, S., Verma, M., and Surampalli, R. Y. (2018). An insight into the adsorption of diclofenac on different biochars: Mechanisms, surface chemistry, and thermodynamics. *Bioresour Technol.*, **249:** 386–394. https://doi.org/10.1016/j.biortech.2017.10.039

Luo, X., Wang, C., Wang, L., Deng, F., Luo, S., Tu, X., and Au, C. (2013). Nanocomposites of graphene oxide-hydrated zirconium oxide for simultaneous removal of As(III) and As(V) from water. *J.Chem. Eng.*, **220**: 98–106. https://doi.org/10.1016/j.cej.2013.01.017

Lv, L., Hor, M. P., Su, F., and Zhao, X. S. (2005). Competitive adsorption of Pb2+, Cu2+, and Cd2+ ions on microporous titanosilicate ETS-10. *J. Colloid Interface Sci.*, **287(1)**: 178–184. https://doi.org/10.1016/j.jcis.2005.01.073

Mahdavinia, G. R., and Mosallanezhad, A. (2016). Facile and green rout to prepare magnetic and chitosan-crosslinked κ-carrageenan bionanocomposites for removal of methylene blue. *J. Water Process. Eng.*, **10**: 143–155. https://doi.org/10.1016/j.jwpe.2016.02.010

Mahdi, C., Pratama, C. A., and Pratiwi, H. (2019). Preventive Study Garlic Extract Water (Allium sativum) Toward SGPT, SGOT, and the Description of Liver Histopathology on Rat (Rattus norvegicus), which were exposed by Rhodamine B. *IOP Conf. Ser.: Mater. Sci. Eng.*, **546(6)**: 062015. https://doi.org/10.1088/1757-899X/546/6/062015

Maiti, A., Basu, J. K., and De, S. (2011). Chemical treated laterite as promising fluoride adsorbent for aqueous system and kinetic modeling. *Desalination.*, **265(1–3)**: 28–36. https://doi.org/10.1016/j.desal.2010.07.026

Malek, A., and Farooq, S. (1996). Comparison of isotherm models for hydrocarbon adsorption on activated carbon. *AIChE J.*, **42(11)**: 3191–3201. https://doi.org/10.1002/aic.690421120

Mandal, B. K., and Suzuki, K. T. (2002). Arsenic round the world: A review. *Talanta*, **58(1)**: 201–235. https://doi.org/10.1016/S0039-9140(02)00268-0

Mao, N., Huang, L., and Shuai, Q. (2019). Facile Synthesis of Porous Carbon for the Removal of Diclofenac Sodium from Water. *ACS Omega*, **4(12)**: 15051–15060. https://doi.org/10.1021/acsomega.9b01838

Marcano, D. C., Kosynkin, D. V., Berlin, J. M., Sinitskii, A., Sun, Z., Slesarev, A., Alemany, L. B., Lu, W., and Tour, J. M. (2010). Improved Synthesis of Graphene Oxide. *ACS Nano*, **4(8)**: 4806–4814. https://doi.org/10.1021/nn1006368

Marin, P., Módenes, A. N., Bergamasco, R., Paraíso, P. R., and Hamoudi, S. (2016). Synthesis, Characterization and Application of ZrCl4-Graphene Composite Supported on Activated Carbon for Efficient Removal of Fluoride to Obtain Drinking Wat. *Air, and Soil Poll.*, **227(12)**: 479. https://doi.org/10.1007/s11270-016-3188-1

Mbayachi, V. B., Ndayiragije, E., Sammani, T., Taj, S., Mbuta, E. R., and khan, A. ullah. (2021). Graphene synthesis, characterization and its applications: A review. *Results Chem.,* **3**: 100163. https://doi.org/10.1016/j.rechem.2021.100163

McArthur, J. M. (2019). Arsenic in Groundwater. In P. K. Sikdar (Ed.), *Groundwater Development and Management* (279–308). Springer International Publishing. https://doi.org/10.1007/978-3-319-75115-3_12

McGrail, B. T., Rodier, B. J., and Pentzer, E. (2014). Rapid Functionalization of Graphene Oxide in Water. *Chem. Mater.*, **26(19)**: 5806–5811. https://doi.org/10.1021/cm5031409

Meenakshi, S., Sundaram, C. S., and Sukumar, R. (2008). Enhanced fluoride sorption by mechanochemically activated kaolinites. *J. Hazard. Mater.*, **153(1–2)**: 164–172. https://doi.org/10.1016/j.jhazmat.2007.08.031

Mekatel, E. H., Amokrane, S., Aid, A., Nibou, D., and Trari, M. (2015). Adsorption of methyl orange on nanoparticles of a synthetic zeolite NaA/CuO. *C R Chim.*, **18(3)**: 336–344. https://doi.org/10.1016/j.crci.2014.09.009

Meloun, M., Bordovská, S., and Galla, L. (2007). The thermodynamic dissociation constants of four non-steroidal anti-inflammatory drugs by the least-squares nonlinear regression of multiwavelength spectrophotometric pH-titration data. *J. Pharm. Biomed. Anal.*, **45(4)**: 552–564. https://doi.org/10.1016/j.jpba.2007.07.029

Miniero, R., and Iamiceli, A. L. (2008). Persistent Organic Pollutants. In *Encyclopedia of Ecology* (2672–2682). Elsevier. https://doi.org/10.1016/B978-008045405-4.00421-3

Miretzky, P., and Cirelli, A. F. (2011). Fluoride removal from water by chitosan derivatives and composites: A review. *J. Fluor. Chem.*, **132(4)**: 231–240. https://doi.org/10.1016/j.jfluchem.2011.02.001

Mkhoyan, K. A., Contryman, A. W., Silcox, J., Stewart, D. A., Eda, G., Mattevi, C., Miller, S., and Chhowalla, M. (2009). Atomic and Electronic Structure of Graphene-Oxide. *Nano Lett.*, **9(3)**: 1058–1063. https://doi.org/10.1021/nl8034256

Mnasri-Ghnimi, S., and Frini-Srasra, N. (2019). Removal of heavy metals from aqueous solutions by adsorption using single and mixed pillared clays. *Appl. Clay Sci.*, **179**: 105151. https://doi.org/10.1016/j.clay.2019.105151

Mobarak, M., Selim, A. Q., Mohamed, E. A., and Seliem, M. K. (2018). Modification of organic matter-rich clay by a solution of cationic surfactant/H2O2: A new product for fluoride adsorption from solutions. *J. Clean. Prod.*, **192**: 712–721. https://doi.org/10.1016/j.jclepro.2018.05.044

Mohan, S. V., and Karthikeyan, J. (1997). Removal of lignin and tannin colour from aqueous solution by adsorption onto activated charcoal. *Environ Pollut.*, **97(1–2)**: 183–187. https://doi.org/10.1016/S0269-7491(97)00025-0

Momčilović, M., Purenović, M., Bojić, A., Zarubica, A., and Ranđelović, M. (2011). Removal of lead(II) ions from aqueous solutions by adsorption onto pine cone activated carbon. *Desalination*, **276(1)**: 53–59. https://doi.org/10.1016/j.desal.2011.03.013

Montalvo, S., Cahn, I., Borja, R., Huiliñir, C., and Guerrero, L. (2017). Use of solid residue from thermal power plant (fly ash) for enhancing sewage sludge anaerobic digestion: Influence of fly ash particle size. *Bioresour. Technol*, **244**: 416–422. https://doi.org/10.1016/j.biortech.2017.07.159

Moore, M. R. (1977). Lead in drinking water in soft water areas—Health hazards. *Sci. Total Environ.*, **7(2)**: 109–115. https://doi.org/10.1016/0048-9697(77)90002-X

Nabbou, N., Belhachemi, M., Boumelik, M., Merzougui, T., Lahcene, D., Harek, Y., Zorpas, A. A., and Jeguirim, M. (2019). Removal of fluoride from groundwater using natural clay (kaolinite): Optimization of adsorption conditions. *C R Chim.*, **22(2–3)**: 105–112. https://doi.org/10.1016/j.crci.2018.09.010

Nachman, K. E., Graham, J. P., Price, L. B., and Silbergeld, E. K. (2005). Arsenic: A Roadblock to Potential Animal Waste Management Solutions. *Environ. Health Perspect.*, **113(9)**: 1123–1124. https://doi.org/10.1289/ehp.7834

Naghipour, D., Hoseinzadeh, L., Taghavi, K., and Jaafari, J. (2018). Characterization, kinetic, thermodynamic and isotherm data for diclofenac removal from aqueous solution by activated carbon derived from pine tree. *Data Br.*, **18**: 1082–1087. https://doi.org/10.1016/j.dib.2018.03.068

Nam, S.-W., Jung, C., Li, H., Yu, M., Flora, J. R. V., Boateng, L. K., Her, N., Zoh, K.-D., and Yoon, Y. (2015). Adsorption characteristics of diclofenac and sulfamethoxazole to graphene oxide in aqueous solution. *Chemosphere*, **136**: 20–26. https://doi.org/10.1016/j.chemosphere.2015.03.061

Neolaka, Y. A. B., Lawa, Y., Naat, J. N., Riwu, A. A. P., Iqbal, M., Darmokoesoemo, H., and Kusuma, H. S. (2020). The adsorption of Cr(VI) from water samples using graphene oxide-magnetic (GO-Fe3O4) synthesized from natural cellulose-based graphite (kusambi wood or Schleichera oleosa): Study of kinetics, isotherms and thermodynamics. *J. Mater. Res. Technol.*, **9(3)**: 6544–6556. https://doi.org/10.1016/j.jmrt.2020.04.040

Nethravathi, C., Viswanath, B., Shivakumara, C., Mahadevaiah, N., and Rajamathi, M. (2008). The production of smectite clay/graphene composites through delamination and co-stacking. *Carbon*, **46(13)**: 1773–1781. https://doi.org/10.1016/j.carbon.2008.07.037

Novoselov, K. S., Fal′ko, V. I., Colombo, L., Gellert, P. R., Schwab, M. G., and Kim, K. (2012). A roadmap for graphene. *Nature*, **490(7419)**: Article 7419. https://doi.org/10.1038/nature11458

Nriagu, J. O. (1994). *Arsenic in the environment. Part I: Cycling and characterization*. https://www.osti.gov/etdeweb/biblio/37811

Oaks, J. L., Gilbert, M., Virani, M. Z., Watson, R. T., Meteyer, C. U., Rideout, B. A., Shivaprasad, H. L., Ahmed, S., Iqbal Chaudhry, M. J., Arshad, M., Mahmood, S., Ali, A., and Ahmed Khan, A. (2004). Diclofenac residues as the cause of vulture population decline in Pakistan. *Nature*, **427(6975)**: Article 6975. https://doi.org/10.1038/nature02317

Pan, L., Zhai, G., Yang, X., Yu, H., and Cheng, C. (2019). Thermosensitive Microgels-Decorated Magnetic Graphene Oxides for Specific Recognition and

Adsorption of Pb(II) from Aqueous Solution. *ACS Omega*, **4(2)**: 3933–3945. https://doi.org/10.1021/acsomega.8b03539

Pandi, K., and Viswanathan, N. (2016). A facile synthesis of metal ion-imprinted graphene oxide/alginate hybrid biopolymeric beads for enhanced fluoride sorption. *RSC Adv.*, **6(79)**: 75905–75915. https://doi.org/10.1039/C6RA11713A

Peng, W., Li, H., Liu, Y., and Song, S. (2017). Areview on heavy metal ions adsorption from water by graphene oxide and its composites. *J. Mol. Liq.*, **230**: 496–504. https://doi.org/10.1016/j.molliq.2017.01.064

Pérez-Estrada, L. A., Malato, S., Gernjak, W., Agüera, A., Thurman, E. M., Ferrer, I., and Fernández-Alba, A. R. (2005). Photo-Fenton Degradation of Diclofenac: Identification of Main Intermediates and Degradation Pathway. *Environ. Sci. Technol.*, **39(21)**: 8300–8306. https://doi.org/10.1021/es050794n

Petrovic, M. (2003). Analysis and removal of emerging contaminants in wastewater and drinking water. *TrAC Trend Anal. Chem.*, **22(10)**: 685–696. https://doi.org/10.1016/S0165-9936(03)01105-1

Pinto, S. S., and Mcgill, C. M. (1953). Arsenic Trioxide Exposure in Industry. *Indust. M. Surg.*, **22(7)**: 281–287.

Poursaberi, T., Ganjali, M. R., and Hassanisadi, M. (2012). A novel fluoride-selective electrode based on metalloporphyrin grafted-grapheneoxide. *Talanta*, **101**: 128–134. https://doi.org/10.1016/j.talanta.2012.08.039

Prasad, M. N. V. (n.d.). Phytoremediation of Metals and Radionuclides in the Environment: The Case for Natural Hyperaccumulators, Metal Transporters, Soil-Amending Chelators and Transgenic Plants. In *Heavy Metal Stress in Plants*. https://doi.org/10.1007/978-3-662-07743-6_14

Ptaszkowska-Koniarz, M., Goscianska, J., and Pietrzak, R. (2018). Removal of rhodamine B from water by modified carbon xerogels. *Colloids Surf. A Physicochem. Eng. Asp.*, **543:** 109–117. https://doi.org/10.1016/j.colsurfa.2018.01.057

Rahman, F. A., Allan, D. L., Rosen, C. J., and Sadowsky, M. J. (2004). Arsenic Availability from Chromated Copper Arsenate (CCA)-Treated Wood. *J. Environ. Qual.*, **33(1)**: 173–180. https://doi.org/10.2134/jeq2004.1730

Rahmani, A., Mousavi, H. Z., and Fazli, M. (2010). Effect of nanostructure alumina on adsorption of heavy metals. *Desalination*, **253(1)**: 94–100. https://doi.org/10.1016/j.desal.2009.11.027

Ramdani, A., Taleb, S., Benghalem, A., and Ghaffour, N. (2010). Removal of excess fluoride ions from Saharan brackish water by adsorption on natural materials. *Desalination*, **250(1)**: 408–413. https://doi.org/10.1016/j.desal.2009.09.066

Ramesha, G. K., Vijaya Kumara, A., Muralidhara, H. B., and Sampath, S. (2011). Graphene and graphene oxide as effective adsorbents toward anionic and cationic dyes. *J. Colloid Interface Sci.*, **361(1)**: 270–277. https://doi.org/10.1016/j.jcis.2011.05.050

Rana, R. S., Singh, P., Kandari, V., Singh, R., Dobhal, R., and Gupta, S. (2017). A review on characterization and bioremediation of pharmaceutical industries' wastewater: An Indian perspective. *Appl. Water Sci.*, **7(1)**: 1–12. https://doi.org/10.1007/s13201-014-0225-3

Rashed, M. N. (2013). Adsorption Technique for the Removal of Organic Pollutants from Water and Wastewater. In *Organic Pollutants—Monitoring, Risk and Treatment*. IntechOpen. https://doi.org/10.5772/54048

Ravenscroft, P. (2007). Predicting the global extent of arsenic pollution of groundwater and its potential impact on human health. *UNICEF Rep.*, 1–35.

Ren, X., Chen, C., Nagatsu, M., and Wang, X. (2011). Carbon nanotubes as adsorbents in environmental pollution management: A review. *J. Chem. Eng.,* **170(2–3)**: 395–410. https://doi.org/10.1016/j.cej.2010.08.045

Repo, E., Mäkinen, M., Rengaraj, S., Natarajan, G., Bhatnagar, A., and Sillanpää, M. (2012). Lepidocrocite and its heat-treated forms as effective arsenic adsorbents in aqueous medium. *J. Chem. Eng,*, **180**: 159–169. https://doi.org/10.1016/j.cej.2011.11.030

Repo, E., Warchol, J. K., Kurniawan, T. A., and Sillanpää, M. E. T. (2010). Adsorption of Co(II) and Ni(II) by EDTA- and/or DTPA-modified chitosan: Kinetic and equilibrium modeling. *J. Chem. Eng.,* **161(1–2)**: 73–82. https://doi.org/10.1016/j.cej.2010.04.030

Rieuwerts, J. (2017). *The Elements of Environmental Pollution* (1st ed.). Routledge. https://doi.org/10.4324/9780203798690

Robertson, F. N. (1989). Arsenic in ground-water under oxidizing conditions, south-west United States. *Environ Geochem Health*, **11(3–4)**: 171–185. https://doi.org/10.1007/BF01758668

Roy, A., Queirolo, E., Peregalli, F., Mañay, N., Martínez, G., and Kordas, K. (2015). Association of blood lead levels with urinary F2-8α isoprostane and 8-hydroxy-2-deoxy-guanosine concentrations in first-grade Uruguayan children. *Environ. Res.*, **140**: 127–135. https://doi.org/10.1016/j.envres.2015.03.001

Saha, R., Nandi, R., and Saha, B. (2011). Sources and toxicity of hexavalent chromium. *J. Coord. Chem.*, **64(10)**: 1782–1806. https://doi.org/10.1080/00958972.2011.583646

Sahoo, S. Ku., and Hota, G. (2018a). Surface functionalization of GO with MgO/MgFe2O4 binary oxides: A novel magnetic nanoadsorbent for removal of fluoride ions. *J. Environ. Chem. Eng.*, **6(2)**: 2918–2931. https://doi.org/10.1016/j.jece.2018.04.054

Sahoo, T. R., and Prelot, B. (2020). Adsorption processes for the removal of contaminants from wastewater. In *Nanomaterials for the Detection and Removal of Wastewater Pollutants* (161–222). Elsevier. https://doi.org/10.1016/B978-0-12-818489-9.00007-4

Sankararamakrishnan, N., Dixit, A., Iyengar, L., and Sanghi, R. (2006). Removal of hexavalent chromium using a novel cross linked xanthated chitosan. *Bioresour. Technol.*, **97(18)**: 2377–2382. https://doi.org/10.1016/j.biortech.2005.10.024

Saravanan, M., Karthika, S., Malarvizhi, A., and Ramesh, M. (2011). Ecotoxicological impacts of clofibric acid and diclofenac in common carp (Cyprinus carpio) fingerlings: Hematological, biochemical, ionoregulatory and enzymological responses. *J. Hazard. Mater.*, **195**: 188–194. https://doi.org/10.1016/j.jhazmat.2011.08.029

Sarkar, M., Banerjee, A., Pramanick, P. P., and Sarkar, A. R. (2006). Use of laterite for the removal of fluoride from contaminated drinking water. *J. Colloid Interface Sci.*, **302(2)**: 432–441. https://doi.org/10.1016/j.jcis.2006.07.001

Scheidegger, A. M., Sparks, D. L., and Fendorf, M. (1996). Mechanisms of Nickel Sorption on Pyrophyllite: Macroscopic and Microscopic Approaches. *Soil Sci Soc Am J.*, **60(6)**: 1763–1772. https://doi.org/10.2136/sssaj1996.03615995006000060022x

Scheurell, M., Franke, S., Shah, R. M., and Hühnerfuss, H. (2009). Occurrence of diclofenac and its metabolites in surface water and effluent samples from Karachi, Pakistan. *Chemosphere*, **77(6)**: 870–876. https://doi.org/10.1016/j.chemosphere.2009.07.066

Selomulya, C., Meeyoo, V., and Amal, R. (1999). Mechanisms of Cr(VI) removal from water by various types of activated carbons. *J. Chem. Technol. Biotechnol.*, **74(2)**: 111–122. https://doi.org/10.1002/(SICI)1097-4660(199902)74:2<111::AID-JCTB990>3.0.CO;2-D

Selvam, S., Antony Ravindran, A., Venkatramanan, S., and Singaraja, C. (2017). Assessment of heavy metal and bacterial pollution in coastal aquifers from SIPCOT industrial zones, Gulf of Mannar, South Coast of Tamil Nadu, India. *Appl. Water Sci.*, **7(2)**: 897–913. https://doi.org/10.1007/s13201-015-0301-3

Shah, J., Rasul, Md. M., Haq, A., and Khan, Y. (2013). Removal of Rhodamine B from aqueous solutions and wastewater by walnut shells: Kinetics, equilibrium and thermodynamics studies. *Front. Chem. Sci. Eng.*, **7**: 428–436. https://doi.org/10.1007/s11705-013-1358-x

Shaji, E., Santosh, M., Sarath, K. V., Prakash, P., Deepchand, V., and Divya, B. V. (2021). Arsenic contamination of groundwater: A global synopsis with focus on the Indian Peninsula. *Geosci. Front.*, **12(3)**: 101079. https://doi.org/10.1016/j.gsf.2020.08.015

Shan, H., Liu, Y., Zeng, C., Peng, S., and Zhan, H. (2022). On As(III) Adsorption Characteristics of Innovative Magnetite Graphene Oxide Chitosan Microsphere. *Materials*, **15(20)**: Article 20. https://doi.org/10.3390/ma15207156

Sharifian, S., Tabrizi, F. F., and Sardarian, A. R. (2022). *Efficient adsorptive removal of diclofenac sodium by acidified MIL101(Cr): Optimizing the content of phosphotungstic acid (PTA), Flow loop thin film slurry flat plate reactor, Kinetic, thermodynamic and recycling studies*. In Review. https://doi.org/10.21203/rs.3.rs-1982409/v1

Shen, J., Zhu, Y., Yang, X., and Li, C. (2012). Graphene quantum dots: Emergent nanolights for bioimaging, sensors, catalysis and photovoltaic devices. *Chem Comm.*, **48(31)**: 3686. https://doi.org/10.1039/c2cc00110a

Shen, K., and Gondal, M. A. (2017). Removal of hazardous Rhodamine dye from water by adsorption onto exhausted coffee ground. *J. Saudi Chem Soc.*, **21**: S120–S127. https://doi.org/10.1016/j.jscs.2013.11.005

Sheng, G., Li, Y., Yang, X., Ren, X., Yang, S., Hu, J., and Wang, X. (2012). Efficient removal of arsenate by versatile magnetic graphene oxide composites. *RSC Adv.*, **2(32)**: 12400. https://doi.org/10.1039/c2ra21623j

Silva, C. P., Otero, M., and Esteves, V. (2012). Processes for the elimination of estrogenic steroid hormones from water: A review. *Environ Pollut.*, **165**: 38–58. https://doi.org/10.1016/j.envpol.2012.02.002

Sokol, R. Z., and Berman, N. (1991). The effect of age of exposure on lead-induced testicular toxicity. *Toxicology*, **69(3)**: 269–278. https://doi.org/10.1016/0300-483X(91)90186-5

Şölener, M., Tunali, S., Özcan, A. S., Özcan, A., and Gedikbey, T. (2008a). Adsorption characteristics of lead(II) ions onto the clay/poly(methoxyethyl)acrylamide (PMEA) composite from aqueous solutions. *Desalination*, **223(1–3)**: 308–322. https://doi.org/10.1016/j.desal.2007.01.221

Soni, R., Bhardwaj, S., and Shukla, D. P. (2020). Various water-treatment technologies for inorganic contaminants: Current status and future aspects. In *Inorganic Pollutants in Water* (273–295). Elsevier. https://doi.org/10.1016/B978-0-12-818965-8.00014-7

Srivastava, S. K., Tyagi, R., Pant, N., and Pal, N. (1989). Studies on the removal of some toxic metal ions. Part II (removal of lead and cadmium by

montmorillonite and kaolinite). *Environ. Technol. Lett.*, **10(3)**: 275–282. https://doi.org/10.1080/09593338909384742

Su, H., Ye, Z., and Hmidi, N. (2017). High-performance iron oxide–graphene oxide nanocomposite adsorbents for arsenic removal. *Colloids Surf A: Physicochem. Eng. Asp.,* **522**: 161–172. https://doi.org/10.1016/j.colsurfa.2017.02.065

Suc, N. V., and Kim Chi, D. (2017). Removal of rhodamine B from aqueous solution via adsorption onto microwave-activated rice husk ash. *J. Dispers Sci Technol.*, **38(2)**: 216–222. https://doi.org/10.1080/01932691.2016.1155153

Sui, Z., Meng, Q., Zhang, X., Ma, R., and Cao, B. (2012). Green synthesis of carbon nanotube–graphene hybrid aerogels and their use as versatile agents for water purification. *J. Mater. Chem.*, **22(18)**: 8767–8771. https://doi.org/10.1039/C2JM00055E

Sulistina, D. R., and Martini, S. (2020). The effect of Rhodamine B on the cerebellum and brainstem tissue of Rattus norvegicus. *J Public Health Res.*, **9(2)**: 1812. https://doi.org/10.4081/jphr.2020.1812

Sun, H., Cao, L., and Lu, L. (2011a). Magnetite/reduced graphene oxide nanocomposites: One step solvothermal synthesis and use as a novel platform for removal of dye pollutants. *Nano Res.*, **4(6)**: 550–562. https://doi.org/10.1007/s12274-011-0111-3

Swain, S. K., Patnaik, T., Patnaik, P. C., Jha, U., and Dey, R. K. (2013). Development of new alginate entrapped Fe(III)–Zr(IV) binary mixed oxide for removal of fluoride from water bodies. *J. Chem. Eng.*, **215–216**: 763–771. https://doi.org/10.1016/j.cej.2012.10.098

Swain, S. K., Patnaik, T., Singh, V. K., Jha, U., Patel, R. K., and Dey, R. K. (2011). Kinetics, equilibrium and thermodynamic aspects of removal of fluoride from drinking water using meso-structured zirconium phosphate. *J. Chem. Eng.*, **171(3)**: 1218–1226. https://doi.org/10.1016/j.cej.2011.05.030

Tam, N. T. M., Liu, Y., Bashir, H., Yin, Z., He, Y., and Zhou, X. (2020). Efficient Removal of Diclofenac from Aqueous Solution by Potassium Ferrate-Activated Porous Graphitic Biochar: Ambient Condition Influences and Adsorption Mechanism. *Int. J. Environ. Res. Public Health.*, **17(1)**: https://doi.org/10.3390/ijerph17010291

Tang, X.-Z., Li, W., Yu, Z.-Z., Rafiee, M. A., Rafiee, J., Yavari, F., and Koratkar, N. (2011). Enhanced thermal stability in graphene oxide covalently functionalized with 2-amino-4,6-didodecylamino-1,3,5-triazine. *Carbon*, **49(4)**: 1258–1265. https://doi.org/10.1016/j.carbon.2010.11.044

Tchounwou, P. B., Yedjou, C. G., Patlolla, A. K., and Sutton, D. J. (2012). Heavy Metal Toxicity and the Environment. In A. Luch (Ed.), *Molecular, Clinical and Environmental Toxicology*., **101**: 133–164. Springer Basel. https://doi.org/10.1007/978-3-7643-8340-4_6

Tehrani, M. S., Azar, P. A., & Dehaghi, M. (2014). *Removal of Lead Ions from Aqueous Solution Using Multi-Walled Carbon Nanotubes: The Effect of Functionalization*.

Thakre, D., Rayalu, S., Kawade, R., Meshram, S., Subrt, J., and Labhsetwar, N. (2010). Magnesium incorporated bentonite clay for defluoridation of drinking water. *J. Hazard. Mate.r*, **180(1–3)**: 122–130. https://doi.org/10.1016/j.jhazmat.2010.04.001

Thanhmingliana, and Tiwari, D. (2015a). Efficient use of hybrid materials in the remediation of aquatic environment contaminated with micro-pollutant diclofenac sodium. *J. Chem. Eng.*, **263**: 364–373. https://doi.org/10.1016/j.cej.2014.10.102

Thanhmingliana, Tiwari, D., and Lee, S.-M. (2016). Hybrid materials in the remediation of arsenic contaminated waters: A physico-chemical study. *Desalination Water Treat.*, **57(5)**: 1995–2005. https://doi.org/10.1080/19443994.2014.979241

Thiele, H. (1953). The Dynamical Character of Adsorption, von H. J. de Boer. Oxford University Press, 1953. 1. Aufl. X V, 239 S., 45 Abb. Gebd. S. 30.—. *Angew Chem.*, **65(16)**: 431–431. https://doi.org/10.1002/ange.19530651619

Thomas, H. C. (1944). Heterogeneous Ion Exchange in a Flowing System. *J. Am. Chem. Soc.*, **66(10)**: 1664–1666. https://doi.org/10.1021/ja01238a017

Tiwari, D., Kim, H.-U., and Lee, S.-M. (2007). Removal behavior of sericite for Cu(II) and Pb(II) from aqueous solutions: Batch and column studies. *Sep. Purif. Technol.*, **57(1)**: 11–16. https://doi.org/10.1016/j.seppur.2007.03.005

Tiwari, D., Lalhriatpuia, C., Lalhmunsiama, Lee, S.-M., and Kong, S.-H. (2015). Efficient application of nano-TiO2 thin films in the photocatalytic removal of Alizarin Yellow from aqueous solutions. *Appl. Surf. Sci.*, **353**: 275–283. https://doi.org/10.1016/j.apsusc.2015.06.131

Tiwari, D., Lalhriatpuia, C., and Lee, S.-M. (2015). Hybrid materials in the removal of diclofenac sodium from aqueous solutions: Batch and column studies. *J Ind Eng Chem.*, **30**: 167–173. https://doi.org/10.1016/j.jiec.2015.05.018

Tiwari, D., Mishra, S. P., Mishra, M., and Dubey, R. S. (1999). Biosorptive behaviour of Mango (Mangifera indica) and Neem (Azadirachta indica) bark for Hg2+, Cr3+ and Cd2+ toxic ions from aqueous solutions: A radiotracer study. *Appl Radiat Isot.*, ***50*(4)**: 631–642. https://doi.org/10.1016/S0969-8043(98)00104-3

Tiwari, J. N., Mahesh, K., Le, N. H., Kemp, K. C., Timilsina, R., Tiwari, R. N., & Kim, K. S. (2013). Reduced graphene oxide-based hydrogels for the efficient capture of dye pollutants from aqueous solutions. *Carbon*, ***56***: 173–182. https://doi.org/10.1016/j.carbon.2013.01.001

Tomar, V., Prasad, S., and Kumar, D. (2013). Adsorptive removal of fluoride from water samples using Zr–Mn composite material. *Microchem. J.*, **111**: 116–124. https://doi.org/10.1016/j.microc.2013.04.007

Tounsadi, H., Khalidi, A., Farnane, M., Abdennouri, M., and Barka, N. (2016). Experimental design for the optimization of preparation conditions of highly efficient activated carbon from Glebionis coronaria L. and heavy metals removal ability. *Process Saf. Environ Prot.*, **102**: 710–723. https://doi.org/10.1016/j.psep.2016.05.017

Third World Academy of Sciences (TWAS) 2002. Safe Drining Water: The Need, the Problem, Solutions and an Action Plan. Trieste, Italy: TWAS;. p. 23

Tzabar, N., and ter Brake, H. J. M. (2016). Adsorption isotherms and Sips models of nitrogen, methane, ethane, and propane on commercial activated carbons and polyvinylidene chloride. *Adsorption*, **22(7)**: 901–914. https://doi.org/10.1007/s10450-016-9794-9

UNDP (2015). Sustainable Development Goal. 17 Goals to Transform Our World. Goal 6: Ensure Access to Water and Sanitation for All. UNDP Report. Available from: http://www.un.org/sustainabledevelopment/water-and-sanitation/

UNESCO (2014). United Nations World Water Assessment Programme (WWAP). The United Nations World Water Development Report: Water and Jobs, Paris

Unuabonah, E. I., and Taubert, A. (2014). Clay–polymer nanocomposites (CPNs): Adsorbents of the future for water treatment. *Appl. Clay Sci.*, **99:** 83–92. https://doi.org/10.1016/j.clay.2014.06.016

Ustun odabasi, S., and Büyükgüngör, H. (2016). *Removal of Micropollutants in Water with Advanced Treatment Processes*.

Vadahanambi, S., Lee, S.-H., Kim, W.-J., and Oh, I.-K. (2013). Arsenic Removal from Contaminated Water Using Three-Dimensional Graphene-Carbon Nanotube-Iron Oxide Nanostructures. *Environ. Sci Technol.*, **47(18)**: 10510–10517. https://doi.org/10.1021/es401389g

Velazquez-Peña, G. C., Olguín-Gutiérrez, M. T., Solache-Ríos, M. J., and Fall, C. (2017). Significance of FeZr-modified natural zeolite networks on fluoride removal. *J. Fluor Chem.*, **202**: 41–53. https://doi.org/10.1016/j.jfluchem.2017.09.004

Wakai, A., Lawrenson, J. G., Lawrenson, A. L., Wang, Y., Brown, M. D., Quirke, M., Ghandour, O., McCormick, R., Walsh, C. D., Amayem, A., Lang, E., & Harrison, N. (2017). Topical non-steroidal anti-inflammatory drugs for analgesia in traumatic corneal abrasions. *Cochrane Database of Syst. Rev.*, **(5)**. https://doi.org/10.1002/14651858.CD009781.pub2

Wang, J., Tsuzuki, T., Tang, B., Hou, X., Sun, L., and Wang, X. (2012). Reduced Graphene Oxide/ZnO Composite: Reusable Adsorbent for Pollutant Management. *ACS Appl. Mater. Interfaces.*, **4(6)**: 3084–3090. https://doi.org/10.1021/am300445f

Wang, J., Wang, T., Burken, J. G., Chusuei, C. C., Ban, H., Ladwig, K., and Huang, C. P. (2008). Adsorption of arsenic(V) onto fly ash: A speciation-based approach. *Chemosphere*, **72(3)**: 381–388. https://doi.org/10.1016/j.chemosphere.2008.02.045

Wang, S., and Peng, Y. (2010). Natural zeolites as effective adsorbents in water and wastewater treatment. *J.Chem. Eng.*, **156(1)**: 11–24. https://doi.org/10.1016/j.cej.2009.10.029

Wang, S., Sun, H., Ang, H. M., and Tadé, M. O. (2013). Adsorptive remediation of environmental pollutants using novel graphene-based nanomaterials. *J.Chem. Eng.*, **226**: 336–347. https://doi.org/10.1016/j.cej.2013.04.070

Wang, X. S., Lu, H. J., Zhu, L., Liu, F., and Ren, J. J. (2010). Adsorption of Lead(II) Ions onto Magnetite Nanoparticles. *Adsorp Sci Technol.*, **28(5)**: 407–417. https://doi.org/10.1260/0263-6174.28.5.407

Wang, Y. h., Zhang, J. c., Song, L. f., Hu, J. y., Ong, S. l., and Ng, W. j. (2005). Adsorption Removal of Phenol in Water and Simultaneous Regeneration by Catalytic Oxidation. *Environ. Eng. Sci.*, **22(5)**: 608–614. https://doi.org/10.1089/ees.2005.22.608

Wani, A. L., Ara, A., and Usmani, J. A. (2015). Lead toxicity: A review. *Interdiscip. Toxicol.*, **8(2)**: 55–64. https://doi.org/10.1515/intox-2015-0009

Wei, H., Deng, S., Huang, Q., Nie, Y., Wang, B., Huang, J., and Yu, G. (2013). Regenerable granular carbon nanotubes/alumina hybrid adsorbents for diclofenac sodium and carbamazepine removal from aqueous solution. *Water Res.*, **47(12)**: 4139–4147. https://doi.org/10.1016/j.watres.2012.11.062

Wongjunda, J., and Saueprasea, P. (2010). Biosorption of Chromium (VI) Using Rice Husk Ash and Modified Rice Husk Ash. *Environ.*, **4(3)**: 244–250. https://doi.org/10.3923/erj.2010.244.250

Xu, C., Li, J., He, F., Cui, Y., Huang, C., Jin, H., and Hou, S. (2016). Al_2O_3–Fe_3O_4–expanded graphite nano-sandwich structure for fluoride removal from aqueous solution. *RSC Adv.*, **6(99)**: 97376–97384. https://doi.org/10.1039/C6RA19390K

Xu, N., Li, S., Li, W., and Liu, Z. (2020a). Removal of Fluoride by Graphene Oxide/Alumina Nanocomposite: Adsorbent Preparation, Characterization, Adsorption Performance and Mechanisms. *Chemistry Select*, **5(6)**: 1818–1828. https://doi.org/10.1002/slct.201904867

Xu, Y., Nakajima, T., and Ohki, A. (2002). Adsorption and removal of arsenic(V) from drinking water by aluminum-loaded Shirasu-zeolite. *J. Hazard. Mater.*, **92(3)**: 275–287. https://doi.org/10.1016/S0304-3894(02)00020-1

Yadav, M., Gupta, R., & Sharma, R. K. (2019). Green and Sustainable Pathways for Wastewater Purification. *Adv. in Water Purification Techniques.,* (pp. 355–383). Elsevier. https://doi.org/10.1016/B978-0-12-814790-0.00014-4

Yagub, M. T., Sen, T. K., Afroze, S., & Ang, H. M. (2014). Dye and its removal from aqueous solution by adsorption: A review. *Adv. Colloid Interface Sci.*, **209**: 172–184. https://doi.org/10.1016/j.cis.2014.04.002

Yang, X., Chen, C., Li, J., Zhao, G., Ren, X., and Wang, X. (2012). Graphene oxide-iron oxide and reduced graphene oxide-iron oxide hybrid materials for the removal of organic and inorganic pollutants. *RSC Adv.*, **2(23)**: 8821–8826. https://doi.org/10.1039/C2RA20885G

Yen Doan, T. H., Minh Chu, T. P., Dinh, T. D., Nguyen, T. H., Tu Vo, T. C., Nguyen, N. M., Nguyen, B. H., Nguyen, T. A., and Pham, T. D. (2020). Adsorptive Removal of Rhodamine B Using Novel Adsorbent-Based Surfactant-Modified Alpha Alumina Nanoparticles. *J Anal Methods Chem.*, **2020**: 1–8. https://doi.org/10.1155/2020/6676320

Yoon, Y., Park, W. K., Hwang, T.-M., Yoon, D. H., Yang, W. S., and Kang, J.-W. (2016). Comparative evaluation of magnetite–graphene oxide and magnetite-reduced graphene oxide composite for As(III) and As(V) removal. *J. Hazard. Mater.*, **304**: 196–204. https://doi.org/10.1016/j.jhazmat.2015.10.053

Yoon, Y., Zheng, M., Ahn, Y.-T., Park, W. K., Yang, W. S., and Kang, J.-W. (2017). Synthesis of magnetite/non-oxidative graphene composites and their application for arsenic removal. *Sep. Purif. Technol.*, **178**: 40–48. https://doi.org/10.1016/j.seppur.2017.01.025

Zhang, K., Dwivedi, V., Chi, C., and Wu, J. (2010). Graphene oxide/ferric hydroxide composites for efficient arsenate removal from drinking water. *J. Hazard. Mater.*, **182(1–3)**: 162–168. https://doi.org/10.1016/j.jhazmat.2010.06.010

Zhang, L., Luo, H., Liu, P., Fang, W., and Geng, J. (2016). A novel modified graphene oxide/chitosan composite used as an adsorbent for Cr(VI) in aqueous

solutions.*Int. J. Biol. Macromol.*,**87**:586–596. https://doi.org/10.1016/j.ijbiomac.2016.03.027

Zhang, W., Shi, X., Zhang, Y., Gu, W., Li, B., and Xian, Y. (2013). Synthesis of water-soluble magnetic graphene nanocomposites for recyclable removal of heavy metal ions. *J. Mater. Chem.*, **1(5)**: 1745–1753. https://doi.org/10.1039/C2TA00294A

Zhang, Z., Luo, H., Jiang, X., Jiang, Z., and Yang, C. (2015). Synthesis of reduced graphene oxide-montmorillonite nanocomposite and its application in hexavalent chromium removal from aqueous solutions. *RSC Adv.*, **5(59)**: 47408–47417. https://doi.org/10.1039/C5RA04288G

Zhao, G., Ren, X., Gao, X., Tan, X., Li, J., Chen, C., Huang, Y., and Wang, X. (2011). Removal of Pb(II) ions from aqueous solutions on few-layered graphene oxide nanosheets. *Dalton Trans.*, **40(41)**: 10945–10952. https://doi.org/10.1039/C1DT11005E

Zhu, J., Sadu, R., Wei, S., Chen, D. H., Haldolaarachchige, N., Luo, Z., Gomes, J. A., Young, D. P., and Guo, Z. (2012). Magnetic Graphene Nanoplatelet Composites toward Arsenic Removal. *ECS J. Solid State Sci. Technol.*, **1(1)**: M1–M5. https://doi.org/10.1149/2.010201jss

Zhu, J., Wei, S., Gu, H., Rapole, S. B., Wang, Q., Luo, Z., Haldolaarachchige, N., Young, D. P., and Guo, Z. (2012). One-Pot Synthesis of Magnetic Graphene Nanocomposites Decorated with Core@Double-shell Nanoparticles for Fast Chromium Removal. *Environ. Sci. Technol.*, **46(2)**: 977–985. https://doi.org/10.1021/es2014133

Zhu, L., Chen, B., and Shen, X. (2000). Sorption of Phenol, *p* -Nitrophenol, and Aniline to Dual-Cation Organobentonites from Water. *Environ. Sci. Technol.*, **34(3)**: 468–475. https://doi.org/10.1021/es990177x

Zou, W., Han, R., Chen, Z., Jinghua, Z., and Shi, J. (2006). Kinetic study of adsorption of Cu(II) and Pb(II) from aqueous solutions using manganese oxide coated zeolite in batch mode. *Colloids Surf. A: Physicochem. Eng. Asp*., **279(1)**: 238–246. https://doi.org/10.1016/j.colsurfa.2006.01.008

BIO-DATA

1. NAME : Ngainunsiami

2. DATE OF BIRTH : 3rd December, 1991.

3. FATHER'S NAME : P.L. Ropianga

4. PERMANENT ADDRESS : C-64/A, Durtlang North, Aizawl, Mizoram, India, 796025

5. EDUCATIONAL QUALIFICATIONS :

Qualification	Year of Passing	Board/University	Subjects	Marks %	Division
HSLC	2007	Indian Certificate of Secondary Education (ICSE)	English, Hindi, Mathematics, Science, Computer science.	71.2	First
HSSLC	2009	Council of Higher Secondary Education (COSEM)	English, Alt. English, Physics, Chemistry, Biology	62.4	First
B.Sc (Chemisty)	2012	Govt. Zirtiri Residential Science College, Mizoram University	Chemistry, Physics, English, Botany, Zoology,	48.25	Second
M.Sc (Chemistry)	2014	Mizoram University	Chemistry (Specializatio in Organic Chemistry)	74.3	First

List of publications

A. Journals

1. Lalhmunsiama, L., Ngainunsiami, N., Kim, D.-J., and Tiwari, D. (2021). Graphene based advanced materials in the remediation of aquatic environment contaminated with fluoride: Newer insights and applicability. *Chem. Eng. Process.:Process Intensif*, **165**: 108428. https://doi.org/10.1016/j.cep.2021.108428

2. Levia Lalthazuala, Lalhmunsiama, **Ngainunsiami**, Diwakar Tiwari, Seung Mok Lee and Suk Soon Choi (2022). Efficient elimination of tetracycline by ferrate (VI): Real water implications. *Applied Chemistry for Engineering,* **34**:3. https://doi.org/10.14478/ace.2023.1012

3. Ngainunsiami, Lalhmunsiama and Tiwari D. (2023). Facile and greener synthesis of novel nanocomposite materials: Insights of interfacial studies in the elimination of arsenic and fluoride in single and binary components. (Communicated: Environmental Science and Pollution Research)
Engineering Journal)

4. Ngainunsiami, Lalhmunsiama and Tiwari D. (2023). Facile synthesis of novel graphene-based magnetized nanocomposite materials for the simultaneous elimination of lead (II) and chromium (VI) in aqueous medium: Insights of interfacial studies. (Communicated: Applied Water Science)

5. Ngainunsiami, Lalhmunsiama and Tiwari D. (2023). Green and facile synthesis of novel mesoporous nanocomposites: Insights of interfacial studies for diclofenac sodium and Rhodamine B. (Communicated: Environmental Research)

B. Conference/ Seminar

1. Presented "Silane grafted bentonite clay in the remediation of Copper from aquatic environment" at International Conference on Chemistry & Environmental Sustainability (ICCES-2019) on 19th to 22nd February, 2019 which was organized by Department of Chemistry, Mizoram university Aizawl, Mizoram, India.

2. Presented "Electrochemical Detection of Emerging Water Contaminants: Voltammetric Determination of Sulfamethoxazole on Nano-composite Modified Glassy Carbon Electrode" at NCFMA- 2019) held on 22nd to 23rd November 2019, organized by Department of BS&HSS (Physics), National Institute of Technology, Aizawl, Mizoram, India.

3. Presented "Heterogeneous Fenton like degradation of diclofenac using synthesized Bentonite /Ag(NPs)/Fe(NPs) nano-composite at National Conference on Emerging Trends In Environmental Research (NACETER 2019), organized by Department of Environmental Science, Pachhunga University College, Aizawl in collaboration with Environment, Forest and Climate Change Department, Government of Mizoram, during 31 October – 2 November 2019.

4. Presented "Synthesis of Graphene Oxide using Sugarcane Syrup: Efficient Use of Graphene Oxide in the Removal of Tetracycline from Aqueous Solutions" at 2nd Annual Convention of North East (India) Academy of Science and Technology (NEAST) & International Seminar on Recent Advances in Science and Technology (ISRAST), 16th -18th November 2020, Organized by NEAST, Mizoram University, Aizawl, Mizoram, India

5. Presented "Efficient use of sugarcane derived graphene oxide-based nanocomposite material for the remediation of aqueous solution contaminated with lead (II)" at the physical sciences discipline technical session in the 4th Mizoram Science Congress held at Aijal Club, Aizawl during 24-25 November,2022.

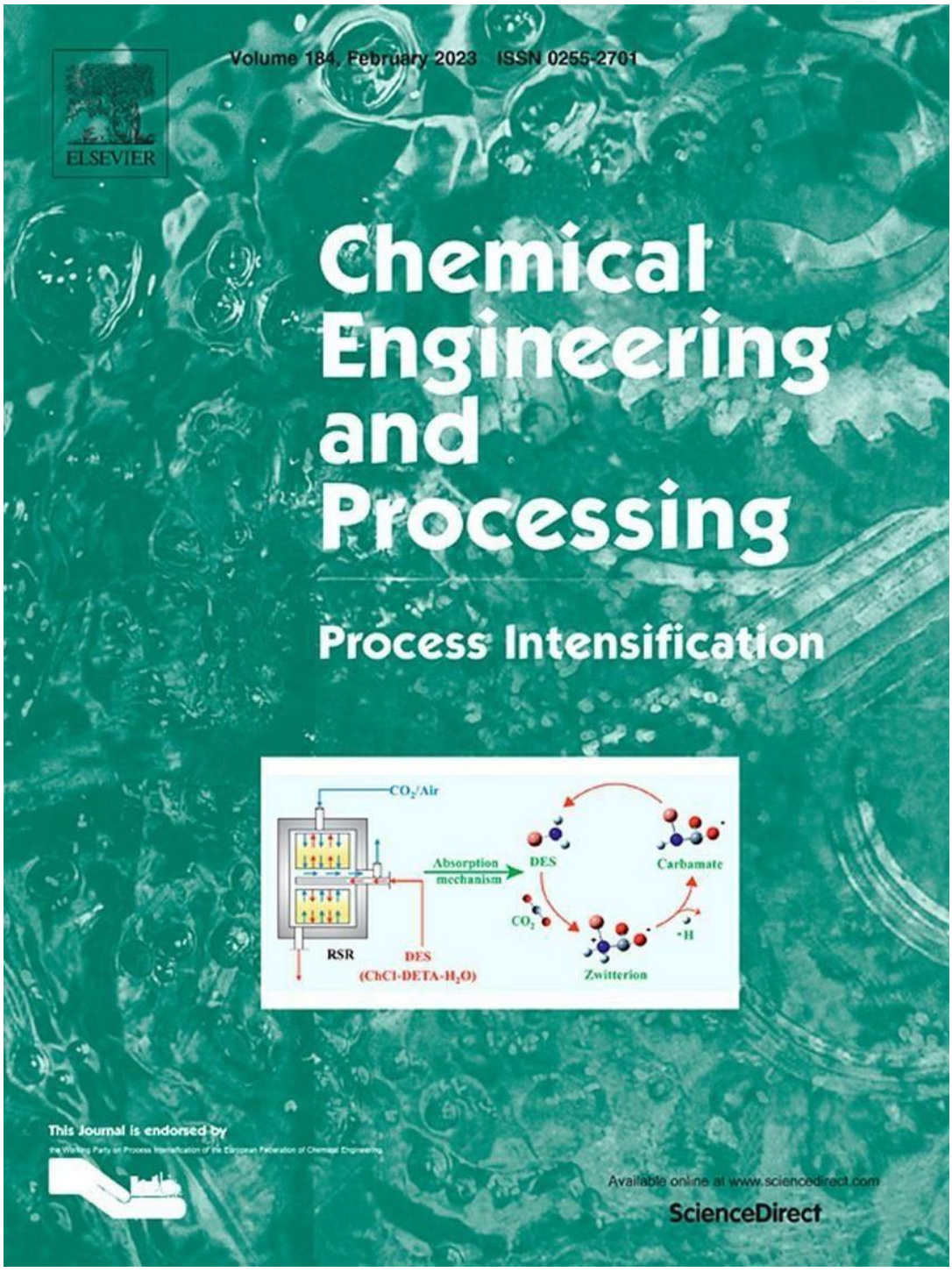
Volume 184, February 2023 ISSN 0255-2701
ELSEVIER
Chemical Engineering and Processing
Process Intensification
CO2/Air
Absorption mechanism
DES
Carbamate
CO2
•H
RSR
DES
(ChCl-DETA-H2O)
Zwitterion
This Journal is endorsed by
Available online at www.sciencedirect.com
ScienceDirect

Chemical Engineering & Processing: Process Intensification 165 (2021) 108428

Contents lists available at ScienceDirect

Chemical Engineering and Processing - Process Intensification

journal homepage: www.elsevier.com/locate/cep

Graphene based advanced materials in the remediation of aquatic environment contaminated with fluoride: Newer insights and applicability

Lalhmunsiama Lalhmunsiama [a], Ngainunsiami Ngainunsiami [b], Dong-Jin Kim [c], Diwakar Tiwari [b,*]

[a] Department of Industrial Chemistry, School of Physical Sciences, Mizoram University, Aizawl, 796004, India
[b] Department of Chemistry, School of Physical Sciences, Mizoram University, Aizawl, 796004, India
[c] Department of Environmental Sciences and Biotechnology & Institute of Energy and Environment, Hallym University, 1 Okcheon, Chuncheon, Gangwon, 24252, Republic of Korea

ARTICLE INFO

Keywords:
Graphene
Functionalized materials
Nanocomposites
Fluoride
Insights of mechanism
Deflouridation

ABSTRACT

Graphene possesses unique physicochemical properties viz., high specific surface area, thermal stability, enormous electron mobility, mechanical flexibility, large elasticity, etc. Due to these distinctive properties, many researchers focused on the modification of graphene or the preparation of graphene-based materials for diverse applications. The review addresses recent advances in the design, synthesis and applications of graphene-based materials in the remediation of aquatic environment contaminated with potential water pollutant fluoride. Overview of major factors influencing the fluoride removal viz., solution pH, temperature, co-existing ions etc. have been included extensively. The fluoride removal mechanisms as investigated with the help of advanced analytical tools viz., Fourier Transform Infrared Spectroscopy (FTIR), X-ray Photoelectron Spectroscopy (XPS), X-ray diffraction (XRD), and Cyclic Voltammetry (CV) are comprehensively demonstrated. Further, regeneration and reusability of the materials are broadly summarized in the review. This review attempted to investigate the updated knowledge of fluoride contamination and remediation with available data and greatly demonstrated the challenges in the existing methods. Therefore, future aspects of studies in intended use of graphene and graphene based advanced materials is elaborated for the greater applicability of the review.

1. Introduction

The contamination of the aquatic environment by fluoride is a serious environmental concern for many countries since fluoride intake to the human body causes various health issues. Fluorine exposure to humans is primarily through the drinking of contaminated water or even through the utilization of fluorine contaminated water in agriculture [1–3]. The naturally occurring fluoride minerals such as fluorspar (CaF_2), fluorapatite [$3Ca_3(PO_4)_2Ca(FCl_2)$], cryolite (Na_3AlF_6) and sellaite (MgF_2) are nearly insoluble in water. However, the fluoride dissolution may take place very slowly under favorable conditions; therefore, the industries effluent are found to be the major sources of fluoride in aqueous media [2,4]. Fluoride shows both lucrative and deleterious effects towards human health [4,5]. Fluoride concentration around 0.7 mg/L is although useful for bones and teeth development and dental cares. However, due to similar ionic radius of F^- and OH^-, i.e., 1.36 Å and 1.40 Å ionic radius respectively; the F^- ions potentially displaces hydroxide ions from hydroxyapatite, $Ca_5(PO_4)_3OH$ (present mainly in human and animal teeth and bones) to form $Ca_5(PO_4)_3F$ which is found to be harder and tougher and eventually resulted in strengthening of enamel to small extent [4]. On the other hand, the fluorine concentration exceeding 1.5 mg/L showed greater adverse effects to the human body and causing osteoporosis, cancer, arthritis, dental fluorosis and skeletal fluorosis [6,7]. A prolonged exposure of fluoride causes enhanced conversion of hydroxyapatite to fluorapatite which makes the teeth and bones more brittle, denser and harder. This finally resulted with dental fluorosis (molting and embrittlement of teeth). Additionally, prolonged exposure of causes skeletal fluorosis [8]. Therefore, because of several severe biological impacts of fluorine towards human health, the removal of excess fluorine from the water bodies is the need of the hour. Various methods viz., precipitation, coagulation, adsorption, ion-exchange, electro-coagulation, reverse osmosis, nano-filtration, etc. are greatly applied in the removal of fluoride from aqueous media. Graphene and graphene based advanced materials have shown

* Corresponding author.
E-mail address: diw_tiwari@yahoo.com (D. Tiwari).

https://doi.org/10.1016/j.cep.2021.108428
Received 22 January 2021; Received in revised form 10 April 2021; Accepted 13 April 2021
Available online 15 April 2021

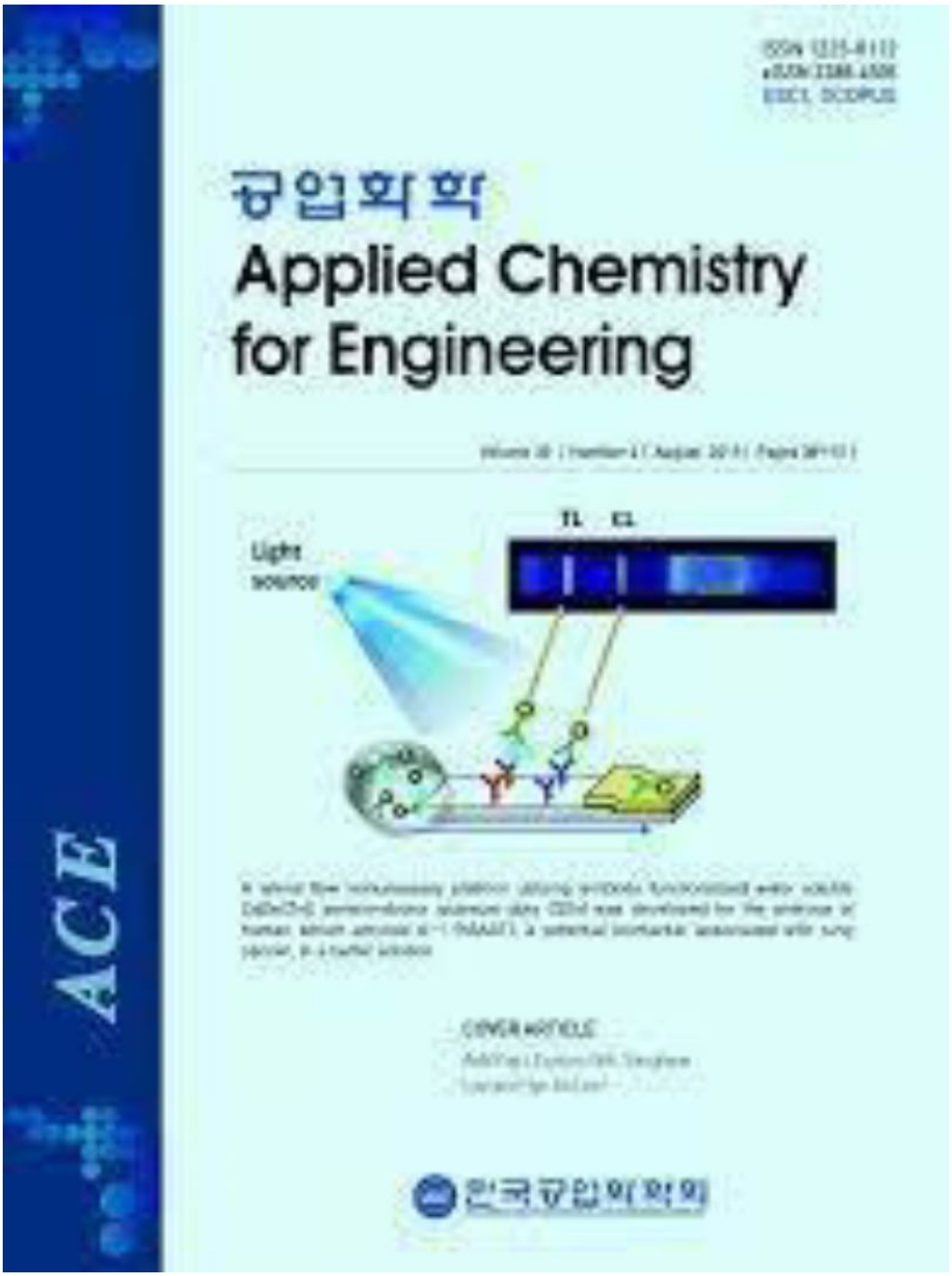
ACE
응용화학
Applied Chemistry
for Engineering
Light
source
한국응용화학회

Appl. Chem. Eng., Vol. 34, No. 3, June 2023, 318-325
https://doi.org/10.14478/ace.2023.1012

Article

Efficient Elimination of Tetracycline by Ferrate (VI): Real Water Implications

Levia Lalthazuala, Lalhmunsiama*, Ngainunsiami, Diwakar Tiwari†, Seung Mok Lee and Suk Soon Choi***,†**

Department of Chemistry, School of Physical Sciences, Mizoram University, Aizawl 796004, India
**Department of Industrial Chemistry, School of Physical Sciences, Mizoram University, Aizawl 796004, India*
***Department of Biosystem and Convergence, Catholic Kwandong University, Gangneung 25601, Republic of Korea*
****Department of Biological and Environmental Engineering, Semyung University, Jecheon 27236, Republic of Korea*
(Received February 3, 2023; Revised March 20, 2023; Accepted March 21, 2023)

Abstract

The detection of antibiotics in treated wastewater is a global concern as it enters water bodies and causes the development of antibiotic resistance genes in humans and marine life. The study specifically aims to explore the potential of ferrate (VI) in eliminating tetracycline (TCL). The degradation of TCL is optimized with parametric studies, *viz.*, the effect of pH and concentration, which provide insights into TCL elimination. The increase in pH (from 7.0 to 10.0) favors the percentage removal of TCL; however, the increase in TCL concentrations from 0.02 to 0.3 mmol/L caused a decrease in percentage TCL removal from 97.4 to 29.1%, respectively, at pH 10.0. The time-dependent elimination of TCL using ferrate (VI) followed pseudosecond-order rate kinetics, and an apparent rate constant (k_{app}) was found at 1978.8 $L^2/mol^2/min$. Coexisting ions, i.e., $NaNO_3$, Na_2HPO_4, NaCl, and oxalic acid, negligibly affect the oxidation of TCL by ferrate (VI). However, EDTA and glycine significantly inhibited the elimination of TCL using ferrate (VI). The mineralization of TCL using ferrate (VI) was favored at higher pH, and it increased from 18.57 to 32.52% when the solution pH increased from pH 7.0 to 10.0. Additionally, the real water samples containing a relatively high level of inorganic carbon spiked with TCL revealed that ferrate (VI) performance in the removal of TCL was unaffected, which further inferred the potential of ferrate (VI) in real implications.

Keywords: *Persistent antibiotics, Elimination of tetracycline, Mineralization of pollutant, Real matrix samples, Potential of ferrate (VI)*

1. Introduction

Antibiotics from all classes are often detected on the ground surface and even in drinking waters around the globe. They frequently escape from existing wastewater treatment plants due to the partial degradation of these pollutants. Additionally, the relaxed legislation, administrative oversights, and unregulated release of pharmaceutical compounds pose serious human health concerns. Moreover, antibiotics in water bodies and their continuous usage cause gene mutations among bacteria, viruses, and fungi that develop antibacterial resistance genes in humans. Therefore, eliminating antibiotics from wastewater is essential before their release into the aquatic environment[1,2].

Tetracycline (TCL) is an extensively used antibiotic to prevent and cure infectious diseases in humans and animals. Due to its reasonable cost and strong antibacterial properties, TCL is a widely prescribed antibiotic. It is prescribed for treating cholera and pneumonia, including several medicinal therapies. TCL is prescribed for several infectious animal diseases, including poultry, swine, sheep, etc.[3-6].

TCL is partially metabolized in the biosystem and releases a significant amount of TCL into wastewater through urine and feces. Moreover, due to its low biodegradability and persistence in nature, TCL is not eliminated efficiently in conventional treatment plants[7]. The occurrence of TCL in treated wastewater suggests that conventional treatment methods are insufficient and need advanced treatment to remove persistent chemicals[7,8]. Several treatment methods have been demonstrated for removing antibiotics from water bodies, including chlorination, activated carbon filtration, microfiltration, ultrafiltration, and advanced oxidation processes such as ozonation, Fenton reaction, photocatalysis, and ultraviolet (UV) radiation[9-15]. However, apart from their removal performance and efficiency, these approaches have limitations, including high sludge production, time consumption, and sometimes toxic byproduct formation[16].

On the other hand, ferrate (VI) is perhaps a suitable alternative oxidant due to its strong oxidizing capacity with a redox potential of 2.20 V, relatively higher than the redox potential of a common oxidant such as permanganate (1.67 V) and ozone (2.07)[17]. Moreover, it is an environmentally friendly oxidant and has received greater attention [18,19]. In aqueous environments, ferrate (VI) exists in four different species, *viz.*, FeO_4^{2-}, $HFeO_4^-$, H_2FeO_4, and $H_3FeO_4^+$. At moderate and alkaline pH, the dominant ferrate (VI) species are $HFeO_4^-$ and FeO_4^{2-}, respectively; nevertheless, the oxidizing ability and strength of ferrate

† Corresponding Author: D. Tiwari: Mizoram University, Department of Chemistry, School of Physical Sciences, Aizawl 796004, India; S. S. Choi: Semyung University, Department of Biological and Environmental Engineering, Jecheon 27236, Republic of Korea
Tel: D. Tiwari: +91-986-232-3015; S. S. Choi: +82-43-649-1337
e-mail: D. Tiwari: drw_tiwari@yahoo.com; S. S. Choi: sschoi@semyung.ac.kr

pISSN: 1225-0112 eISSN: 2288-4505

PARTICULARS OF THE CANDIDATE

NAME OF THE CANDIDATE	:	Ngainunsiami
DEGREE	:	Doctor of Philosophy (Ph.D.)
DEPARTMENT	:	Department of Chemistry
TITLE OF THESIS	:	Magnetite graphene oxide - clay nanocomposites in the remediations of aquatic environment contaminated with arsenic and fluoride.
DATE OF ADMISSION	:	18th August, 2017

APPROVAL OF RESEARCH PROPOSAL:

1. DRC	:	5th April, 2018
2. BOS	:	13th April, 2018
3. SCHOOL BOARD	:	24th April, 2018
4. MZU REGISTRATION NUMBER	:	3173 of 2009-10
5. Ph.D. REGISTRATION NO. & DATE	:	MZU/Ph.D/1104 of 24.04.2018

Head

Department of Chemistry